Final Report

FHWA/IN/JTRP – 2005/16-2

Fatigue of Older Bridges in Northern Indiana due to Overweight and Oversized Loads

Volume 2: Analysis Methods and Fatigue Evaluation

by

Piya Chotickai
Graduate Research Assistant

and

Mark D. Bowman
Professor of Civil Engineering

School of Civil Engineering
Purdue University

Joint Transportation Research Program
Project No: C-36-56DDD
File No: 7-4-55
SPR-2385

Conducted in Cooperation with the
Indiana Department of Transportation
And the U.S. Department of Transportation
Federal Highway Administration

Purdue University
West Lafayette, Indiana
July 2006

INDOT Research

TECHNICAL *Summary*

Technology Transfer and Project Implementation Information

TRB Subject Code: 25-1 Bridges *July 2006*
Publication No.: FHWA/IN/JTRP-2005/16-2, SPR-2385 *Final Report*

Fatigue of Older Bridges in Northern Indiana due to Overweight and Oversized Loads

Volume 2: Analysis Methods and Fatigue Evaluation

Introduction

An important part of the economy of northwestern Indiana is the shipping of steel and other various products to Michigan for the manufacturing of automobiles and other commodities. The extra heavy-duty corridor is composed of segments of roads totaling 94 miles in northwest Indiana. It was put into place to facilitate the shipping of large truck loads, such as coils of sheet steel. The extra heavy-duty corridor highway permits truck loads of up to 134,000 lbs. transported by multiple trailer, multiple axle "Michigan Train" trucks. The purpose of this study is to examine and evaluate the fatigue strength of the steel bridges along the extra heavy duty corridor.

The work in this study consisted of two portions: field measurements (Vol. 1) to determine the spectrum of the truck axle loads on the heavy-weight corridor and the influence of those loads on the response of one steel bridge located relatively close to the WIM, and fatigue analysis and evaluation (Volume 2) to estimate the response and remaining fatigue life of steel bridges along the heavy weight corridor.

Findings

An analytical model was developed to evaluate the fatigue strength of the steel bridges along the extra heavy weight corridor. Fatigue load models that are representative of the loading history on the extra heavy duty corridor were used to predict the stresses at critical fatigue details. It was found that fatigue truck models given by AASHTO (1990) and Laman and Nowak (1996) do not provide an accurate estimate of the fatigue damage for a wide range of span lengths when compared to the damage predicted using the WIM database. The fatigue damage estimated by these fatigue truck models could be significantly overestimated in short spans. Accordingly, new 3-axle and 4-axle fatigue trucks were developed to more accurately estimate the fatigue damage for a wide range of spans lengths. Moreover, a statistical database of resistance parameters was incorporated in the analytical model so that an estimate of the fatigue life could be predicted for a level of safety selected by the user. The safety factor for the fatigue evaluation was developed for both an extension of the S-N line approach and the variable amplitude fatigue limit concept.

An application of the fatigue model was demonstrated through a field investigation of two different steel bridge structures. Strain gage instrumentation was used to investigate actual bridge response under routine truck traffic. Strain data were collected for more than three weeks at one site and more than four weeks at the second site. By comparing the week-by-week results with the aggregate results, it was found that routine traffic strain data could generally be modeled accurately with only one week of strain data. Additionally, the response was compared to the fatigue life estimated by using traffic count data only. It was found that use of traffic count data can provide a relatively accurate estimate of the effective gross weight when the frequency of occurrence and average gross weight of each truck type at an investigated site is used in the calculation.

The fatigue behavior of thirteen steel bridge structures along the extra heavy duty

corridor was evaluated using the fatigue reliability model; one steel bridge on an interstate route was also investigated. The bridges on the extra heavy duty corridor were evaluated using WIM data to obtain the effective gross vehicle weight for the fatigue truck. The dimensions of the longitudinal members, deck thickness, and location of the fatigue critical details were taken from the bridge plans for each structure. Moreover, a field bridge inspection was preformed to verify the fatigue critical details used in each structure. A one-dimensional, beam-line analysis was then conducted for each of the structures. It was found that a remaining fatigue life in excess of 25 years was found for all bridges along the corridor, and most bridge details had fatigue lives well in excess of fifty years. Moreover, it is believed that a life well in excess of 25 years still remains for the two bridges that had the shortest remaining lives since the one-dimensional beam analysis is known to provide conservative fatigue life estimates.

Finally, by comparing the structural response from measured strain data and that from analytical bridge models, it was found that a three-dimensional bridge model provides a more accurate estimate of the effective stress range than a one-dimensional model. Also, strain gage monitoring of a detail provides the most realistic estimate of the structural response and tends to produce fatigue life predictions longer than the lives predicted by structural analysis of the bridge models.

Implementation

A reliability-based analytical model was developed to predict the fatigue life of steel bridge structures. Based upon truck gross vehicle weights measured using a weigh-in-motion sensor installed on the extra heavy-weight corridor, the effective gross weight of a four-axle fatigue truck was determined. By using stresses predicted for the fatigue truck loading along with the reliability-based model, the fatigue strength for thirteen bridge structures on the extra heavy-weight corridor was evaluated. Based upon this information, the following implementation recommendations are provided. First, the fatigue critical details for the steel bridges along the extra heavy-duty corridor should continue to be monitored through the routine biennial inspections. Second, a closer, arms-length inspection should be conducted if any cracking or unusual rusting is detected during the routine biennial inspections, especially for the bridges which had the shortest predicted remaining fatigue lives. Third, the characterization of the loading on the extra heavy-weight corridor should be periodically monitored if the trends in truck weights change significantly. Lastly, the analytical model developed in this study can be used to evaluate steel bridge structures at locations other than the extra heavy duty corridor. To perform such an evaluation, the user would need to define the stress at the fatigue detail using either structural analysis along with the appropriate fatigue truck or strain data to infer the stress level.

Contacts

For more information:

Prof. Mark D. Bowman
Principal Investigator
School of Civil Engineering
Purdue University
West Lafayette, IN 47907-2051
Phone: (765) 494-2220
Fax: (765) 496-1105
E-mail: bowmanmd@ecn.purdue.edu

Indiana Department of Transportation
Division of Research
P.O. Box 2279
West Lafayette, IN 47906
Phone: (765) 463-1521
Fax: (765) 497-1665

Purdue University
Joint Transportation Research Program
School of Civil Engineering
West Lafayette, IN 47907-1284
Phone: (765) 494-9310
Fax: (765) 496-7996
E:mail: jtrp@ecn.purdue.edu
http://www.purdue.edu/jtrp

TECHNICAL REPORT STANDARD TITLE PAGE

1. Report No.	2. Government Accession No.	3. Recipient's Catalog No.
FHWA/IN/JTRP-2005/16-2		

4. Title and Subtitle	5. Report Date
Fatigue of Older Bridges in Northern Indiana due to Overweight and Oversized Loads Volume 2: Analysis Methods and Fatigue Evaluation	July 2006
	6. Performing Organization Code
7. Author(s) Piya Chotickai and Mark D. Bowman	8. Performing Organization Report No. FHWA/IN/JTRP-2005/16-2
9. Performing Organization Name and Address Joint Transportation Research Program 550 Stadium Mall Drive Purdue University West Lafayette, Indiana 47907-2051	10. Work Unit No.
	11. Contract or Grant No. SPR-2385
12. Sponsoring Agency Name and Address Indiana Department of Transportation State Office Building 100 North Senate Avenue Indianapolis, IN 46204	13. Type of Report and Period Covered Final Report
	14. Sponsoring Agency Code

15. Supplementary Notes

Prepared in cooperation with the Indiana Department of Transportation and Federal Highway Administration.

16. Abstract

This report is the second of a two-volume final report presenting the findings of the research work that was undertaken to evaluate the fatigue behavior of steel highway bridges on the extra heavy weight corridor in Northwest Indiana. The purpose of the study was to evaluate the type and magnitude of the loads that travel along the corridor and then assess the effect of those loads on the fatigue strength of the steel bridges on the corridor. This volume presents the results of an evaluation of the fatigue strength of steel bridge structures along the extra heavy weight corridor. A fatigue load model was developed based on a three-axle and four-axle fatigue truck to accurately represent the fatigue damage caused by the actual truck load history. A fatigue damage model was also developed using a statistical database of resistance parameters to assess the fatigue strength for a level of safety selected by the user. The utility of the model was evaluated through a field investigation of two different bridge structures. Strain data were collected for more than three weeks at both sites. The behavior predicted by two-dimensional and three-dimensional analytical bridge models were compared with measured strain data. It was found that both the 1D and 3D models provided conservative fatigue life estimates, although the 3D model was considerably closer to the measured strain behavior. The fatigue truck along with the fatigue damage model was then used to assess thirteen steel bridge structures along the corridor. A remaining fatigue life of more than 25 years was found for the critical details for all bridges using the most conservative 1D model. Most remaining fatigue lives, however, were considerably longer than 25 years.

The titles of the two volumes (Report Number in parentheses) are listed below:

Volume 1: Bridge and Weigh-In-Motion Measurements (FHWA/IN/JTRP-2005/16-1)
Volume 2: Analysis Methods and Fatigue Evaluation (FHWA/IN/JTRP-2005/16-2)

17. Key Words	18. Distribution Statement
fatigue, bridge, steel, girder, heavy truck, fatigue truck, strain measurement, analytical model, inspection, cyclic damage, remaining life	No restrictions. This document is available to the public through the National Technical Information Service, Springfield, VA 22161

19. Security Classif. (of this report)	20. Security Classif. (of this page)	21. No. of Pages	22. Price
Unclassified	Unclassified	232	

Form DOT F 1700.7 (8-69)

ACKNOWLEDGMENTS

This research project was financially supported by the Federal Highway Administration and the Indiana Department of Transportation through the auspices of the Joint Transportation Research Program. The authors would like to express their grateful acknowledgement for sponsorship of this research.

The advice and input provided by the Study Advisory Committee throughout the study is greatly appreciated. Members of the Study Advisory Committee include Mr. William Dittrich, Mr. Richard Fieberg, Dr. Tommy Nantung, and Mr. Wayne Skinner of the Indiana Department of Transportation and Mr. Keith Hoernschemeyer of the Federal Highway Administration. The advice and input of Dr. Garrett D. Jeong, Dr. Judy Liu, and Dr. Alten F. Grandt is also gratefully acknowledged.

Appreciation is expressed to Harry Tidrick, Andrew Nichols, and James Reisert for their guidance and technical help in various aspects of the study. Lastly, special thanks also extend to Richard Fieberg and Scott Wood for their assistance during the instrumentation of the bridge structure.

TABLE OF CONTENTS

Page

Page

Page

LIST OF TABLES

Table Page

Table Page

LIST OF FIGURES

Figure Page

Figure Page

Figure Page

Figure Page

CHAPTER 1. INTRODUCTION

1.1. Problem Statement

Steel bridge structures are subjected to repeated cyclic stresses due to traffic load. The damage accumulation of these cyclic stresses can initiate cracks in a member, leading to fatigue failure and jeopardizing the structural integrity. Generally, a certain safety level of designed structures can be achieved by using the procedures specified in the AASHTO bridge design code (1998). However, changes in the operating environment can impact the service life of a bridge structure. Traffic volume and vehicle weight might increase and differ significantly from assumptions utilized during the design process due to the growth of industry. Also, deterioration of the bridge deck surface, as well as human errors during design and construction, can cause unexpected increases in the stress level in the bridge. As a result, the useful service life of the bridge could be significantly reduced.

Truck traffic loadings can vary considerably from site to site. Bridge live load spectra caused by a variety of gross vehicle weights, axle configurations, and axle weights of the truck population are, therefore, site-specific. To accurately estimate a fatigue life, it is necessary to incorporate truck traffic characteristics into the fatigue life calculation. The AASHTO bridge design code (1998) and the AASHTO Fatigue Guide Specifications (1990) provide a single fatigue truck that can be used for fatigue design and evaluation. An attempt to use this single truck as a representative of the actual truck traffic at different sites can, however, result in significant errors. To ensure a particular level of bridge safety, it is essential to evaluate the accuracy of the AASHTO fatigue truck in estimating the fatigue damage accumulation of actual truck traffic loadings at a given site.

The AASHTO Fatigue Guide Specifications (1990) are currently used for bridge evaluations. These specifications were developed based on the parameters provided in the LFD and ASD AASHTO code provisions (1984). Some of these parameters, such as girder distribution factor, dynamic load factor, and fatigue resistance curves, have been investigated by many researchers during the past decade. New formulations have been proposed and shown to provide a more accurate prediction of the structural response and fatigue resistance. Therefore, a refined evaluation procedure for the Guide Specifications (1990) is desirable so that the remaining fatigue life of an in-service bridge can be more accurately estimated.

1.2. Objective and Scope

The structural reliability concept has been widely applied in many fields, including civil engineering applications during the past two decades to systematically incorporate uncertainties inherent in parameters, modeling, and the calculation procedure. The reliability concept can be effectively used in the fatigue evaluation process to provide an estimate of the fatigue life with a certain confidence level. Therefore, it has been selected for developing the fatigue evaluation procedure used in this study.

The study is focused on a fatigue evaluation of short-to-medium-span steel bridge girders. Four main objectives are investigated:

1. To evaluate the accuracy of current available fatigue truck models in estimating a fatigue damage accumulation caused by actual truck traffic.
2. To investigate the potential of using traffic count data in a fatigue evaluation.
3. To examine the validity of using the racetrack method as a pre-filtering process in a cycle counting procedure.
4. To develop a refined evaluation procedure of the Fatigue Guide Specifications (1990).

The first objective is associated with a comparison of the fatigue damage accumulation caused by the actual truck traffic data collected from three weigh-in-motion (WIM) sites and the damage predicted by the 54-kip AASHTO fatigue truck, the modified AASHTO fatigue truck with an equivalent effective gross weight, and other fatigue truck models. The sites include one station on the extra heavy duty corridor in northwest Indiana and two stations on other highways in Indiana. Typical trucks traveling along the extra heavy duty corridor are multi-trailer, multi-axle vehicles generally referred to as “Michigan Train” trucks.

Secondly, to incorporate site-specific information into a fatigue evaluation, several alternatives, such as strain gage instrumentation, static weigh station, and weigh-in-motion (WIM) measurements, are generally used to determine stress range levels in the bridge structures. However, in many cases, these alternatives are not available at an investigated site. Therefore, it would be worthwhile if the information commonly recorded at a site, such as traffic count data, can be utilized to estimate the structural response. This objective can be achieved by an analysis of the vehicle database developed in this study.

One of the most accurate ways to evaluate the actual structural response in a bridge girder at a particular detail is to install strain instrumentation and collect field data. A cycle counting procedure is then needed to decompose the complex strain history. By utilizing an appropriate counting procedure, the total number of cycles and strain range magnitudes of a given strain history can be determined. The third objective is related to a verification of the racetrack method, a procedure for condensing and revealing significant events in a complex reversal history, to facilitate a cycle counting procedure so that the computational time can be reduced significantly.

The fourth objective is associated with an extensive review of the previous fatigue load and resistance models, development of a fatigue reliability model, and calibration of the safety factor for fatigue evaluation. Based on the developed fatigue evaluation procedure, it is anticipated that a more accurate estimate of the fatigue life can be obtained. As a result, appropriate decisions regarding inspection, maintenance, repair or replacement can be made.

1.3. Report Organization

The report is organized into six chapters. Chapter 1 includes an introduction, a discussion of the problem statement, and the scope of the research. Chapter 2 provides a review of the previous research on fatigue load and resistance models, as well as a discussion of the structural reliability concept. Chapter 3 presents detailed information on the vehicle database developed in this study and a discussion of uncertainty associated with use of traffic count data for a fatigue evaluation. A discussion of the accuracy of current available fatigue truck models in estimating fatigue damage and a new fatigue truck design are also presented in this chapter. Next, Chapter 4 provides a statistical database of fatigue load and resistance parameters, as well as the proposed fatigue reliability model. The safety factor developed for fatigue evaluation is also presented in this chapter. Chapter 5 includes a discussion of the results obtained from field investigations, an application of the proposed fatigue reliability model, and a simplified evaluation procedure for the fatigue reliability-based analysis. The conclusions and recommendations are provided in Chapter 6.

CHAPTER 2. LITERATURE REVIEW

2.1. Introduction

Structural reliability concepts are used in civil engineering applications to ensure that structural performance requirements will be satisfied with a certain confidence level. Reliability concepts can be utilized in a fatigue evaluation to rationally incorporate uncertainties inherent in fatigue load and resistance parameters. To develop a fatigue reliability model, three essential components are needed: fatigue resistance model, fatigue load model, and background on the structural reliability concept. A brief discussion of these three aspects is presented below.

2.2. Fatigue Resistance Model

A fatigue resistance model is used to evaluate the fatigue strength of a structure subjected to repeated cyclic loads. The two most widely used procedures in bridge applications are linear elastic fracture mechanics and stress-life approach. The linear elastic fracture mechanics is based on a theory of elasticity, while the stress-life approach is primarily based on experimental data. A review of these two procedures is provided in the following. Moreover, bridges are subjected to random loadings of truck traffic. Therefore, an understanding of variable amplitude fatigue behavior is necessary for development of a fatigue resistance model for steel bridge structures. A brief discussion of previous research studies on this aspect is also summarized herein.

2.2.1. Linear Elastic Fracture Mechanics

Linear elastic fracture mechanics (LEFM) is associated with a stress analysis or stress distribution in the vicinity of a notch or crack. It is based on a theory of elasticity;

therefore, a linear stress-strain relationship and small displacements are assumed to be valid.

Linear elastic fracture mechanics uses a stress-intensity factor (K) to characterize the stress field ahead of a sharp crack. The stress-intensity factor is a function of a remote applied stress (σ) and a crack or flaw size (a) and can be expressed as Eq. 2.1, where f(g) is a correction factor depending on specimen and crack geometry. The extensive stress-intensity-factor solutions for a variety of geometries and loading conditions are available in the literature (Tada *et al*., 1985; Sih, 1973).

$$K = f(g) \times \sigma \times \sqrt{\pi a} \tag{2.1}$$

A relationship between stable crack growth and the stress-intensity factor range was established by Paris and Erdogan (1963). This relationship is given as:

$$\frac{da}{dN} = C(\Delta K)^m \tag{2.2}$$

where $\frac{da}{dN}$ is the crack growth rate, C and m are material constants, and ΔK is the stress intensity range ($\Delta K = K_{max}-K_{min}$). Experimental testing can be used to empirically establish the material constants.

Stable crack growth only occurs within certain limits of ΔK. When the stress intensity range is below a threshold value (ΔK_{TH}), a fatigue crack will not propagate. The fatigue threshold for steel is usually between 5 and 15 $\text{ksi}\sqrt{\text{in}}$ (Bannantine *et al*., 1990). When the stress intensity factor approaches a critical value known as the fracture toughness (K_c), an unstable crack growth occurs. This critical stress intensity factor is dependent on a material property, thickness, temperature, and loading rate. By employing the critical stress intensity, a theoretical critical flaw size can be determined.

By using the Paris equation, the fatigue strength or a number of cycles to propagate a crack from a particular known size to failure (N_f) can be determined from Eq. 2.3:

$$N_f = \int_{a_i}^{a_f} \frac{da}{C(\Delta K)^m} \tag{2.3}$$

where a_i and a_f are the initial and final (critical) crack sizes, respectively. Obviously, the initial crack size is required to calculate the fatigue crack propagation life. However, both the initial crack size and the expression for the stress intensity factor are generally difficult to obtain for complex geometries.

2.2.2. Stress-Life Approach

The stress-life approach was the first method used to understand fatigue behavior. It is widely used in high-cycle applications. The approach is based upon the collection of suitable experimental data for a given structural detail. A regression analysis well known as the S-N curve is used to provide a relationship between stress range and fatigue life, which is log-log in nature and can be expressed as Eq. 2.4:

$$LogN = b - mLogS_r \tag{2.4}$$

where N is the total fatigue life in cycles, S_r is the stress range, b and m are the intercept and slope constant obtained from the regression analysis. For steel structures, the slope (m) is typically taken to be approximately equal to 3.0 (Keating and Fisher, 1986) for convenience and ease of use.

An extensive research program has been performed under the auspices and funding of the National Cooperative Highway Research Program (NCHRP) in order to develop a fatigue strength database of typical fatigue details in steel bridge structures (Fisher *et al*., 1970, 1974 and 1979). The studies indicated that small-scale specimens

always provide higher cycle life than large-scale beam-type specimens. This is because residual stresses in small-scale specimens are lower than those found in full-scale specimens. Frequency of occurrence of defects, secondary stresses due to misalignment of the specimens during testing can also cause shorter fatigue lives in full-scale specimens. It has been shown that stress ratio and mean stress effects do not have a significant influence in the fatigue strength of welded details because the high residual stresses caused by the welded processes make the maximum stress at a point of fatigue initiation and growth always close to the yield point. The most important parameters governing the fatigue resistance, however, are the stress range and the type of detail.

Another important characteristic of the S-N curve is the constant amplitude fatigue limit (CAFL). The fatigue limit is a limiting stress level that will result in an infinite fatigue life when the stress range of the constant amplitude fatigue loading is below this limit. However, the fatigue limit can disappear when a structure is subjected to periodic overloads, corrosive environments, and high temperatures (Bannantine *et al*., 1990).

The AASHTO Specifications (1998) provide a nominal fatigue resistance for fatigue design. The fatigue resistance is a function of the detail category and expressed as Eq. 2.5:

$$(\Delta F)_n = \left(\frac{A}{N}\right)^{\frac{1}{3}} \geq \frac{1}{2}(\Delta F)_{TH} \qquad (2.5)$$

where $(\Delta F)_n$ is the nominal fatigue resistance, A is the detail constant for each fatigue category (Table 2.1), and $(\Delta F)_{TH}$ is the nominal constant amplitude fatigue threshold (Table 2.1). The Specifications (1998) use the S-N curves at two standard deviations below the mean S-N curves, which corresponds to a confidence limit of 95 percent (Fisher, 1997). Figure 2.1 shows the S-N curves provided in the Specifications (1998).

By considering Eq. 2.5, it can be viewed that the Specifications (1998) assume an extension of S-N line for a stress range greater than half of the nominal constant amplitude fatigue limit. The value at half of the constant amplitude is used to check

whether the maximum stress range in a variable amplitude spectrum exceeds the constant amplitude fatigue limit. It is assumed that the maximum stress range is twice as great as the calculated nominal stress range.

2.2.3. Cumulative Fatigue Damage and Miner's Rule

Miner (1945) formulated a linear damage criterion that was first suggested by Palmgren (1924). The Palmgren-Miner hypothesis, which is often referred to as Miner's rule, is one of the most widely used damage accumulation models. One of the reasons for it's popularity is the simplicity and ease of use since it assumes a linear damage accumulation. Although other nonlinear models have been proposed, they are more complicated than the Miner's rule and cannot provide consistently better results (Committee on Fatigue, 1982). Several current design codes, such as AWS (American Welding Society), ASME (American Society of Mechanical Engineers) and AASHTO Specifications (American Association of State Highway and Transportation Officials) suggest that the Miner's rule can be used to account for the fatigue damage accumulation.

Miner's rule neglects sequence and mean stress effects. The damage of each cycle in a stress history is independent. The study performed by Fisher *et al.* (1998) suggested that the Miner's rule can provide a reasonable estimate of the fatigue damage accumulation in steel bridge structures because of the high residual stresses restraining the plasticity at welded locations. Accordingly, the mean stress will have a small effect on the fatigue life. Based on Miner's rule, the total fatigue damage (D) can be defined as a summation of the fatigue damage caused by each stress range, as shown in Eq. 2.6:

$$D = \sum_{i=1}^{k} \Delta D_i = \sum_{i=1}^{k} \frac{n_i}{N_i} \tag{2.6}$$

where N_i and n_i are the fatigue resistance and a number of cycles of the i^{th} stress range, respectively.

2.2.4. Variable Amplitude Fatigue Behavior

An equivalent stress range is used to relate variable amplitude fatigue behavior to a constant amplitude fatigue behavior. It is often referred to as the effective stress range of a given stress range distribution. The fatigue damage caused by a given number of cycles of the effective stress range is the same as the damage caused by a variable amplitude fatigue loading with an equivalent number of cycles. By means of the effective stress range, a fatigue life of the structure subjected to a variable amplitude fatigue loading can be predicted with the constant amplitude S-N data. Based on Miner's rule, the effective stress range, S_{re}, can be expressed as Eq. 2.7:

$$S_{re} = \left(\sum f_i S_{ri}^m\right)^{\frac{1}{m}} \tag{2.7}$$

where f_i is the frequency of occurrence of the i^{th} stress range (S_{ri}), and m is the slope constant of S-N lines, which is approximately equal to 3.0.

The levels of maximum and effective stress ranges in steel bridges can be one of the three following situations:

Case 1	maximum and effective stress ranges > constant amplitude fatigue limit
Case 2	maximum stress range > constant amplitude fatigue limit, but the effective stress range < constant amplitude fatigue limit
Case 3	maximum and effective stress ranges < constant amplitude fatigue limit

For Case 1, the effective stress range can be used as a representative of a variable amplitude spectrum and applied to a constant amplitude S-N curve to determine a fatigue life. When the maximum stress range, however, is lower than the constant amplitude fatigue limit (Case 3), the fatigue life is infinite. Accordingly, a variable amplitude

fatigue limit can be calculated from a ratio of the effective to maximum stress ranges (ρ_e), as shown in Eq. 2.8:

$$f_{VAFL} = \rho_e \times f_{FL} \tag{2.8}$$

where f_{VAFL} and f_{FL} are the stress levels at the variable and constant amplitude fatigue limits, respectively. The variable amplitude fatigue limit can be changed since it depends on the stress range distribution, while the constant amplitude fatigue limit is a constant parameter for a specific set of specimens. As mentioned earlier, the AASHTO LRFD Bridge Specifications (1998) assume that the ratio of the equivalent to maximum stress ranges (ρ_e) is equal to 0.5.

Bridge structures are often subjected to a stress spectrum that has the effective stress range below the constant amplitude fatigue limit and the maximum stress range above the constant amplitude fatigue limit (Case 2). A review of previous research studies on long-life fatigue loadings is provided below.

2.2.4.1. Fisher *et al*. (1983)

The study was aimed to investigate a fatigue crack growth behavior of steel bridge members under variable amplitude loadings in the fatigue limit region. The fatigue tests were performed on center-crack specimens, cruciform specimens, and eight full-scale welded beams with Category E′ web attachments and Category E or E′ cover plates. The specimens were tested under random block variable amplitude load spectra defined by the Rayleigh distribution with most stress cycles below the constant amplitude fatigue limit. The percentage of cycles exceeding a constant amplitude fatigue limit was varied from 0.10 percent to 11.72 percent.

The study demonstrates that no fatigue crack propagation occurs when none of the stress range cycles exceeds the constant amplitude fatigue limit. The results from the investigation also indicated that the S-N curves developed for details subjected to constant amplitude loading can be used to predict the fatigue life of the details subjected

to variable amplitude loading. The fatigue lives of the web attachment details and cover plate details either equaled or exceeded the ones predicted by simply extending the sloped portion of the S-N curve.

2.2.4.2. Fisher *et al*. (1993)

Fisher *et al*. (1993) performed the long life fatigue tests on eight full-scale girders including three types of welded details: 1) transverse web stiffeners, 2) partial length cover plates, and 3) longitudinal web attachments. The flange thickness and detail geometry of the partial length cover plates and web attachments provide a fatigue category classification of E′. The transverse web stiffeners* can be classified as fatigue category C per AASHTO (1992). (Note that the classification for transverse web stiffeners was changed by AASHTO in 1998 from category C to category C'.) The wide-band Rayleigh-type probability-density curve was used to define a stress range spectrum. The effective stress ranges of the transverse stiffeners, cover plates, and web attachments were varied from 5.59 to 8.83 ksi, 1.66 to 4.09 ksi, and 1.36 to 3.05 ksi, respectively.

The results obtained from web attachment and cover plate details demonstrated that fatigue cracking developed when a maximum stress range of the variable amplitude stress spectrum exceeded the constant amplitude fatigue limit, although the effective stress range of the load spectrum was below the constant amplitude fatigue limit. It was concluded that a straight-line extension of the sloped S-N curve should be used in estimating fatigue life of the web gusset plates. However, for cover-plate details, all stress cycles above 50 percent of the constant amplitude fatigue limit should be counted towards inducing fatigue damage. The tests on transverse stiffener details suggested that fatigue cracks are not likely to develop at these details in an actual bridge unless an out-of-plane distortion develops. The results also showed that an extension of the S-N line underestimated the fatigue life of the transverse stiffener details.

2.2.4.3. Albrecht and Wright (2000)

Albrecht and Wright (2000) performed a series of tests to investigate the long-life fatigue behavior of a typical fatigue detail in steel bridges. Constant-amplitude and variable-amplitude fatigue tests were performed on a transverse stiffener detail. Twenty-nine specimens were tested under constant amplitude loading with various stress ranges between 13 and 42 ksi. Twenty-six specimens were tested under variable amplitude loading with seven levels of equivalent stress ranges and a minimum stress of 2 ksi.

The results of the variable-amplitude fatigue tests showed that when the equivalent stress range decreased, and few cycles had stress ranges exceeding the constant amplitude fatigue limit, the specimens failed at cyclic lives longer than those predicted by an extension of the straight S-N line. This trend was consistent with the study on transverse stiffener welded details performed by Albrecht and Friedland (1979). A numerical model proposed by Albrecht and Friedland was derived in a closed-form equation. A basic concept of the model is that only stress ranges greater than a constant amplitude fatigue limit propagate cracks. Therefore, the fatigue life can be calculated using Eq. 2.9, which was referred in the literature as the equivalent stress range model:

$$N = \frac{10^{b}}{\sum_{i=a}^{k} \gamma_i S_{ri}^{m}} \tag{2.9}$$

where γ_i is the frequency of occurrence of the stress range (S_{ri}), and b and m are the intercept and slope constant of the log-log mean S-N line. The stress range magnitudes from a to k are those greater than the constant amplitude fatigue limit. A simplification model of Eq. 2.9 was developed by utilizing a concept of the fatigue threshold in fracture mechanics and are expressed as Eq. 2.10:

$$N = \frac{10^{b}}{S_{re}^{m} - f_{VAFL}^{m}} \tag{2.10}$$

where S_{re} is the effective stress range of a stress range spectrum, and f_{VAFL} is the variable amplitude fatigue limit determined from Eq. 2.8. A comparison of the fatigue test data obtained in the study and the predicted fatigue lives provided by the equivalent and simplified stress range models is graphically presented in Figure 2.2. The results indicated that the simplified stress range model provided the best predicted mean trend of the data and was easy to use when compared with the equivalent stress range model.

2.3. Fatigue Load Model

The effective stress range is one of the most important parameters in a fatigue evaluation of a structural detail. It can be predicted from several alternatives, including a fatigue truck analysis and strain gage instrumentation. For the first alternative, the effective stress range is calculated from a structural analysis of a suitable bridge model with an applied load given in terms of an equivalent fatigue truck. The accuracy in estimating the effective stress range is obviously dependent on the selected configuration of the fatigue truck. In addition, parameters such as the girder distribution factor and the dynamic load factor are important in the calculation for this alternative. When strain gage data are employed in the evaluation, the stress range spectrum can be obtained by utilizing a cycle counting procedure to decompose the recorded stress history.

2.3.1. Available Fatigue Truck Model

The fatigue truck is typically used to represent truck traffic at a given site with a variety of gross weights and truck configurations. Its configuration should be selected so that the fatigue damage caused by the fatigue truck is the same as the fatigue damage caused by actual truck traffic with an equivalent number of passages. Truck traffic is site-specific and can vary considerably from site to site; therefore, several fatigue truck models have been proposed by researchers to be a representative of the truck traffic observed at the investigated sites.

2.3.1.1. AASHTO Fatigue Truck

The AASHTO Fatigue Guide Specifications (1990) provide a single fatigue truck that can be used for the fatigue evaluation. The AASHTO fatigue truck was developed based on a configuration of the fatigue truck proposed by Schilling and Klippstein (1978). However, instead of using a 50-kip gross weight as proposed for the Schilling fatigue truck, the Guide Specifications (1990) stipulate a 54-kip gross weight of the fatigue truck for a basic evaluation procedure. This gross vehicle weight represents the actual truck traffic spectrum obtained from WIM studies (Synder *et al*., 1985), including more than 27,000 trucks and 30 sites nationwide. Its configuration was approximated based on the axle weight ratios and axle spacings of 4- and 5-axle trucks, which dominated a high percentage of the fatigue damage in typical bridges. The AASHTO fatigue truck has front and rear axle spacings of 14 ft and 30 ft, respectively, with a 6-ft axle width, as shown in Figure 2.3. It should be noted that this fatigue truck is also specified in the AASHTO LRFD Bridge Design Specifications (1998) as a factored live load for the fatigue limit state.

A gross weight of the fatigue truck should be selected so that the fatigue truck causes the same amount of fatigue damage as the actual traffic for a given number of passages. Therefore, when a gross weight distribution at an investigated site is available, an effective gross weight determined from Eq. 2.11 can be used to modify the gross weight of the AASHTO fatigue truck:

$$W = \left(\sum f_i W_i^3\right)^{\frac{1}{3}} \tag{2.11}$$

where f_i is the frequency of occurrence of trucks with a gross vehicle weight of W_i. This effective weight must be distributed to each axle in the same proportion as noted in Figure 2.3. By using this modification, it is anticipated that a more accurate estimate of the fatigue damage accumulation can be obtained for a given site. This effective gross weight was developed based on the concept that a variable amplitude fatigue spectrum is related to a constant stress range by means of an effective stress range and Miner's rule. The effective gross weight is, therefore, analogous to the effective stress range.

2.3.1.2. Laman and Nowak Fatigue Truck Model

Laman and Nowak (1996) developed a fatigue load model based on WIM measurements at five steel bridge structures. The effective gross weights at these structures were in a range of 62.4 to 78.1 kips. A simulation technique was utilized to investigate moment range responses caused by actual traffic flow over analytical simple-beam bridge models. By using the S-N line approach and Miner's rule, it was found that a high percentage of the fatigue damage in the monitored structures was dominated by 10- and 11-axle trucks. In addition, based on simulation results and an analysis of the WIM data, Laman and Nowak (1996) proposed two new fatigue trucks (see Figure 2.4). The 3-axle fatigue truck was suggested to be representative of 2- to 9-axle trucks, while the 4-axle truck was suggested for the 10- and 11-axle trucks. The damage accumulation caused by passages of these fatigue trucks is equivalent to the fatigue damage caused by the corresponding truck spectrum with an equivalent number of passages. It was demonstrated that for the WIM database developed in the study, these two fatigue trucks could provide a relatively accurate estimate of the fatigue damage accumulation over a range of bridge spans.

2.3.2. Girder Distribution Factor

Girder distribution factor (GDF) is defined as the ratio of the load effect in a girder to the total moment or shear force. It can be applied to a one-dimensional-analysis moment to obtain the moment per girder. In bridge structures, vehicle loadings are distributed to a girder by a statistically indeterminate floor system. Therefore, complicated analyses, such as orthotropic plate method, finite element procedure, and Grillage method, are generally used by researchers to obtain the girder distribution factor (Aziz and Alizadeh, 1976; Schilling, 1982; Mabsout *et al*., 1998).

The simplified girder distribution formulas specified in the AASHTO LRFD Specifications (1998) were developed under the study of the NCHRP 12-26, entitled "Distribution of Live Loads on Highway Bridges" (Zokaie, 1992). A database of bridge parameters was built in the study by randomly selecting several hundred bridges from the National Bridge Inventory File (NBIF). A sensitivity study was performed to investigate

considerable importance of each bridge parameter to the live load distribution. The simplified girder distribution formulas were developed for beam-and-slab bridges with steel, prestressed, or T-beam girders, multicell box girder bridges, side-by-side box beam bridges, and solid slab decks with spread box beam bridges.

The axle live load distribution factor of interior beams for one-lane-loaded steel-beam bridges with a concrete deck can be determined from Eq. 2.12:

$$GDF = 0.06 + \left(\frac{S}{14}\right)^{0.4}\left(\frac{S}{L}\right)^{0.3}\left(\frac{K_g}{12Lt_s^3}\right)^{0.1} \tag{2.12}$$

$$K_g = n\left(I_g + Ae^2\right) \tag{2.13}$$

where S is the girder spacing (3.5 ft ≤ S ≤16 ft), L is the span length (20 ft ≤ L ≤ 240 ft), t_s is the deck thickness (4.5 inches ≤ t_s ≤ 12.0 inches), K_g is the girder stiffness, n is the modular ratio of girder material to slab material, I_g is the girder moment of inertia, A is the girder area, and e is the girder eccentricity. Eq. 2.12 is applicable to both simple and continuous beams.

The girder stiffness (K_g) was introduced in order to reduce the number of variables. It was found that the girder distribution factors were not significantly affected by a variation of girder moment of inertia, girder area, and girder eccentricity, while the girder stiffness (K_g) of the bridges was still the same. It should be noted that a multiple presence factor of 1.20 was included in Eq. 2.12 to account for combinations of loaded lanes (AASHTO, 1998). Therefore, the distribution factor obtained from Eq. 2.12 must be divided by this multiple presence factor for fatigue calculation purposes. A reduction factor (f_s) for correcting the effect of skewed supports was also introduced, as shown in Eq. 2.14:

$$f_s = 1 - c_1\left(\tan\theta\right)^{1.5} \tag{2.14}$$

$$c_1 = 0.25\left(\frac{K_g}{12Lt_s^3}\right)^{0.25}\left(\frac{S}{L}\right)^{0.5} \tag{2.15}$$

where c_1 is equal to 0 for skew angles less than 30°, and θ is equal to 60° for skew angles greater than 60°. In addition, it was found that edge girders were more sensitive to truck placement location than other factors. In many cases, a lever rule provided more accurate results than applying a correction factor to the base formulas.

2.3.3. Dynamic Load Factor

Dynamic load is inherent in a bridge response when a vehicle is moving across a structure. It is random in nature and also site-specific. The dynamic response is affected by dynamic characteristics of both bridge and vehicle and by the bridge surface conditions. These parameters interact with each other. Vehicle speed, bridge vibration frequency, weight of vehicles, and vehicle suspension are also important parameters affecting the dynamic response. Vehicles moving across the bridge at a given speed near the bridge natural vibration frequency can cause resonance phenomena.

Many studies have been performed to evaluate the dynamic response of bridges. Several definitions are used to calculate dynamic load factor or impact factor. Only the common definitions are reviewed here. All of these definitions use the static response due to a truck crawling across a bridge (McLean and Marsh, 1998).

Definition 1: Dynamic load factor is defined as a ratio of the maximum instantaneous dynamic response to the maximum static response.

Definition 2: Dynamic load factor can be determined by dividing the dynamic response that occurs at the same location as the maximum static response by the maximum static value.

Definition 3: Dynamic load factor is defined as a ratio of the maximum dynamic response to the static response that occurs simultaneously with the maximum dynamic response.

It should be noted that the maximum dynamic response does not occur at the same time as the maximum static response, nor at the location of the truck. Therefore, for the bridge response shown in Figure 2.5, Definition 3 provides a higher dynamic load factor than Definition 1. Definition 3 is perhaps the most precise of the three given here and was used to interpret many of the Ontario tests (Bakht and Pinjarkar, 1989). However, the first definition appears to be the most rational for design purposes because the maximum bridge response is involved. The AASHTO Specifications (1998) specify the dynamic load as an additional static live load and suggest a 15 percent dynamic load allowance for fatigue and fracture limit states.

The theoretical and experimental studies of dynamic load factor for highway bridges performed by Schilling (1982) have shown that dynamic load factors for individual trucks in actual traffic should be generally less than 0.25. In the studies aimed to determine a peak dynamic load factor for non-fatigue design, a dynamic load factor as high as 1.0 was observed. This high dynamic load factor could be obtained under unusual conditions, such as a bump or pavement irregularity at a critical location. However, the dynamic load factors determined from individual trucks in traffic or from test trucks are generally much lower and should be used in fatigue design and evaluation.

Nassif and Nowak (1995) performed experimental studies on four steel girder bridges to investigate the effects of various parameters, such as truck gross weight, truck speed, truck type, girder static stress, and girder position, on dynamic load factor. A WIM measurement and strain transducers were used in the study. By employing a numerical procedure, dynamic load factors were determined under normal traffic of various load ranges and axle configurations. It was concluded that a dynamic component of stress was practically independent of static component. Accordingly, the dynamic load factor deceased when static stress increased. This is because a ratio of the dynamic increment to the static response is typically determined. Observations indicated that among all types of vehicles, excluding light-weight vehicles, four- and five-axle trucks caused the largest impact values. Large values of the dynamic load factor were observed in an exterior girder. This was because of a relatively small strain in this girder. Therefore, it was

recommended that the dynamic load factor should be obtained from the most loaded interior girders.

2.3.4. Cycle Counting Method

In-service steel bridges are subjected to randomly applied traffic loads. This traffic load induces a primary or static stress and secondary stresses of a structural dynamic response. Therefore, the stress history is generally complex and cannot be applied directly in a fatigue calculation. Consequently, cycle counting methods are employed to decompose this complex stress history. Different cycle-counting strategies are available; however, they can lead to different stress ranges and different counts. As a result, the number of cycles to failure predicted by various counting methods are not similar. ASTM E1049-85 (Standard Practices for Cycle Counting in Fatigue Analysis) provides several counting procedures for a fatigue analysis, such as level-crossing, peak, range-pair, and rainflow cycle counting methods. Only the rainflow counting and racetrack methods are reviewed here.

2.3.4.1. Rainflow Counting Method

The rainflow counting method was proposed by Matsuishi and Endo in 1968 to count the number of cycles of each stress range in a stress history. Based on an extensive series of axial strain controlled fatigue tests, Dowling (1972) demonstrated that the rainflow counting method accurately identified closed hysteresis loops in a variable amplitude histogram. He also concluded that counting methods other than range-pair and rainflow methods resulted in enormous differences in predicted and actual fatigue lives. To apply the rainflow counting method, a stress history has to be oriented vertically with positive time pointing downward. Then, the fall of rain from top of the stress history is used to facilitate the method. The rainflow paths are defined according to the following rules (Committee on Fatigue and Fracture Reliability, 1982):

a) A rainflow path is started at each peak and trough.

b) When a rainflow path that started at a trough comes to the tip of a roof , the flow stops if the opposite trough is more negative than that at the start of the path under consideration. Conversely, a path that started at a peak is stopped by a peak which is more positive than that at the start of the rain path under consideration.

c) If the rain flowing down a roof intercepts flow from previous path the present path is stopped.

d) A path is not started until the path under consideration is stopped.

Figure 2.6 illustrates an example of rainflow counting method. Each segment of the flow path is counted as half cycle.

2.3.4.2. Racetrack Counting Method

The racetrack counting method is originally called the ordered overall range method (Fuchs *et al*., 1973). Its objective is to condense and reveal significant events in a complex reversal history. It is based on an assumption that the highest peak to the lowest valley is the most important feature in the history. The second highest peak to the second lowest valley is the next most important feature in the history. Continuing this manner, all reversals can be counted or counting can be performed until a reversal range is less than a selected value.

A procedure of the racetrack counting method is illustrated in Figure 2.7. The original history of Figure 2.7a is condensed to the history in Figure 2.7c. For this procedure, a racetrack width (s) must be defined first. The track has a similar profile as the original history. Only reversal points at which a racer would have to change from upward to downward or vice versa are counted. It is obvious that the track width determines the number of counted reversals. Applying this method, the original complex history is condensed to a smoother history, and small amplitude ranges causing negligible fatigue damage are discarded.

2.3.5. Equivalent Number of Cycles Per Passage

The concept of an equivalent number of cycles per passage was proposed by Schilling (1984) to represent a complex stress history with a number of cycles of a single stress range. By utilizing the rainflow counting method, the stress history can be decomposed into a primary and one or more higher order stress ranges. The primary stress range is defined as the stress range between the maximum and minimum stresses in the load excursion, while the remaining cycles are higher order stress ranges. Based on Miner's rule, an equivalent number of cycles can be calculated from Eq. 2.16:

$$N_e = 1 + \left(\sum_{i=1}^{k} \frac{S_{ri}}{S_{rp}} \right)^m \tag{2.16}$$

where S_{ri} is the stress range in a complex stress history, S_{rp} is the primary stress range, and m is the slope constant of the S-N curves, which is approximately equal to 3.0. The stress history caused by truck loading is composed of static and dynamic responses. The static response can be calculated from a structural analysis of a bridge structure and accounts for the greatest percentage of the fatigue damage. Meanwhile, the dynamic response tends to increase the magnitude of the stress range and superimposes wiggles to the static cycle. The first effect can be addressed by using a dynamic load factor. Based on the study of actual bridge responses, Schilling (1984) concluded that the additional fatigue damage caused by superimposed dynamic responses was negligible and had a small effect on the equivalent number of cycles.

The equivalent number of cycles per passage of the Schilling fatigue truck (Schilling and Klippstein, 1978) are listed below. It should be noted that the Schilling fatigue truck has a 50-kip gross weight with similar axle weight ratios and axle spacings as the AASHTO fatigue truck.

- Simple-span girders: $N_e = 2.0$ for span < 40 ft and $N_e = 1.0$ for span > 40 ft
- Continuous-span girders near interior support (within a distance equal to

0.1 of the span on each side of the support): $N_e = 2.0$ for span < 40 ft and $N_e = 1.5$ for span > 40 ft

- Continuous-span girders elsewhere: $N_e = 2.0$ for span < 40 ft and $N_e = 1.0$ for span > 40 ft
- Cantilever girders: $N_e = 10$
- Trusses: $N_e = 1.0$
- Transverse members: $N_e = 2.0$ for span < 20 ft and $N_e = 1.0$ for span > 20 ft

The AASHTO Specifications (1990) adopted the concept of an equivalent number of cycles and prescribed the values shown in Table 2.2 for conducting a fatigue evaluation.

2.4. Structural Reliability Theory

Reliability theory provides a rational analysis procedure that can be used to calculate a probability of failure in a structure subjected to various types of loads. The theory affords an opportunity to include a target level of safety and uncertainties about structural properties, load estimation, model imperfections, and human errors into both the design and evaluation process.

The first step involves the definition of the inherent uncertainties. Hence, a probability function of each random variable is formulated based upon critical information. This information can be obtained from extensive studies or it can be based upon an analyst's knowledge and experience. A boundary between safe and unsafe regions can be expressed in a mathematical formulation called a limit state function. In actual applications, the limit state function is normally related to multi random variables; therefore, an exact solution is difficult to obtain. Numerical procedures are used to approximate the probability of failure and solve the limit state function. Some of these numerical procedures are discussed below.

2.4.1. Limit State Function

A limit state is defined as a boundary between desired and undesired performance of a structure. A mathematical formulation of the limit state is well known as a limit state function. The limit state function might include ultimate capacity, serviceability, fatigue or other strength or serviceability related criteria. The ultimate limit states are mostly related to loss of load-carrying capacity. Examples of the criteria for the ultimate limit states are axial, torsional, flexural and shear capacities. The serviceability limit states are mostly related to gradual deterioration, user discomfort, and maintenance costs. They are generally not related to structural integrity. Violating these limit states does not necessarily mean a sudden failure of the structure. Examples of the criteria for the serviceability limit states are deflection, vibration, and local damage. The fatigue limit state is related to loss of strength under repeated loads.

A basic structural reliability problem considers only one load effect (Q) and one resistance (R). If both load effect and resistance are described by known probability density functions, the probability of failure can be stated as follows (Melchers, 1987):

$$P_f = P(R\text{-}Q \le 0) \tag{2.17}$$

$$= P(R/Q \le 1) \tag{2.18}$$

$$= P(\ln R\text{-}\ln Q \le 0) \tag{2.19}$$

Or in general,

$$P_f = P[G(R,Q) \le 0] \tag{2.20}$$

where G(R,Q) is the limit state function defining a safety margin of the structure. When the limit state function is set to be zero, a domain of the model can be divided into two sets, the safe set and the failure set, in which the performance or function of a structure is satisfied and not satisfied, respectively.

In general, R and Q are a function of many variables; therefore, the limit state function can be expressed in terms of many random variables, as shown Eq. 2.21. The probability of failure can be determined from Eq. 2.22:

$$Z = G(x) = G(x_1, x_2, ...x_n) \tag{2.21}$$

$$P_f = \int_{x_1}\int_{x_2}\cdots\int_{x_n} f_{\underline{x}}(x_1, x_2, \ldots, x_n)\,dx_1\,dx_2\ldots dx_n \quad (2.22)$$

where $f_{\underline{x}}(x_1, x_2, \ldots, x_n)$ is the joint probability density function of load and resistance random variables, x_1, x_2, …, and x_n. The above integral is performed over the failure region where $G(x)$ is less than zero. In general, the integration of all random variables in Eq. 2.22 is difficult to obtain. Therefore, analytical approximation and simulation methods are often used to determine the probability of failure. Among these methods are the second moment methods, Rackwitz-Fiessler procedure, and Monte Carlo simulation.

2.4.2. Reliability Index

The reliability index is used to represent a level of structural safety. A probability of failure (P_f) can be defined in terms of the reliability index, as shown in Eq. 2.23. The corresponding probability of survival (P_s) of a structural element or system is defined as Eq. 2.24:

$$P_f = \Phi(-\beta) \quad (2.23)$$

$$P_s = 1 - P_f \quad (2.24)$$

where Φ is the cumulative density function of the standard normal distribution. The relationship between a selected value of the reliability index (β) and a probability of failure (P_f) is shown in Table 2.3.

2.4.3. Second Moment Methods

Second moment methods can be used to simplify the probability density functions. The methods require the knowledge of only two parameters for each random variable, mean and standard deviation. Higher moment parameters, which describe skew

and flatness of distribution, are not considered. The methods are simply used and powerful for solving a wide range of practical problems.

Second moment methods provide exact solutions only when the parameters in a limit state function are all defined by a normal or lognormal distribution. Otherwise, only approximate solutions will be obtained. If the limit state function is linear and both R and Q are statistically independent normally distributed random variables, the reliability index can be determined from Eq. 2.25:

$$\beta = \frac{\mu_R - \mu_Q}{\sqrt{\sigma_R^2 + \sigma_Q^2}} \tag{2.25}$$

where μ_R and σ_R are the mean and standard deviation of the resistance variable R, and μ_Q and σ_Q are the mean and standard deviation of the load variable Q.

Limit state functions are generally not linear. Thus, the limit state functions will not typically be normally distributed, even though all of the random variables may be normally distributed. In this case, the limit state function can be linearized by using a first-order Taylor series expansion. The nonlinear failure surface is approximated by a linear one, as shown in Eq. 2.26, while the mean and variance can be determined from Eq. 2.27 and 2.28 (Madsen *et al.*, 1986):

$$Z \approx G(\mu_1,\mu_2,....,\mu_n) + \sum_{i=1}^{n} (x_i - \mu_i) \left.\frac{\partial G}{\partial x_i}\right|_{x_i=\mu_i} \tag{2.26}$$

$$\mu_Z \approx G(\mu_1,\mu_2,....,\mu_n) \tag{2.27}$$

$$\sigma_Z^2 \approx \sum_{i=1}^{n}\sum_{j=1}^{n} \left.\frac{\partial G}{\partial x_i}\right|_{x_i=\mu_i} \left.\frac{\partial G}{\partial x_j}\right|_{x_j=\mu_j} \mathrm{cov}(x_i, x_j) \tag{2.28}$$

If the random variables are independent, $\mathrm{cov}(x_i,x_j)$ will equal zero. The variance in Eq. 2.28 can be simplified further, as expressed in Eq. 2.29. The reliability index can then be obtained from 2.30:

$$\sigma_Z^2 \approx \sum_{i=1}^{n} \left[\left. \frac{\partial G}{\partial x_i} \right|_{x_i=\mu_i} \right]^2 \mathrm{Var}(x_i) \tag{2.29}$$

$$\beta = \frac{\mu_Z}{\sigma_Z} \quad \text{and} \quad P_f = \Phi(-\beta) \tag{2.30}$$

Because the first-order Taylor series expansion is used in the approximation, the above procedure is so called the first-order second moment method. This method has some drawbacks that should be noted here. The distribution information of random variables is not considered in this method. In addition, the reliability index is not consistent under different formulations of the same limit state function. The lack of invariance problem can be overcome by the Hasofer-Lind transformation (Hasofer and Lind, 1974).

Unlike the first-order second-moment method, the Hasofer-Lind transformation calculates a reliability index based on a geometry of the limit state function. To apply this method, all random variables have to be uncorrelated and normally distributed. However, when the variables are correlated, an intermediate step is required to obtain the uncorrelated random variables. The procedure used to obtain these variables is essentially an eigen-value problem.

To apply the Hasofer-Lind transformation, all variables have to be first transformed to standard normal variables (u_i), by using Eq. 2.31. As a result of this transformation, u_i will have zero mean and standard deviation equal to 1. The limit state function is also be transformed and is given by $g(u_i)$.

$$u_i = \frac{x_i - \mu_i}{\sigma_i} \tag{2.31}$$

The reliability index can be calculated from a minimum distance from the origin of the axes of transformed coordinate system to the limit state surface ($g(u_i) = 0$), as shown in Figure 2.8 and given in Eq. 2.32. The particular point satisfying Eq. 2.32 is called a design point. The reliability index obtained from this definition is invariant

because regardless of the form used for the limit state function, its distance from the origin remains constant.

$$\beta=\min\left(\sum_{i=1}^{n} u_i^2\right)^{1/2} \tag{2.32}$$

From the geometry of surfaces, the reliability index in Eq. 2.32 can be determined from Eq. 2.33 to 2.35. An iterative procedure is required to compute the reliability index and proceeds until a convergent value of the reliability index is obtained.

$$\beta = -\frac{\sum_{i=1}^{n} u_i^* \left(\frac{\partial g}{\partial u_i}\right)\Big|_{\underline{u}^*}}{\sqrt{\sum_{i=1}^{n}\left(\frac{\partial g}{\partial u_i}\right)^2\Big|_{\underline{u}^*}}} \tag{2.33}$$

Where $\underline{u}^*$ is the design point $(u_1^*,u_2^*,...,u_n^*)$.

$$u_i^*=-\alpha_i\beta \tag{2.34}$$

$$\alpha_i=\frac{\left(\frac{\partial g}{\partial u_i}\right)\Big|_{\underline{u}^*}}{\sqrt{\sum_{i=1}^{n}\left(\frac{\partial g}{\partial u_i}\right)^2\Big|_{\underline{u}^*}}} \tag{2.35}$$

2.4.4. Rackwitz - Fiessler Method

Unlike the second-moment methods, the iterative procedure developed by Rackwitz and Fiessler (1978) solves a point of maximum probability on the failure surface or a design point without requiring a solution of the reliability index in each iteration. A value of the design point $\left(x_i^*\right)$ has to be guessed first. Then, all non-normal

variables have to be transformed into equivalent normal variables. The equivalent normal mean $\left(\mu_i^N\right)$ and standard deviation $\left(\sigma_i^N\right)$ of the guessed design point are determined based on the constraints provided in Eq. 2.36 and 2.37:

$$f_x^{/}\left(x_i^*\right) = f_x\left(x_i^*\right) \tag{2.36}$$

$$F_x^{/}\left(x_i^*\right) = F_x\left(x_i^*\right) \tag{2.37}$$

where $f_x^{/}$ and $F_x^{/}$ are the normal probability density function and normal cumulative density function, and f_x and F_x are the probability density function and cumulative density function of variable x_i. The equivalent normal variables can be calculated from Eq. 2.38 and 2.39:

$$\mu_i^N = x_i^* - \sigma_i^N \Phi^{-1}\left[F_{x_i}\left(x_i^*\right)\right] \tag{2.38}$$

$$\sigma_i^N = \frac{\varphi\left\{\Phi^{-1}\left[F_{x_i}\left(x_i^*\right)\right]\right\}}{f_{x_i}\left(x_i^*\right)} \tag{2.39}$$

where μ_i^N and σ_i^N are the equivalent normal distribution parameters, and φ and Φ are the probability and cumulative density functions of the standard normal distribution. These equivalent normal mean and standard deviation values need to be updated in each iteration.

Then, the design point, u_i^*, in the transformed coordinate system can be obtained from Eq. 2.40:

$$u_i^* = \frac{x_i^* - \mu_i^N}{\sigma_i^N} \tag{2.40}$$

The design point of the next iteration, $u^*_{(i+1)}$, can be obtained from Eq. 2.41. This equation is derived from the first-order Taylor series expansion about u^*_i.

$$\underline{u}^*_{(i+1)} = \frac{1}{\left|\nabla G\left(\underline{u}^*_i\right)\right|^2}\left[\left(\nabla G\left(\underline{u}^*_i\right)\right)^T \underline{u}^*_i - G\left(\underline{u}^*_i\right)\right]\nabla G\left(\underline{u}^*_i\right) \tag{2.41}$$

Where

$$\left(\nabla G\left(\underline{u}^*_i\right)\right)^T = \left[\frac{\partial G}{\partial u_1} \quad \frac{\partial G}{\partial u_2} \quad \ldots \quad \frac{\partial G}{\partial u_n}\right]_{\underline{u}^*_i} \tag{2.42}$$

$$\left(u^*_i\right)^T = \left[u_{1(i)} \quad u_{2(i)} \quad \ldots \quad u_{n(i)}\right] \tag{2.43}$$

The iterative procedure is used in this method. The algorithm iterations proceed until the constraints provided in Eq. 2.44 and 2.45 are satisfied:

$$\left|u^*_{(i+1)} - u^*_i\right| \le \delta \tag{2.44}$$

$$\left| \; G\left(u^*_{(i+1)}\right) \; \right| \le \varepsilon \tag{2.45}$$

where δ and ε are the specified tolerance values. A convergence of the Rackwitz-Fiessler method is often slower than the second-moment methods.

2.4.5. Monte Carlo Simulation

Monte Carlo simulation is a powerful tool in solving integration problems when random variables are related through nonlinear equations. It is very useful for evaluating limit states especially when these are implicit functions of the random variables. The Monte Carlo simulation is based on the fact that sampling averages become more stable

as the sample size increases. Therefore, the method involves randomly sampling to simulate artificially a large number of experiments.

The first step of this method is to define a problem in terms of random variables with known distributions. These random variables will then be generated. The corresponding value of safety margin can be determined from the simulation. The procedure will be repeated many times. With a suitable large number of generations, a probability of failure can be approximated by Eq. 2.46 (Melchers, 1987):

$$P_f \approx \frac{n(G \le 0)}{N} \tag{2.46}$$

where $n(G \le 0)$ is a number of trials for which $G \le 0$, and N is a total number of trials. Obviously, the accuracy of the probability of failure (P_f) depends on the number of simulations. Although the Monte Carlo simulation can be employed to solve a complex limit state function, it tends to be expensive when the limit state function is related to a very large number of random variables.

Table 2.1 – AASHTO Detail Constant and Threshold (AASHTO, 1998)

Detail Category	$A \times 10^8$ (ksi^3)	Threshold (ksi)
A	250.0	24.0
B	120.0	16.0
B′	61.0	12.0
C	44.0	10.0
C′	44.0	12.0
D	22.0	7.0
E	11.0	4.5
E′	3.9	2.6

Table 2.2 – Number of Cycles Per Truck Passage (AASHTO, 1990)

Longitudinal Members	Span ≤ 40 ft	40 ft < Span < 80 ft	80 ft ≤ Span
Simple Span Girders	1.8	1	1
Continuous Girders			
1. Near Interior Support	1.5	1	1+(Span-80)/400
2. Elsewhere	1.5	1	1
Cantilever Girders	2		
Trusses	1		
Transverse Members	Spacing ≤ 20 ft	20 ft < Spacing	
	2	1	

Table 2.3 - Relationship between Reliability Index and Probability of Failure for a Normally Distributed Variable

Reliability Index	Probability of Failure
0	0.5
1	0.159
2	0.0228
3	0.00135
4	0.0000317
5	0.000000287
6	0.000000000987

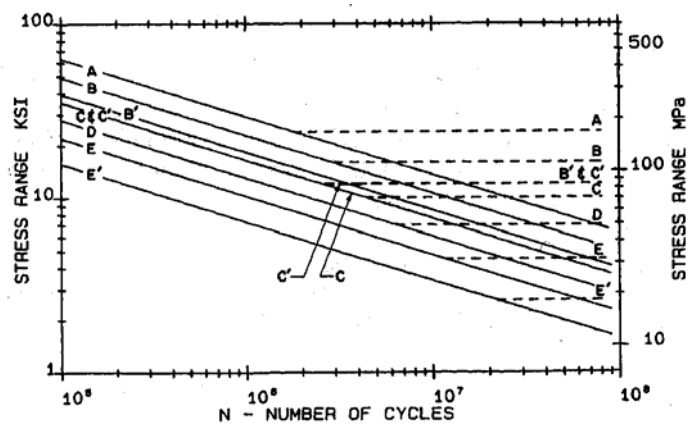

Figure 2.1 – AASHTO S-N Curves (AASHTO, 1998)

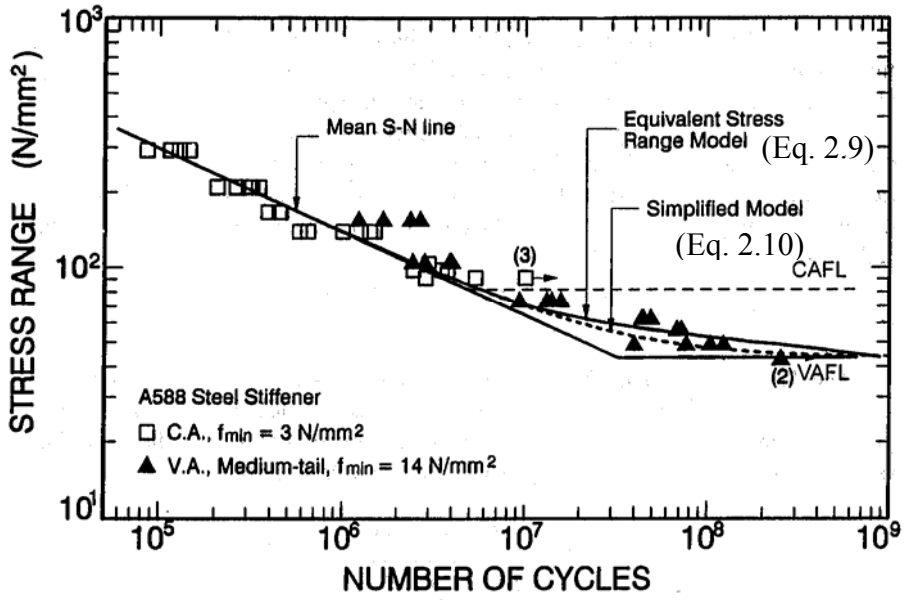

Figure 2.2 – Comparison of Fatigue Test Data and Predicted Fatigue Lives of Equivalent and Simplified Stress Range Models (Albrecht and Wright, 2000)

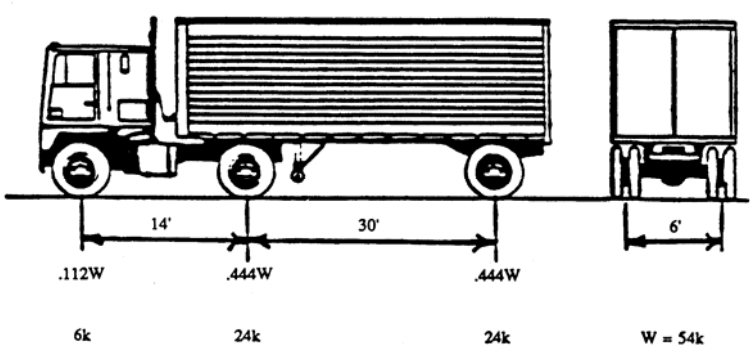

Figure 2.3 – AASHTO Fatigue Truck (AASHTO, 1990)

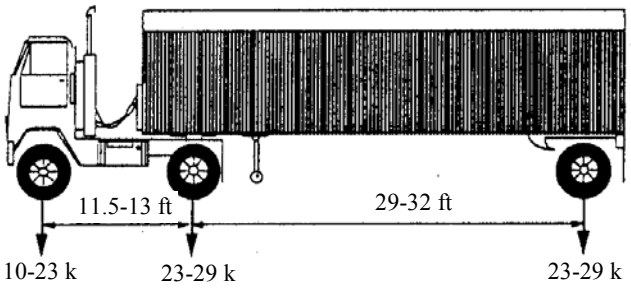

a) Three-Axle Fatigue Truck

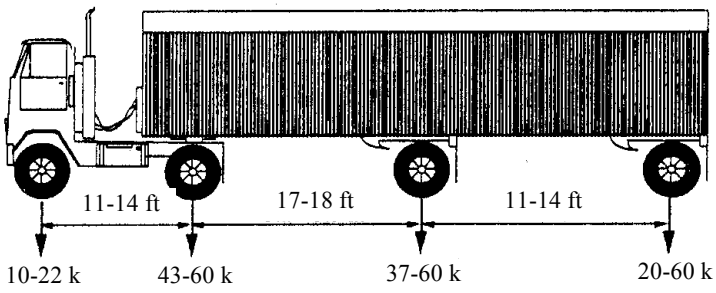

b) Four-Axle Fatigue Truck

Figure 2.4 – Laman and Nowak Fatigue Trucks (1996)

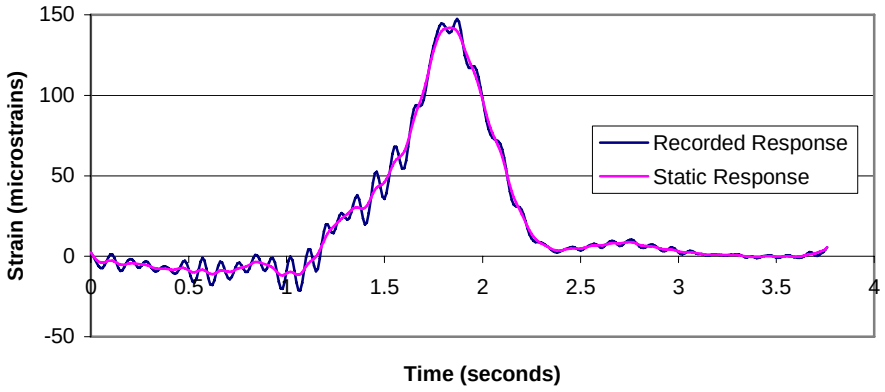

Figure 2.5 – Example of Bridge Response

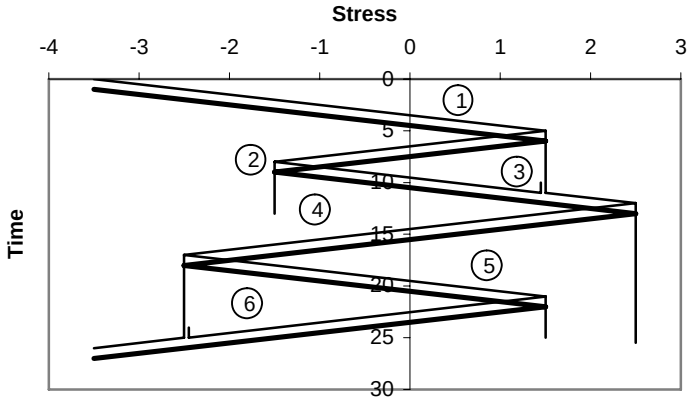

Range Number	Stress Range
1	6
2	3
3	3
4	6
5	4
6	4

Figure 2.6 – Example of Rainflow Counting Method

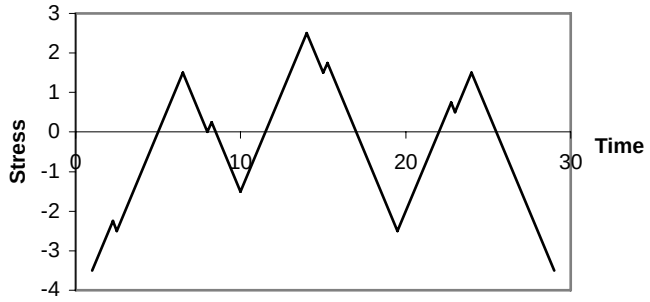

a) Original Stress History

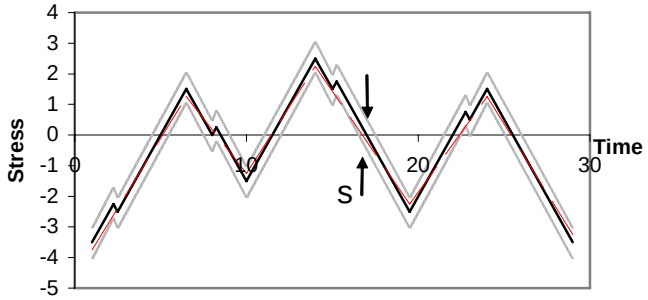

b) Racetrack Counting Method

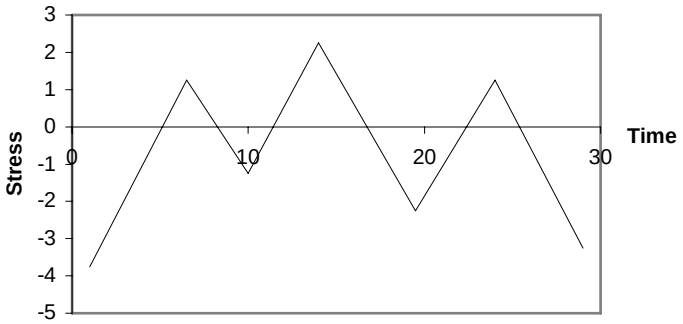

c) Condensed Stress History

Figure 2.7 – Example of Racetrack Counting Method

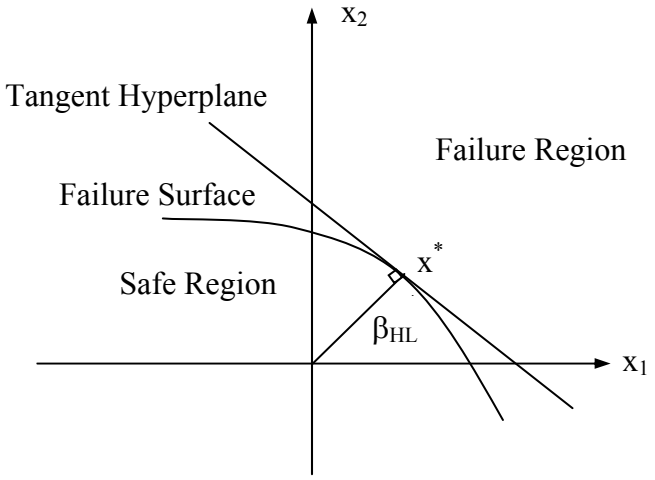

Figure 2.8 – Description of Hasofer-Lind Reliability Index

CHAPTER 3. FATIGUE LOAD MODEL

3.1. Introduction

The loading model is an important parameter in a fatigue evaluation. In general, the effective stress range, which is based on Miner's hypothesis (Miner, 1945), is used to relate the variable amplitude fatigue behavior to a constant amplitude fatigue behavior. The effective stress range can be obtained from a couple of alternatives, namely spectrum analysis using strain gage data or structural analysis using a suitable fatigue truck.

For the first alternative, the effective stress range can be determined from a root-mean-cube (RMC) value of the stress range spectrum obtained by decomposing a complex stress (strain) history with a suitable cycle counting procedure. This alternative tends to provide an accurate estimate of the actual bridge response under routine truck traffic; however, significant time and expense are required to acquire and evaluate the data.

For the fatigue truck analysis, the effective stress range is computed from a structural analysis of a suitable bridge model with an applied load given in terms of an equivalent fatigue truck. An attractive feature of the method is that it can be conveniently used to determine an effective stress range. Accuracy in the estimated effective stress range is, obviously, dependent upon the configuration of the fatigue truck. Ideally, the fatigue truck configuration should be selected so that it will cause the same fatigue damage as actual truck traffic for a given equivalent number of passages.

To incorporate site-specific information into a fatigue life calculation, truck traffic data collected from static weigh station and weigh-in-motion (WIM) measurements are generally used to estimate an effective gross weight of the fatigue truck. However, both static weigh station and WIM measurements are currently available at a limited number of highway sections due to economical reasons. The installation cost of a permanent

WIM site can range from $50,000 to $120,000, depending upon the type of equipment, number of lanes, and other factors (Najafi and Blackadar, 1998). Therefore, the possibility of using commonly recorded information at particular sites, such as traffic count data, is of particular interest. By employing the WIM data collected at several sites in Indiana and the traffic database software (VTRIS), a biased value and the amount of uncertainty inherent with use of traffic count data can be determined. These parameters will serve as crucial information in developing a fatigue reliability model.

In addition, the accuracy of current available fatigue truck models in estimating fatigue damage accumulation was examined in this study. Weigh-in-motion (WIM) data collected from three sites in Indiana were investigated and used as applied loads on analytical bridge models. Fatigue damage accumulations were computed based on using Miner's hypothesis for the truck traffic profile constructed using the WIM data. These damage accumulations were then compared with the fatigue damage predicted by the current available fatigue trucks and used as a basis in developing a new design of the fatigue trucks.

3.2. Vehicle Database

Weigh-in-motion (WIM) sensors have been extensively used in recent years by highway and bridge engineers to monitor truck traffic. A WIM system can be used to measure vehicle gross weights, axle weights, and axle spacings of the actual truck traffic. Typically, the WIM sensor, such as a load cell or a piezoelectric strip, is installed directly in the roadway and is relatively unobtrusive. Consequently, an advantage of the technology is that it can be operated without being detected by roadway users. As a result, in contrast to static weigh stations that tend to be avoided by heavy trucks, unbiased truck traffic data can be obtained.

The WIM data recorded at nine sites in Indiana were included in a vehicle database in the study. A view of the WIM for one site is shown in Figure 3.1. The WIM sites were selected such that they were not located on a same highway section, which might have a similar truck population. Consequently, actual statistics of traffic count data in estimating the effective gross weight can be obtained.

The assigned nomenclature, location, and recording period of each WIM site are provided in Table 3.1. Figure 3.2 provides an overview of the WIM site locations. The WIM database included four different sites on three interstate highways, three different U.S. highways, and two different state routes. The WIM data, except at Station 001, were collected by another researcher, Andrew Nichols. The truck traffic was recorded in both traffic directions at each WIM site. Stations 400 and 401 were located at the same location on I-80 but on opposite traffic directions. A substantial number of trucks had been observed in both traffic directions at this site; therefore, two separate WIM data files and nomenclatures were assigned for these stations.

Highway functional classification is used in highway planning and design to group highways into classes or systems according to their provided characters of traffic service. The two main characters of service are the degree of land access and travel mobility. All streets and highways can be categorized into one of three classifications: arterial, collector, and local roads, depending on characters of their service. Among these three classifications, arterials provide the highest mobility level and the greatest access control. The geometric design of an individual highway, including design speed, roadway width, roadside safety elements, and other design values, must be selected regarding to its functional classification (Indiana Design Manual, 1994). The functional classifications of all WIM sites included in this study are shown in Table 3.1. They can be grouped into either principal arterial interstate or other principal arterial. These two functional classifications are a subdivision of the arterial. The principal arterial interstate provides higher mobility and greater access control than the other principal arterial routes.

Statistics of all recorded trucks, including average daily truck traffic (ADTT), mean gross weight, standard deviation, maximum gross weight, and effective gross weight in both traffic directions are summarized in Table 3.2. ADTT was computed by dividing a total number of trucks with recording period in days. Although no seasonal factors were applied, the estimated ADTT of five sites in the vehicle database with one-year recording period in 2002 can be referred as the average annual daily truck traffic (AADTT). The ADTT at the other sites however are not equal to the AADTT because of the variation in a number of trucks that can occur throughout the year. In addition,

minimum and maximum effective gross weights of the WIM database were found to be 31.7 kips at Station 640 and 75.3 kips at Station 001, respectively. The results indicate that the effective gross weight is site-specific and can be dramatically different from a 54-kip gross weight of the AASHTO fatigue truck.

The gross weight histograms in both traffic directions at each site are shown in Figures 3.3 to 3.11. All Class-4-to-Class-13 trucks are included in these figures. A description of the FHWA truck classification is provided in Appendix A. The histograms indicate that the gross vehicle weight varies significantly from site to site and the maximum gross weight was observed to be as high as 200 kips; however, most of the truck population have gross weights less than 80 kips.

A percentage of each truck type classified per FHWA is shown in Table 3.3. Class-5 and Class-9 trucks governed the highest percentages of the truck population at all stations. Only Station 001 had a high percentage of Class-13 trucks, which correspond to 7-or-more axle multi-trailer trucks.

Statistics of the gross weight of each truck type are summarized in Table 3.4. The results demonstrate that the mean gross weight of a certain truck type can be significantly different from site to site. For example, the highest and lowest mean gross weights of Class-9 trucks were found to be 73.5 kips at Station 120 and 41.0 kips at Station 640, respectively. The main factor causing this variation is the percentages of loaded and unloaded trucks at a specific site.

In addition to the WIM database, the Vehicle Travel Information System (VTRIS) software was also included in the vehicle database. The VTRIS software was developed by Signal Corporation and the FHWA Office of Highway Policy Information (HPPI). It is available to all public through the FHWA website (http://apps.fhwa.dot.gov/vtris). The VTRIS system maintains a permanent database of station descriptions, vehicle classifications, and gross weights of many truck weight sites in several states. The software allows users to generate truck statistics, such as average daily count, truck distribution, and average gross weight of truck as classified by the FHWA.

The average gross weights of each truck type collected in Indiana in 1999 for several different highway functional classifications are summarized in Table 3.5. Truck

traffic statistics corresponding to the period that the WIM data were collected (2001 to 2002) are not available in the VTRIS software. It is assumed in the study that there is no substantial difference in truck traffic characteristics between 1999 and 2002.

3.3. Statistics of Using Traffic Count

The statistics related to use of traffic count data for estimating an effective gross weight were determined based on the WIM database and the VTRIS software. A number of trucks grouped by the FHWA truck classification and an average gross weight of each truck type are assumed to be employed when traffic count data are utilized in the evaluation. This is because the traffic data are generally provided in terms of vehicle types. The intention is to use the traffic count data when actual gross vehicle weight histograms are not available at the investigated sites. Based upon the described assumptions, an effective gross weight can be determined from Eq. 3.1:

$$W = \left(\sum f_{ci} W_{ci}^{3}\right)^{\frac{1}{3}} \tag{3.1}$$

where f_{ci} is the frequency of occurrence of Class-i trucks, and W_{ci} is the average gross weight of Class-i trucks.

There are several alternatives that can be used to estimate the effective gross weight based on traffic count data and average gross weights of the WIM database and the VTRIS software. However, only four different combinations were considered in the study:

- Combination 1: Use both frequencies of occurrence and average gross weights obtained from the WIM database.
- Combination 2: Use frequencies of occurrence obtained from the WIM database and average gross weights corresponding to highway functional classification provided in the VTRIS software.

- Combination 3: Use frequencies of occurrence obtained from the WIM database and VTRIS statewide average gross weights.
- Combination 4: Use frequencies of occurrence corresponding to highway functional classification provided in the VTRIS software and VTRIS statewide average gross weights.

The estimated effective gross weights provided by each combination in both traffic directions at all sites were determined. A biased value or a ratio of the actual effective gross weight (Table 3.2) and the estimated effective gross weight was then computed and is graphically presented in Figure 3.12. The results indicate that actual effective gross weights tend to be underestimated at all sites and can be significantly underestimated when frequencies of occurrence corresponding to highway function classification and statewide average gross weights are used in the calculation (Combination 4). On the other hand, use of traffic count data provides estimated effective gross weights relatively close to the actual values and has a small degree of uncertainty when both traffic count data and average gross weights of the investigated sites are employed in the calculation (Combination 1).

Mean biased value, standard deviation, and coefficient of variation for each combination are presented in Table 3.6. Comparison of the results obtained from Combinations 3 and 4 shows that use of the truck distribution corresponding to the highway functional classification (Combination 4) can introduce a significant amount of uncertainty into the traffic count procedure. Moreover, both biased values and coefficients of variation of Combinations 2 and 3 are not statistically different, although additional information regarding to the highway functional classification is employed in Combination 2. Therefore, the statewide average gross weights are suggested to be used when average gross weights at an investigated site or other sites with similar truck traffic characteristics are not available. However, it cannot be concluded at this point that highway functional classification has no relation with truck gross weights due to a limited number of sites.

The analysis results of the WIM database and the VTRIS software have shown promise in using traffic count data as another alternative procedure in a fatigue evaluation. Use of traffic count data provides an estimate relatively close to an actual effective gross weight when the frequency of occurrence and average gross weight of each truck classification at an investigated site or other sites with similar traffic characteristics are utilized in the calculation (Combination 1). It has been found that a mean biased value and a coefficient of variation corresponding to this procedure are equal to 1.10 and 5 percent. However, when average gross weights are not available at an investigated site or other similar highways, the statewide average gross weights can be employed with a mean biased value of 1.21 and a coefficient of variation of 15 percent (Combination 3).

3.4. Proposed Fatigue Truck Model

A sample of the WIM data collected at three sites in Indiana was used to examine the accuracy of current available fatigue truck models for estimating fatigue damage accumulation. The WIM data were simulated over analytical bridge models, including simple and two-equally continuous spans. Fatigue damage accumulations were computed using Miner's hypothesis and compared with the fatigue damage predicted by current available fatigue truck models. In addition, based on the simulation results, a new fatigue truck model was developed.

3.4.1. WIM Database

The WIM data collected at three sites in Indiana were selected from the vehicle database (Section 3.2). These three sites were used to represent a variety of truck traffic characteristics that practicing engineers might encounter when performing a fatigue evaluation. Statistics of the WIM data were examined to evaluate the truck traffic characteristics at these sites. The number of axles was used to classify trucks and was considered to be an appropriate criterion in evaluating fatigue truck configurations

The first WIM site, which will be referred to as Station 001, is located on U.S. 20 along the extra heavy duty corridor in northwest Indiana. The corridor provides an important route for steel producers and other manufacturers to transport cargos between northwest Indiana and the state of Michigan. An overview of the highways designated as part of the extra heavy duty corridor is presented in Figure 3.13. The corridor is composed of segments of roads totaling 94 miles. With a special permit, the legal weight limit of trucks passing on this route is 134 kips, which is much heavier than the legal limit of 80 kips for typical interstate and state highways (Reisert, 2003). A common truck type traveling along this route is a multi-trailer, multi-axle vehicle generally referred to as "Michigan Train" trucks. Two configurations of "Michigan Train" trucks used in Indiana are Michigan Train Truck Numbers 5 and 8 (Figures 3.14 and 3.15).

The eastbound truck traffic data collected at Station 001 in January 2002 included a sample of 22,992 trucks. A percentage distribution of trucks classified by the number of axles is provided in Table 3.7. It was found that approximately 45 percent of the truck traffic was 5-axle trucks, while 8- to 11-axle trucks accounted for 14 percent of the total truck traffic. A gross weight distribution of the truck traffic recorded at this station is shown in Figure 3.16. The maximum gross weight was found to be as high as 216 kips. The statistics of average gross weight, axle weight, and axle spacing of each truck type are summarized in Tables 3.8 and 3.9. The statistics revealed that although average gross weights of 7- to 11-axle trucks were considerably heavier than the other trucks with fewer axles, the average axle weights of these trucks were not significantly different from the average axle weights of the others and still in a range of 10 to 15 kips.

The second WIM site, referred to as Station 410, is located on I-65 in northwestern Indiana. The four-day southbound truck traffic data collected in August 2002 included a sample of 21,856 trucks. The gross weight distribution is graphically presented in Figure 3.16. A maximum gross weight of 102.3 kips was observed. The majority of truck traffic at this site are 5-axle trucks, with approximately 84 percent of the total truck population. The statistics of average gross weight, axle weight, and spacing of each truck type are provided in Tables 3.10 and 3.11. The average gross weights of both 7-axle and 8-axle trucks at this station were found to be 46.2 and 68.1 kips. These

average gross weights were considerably less than the average gross weights of the same trucks of 101.7 and 108.3 kips at Station 001. As mentioned earlier, the AASHTO fatigue truck was calibrated to represent the fatigue damage caused by 5-axle trucks. Therefore, comparing a configuration of the AASHTO fatigue truck with actual 5-axle trucks would provide intuitive information. An average first axle weight of the 5-axle trucks at this station was found to be 26 percent of the average gross weight. This percentage is relatively high compared with a first axle weight-to-gross weight ratio of 11 percent for the AASHTO fatigue truck (see Figure 2.3). In addition, an average total length of the 5-axle trucks was equal to 52.9 ft, which is much longer than the 44-ft length for the AASHTO fatigue truck.

The third WIM site, referred to as Station 520, is located on U.S. 50 in southeastern Indiana. The eastbound truck traffic data collected in May 2002 included a sample of 16,696 trucks. Figure 3.16 shows the gross weight distribution of the recorded truck traffic. The maximum recorded gross weight was found to be 160.3 kips. The highest percentage of truck traffic at this station was dominated by 2-axle trucks, approximately 47 percent of the total truck traffic (see Table 3.7). Moreover, only 0.25 percent of the truck traffic had more than 5 axles. Tables 3.12 and 3.13 provide the statistics of gross weight, axle weight, and axle spacing of each truck type at Station 520. The statistics indicated that an average of the first axle weight-to-gross weight ratios of 5 axle trucks was approximately equal to 20 percent. Similar to Station 410, this percentage is relatively high compared with the configuration given for the AASHTO fatigue truck (see Figure 2.3). The average axle spacings of the 5-axle trucks at this station are approximately equal to the configuration of the same trucks observed at Station 410.

3.4.2. Analysis Results of WIM Database

Damage accumulation models are used to relate fatigue performance under variable amplitude fatigue loadings to well known constant amplitude fatigue data. Among the available damage models, the Palmgren-Miner's hypothesis is widely applied in bridge applications due to its simplicity and capability to provide a reasonable estimate of the fatigue damage for details typically used in bridge structures (Fisher *et al*., 1998).

Because the damage accumulation is linear, the total fatigue damage is simply the summation of the damage caused by each cycle.

The stress history in bridge girders for each truck passage is complex due to the composition of static and dynamic responses. By utilizing a rainflow counting method the stress history can be decomposed into primary and higher order stress ranges. The primary stress range is the maximum stress range in the stress history while the remaining reversals are the higher order stress ranges. Based on Miner's rule, Schilling (1984) demonstrated that the fatigue damage accumulation of the complex stress cycles caused by an individual truck passage can be represented by the fatigue damage of the primary or maximum stress range with an equivalent number of cycles (N_e) determined from:

$$N_e = 1 + \left(\frac{S_{r1}}{S_{rp}}\right)^m + \left(\frac{S_{r2}}{S_{rp}}\right)^m \ldots + \left(\frac{S_{ri}}{S_{rp}}\right)^m \tag{3.2}$$

where m is the slope constant of the S-N line, S_{rp} is the maximum stress range, and S_{ri} is the higher order stress range. The slope constant (m) is approximately equal to 3 for all AASHTO fatigue category details (Keating and Fisher, 1986).

Although Eq. 3.2 is expressed in terms of stress ranges, it can also be calculated from moment ranges for linear elastic behavior based on the assumption that they are proportional. By using the concept of an equivalent number of cycles and Miner's rule, the fatigue damage accumulation caused by each truck passage can be written as:

$$D = \sum \frac{1}{N_i} = \sum \frac{S_{ri}^3}{10^b} = \frac{N_e S_{rp}^3}{10^b} \tag{3.3}$$

where N_i is the fatigue strength (cycles) corresponding to each stress range in a stress history, and b is the intercept of S-N line for the detail being evaluated.

A computer program was developed to simulate the actual truck traffic flow over analytical bridge models, including a simple span and a two-span structure with equal span lengths. The simulated bridge spans ranged from 30 ft to 120 ft with a 10-foot

increment. The WIM database developed for the three bridge sites was used for the input loading. Static moment ranges were monitored at the middle span of the simple beam, the middle support of the continuous beam, and the middle span of the continuous beam. The moment cycles caused by each truck passage were decomposed using a rainflow counting method. The maximum moment range and equivalent number of cycles for each truck passage were then determined. This procedure was applied to all trucks in the WIM database.

A sample of selected simulation results is provided in Tables 3.14 to 3.16. The maximum moment range, effective moment range, and cumulative probability at twice of the value of the effective moment range in 30-, 60-, and 120-ft bridge spans are included in the tables. The maximum moment range is the single greatest moment difference caused by the trucks within the loading spectrum, while the effective moment range is the effective weighted moment difference caused by the truck load spectrum. The latter value is given by:

$$M_{re} = \left(\sum f_i Mr_i^3\right)^{\frac{1}{3}} \tag{3.4}$$

where f_i is the frequency of trucks within a particular moment range, Mr_i. The results indicate that among the recorded truck traffic data, Station 001 had the highest effective moment ranges in all spans, followed by Stations 520 and 410, respectively. This is consistent with the order of the effective gross weights observed at these three stations.

The effective moment range was found to be approximately 2 to 3 times less than the maximum moment range, depending on a shape of the moment range distribution. Cumulative distributions of moment range in a 60-ft span are graphically presented in Figure 3.17. The cumulative probabilities for other span lengths were found to have a trend similar to that depicted in Figure 3.17. The cumulative probabilities for both simple and continuous beams tend to approach 100 percent as the moment ranges exceed 60 percent of the maximum moment ranges. The cumulative probabilities at twice of the effective moment ranges were found to be in a range of 98.4 and 99.9 percent. This indicates that moment ranges above this level are associated with the tail region of the

distributions. Therefore, the assumption used in the AASHTO LRFD Specifications (1998) that the peak stress range can be assumed to be a stress level at twice of the effective stress range seems to be appropriate when field-measured data are not available.

An average of the equivalent numbers of cycles per passage of all trucks is graphically presented in Figure 3.18 for the three sites. It is evident that the average number of cycles per truck passage at the middle span of the simple beam and the continuous beam approaches one when the span length exceeds 50 ft. However, the average number of cycles at the middle support of continuous beams increases in spans above 40 ft. The results also indicate that Station 520 had a higher average number of cycles per passage at the middle support of the continuous beam than Station 410. This is because Station 520 had a high percentage of 2- and 3-axle trucks, which tends to cause a higher equivalent number of cycles in long spans than trucks with a greater number of axles. On the other hand, Station 410 had a somewhat higher average number of cycles at midspan of the simple beam and the continuous beam than Station 520. The primary reason for the difference is that 5-axle trucks, the majority truck type at Station 410, tend to cause a greater number of cycles than 2- and 3-axle trucks at the middle span of short beam members.

By employing Eq. 3.3, the percent fatigue damage accumulation caused by each truck type was computed. Figure 3.19 graphically presents the percent fatigue damage caused by 2- and 3-axle, 4- and 5-axle, and 8- to 11-axle trucks at midspan of a simple beam member. The results indicate that the summation of the fatigue damage caused by 4- and 5-axle, and 8- to 11-axle trucks contributed to more than 86 percent of the total damage accumulation at Station 001. Moreover, the 8- to 11-axle trucks caused more than 50 percent of the total fatigue damage at the middle span of simple beam in spans above 50 ft. This percentage was relatively high given that a total number of these trucks was only 14 percent of the truck traffic. In long bridge spans, the fatigue damage caused by 8- to 11-axle trucks tends to overcome the damage caused by 4- and 5-axle trucks. This is because the heavy loaded 8- to 11-axle trucks cause considerably higher moments than the 4- and 5-axle trucks in long spans.

At Station 410, 4- and 5- axle trucks contributed to more than 95 percent of the total fatigue damage. A majority of the fatigue damage was also dominated by 4- and 5-axle trucks at Station 520. They accounted for roughly 70 percent of the total fatigue damage, while 2- and 3-axle trucks caused approximately 30 percent of the fatigue damage at this station. The percent fatigue damage of the multiple axle trucks at the middle support and middle span of continuous beam members are shown in Figures 3.20 and 3.21 and were found to have a similar trend as depicted in Figure 3.19 for simple beam members.

3.4.3. Evaluation of Various Fatigue Trucks

Fatigue damage accumulations obtained from the simulation of the truck database were compared with the fatigue damage predicted by the 54-kip AASHTO fatigue truck, the modified AASHTO fatigue truck, and the Laman fatigue trucks. The effective gross vehicle weights computed from the WIM data were used for the gross weight of the modified AASHTO fatigue truck. To compare the fatigue damage accumulation caused by actual truck traffic and the various fatigue trucks, a damage ratio is introduced as follows:

$$\text{Damage Ratio} = \frac{D_{actual}}{D_{truck}} = \left(\frac{\sum N_{ei} S_{rpi}^3}{NC \times N_t \times S_{FT}^3} \right) = \left(\frac{\sum N_{ei} M_{rpi}^3}{NC \times N_t \times Mr^3} \right) \tag{3.5}$$

where S_{rpi} is the primary or maximum stress range of truck i, S_{FT} is the stress range of the fatigue truck, M_{rpi} is the primary or maximum moment range of truck i, Mr is the moment range of the fatigue truck, N_{ei} is an equivalent number of cycles per passage of truck i, NC is an equivalent number of cycles per passage of the fatigue truck, and N_t is the total number of fatigue truck passages. The damage ratio is used in the comparison because it does not require information on the fatigue detail or category classification; the detail expression is in the denominator of both damage terms and cancels out accordingly.

By simulating the fatigue trucks over analytical bridge models, effective moment ranges and an equivalent number of cycles per passage of these fatigue trucks were determined. The damage ratio for each fatigue truck model was then computed. It should be noted that Laman and Nowak (1996) provide a range of axle weights and axle spacings for the fatigue trucks (see Figure 2.4). Therefore, to obtain a configuration of the Laman fatigue trucks for each station, an iterative procedure was utilized. Each range of the axle weights and axle spacings was divided into more than 10 increments. During each iteration, one of the axle weights and axle spacings of the Laman fatigue trucks was modified within the range provided in Figure 2.4. The procedure continued until a minimum sum of squared error of the fatigue damage over a range of bridge spans was obtained.

Figure 3.22 shows the damage ratios computed for the loading spectrum gathered for each of the three stations when compared with the 54-kip fatigue truck and modified AASHTO fatigue truck. The moment ranges obtained from simulation and the number of cycles per passage as provided in the AASHTO Fatigue Guide Specifications (1990) were used in the calculation. The results indicate that the modified AASHTO fatigue truck provides a notably better estimate of the fatigue damage accumulation than the original 54-kip AASHTO fatigue truck at all three stations (i.e., values closer to unity). The fatigue damage predicted by the 54-kip AASHTO fatigue truck is significantly underestimated at Station 001 and overestimated at Station 410.

It can also be observed in Figure 3.22 that the modified AASHTO fatigue truck does not provide an accurate estimate of the fatigue damage accumulation over the full range of the bridge spans investigated. The fatigue damage was significantly overestimated in both simple and continuous beams with short span lengths at all stations. It also should be noted that the AASHTO Fatigue Guide Specifications (1990) provide a number of cycles per passage in the form of step functions for both simple and continuous beams with short span lengths. When the actual number of cycles per passage of the modified AASHTO fatigue truck was used in the comparison, damage ratios of approximately 0.35, 0.47, and 0.57 were obtained in simple and continuous beams with a 30-ft span length at Stations 001, 410, and 520, respectively.

A comparison of the fatigue damage caused by the actual truck traffic and the Laman fatigue trucks are shown in Figure 3.23. The moment ranges and equivalent numbers of cycles per passage of the Laman fatigue trucks obtained from simulation were used in this figure. The results indicate that the Laman fatigue trucks provide a reasonable estimate of the fatigue damage accumulation at Station 001. The fatigue damage at Stations 001 and 520 is slightly overestimated in spans shorter than 60 ft and slightly underestimated at the middle support of continuous beam in 60- to 100-ft spans. The Laman fatigue trucks, however, overestimate fatigue damage in all span ranges at Station 410 because the effective gross weight at this station is significantly less than a minimum gross weight of the truck configurations provided in Figure 2.4.

3.4.4. Proposed Fatigue Truck

A new fatigue truck design was developed by utilizing an iterative procedure. During the iteration, both the axle weight ratios and the axle spacings of the fatigue truck were modified. The effective gross weights obtained from the WIM database were assigned for a gross weight of the fatigue trucks. Maximum moment ranges, equivalent number of cycles per passage, and damage ratios for a given truck configuration were determined for the variables used during each iteration. Then, one of the axle weight ratios or axle spacings was changed at a time. The adjustment was performed until a minimum sum of the squared error of the fatigue damage accumulation over a range of bridge spans was obtained.

The iterative procedure was first used to find a configuration of the 3-axle fatigue truck best representing truck traffic at Station 001. It was found, however, that a single 3-axle fatigue truck cannot provide an accurate estimate of the fatigue damage over a range of the bridge spans at this station. The fatigue damage tended to be significantly overestimated in short span girders. Consequently, the iterative procedure was then applied to find the best configuration of a 4-axle fatigue truck at this station, since it was expected that the addition of an axle to the original 3-axle fatigue truck would more accurately estimate the fatigue damage caused by 8- to 11-axle trucks. The configuration of the optimal 4-axle fatigue truck produced by the iterative procedure is shown in Figure

3.24b. Axle weights are shown as a function of the fatigue truck gross weight (W) in this figure.

A comparison of the actual fatigue damage accumulation at Station 001 and the 4-axle fatigue truck is depicted graphically in Figure 3.25. Clearly, the new 4-axle fatigue truck can provide a relatively accurate estimate of the fatigue damage accumulation over a wide range of bridge spans in both simple and continuous beams.

Based on an analysis of the fatigue damage at Stations 410 and 520, it was found that most of the fatigue damage at these stations was dominated by 2- to 5-axle trucks, which can be reasonably represented by a 3-axle fatigue truck. Therefore, a new design of the 3-axle fatigue truck was developed to be representative of the truck traffic at these stations. Its configuration was adjusted until a minimum sum of the squared error of the damage accumulation at Stations 410 and 520 was obtained. A configuration of the new 3-axle fatigue truck is shown in Figure 3.24a. Front and rear axle spacings of the new 3-axle fatigue truck are wider than the AASHTO fatigue truck. In addition, a higher percentage of the gross weight is distributed to the front axle, compared with a ratio of a 6-kip front axle weight to a 54-kip gross weight of the AASHTO fatigue truck. These adjustments are consistent with statistics of the axle configurations of truck traffic observed in the WIM database. Average front axle weight-to-gross weight ratios of 5-axle trucks, a truck type dominating the highest percentage of the fatigue damage at Stations 410 and 520, were found to be 26 percent and 21 percent, respectively, while average total lengths of 5-axle trucks at these stations were equal to 53 ft and 58 ft.

Damage ratios of the actual truck traffic at all three stations and the new 3-axle fatigue truck are shown in Figure 3.26. The results indicate that the 3-axle fatigue truck accurately estimates the fatigue damage accumulation at Stations 410 and 520. The fatigue damage at midspan of the simple beam and the continuous beam at Station 410 is slightly overestimated by the new 3-axle fatigue truck in spans below 60 ft. For truck traffic at Station 001, however, the 3-axle truck does not provide a particularly accurate prediction of the fatigue damage for the full range of spans and tends to significantly overestimate the fatigue damage at midspan of the simple beam and the continuous beam for span lengths shorter than 50 ft.

By comparing the analysis results shown in Figures 3.22, 3.23, 3.25, and 3.26, it can be seen that an accurate estimate of the fatigue damage accumulation can be obtained over a wide range of bridge spans from a new design of the 3-axle and 4-axle fatigue trucks. The new 4-axle fatigue truck was most effective when a significant number of 8- to 11-axle trucks pass over the bridge, while the new 3-axle fatigue truck was most effective otherwise. Additionally, with the constant axle spacings and axle weight ratios assigned for the new trucks, the fatigue damage accumulation caused by truck traffic loadings can be conveniently determined. The site-specific information, such as an effective gross weight, can be incorporated into the fatigue load model by using the axle weight ratios provided in Figure 3.24.

3.4.5. Number of Loading Cycles

An equivalent number of cycles per passage for the 3- and 4-axle fatigue trucks was determined for bridge spans ranging from 30 ft to 120 ft, with a 2.5-ft increment. The results are presented graphically in Figure 3.27. The curve trends for the number of cycles per passage at midspan of the simple beam and the continuous beam are similar for both 3-axle and 4-axle fatigue trucks. They approach unity for span lengths greater than 40 ft. The number of cycles per passage at the middle support of continuous beams for both 3- and 4-axle trucks increase to a value greater than unity for span lengths greater than 80 ft.

A linear regression analysis of the number of cycles per passage was conducted using the least squares method. The best fit linear regression lines are shown in Figure 3.27 along with the number of cycles per passage provided in the AAHTO Fatigue Guide Specifications (1990). The parameters obtained from the linear regression analysis are summarized in the following:

For the new 3-axle fatigue truck:

<u>At midspan of a simple beam</u>

$$NC = 1 + \frac{(50 - L)}{37} \qquad \text{when } 30 \text{ ft} \le \text{span length (L)} < 50 \text{ ft}$$

$$NC = 1 \qquad \text{when span length (L)} \ge 50 \text{ ft}$$

At the middle support of two-equally continuous spans

$$NC = 1 + \frac{(40 - L)}{32} \qquad \text{when } 30 \text{ ft} \le \text{span length (L)} < 40 \text{ ft}$$

$$NC = 1 \qquad \text{when } 40 \text{ ft} \le \text{span length (L)} < 80 \text{ ft}$$

$$NC = 1 + \frac{(L - 80)}{415} \qquad \text{when } 80 \text{ ft} \le \text{span length (L)} < 120 \text{ ft}$$

At midspan of two-equally continuous spans

$$NC = 1 + \frac{(40 - L)}{27} \qquad \text{when } 30 \text{ ft} \le \text{span length (L)} < 40 \text{ ft}$$

$$NC = 1 \qquad \text{when span length (L)} \ge 40 \text{ ft}$$

For the new 4-axle fatigue truck:

At midspan of a simple beam

$$NC = 1 + \frac{(40 - L)}{66} \qquad \text{when } 30 \text{ ft} \le \text{span length (L)} < 40 \text{ ft}$$

$$NC = 1 \qquad \text{when span length (L)} \ge 40 \text{ ft}$$

At the middle support of two-equally continuous spans

$$NC = 1 + \frac{(40 - L)}{233} \qquad \text{when } 30 \text{ ft} \le \text{span length (L)} < 40 \text{ ft}$$

$$NC = 1 \qquad \text{when } 40 \text{ ft} \le \text{span length (L)} < 65 \text{ ft}$$

$$NC = 1 + \frac{(L - 65)}{713} \qquad \text{when } 65 \text{ ft} \le \text{span length (L)} < 120 \text{ ft}$$

At midspan of two-equally continuous spans

$$NC = 1 + \frac{(40 - L)}{80} \qquad \text{when } 30 \text{ ft} \le \text{span length (L)} < 40 \text{ ft}$$

$$NC = 1 \qquad \text{when span length (L)} \ge 40 \text{ ft}$$

The estimates obtained from the regression lines are close to the actual numbers of cycles per passage in all span lengths. The AASHTO Specifications (1990) provide values relatively conservative in spans shorter than 40 ft and only slightly unconservative for the new 3-axle fatigue truck in 40- to 50-ft span lengths for simple beams. However,

for simplification purposes, the number of cycles per passage presented in the AASHTO Specifications (1990) may be used for the proposed fatigue trucks with very little error.

3.5. Conclusions

Based upon the analysis results of the vehicle database and the simulation of truck traffic over the analytical bridge models, the following conclusions can be made:

1. Traffic count data can be used to estimate an effective gross weight of the truck traffic. When average gross weights at an investigated site or other similar highways are included in the calculation, use of traffic count data can provide relatively accurate estimates. However, statewide average gross weights can also be utilized when no information regarding the average gross weights at an investigated site is available.
2. An effective gross weight is site-specific and can be dramatically different than the 54-kip gross weight of the AASHTO fatigue truck.
3. Based upon the moment ranges obtained from simulating truck traffic flow over analytical bridge models, it has been found that a cumulative probability of the moment range distribution at twice of its effective value is in a range of 98.4 percent and 99.9 percent. This indicates that most of the moment ranges in the distribution are less than twice of the effective value.
4. The simulation results indicate that the fatigue trucks given by AASHTO (1990) and Laman and Nowak (1996) do not provide an accurate estimate of the fatigue damage accumulation for a wide range of span lengths when compared with damage predicted using the WIM database. The fatigue damage predicted by these fatigue truck models could be significantly overestimated, especially in short bridge spans.
5. A new design of the fatigue trucks provides a relatively accurate estimate of the fatigue damage accumulation over a range of bridge spans. In addition, the fatigue damage accumulation caused by truck traffic loadings

can be conveniently determined using the configurations (fixed axle spacing and weight distributions) developed for the new trucks.

6. The new 3-axle fatigue truck can be used as a representative of truck traffic on typical highways, while the 4-axle fatigue truck can better represent truck traffic on heavy duty highways with a high percentage of the fatigue damage dominated by 8- to 11-axle trucks.
7. The AASHTO Specifications (1990) provide relatively conservative estimates of the number of cycles per passage of the proposed fatigue trucks in most bridge spans.

Table 3.1 - Site Description

Station	Description (Location - City)	Period (Month/Year)	Highway Functional Class
001	U.S. 20 at Milepost 36.4 - Michigan City	11/01-10/02	Urban Other Principal Arterial
120	I-74 at Milepost 5.2 – Covington	1/02-12/02	Rural Principal Arterial Interstate
240	U.S. 24 at Milepost 158.1 - New Haven	1/02-12/02	Rural Other Principal Arterial
400	I-80 at Milepost 6.0 - Gary	1/02-12/02	Urban Principal Arterial Interstate
401	I-80 at Milepost 6.0 - Gary	1/02-12/02	Urban Principal Arterial Interstate
410	I-65 at Milepost 218.4 – Rensselaer	7/02-12/02	Rural Principal Arterial Interstate
470	S.R. 49 at Milepost 35.3 – Valparaiso	8/02-12/02	Rural Other Principal Arterial
510	I-65 at Milepost 79.1 – Edinburgh	1/02-12/02	Rural Principal Arterial Interstate
520	U.S. 50 at Milepost 137.4 – Versailles	1/02-9/02	Rural Other Principal Arterial
640	S.R. 66 at Milepost 18.7 – Evansville	9/02-12/02	Urban Other Principal Arterial

Table 3.2 - Traffic Characteristics of WIM Sites

Station	Direction	ADTT	Statistics of Gross Weight (kips)			Effective Gross Weight (kips)
			Mean	Std.	Maximum	
001-E	Eastbound	776	51.3	40.3	220.4	75.3
001-W	Westbound	598	45.8	37.0	220.2	67.4
120-E	Eastbound	2968	65.0	28.2	218.4	73.9
120-W	Westbound	2813	61.5	28.1	218.3	70.7
240-E	Eastbound	1652	50.3	20.3	166.4	56.9
240-W	Westbound	1593	50.4	21.8	194.1	57.9
400-E	Eastbound	18272	48.9	23.6	213.8	57.5
401-W	Westbound	17032	48.1	21.5	214.3	55.4
410-N	Northbound	4534	41.2	21.0	214.1	51.1
410-S	Southbound	4944	37.5	17.8	207.9	45.0
470-N	Northbound	2195	38.8	26.2	193.7	52.6
470-S	Southbound	1880	41.7	24.2	187.7	52.3
510-N	Northbound	3473	34.0	26.4	203.3	49.7
510-S	Southbound	2835	33.2	28.9	211.6	49.8
520-E	Eastbound	564	39.6	31.7	203.9	59.2
520-W	Westbound	455	32.0	22.6	179.2	44.2
640-E	Eastbound	256	19.0	17.4	117.3	31.7
640-W	Westbound	218	24.0	19.7	145.0	35.7

Table 3.3 - Percent Trucks Per FHWA Truck Classification

Station	FHWA Truck Classification										Total
Number	4	5	6	7	8	9	10	11	12	13	Trucks
001-E	2.70	25.67	4.30	0.64	2.57	44.60	2.34	0.13	0.82	16.22	283363
001-W	3.14	26.07	6.73	0.99	3.64	43.76	3.30	0.21	0.49	11.68	218280
120-E	0.88	11.14	1.76	0.19	1.76	81.30	0.42	1.85	0.64	0.06	1083381
120-W	0.98	11.57	1.84	0.53	2.02	79.93	0.42	1.92	0.73	0.06	1026610
240-E	1.19	7.50	1.25	0.30	1.41	85.34	0.69	1.76	0.53	0.05	602868
240-W	1.23	8.79	1.48	0.17	1.50	84.01	0.73	1.61	0.44	0.03	581433
400-E	1.98	12.72	2.30	0.21	1.69	77.55	0.77	2.06	0.65	0.07	6669431
401-W	2.00	10.00	3.07	0.16	1.63	79.26	0.95	2.18	0.62	0.13	6216768
410-N	0.91	4.93	1.83	0.20	2.13	85.26	0.48	3.50	0.76	0.02	834273
410-S	0.94	11.30	2.18	0.23	2.38	78.11	0.45	3.56	0.84	0.03	909659
470-N	1.13	24.65	3.14	0.86	2.63	64.76	1.17	1.39	0.20	0.09	335838
470-S	1.10	20.62	3.42	1.07	2.54	67.77	1.55	1.66	0.24	0.03	287649
510-N	1.98	35.48	2.22	0.61	3.01	52.40	1.69	1.95	0.63	0.02	1267823
510-S	0.99	52.99	1.34	0.46	3.11	39.23	0.18	1.38	0.30	0.01	275302
520-E	2.40	39.42	2.62	0.70	7.84	46.23	0.52	0.21	0.02	0.03	136995
520-W	0.60	27.40	3.57	0.80	3.25	62.92	1.00	0.24	0.16	0.06	110491
640-E	1.84	58.14	15.01	0.20	5.60	18.86	0.25	0.04	0.06	0.01	31197
640-W	1.33	50.65	6.96	12.77	5.43	22.53	0.27	0.04	0.00	0.02	26634

Table 3.4 - Statistics of Truck Gross Weight Per
FHWA Truck Classification

Station Number	Gross Wt. (kips)	FHWA Truck Classification									
		4	5	6	7	8	9	10	11	12	13
001-E	Mean	24.9	9.3	29.7	66.8	28.1	54.8	68.5	44.6	88.1	116.7
	Std.	10.3	6.7	16.0	21.8	10.7	23.3	23.4	13.4	26.7	25.3
	Max	117.0	82.3	122.9	178.4	111.6	218.5	217.4	92.7	217.1	220.4
001-W	Mean	25.6	10.3	30.8	71.9	28.6	51.3	61.1	48.0	73.1	115.8
	Std.	11.3	7.5	17.3	20.6	10.6	23.4	24.4	12.7	27.2	27.1
	Max	119.4	72.7	135.9	172.3	113.1	214.3	212.3	131.5	208.4	220.2
120-E	Mean	30.8	12.0	35.0	75.4	33.7	73.5	87.0	71.5	78.1	138.2
	Std.	10.9	7.0	13.2	12.4	14.3	20.7	27.9	15.4	16.4	34.2
	Max	83.2	54.1	97.6	133.5	100.4	136.4	204.5	116.1	161.9	218.4
120-W	Mean	32.3	12.1	33.8	82.1	36.2	69.6	83.0	70.0	75.5	121.1
	Std.	10.9	7.6	13.1	11.4	15.0	21.9	27.9	14.3	13.2	38.3
	Max	82.0	63.4	99.5	134.8	107.6	150.6	195.2	112.1	157.6	218.3
240-E	Mean	24.5	10.5	27.5	64.7	33.8	54.1	65.3	64.6	70.7	78.3
	Std.	7.6	6.8	11.5	9.2	10.0	16.7	19.6	12.0	14.2	31.1
	Max	78.8	45.1	79.1	91.8	77.0	123.7	127.3	109.7	120.3	166.4
240-W	Mean	23.2	9.4	25.8	58.6	29.9	55.6	65.1	49.6	59.3	92.8
	Std.	8.2	5.8	11.6	13.0	10.1	17.7	21.1	9.9	13.9	29.7
	Max	69.8	45.0	77.0	96.3	77.5	135.9	189.6	106.1	148.5	194.1
400-E	Mean	24.4	9.4	24.0	62.6	32.0	56.5	63.8	57.7	59.4	71.7
	Std.	7.9	5.2	10.3	13.9	11.0	18.4	22.3	10.4	13.5	29.3
	Max	81.8	50.3	92.5	110.4	89.9	143.1	192.5	105.3	147.3	213.8
401-W	Mean	25.0	10.3	25.9	61.1	32.4	54.0	53.0	59.6	62.7	70.2
	Std.	7.7	5.8	10.6	14.3	10.7	17.3	22.6	10.9	13.6	23.2
	Max	81.9	51.9	86.5	106.3	84.7	135.7	180.3	106.6	159.6	214.3
410-N	Mean	25.1	10.3	25.9	61.0	32.3	54.0	53.3	59.5	62.7	70.5
	Std.	7.7	5.7	10.6	14.3	10.8	17.2	22.5	10.8	13.5	23.0
	Max	81.9	51.9	86.5	106.3	84.7	135.7	180.3	106.6	159.6	214.3
410-S	Mean	24.2	10.1	19.5	49.6	25.1	42.0	50.3	42.8	45.0	59.6
	Std.	9.5	5.3	9.7	17.7	10.6	15.4	20.0	11.8	12.3	23.4
	Max	80.7	92.1	113.3	128.4	110.2	207.9	182.0	137.2	143.4	186.7
470-N	Mean	26.5	8.9	27.4	58.4	29.9	50.0	61.6	56.2	57.1	68.3
	Std.	10.1	5.4	15.4	21.1	13.0	22.5	24.3	17.4	17.6	29.7
	Max	83.9	68.4	115.2	141.4	109.0	193.7	186.4	133.2	136.0	188.8
470-S	Mean	25.9	8.3	25.1	61.9	26.4	52.3	62.1	51.5	63.3	87.9
	Std.	8.9	5.6	10.2	12.5	9.3	18.2	18.0	10.6	20.6	29.5
	Max	78.1	47.3	95.3	156.7	78.4	169.9	187.7	113.7	166.5	154.0

Table 3.4 (Cont.) - Statistics of Truck Gross Weight Per FHWA Truck Classification

Station Number	Gross Wt. (kips)	FHWA Truck Classification									
		4	5	6	7	8	9	10	11	12	13
510-N	Mean	21.4	6.7	23.8	51.7	23.2	52.0	59.8	54.0	54.4	107.4
	Std.	8.0	4.1	11.0	20.6	11.3	19.5	19.4	11.5	11.9	35.7
	Max	80.2	52.7	79.7	101.1	96.7	127.5	180.4	110.5	129.3	203.3
510-S	Mean	30.3	11.7	29.8	54.2	25.4	60.7	71.2	70.0	67.8	101.6
	Std.	13.2	8.3	15.0	30.6	17.1	22.6	30.5	24.8	15.2	55.3
	Max	83.9	85.0	97.2	151.7	129.9	184.7	172.8	183.5	179.0	211.6
520-E	Mean	26.8	10.2	33.6	82.5	38.8	64.3	80.9	48.3	61.5	127.1
	Std.	9.6	6.7	13.4	18.1	25.1	24.5	28.6	17.5	35.2	49.1
	Max	99.9	86.9	99.7	134.9	144.5	188.9	166.9	133.9	148.4	203.9
520-W	Mean	23.6	7.2	23.1	48.2	27.7	42.6	59.3	48.6	69.3	85.0
	Std.	6.0	6.4	10.6	13.3	9.3	19.1	20.3	10.8	19.0	25.9
	Max	55.4	46.0	79.5	99.7	75.3	164.4	179.2	93.5	125.5	145.8
640-E	Mean	22.2	8.1	24.7	52.9	25.4	44.0	55.5	40.7	51.1	22.7
	Std.	8.4	5.2	8.5	13.9	10.1	18.7	20.0	11.8	31.1	43.3
	Max	76.1	47.9	74.3	77.0	76.0	98.6	117.3	61.4	84.2	97.4
640-W	Mean	20.9	8.4	27.9	51.6	25.0	41.1	47.3	39.3	4.2	50.3
	Std.	5.9	4.7	12.2	7.1	9.3	16.5	17.7	15.9	13.6	58.2
	Max	46.5	44.4	75.1	77.7	51.2	87.1	90.4	54.4	37.9	145.0

Table 3.5 - Average Gross Weight of Trucks in Indiana Classified by Highway Functional Classification in 1999 (VTRIS)

Highway Functional Class	Parameter	FHWA Truck Classification									
		4	5	6	7	8	9	10	11	12	13
Rural Principal Arterial Interstate	Ave. Wt. (kips)	24.5	13.3	24.4	50.3	29.0	48.8	55.1	56.9	60.2	96.8
	Percent Truck	4.97	19.8	3.51	7.85	9.86	47.7	1.01	3.64	0.63	1.01
Rural Other Principal Arterial	Ave. Wt. (kips)	23.8	10.7	21.8	54.5	28.4	48.2	64.2	51.7	61.3	79.2
	Percent Truck	3.48	13.4	5.93	2.45	8.81	59.5	2.99	2.06	1.03	0.39
Rural Minor Arterial	Ave. Wt. (kips)	25.2	12.9	30.8	54.3	33.8	57.7	67.3	59.2	81.3	97.5
	Percent Truck	4.32	34.9	6.75	3.38	9.7	36.8	0.84	1.27	0.53	1.48
Rural Major Collector	Ave. Wt. (kips)	25.3	9.9	31.2	70.2	30.9	53.5	63.7	55.0	34.7	62.3
	Percent Truck	3.07	35.9	6.32	10.2	7.32	6.96	0.63	1.45	1.26	26.9
Urban Principal Arterial Interstate	Ave. Wt. (kips)	26.1	5.7	16.1	48.4	20.2	36.8	42.6	37.2	40.8	62.8
	Percent Truck	1.58	37.9	3.04	1.46	6.62	43	1.12	3.16	1.23	0.89
Urban Other Principal Arterial	Ave. Wt. (kips)	22.4	13.4	29.9	51.8	31.2	54.0	65.0	55.4	62.1	80.9
	Percent Truck	2.73	79.2	1.85	0.88	3.08	10.4	0.26	0.97	0.18	0.44
All Functional Classes (Statewide)	Ave. Wt. (kips)	26.0	10.9	25.4	53.8	28.9	49.8	58.7	52.7	60.3	83.5
	Percent Truck	2.92	34.6	3.75	3.36	7.64	41.6	1.12	2.77	0.92	1.36

Table 3.6 – Statistics of Using-Traffic-Count Procedure

Combination	Mean Biased Value	Standard Deviation	Coefficient of Variation
1	1.10	0.05	0.05
2	1.27	0.23	0.18
3	1.21	0.18	0.15
4	1.26	0.50	0.40

Table 3.7 – Percent Truck Classified by Number of Axles

Number of Axles	Station Number		
	001	410	520
2	27.91	8.13	47.06
3	6.12	3.38	12.69
4	2.22	2.74	8.71
5	45.21	84.17	31.30
6	2.82	1.54	0.22
7	1.30	0.03	0.03
8	3.07	0.01	0
9	6.82	0	0
10	1.99	0	0
11	2.54	0	0

Table 3.8– Statistics of Axle Weight of Trucks at Station 001

Number of Axles	Parameter	Weight of i th Axle (kips)											Gross Weight (kips)
		1	2	3	4	5	6	7	8	9	10	11	
2	Mean	4.6	5.6	-	-	-	-	-	-	-	-	-	10.2
	Std.	3.0	5.2	-	-	-	-	-	-	-	-	-	7.8
3	Mean	11.4	9.5	8.8	-	-	-	-	-	-	-	-	29.6
	Std.	5.4	5.9	6.2	-	-	-	-	-	-	-	-	15.4
4	Mean	9.1	11.9	8.7	9.0	-	-	-	-	-	-	-	38.6
	Std.	3.9	6.3	8.6	9.2	-	-	-	-	-	-	-	24.1
5	Mean	9.9	11.4	11.2	10.3	10.2	-	-	-	-	-	-	53.0
	Std.	2.4	5.4	5.4	6.1	5.9	-	-	-	-	-	-	22.3
6	Mean	10.3	12.8	12.7	10.8	12.1	11.9	-	-	-	-	-	70.7
	Std.	2.4	5.4	5.4	5.8	6.1	6.0	-	-	-	-	-	24.3
7	Mean	10.8	15.2	15.2	13.6	15.2	16.5	15.2	-	-	-	-	101.7
	Std.	2.7	4.4	4.7	5.7	6.1	7.4	6.8	-	-	-	-	24.2
8	Mean	10.9	14.3	14.4	14.2	14.6	14.7	12.4	12.8	-	-	-	108.3
	Std.	2.4	3.9	4.2	5.2	6.2	6.6	5.3	5.9	-	-	-	26.3
9	Mean	10.9	14.1	14.3	14.0	12.1	12.6	12.2	11.1	12.4	-	-	113.8
	Std.	2.4	3.9	4.1	4.7	4.9	4.8	4.1	4.1	4.4	-	-	22.2
10	Mean	11.5	13.8	14.2	12.4	11.4	11.1	11.5	11.3	10.6	10.8	-	118.7
	Std.	2.8	3.7	4.0	4.5	4.0	3.7	3.7	4.3	3.7	3.9	-	21.7
11	Mean	11.0	13.6	13.8	11.6	11.0	11.6	11.3	10.7	11.1	11.0	11.2	127.8
	Std.	2.7	4.0	4.1	4.3	4.1	4.6	4.0	3.9	4.3	4.0	4.5	26.2

Table 3.9– Statistics of Axle Spacing of Trucks at Station 001

Number of Axles	Parameter	Spacing of i th Axle (ft)									
		1	2	3	4	5	6	7	8	9	10
2	Mean	14.3	-	-	-	-	-	-	-	-	-
	Std.	3.8	-	-	-	-	-	-	-	-	-
3	Mean	16.8	7.1	-	-	-	-	-	-	-	-
	Std.	3.1	7.0	-	-	-	-	-	-	-	-
4	Mean	12.9	23.0	6.2	-	-	-	-	-	-	-
	Std.	1.9	12.8	7.1	-	-	-	-	-	-	-
5	Mean	15.7	4.5	29.3	5.4	-	-	-	-	-	-
	Std.	2.7	1.1	6.8	2.6	-	-	-	-	-	-
6	Mean	16.9	4.4	17.0	7.0	5.9	-	-	-	-	-
	Std.	2.4	0.1	7.3	2.7	3.3	-	-	-	-	-
7	Mean	18.0	4.5	13.7	8.6	7.9	8.5	-	-	-	-
	Std.	2.2	0.1	5.0	4.3	3.0	3.9	-	-	-	-
8	Mean	17.8	4.5	12.7	8.7	6.3	8.6	7.0	-	-	-
	Std.	2.1	0.1	3.9	3.3	2.7	5.2	2.6	-	-	-
9	Mean	17.1	4.5	12.2	8.6	5.0	5.0	6.0	7.7	-	-
	Std.	2.0	0.1	2.5	1.9	2.3	2.4	3.9	2.4	-	-
10	Mean	17.9	4.4	11.2	7.5	4.1	4.1	6.8	7.5	4.4	-
	Std.	2.3	0.1	2.1	2.7	0.7	1.6	3.4	4.1	1.5	-
11	Mean	18.3	4.4	10.7	7.2	4.0	4.0	3.9	7.0	8.0	5.0
	Std.	1.9	0.1	1.1	2.6	0.2	0.8	0.3	3.0	2.7	2.1

Table 3.10– Statistics of Axle Weight of Trucks at Station 410

Number of Axles	Parameter	Weight of i th Axle (kips)								Gross Weight (kips)
		1	2	3	4	5	6	7	8	
2	Mean	5.9	5.3	-	-	-	-	-	-	11.2
	Std.	2.8	3.2	-	-	-	-	-	-	5.7
3	Mean	9.8	5.4	4.8	-	-	-	-	-	20.0
	Std.	2.8	3.6	3.4	-	-	-	-	-	8.4
4	Mean	7.6	6.8	5.4	5.5	-	-	-	-	25.3
	Std.	3.0	3.1	3.3	3.7	-	-	-	-	10.9
5	Mean	10.8	7.8	7.5	7.4	7.6	-	-	-	41.0
	Std.	2.0	2.6	2.6	3.2	3.4	-	-	-	11.6
6	Mean	10.2	6.9	6.7	7.6	7.1	7.1	-	-	45.6
	Std.	2.0	2.0	1.9	2.4	2.2	2.2	-	-	9.4
7	Mean	9.2	6.6	6.7	5.6	5.9	6.2	6.0	-	46.2
	Std.	1.5	2.1	2.0	2.1	1.1	2.5	2.0	-	5.9
8	Mean	11.0	4.7	12.3	11.3	6.9	7.0	7.6	7.5	68.1
	Std.	0.4	0.1	3.5	3.1	2.1	2.0	4.2	2.5	17.6

Table 3.11– Statistics of Axle Spacing of Trucks at Station 410

Number of Axles	Parameter	Spacing of i th Axle (ft)						
		1	2	3	4	5	6	7
2	Mean	13.4	-	-	-	-	-	-
	Std.	5.0	-	-	-	-	-	-
3	Mean	16.1	5.4	-	-	-	-	-
	Std.	3.8	5.1	-	-	-	-	-
4	Mean	12.6	20.3	4.9	-	-	-	-
	Std.	2.5	9.5	6.0	-	-	-	-
5	Mean	14.9	4.9	27.9	5.2	-	-	-
	Std.	2.2	3.8	5.9	4.1	-	-	-
6	Mean	13.6	4.1	19.7	7.1	15.1	-	-
	Std.	2.7	1.5	4.6	2.1	7.7	-	-
7	Mean	13.8	4.0	13.5	5.6	5.9	13.5	-
	Std.	1.2	0.3	4.6	2.5	2.0	8.4	-
8	Mean	11.1	3.7	4.0	30.2	4.1	4.1	4.1
	Std.	0.4	0.1	0.1	0.7	0.0	0.1	0.1

Table 3.12– Statistics of Axle Weight of Trucks at Station 520

Number of Axles	Parameter	Weight of i th Axle (kips)							Gross Weight (kips)
		1	2	3	4	5	6	7	
2	Mean	6.1	6.4	-	-	-	-	-	12.5
	Std.	3.8	6.3	-	-	-	-	-	9.5
3	Mean	14.6	22.0	19.5	-	-	-	-	56.2
	Std.	5.5	12.6	11.9	-	-	-	-	26.2
4	Mean	11.9	15.8	10.8	14.1	-	-	-	52.5
	Std.	5.5	10.2	7.0	11.3	-	-	-	28.9
5	Mean	13.2	13.6	13.1	12.1	12.0	-	-	64.0
	Std.	3.0	5.6	5.4	6.3	6.3	-	-	23.7
6	Mean	12.7	15.3	14.6	10.1	13.2	12.8	-	78.8
	Std.	2.6	4.5	4.8	5.8	6.7	6.0	-	24.6
7	Mean	14.7	16.8	24.9	23.5	22.8	20.8	21.3	144.7
	Std.	2.3	6.6	3.3	5.7	4.4	4.2	5.7	12.9

Table 3.13– Statistics of Axle Spacing of Trucks at Station 520

Number of Axles	Parameter	Spacing of i th Axle (ft)					
		1	2	3	4	5	6
2	Mean	12.4	-	-	-	-	-
	Std.	4.2	-	-	-	-	-
3	Mean	15.5	26.5	-	-	-	-
	Std.	2.8	13.5	-	-	-	-
4	Mean	15.0	18.3	13.5	-	-	-
	Std.	2.8	12.9	13.8	-	-	-
5	Mean	16.2	4.8	31.7	5.2	-	-
	Std.	2.5	2.7	5.3	2.9	-	-
6	Mean	15.9	4.4	23.5	4.4	4.8	-
	Std.	2.3	0.1	7.5	0.9	2.9	-
7	Mean	16.3	4.5	10.5	28.3	4.7	4.7
	Std.	3.8	0.3	13.1	13.3	0.3	0.2

Table 3.14– Simulation Results of Trucks at Station 001

Location	Span (ft)	Moment Range (kip-ft)				Cumulative Probability at 2xEffective Moment (%)
		Mean	Std.	Maximum	Effective	
Middle Span Of Simple Beam	30	145.1	97.6	714.6	198.8	98.63
	60	395.3	283.7	1824.3	561.7	98.39
	120	1096.9	835.1	4866.7	1602.7	98.36
Middle Support of Continuous Beam	30	102.0	75.4	454.0	146.1	98.63
	60	243.6	179.9	975.7	346.5	98.87
	120	508.2	393.8	2234.1	748.2	98.38
Middle Span of Continuous Beam	30	135.3	87.2	673.7	181.9	98.78
	60	388.3	279.0	1835.3	552.4	98.40
	120	1107.0	840.5	4895.8	1614.0	98.40

Table 3.15– Simulation Results of Trucks at Station 410

Location	Span (ft)	Moment Range (kip-ft)				Cumulative Probability at 2xEffective Moment (%)
		Mean	Std.	Maximum	Effective	
Middle Span of Simple Beam	30	107.5	38.3	381.4	120.7	99.44
	60	283.8	94.6	907.1	313.6	99.68
	120	814.1	294.4	2270.2	909.6	99.87
Middle Support of Continuous Beam	30	76.4	29.7	241.6	86.9	99.67
	60	193.6	73.3	515.0	217.8	99.92
	120	381.8	142.6	1060.2	428.9	99.84
Middle Span of Continuous Beam	30	102.3	34.6	356.1	113.7	99.53
	60	277.1	93.1	910.1	306.9	99.61
	120	822.9	298.8	2279.3	920.2	99.85

Table 3.16– Simulation Results of Trucks at Station 520

Location	Span (ft)	Moment Range (kip-ft)				Cumulative Probability at 2xEffective Moment (%)
		Mean	Std.	Maximum	Effective	
Middle Span Of Simple Beam	30	126.0	89.2	565.2	177.8	98.95
	60	317.1	218.6	1442.3	440.2	99.11
	120	844.3	634.5	3434.9	1217.4	99.32
Middle Support of Continuous Beam	30	79.7	61.2	321.4	116.7	98.71
	60	199.5	163.4	875.2	300.7	99.33
	120	387.9	305.0	1546.0	572.1	99.33
Middle Span of Continuous Beam	30	122.6	84.9	562.1	171.4	98.88
	60	310.0	211.7	1446.1	429.4	99.09
	120	854.7	645.3	3459.7	1235.7	99.31

Figure 3.1 – WIM Sensors and Control Loops

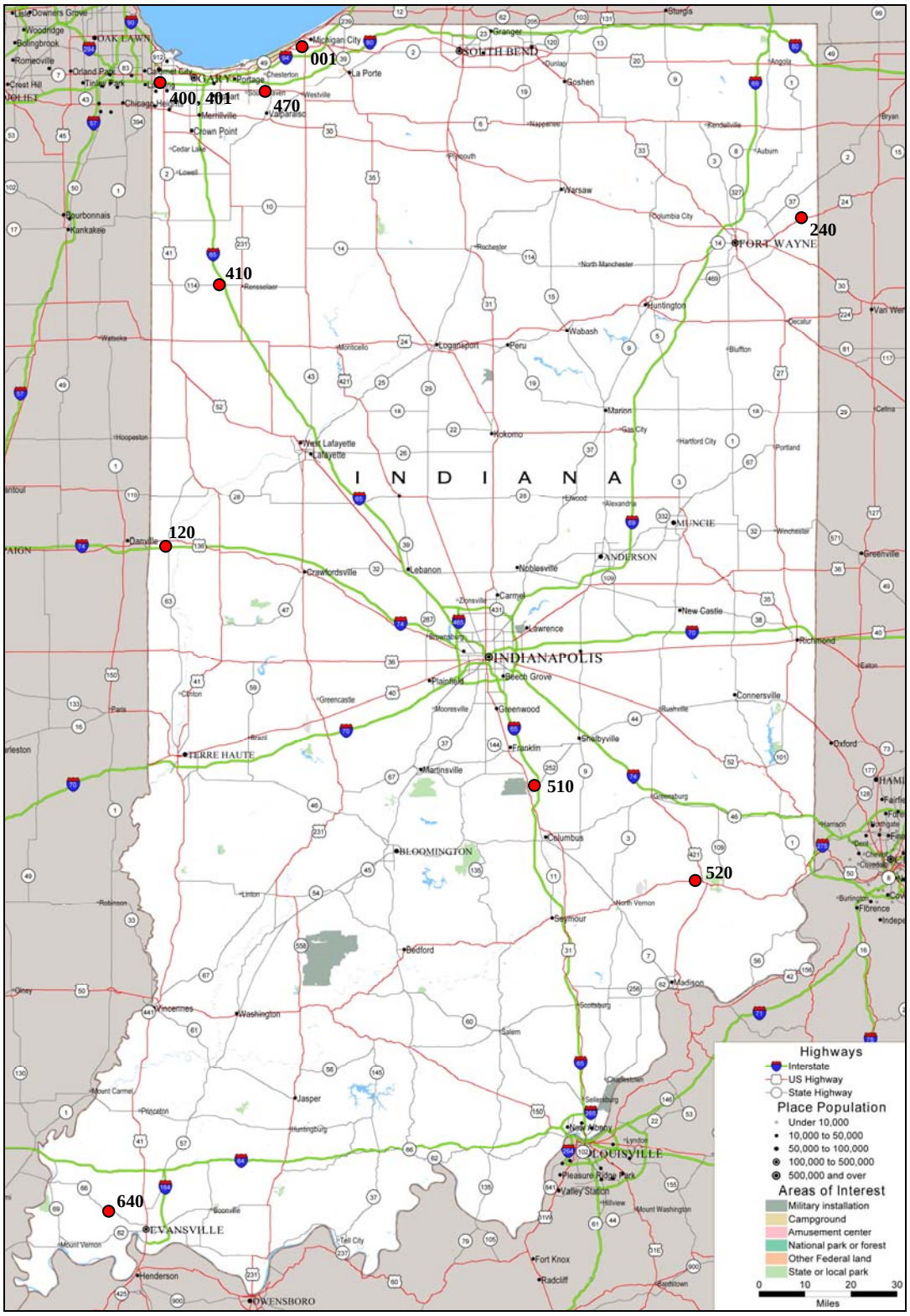

Figure 3.2 – Locations of WIM Sites Included in Vehicle Database

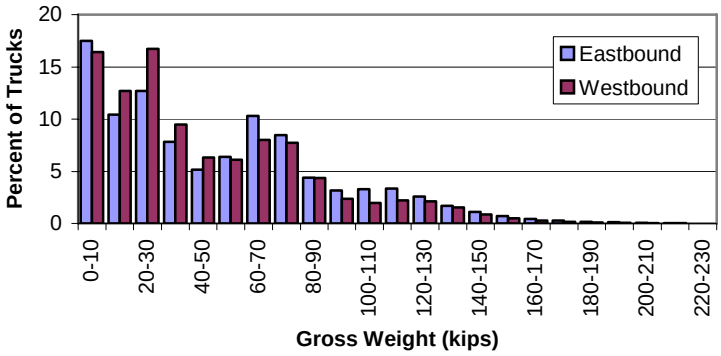

Figure 3.3 – Gross Weight Distribution of Station 001

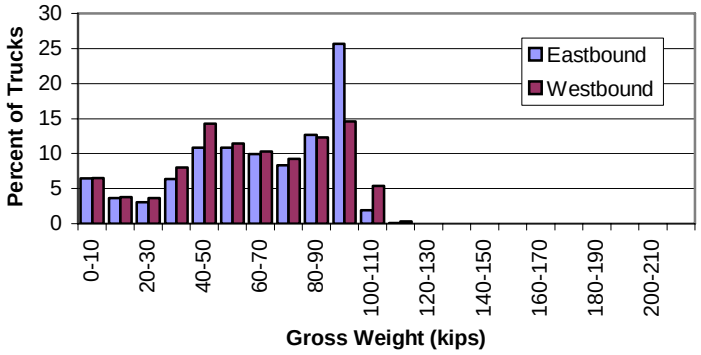

Figure 3.4 – Gross Weight Distribution of Station 120

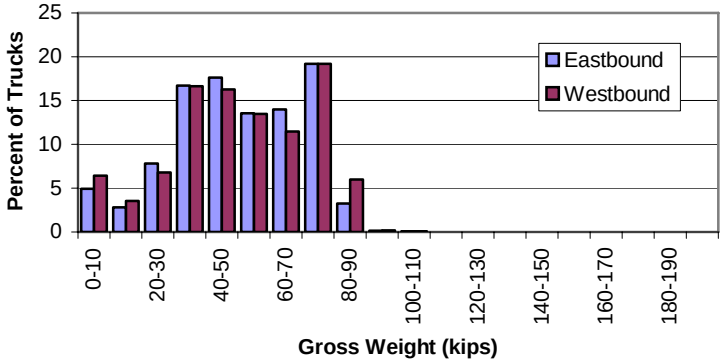

Figure 3.5 – Gross Weight Distribution of Station 240

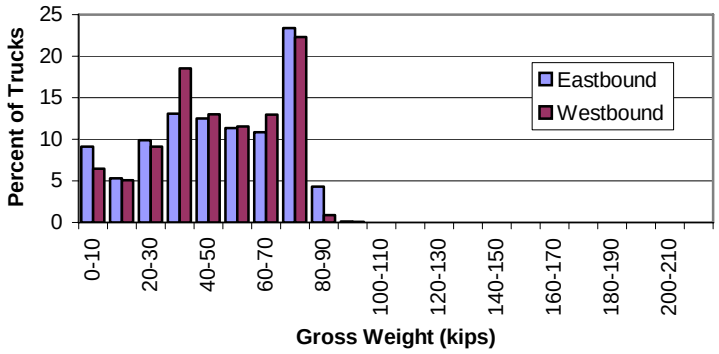

Figure 3.6 – Gross Weight Distribution of Stations 400 and 401

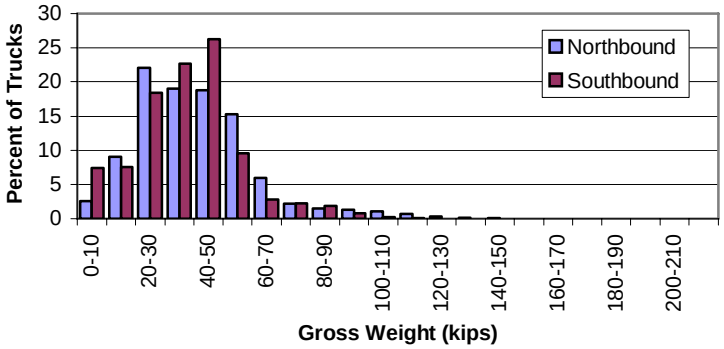

Figure 3.7 – Gross Weight Distribution of Station 410

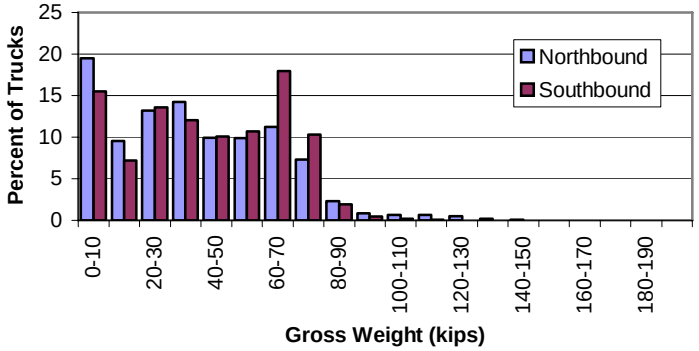

Figure 3.8 – Gross Weight Distribution of Station 470

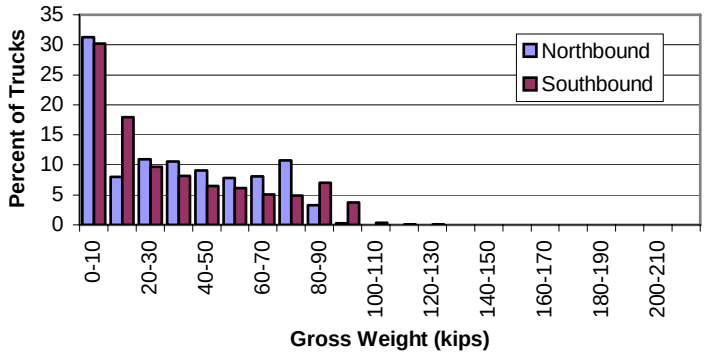

Figure 3.9 – Gross Weight Distribution of Station 510

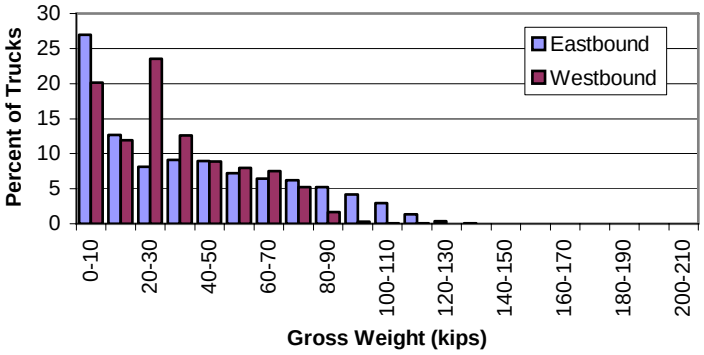

Figure 3.10 – Gross Weight Distribution of Station 520

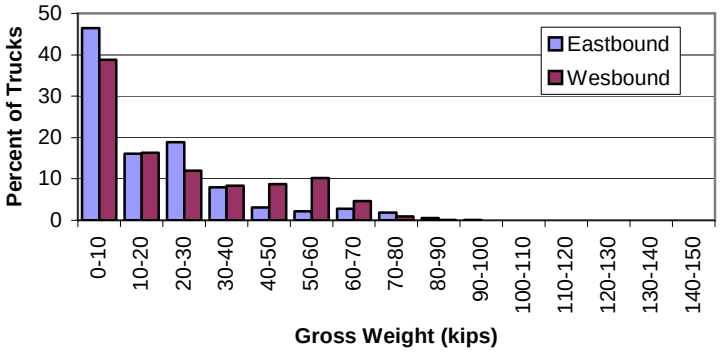

Figure 3.11 – Gross Weight Distribution of Station 640

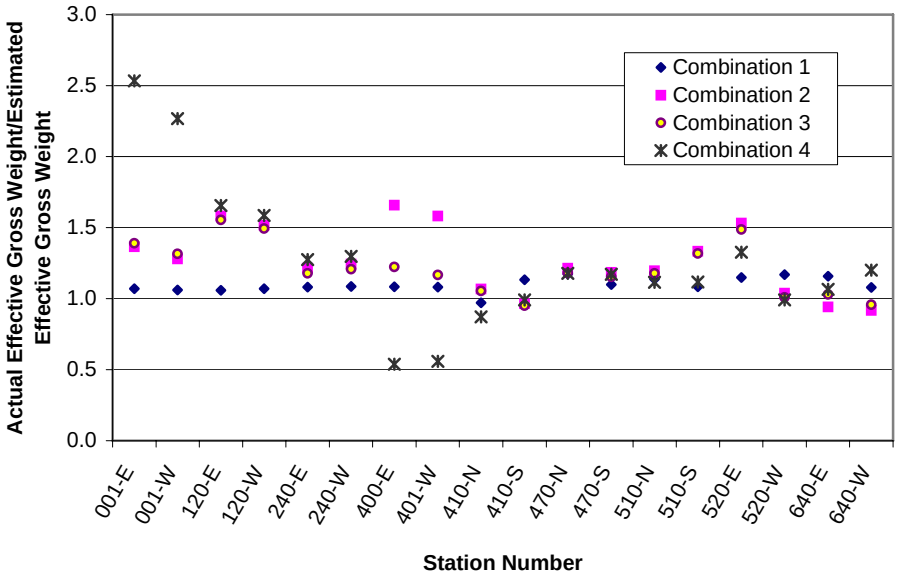

Figure 3.12 – Biased Value of Use of Traffic Count Data in Estimating Effective Gross Weight

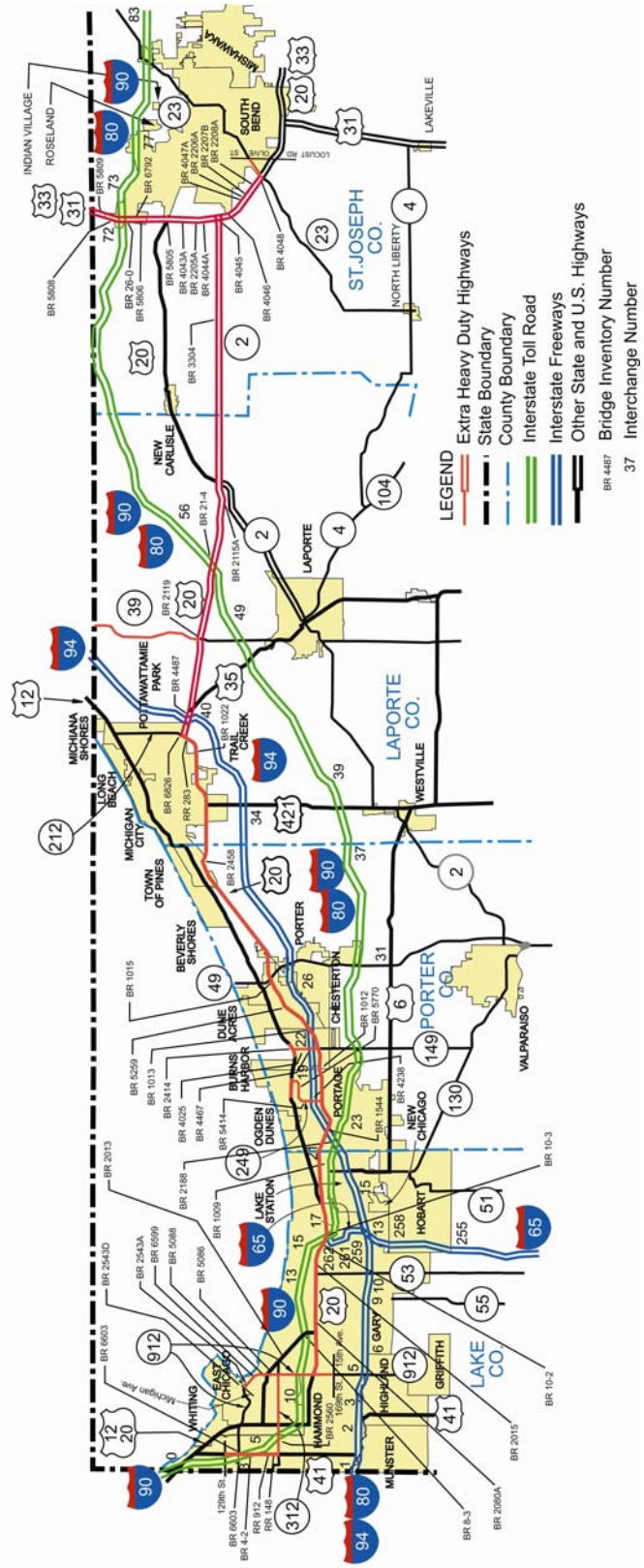

Figure 3.13 – Overview of Extra Heavy Duty Corridor

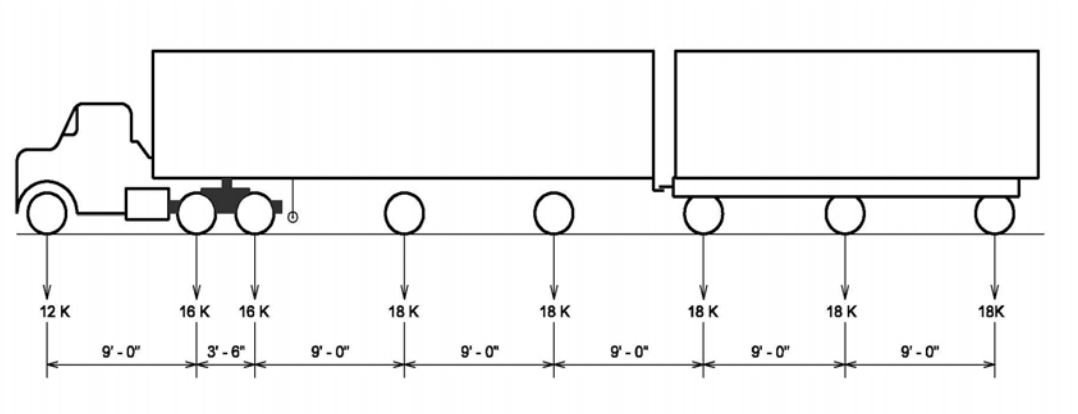

Figure 3.14 - Michigan Train Truck Number 5

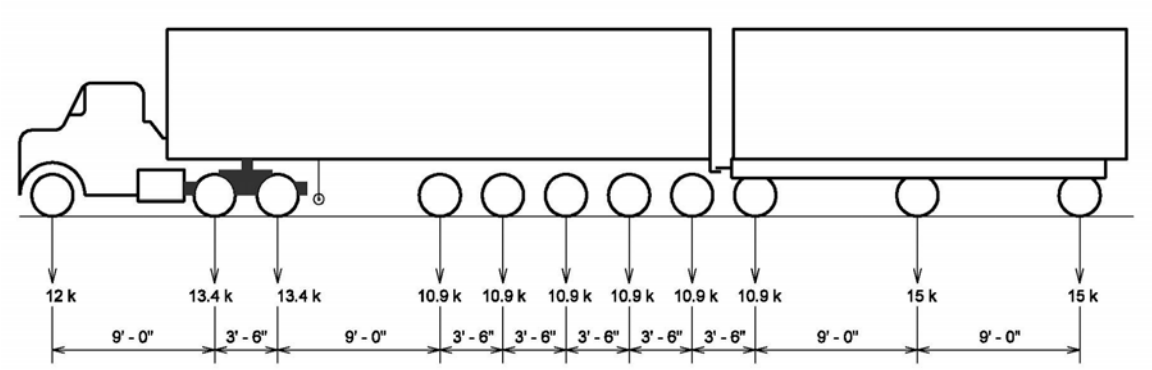

Figure 3.15 – Michigan Train Truck Number 8

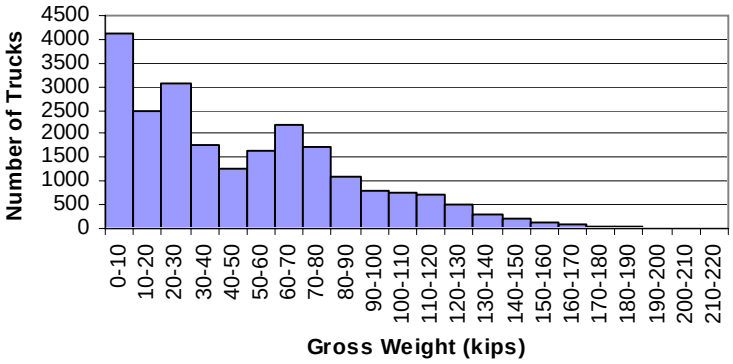

a) Station 001

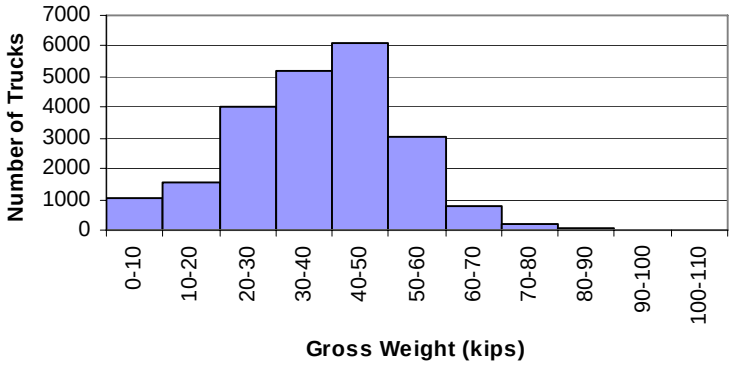

b) Station 410

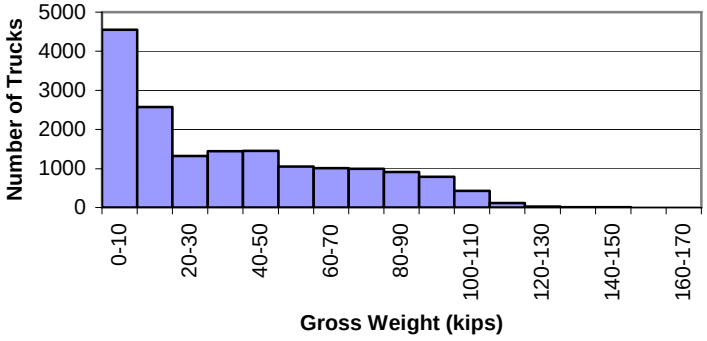

c) Station 520

Figure 3.16 – Gross Weight Distribution of Sampled Truck Traffic

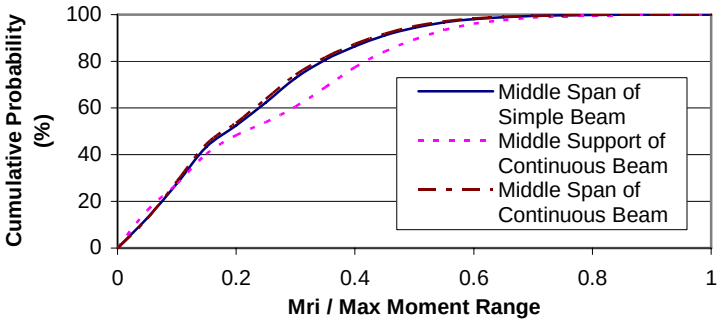

a) Station 001

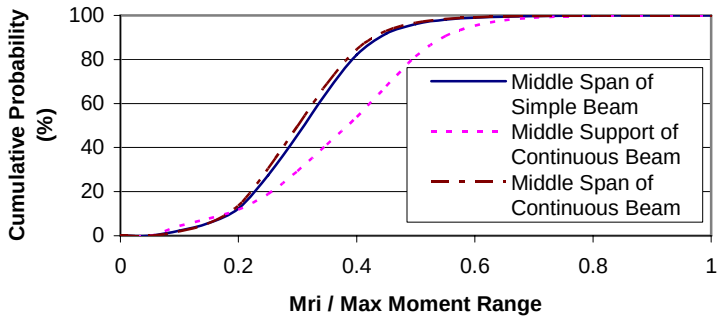

b) Station 410

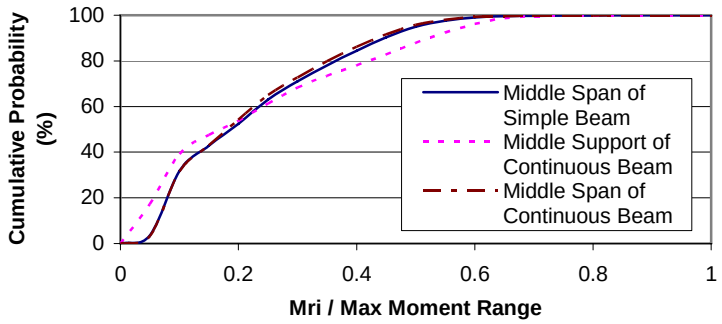

c) Station 520

Figure 3.17 – Cumulative Distribution of Moment Range in 60-Foot Span Bridge

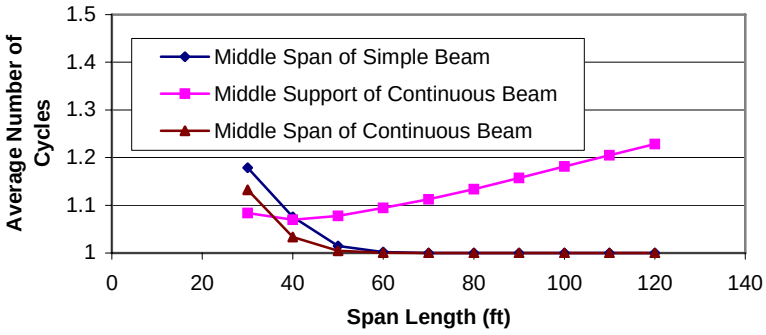

a) Station 001

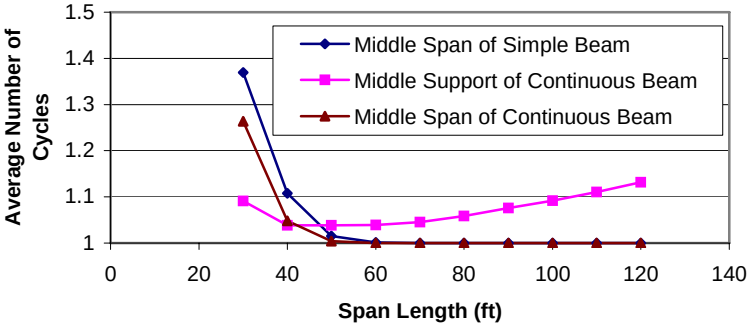

b) Station 410

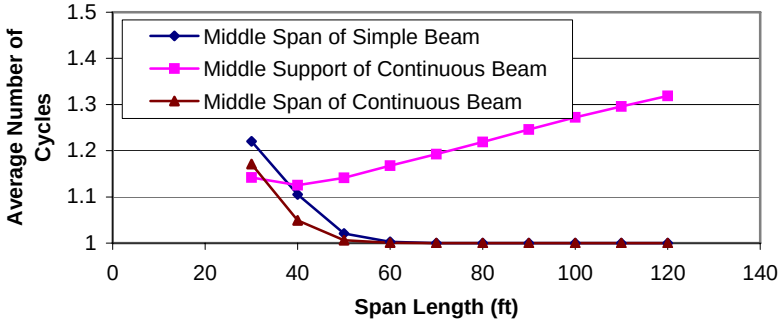

c) Station 520

Figure 3.18 – Average Number of Cycles Per Passage

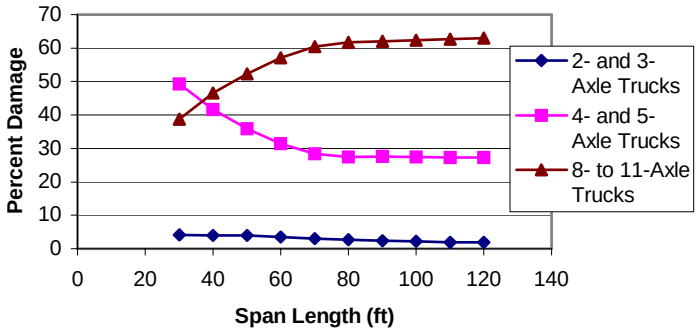

a) Station 001

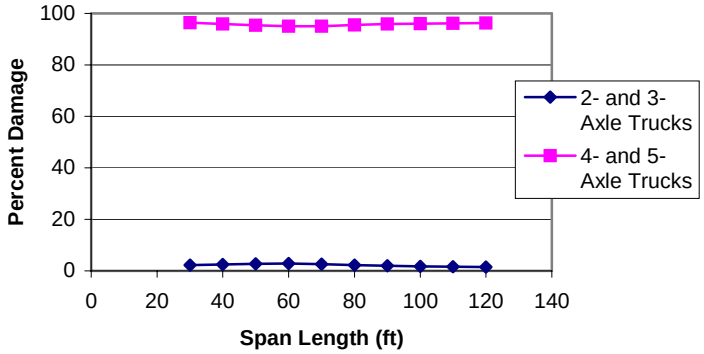

b) Station 410

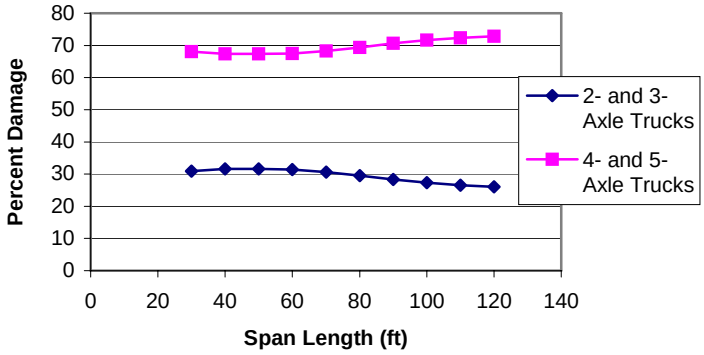

c) Station 520

Figure 3.19 – Percent Fatigue Damage Accumulation at Midspan of Simple Beam Members

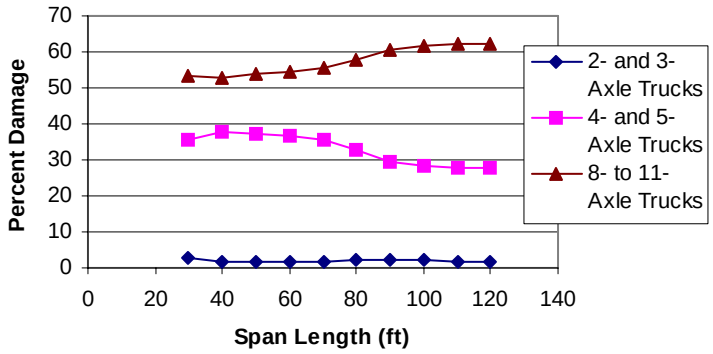

a) Station 001

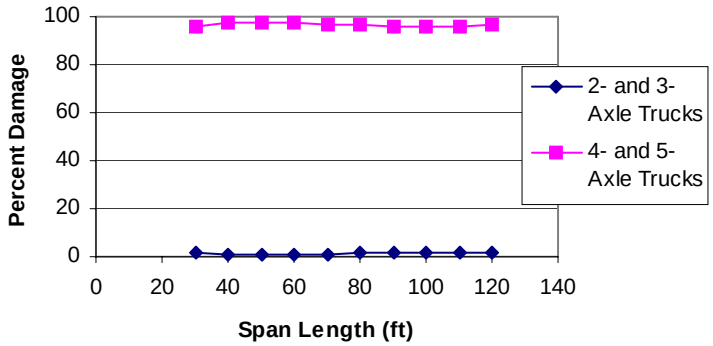

b) Station 410

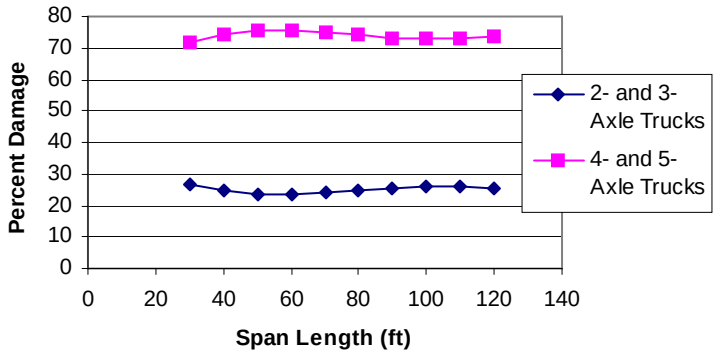

c) Station 520

Figure 3.20 – Percent Fatigue Damage Accumulation at Middle Support of Continuous Beam Members

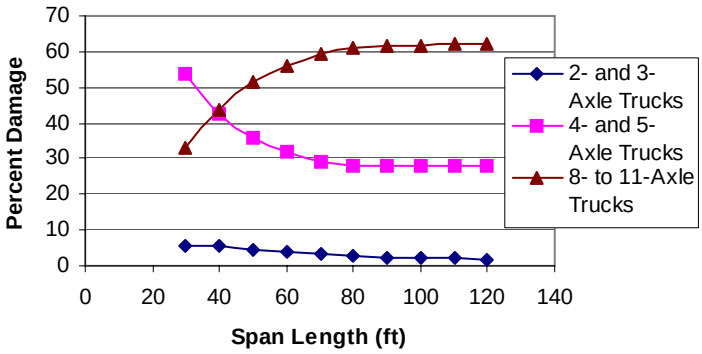

a) Station 001

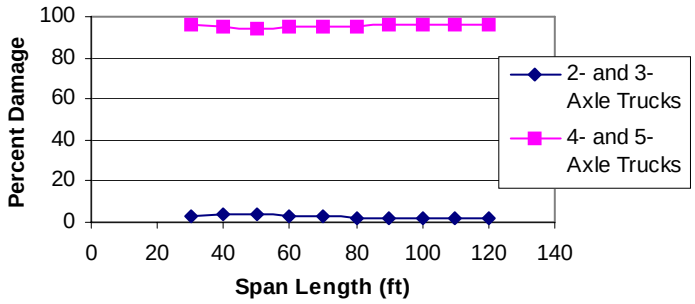

b) Station 410

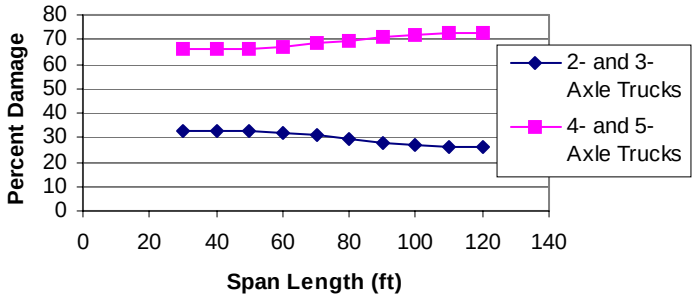

c) Station 520

Figure 3.21 – Percent Fatigue Damage Accumulation at Midspan of Continuous Beam Members

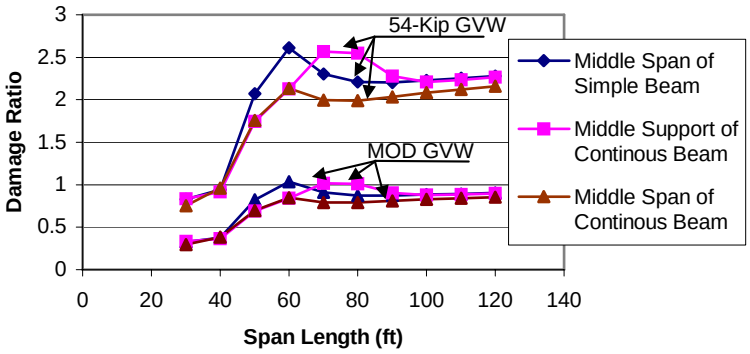

a) Station 001

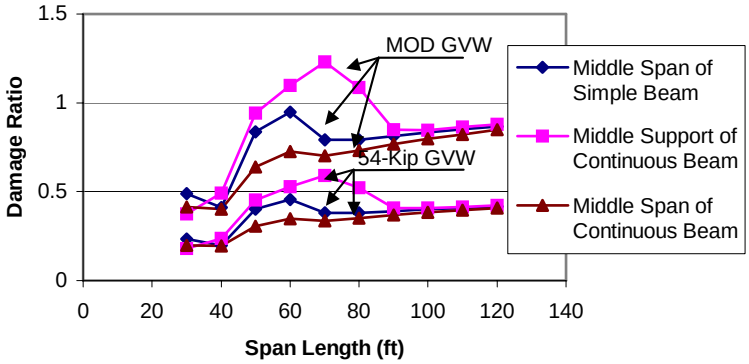

b) Station 410

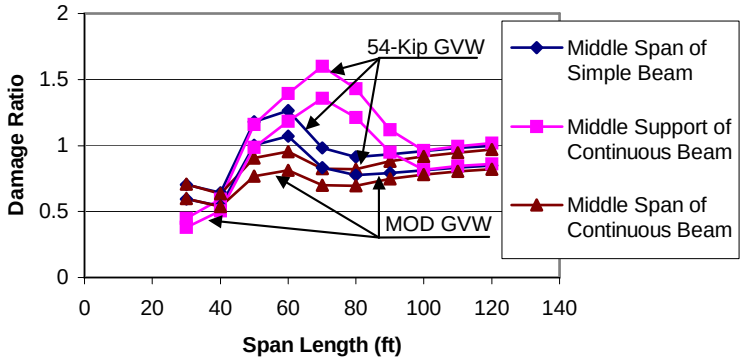

c) Station 520

Figure 3.22 - Damage Ratio of 54-kip and Modified AASHTO Fatigue Trucks

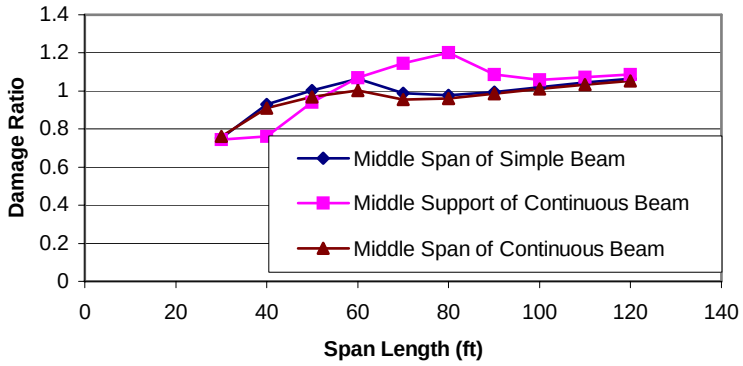

a) Station 001

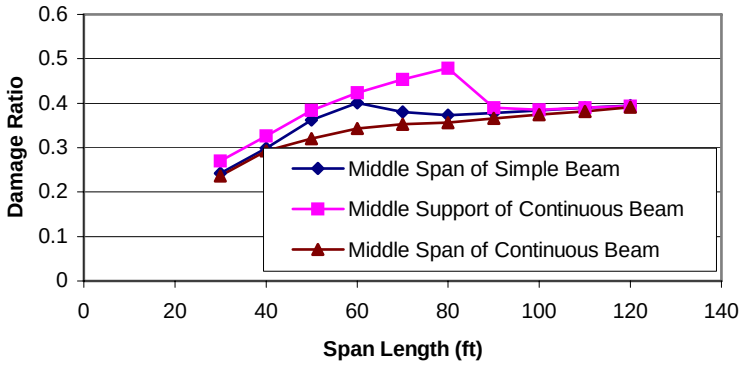

b) Station 410

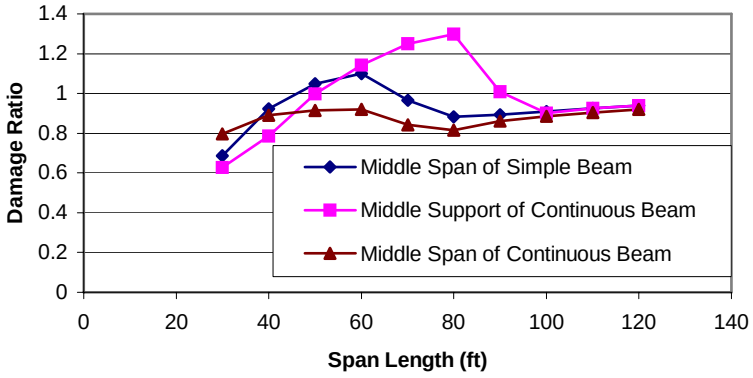

c) Station 520

Figure 3.23 – Damage Ratio of Laman Fatigue Trucks

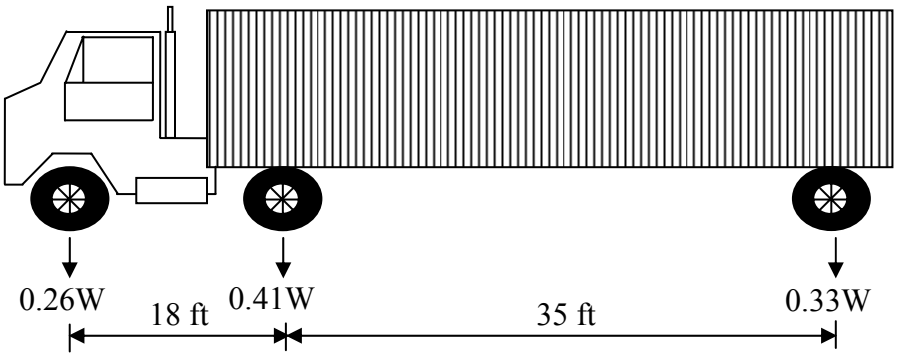

a) 3-Axle Fatigue Truck

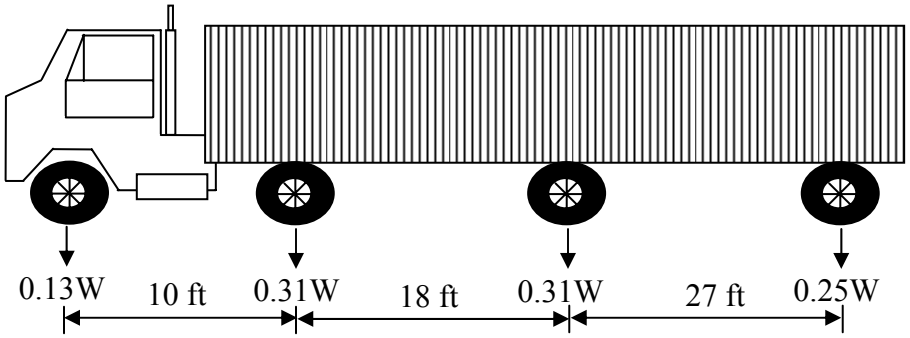

b) 4-Axle Fatigue Truck

Figure 3.24 – Proposed Fatigue Trucks

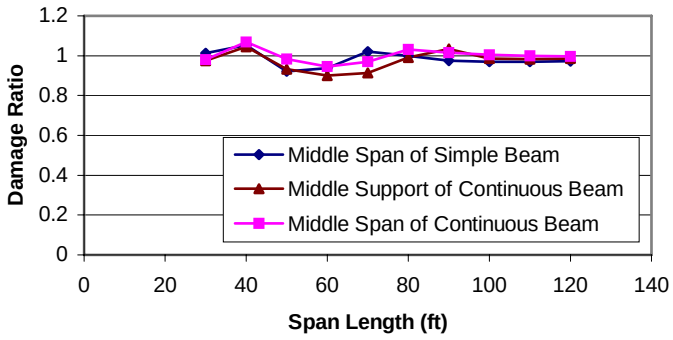

Figure 3.25 – Damage Ratio of New 4-Axle Fatigue Truck at Station 001

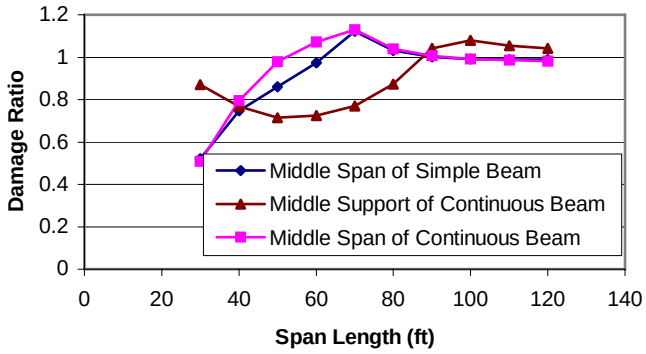

a) Station 001

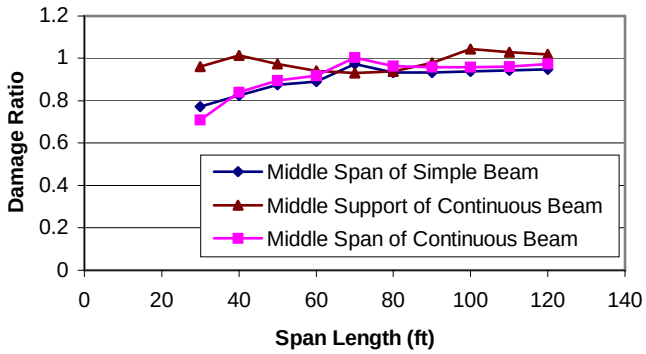

b) Station 410

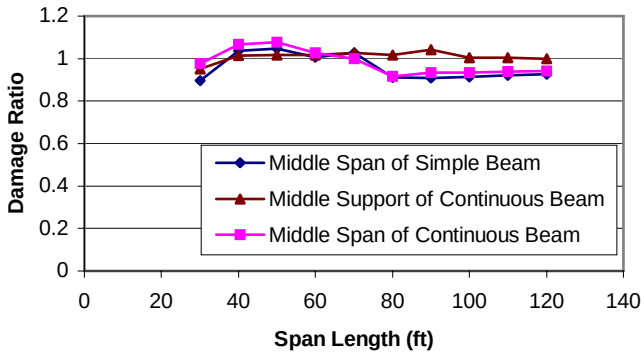

c) Station 520

Figure 3.26 – Damage Ratio of New 3-Axle Fatigue Truck

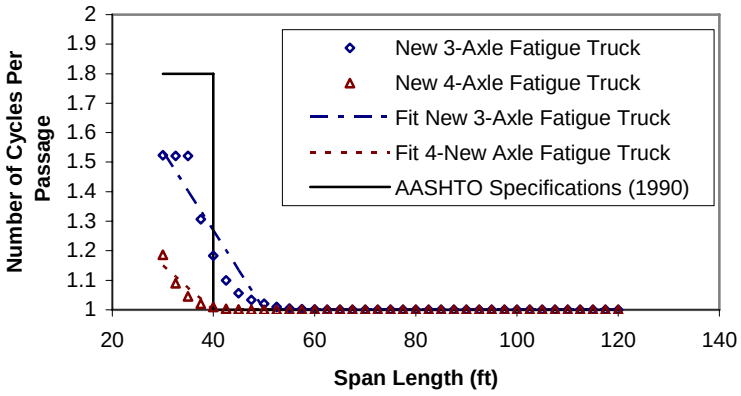

a) Midspan of a Simple Beam

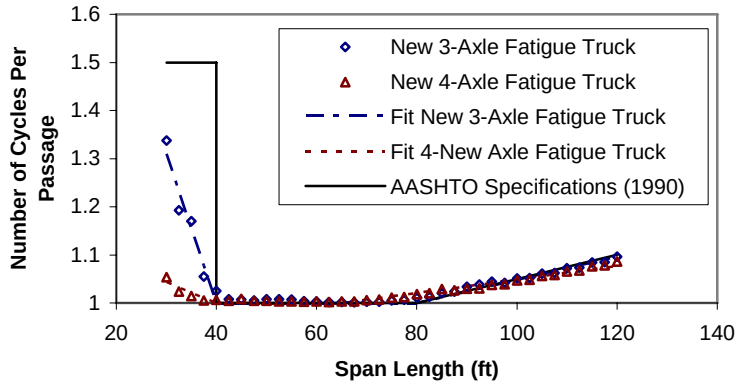

b) Middle Support of a Two-Span Continuous Beam

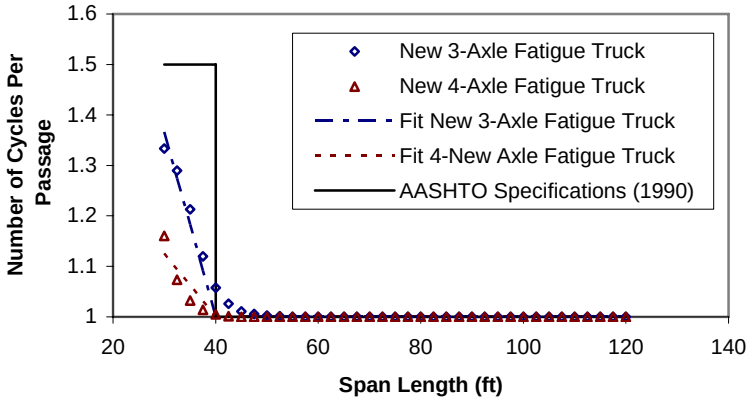

c) Midspan of a Two-Span Continuous Beam

Figure 3.27 – Number of Cycles Per Passage of Proposed Fatigue Trucks

CHAPTER 4. FATIGUE RELIABILITY MODEL

4.1. Introduction

A fatigue reliability model should be developed in such a way that it can incorporate information obtained from an inspection at a specific site. It should also include uncertainties inherent in fatigue load and resistance parameters. In the present study, a fatigue reliability model was developed based on an extensive literature review and the analysis results of the vehicle database described in Chapter 3. It can be used to provide an estimate of the fatigue life with a certain confidence level. In addition, a safety factor corresponding to the proposed fatigue reliability model was developed. Its application and provided range of the level of safety are demonstrated through two calculation examples.

4.2. Fatigue Limit State Function

A fatigue limit state function is used to define the failure limit for structures subjected to repeated cyclic loads. The fatigue limit state function can be expressed as Eq. 4.1:

$$G(\Delta, n, N) = \Delta - \frac{n}{N} \tag{4.1}$$

where Δ is an uncertainty in estimating the fatigue damage at failure predicted by Miner's rule, n is an estimated number of cycles over an entire fatigue life, and N is the fatigue strength. The total number of cycles (n) can be calculated from Eq. 4.2:

$$n = ADTT_{ave} \times 365 \times t \times NC \times p \tag{4.2}$$

where $ADTT_{ave}$ is the average daily truck traffic over an entire fatigue life, t is the total fatigue life in years, NC is a number of cycles per truck passage, and p is a fraction of truck traffic in a single lane.

The fatigue strength (N) in Eq. 4.1 is the total number of cycles that a structure can resist for a given loading history. It is primarily a function of the applied stress range and category fatigue detail. Estimated values of the fatigue strength (N) can vary, depending on the methodologies used in a fatigue limit consideration. An extension of the S-N line can be employed when all stress range levels are assumed to cause fatigue damage. For this methodology, a fatigue limit is not included in the calculation. Based on this assumption, the fatigue strength (N) can be calculated from Eq. 4.3. However, when a variable amplitude fatigue limit (VAFL) exists, the fatigue strength (N) can be determined from Eq. 4.4 (Albrecht and Wright, 2000):

$$N = 10^{b - m\log(S_{re})} \tag{4.3}$$

$$N = \frac{10^{b}}{S_{re}^{\ m} - f_{vafl}^{\ m}} \tag{4.4}$$

where b and m are the intercept and slope constant of the S-N line, S_{re} is the effective stress range, and f_{vafl} is the stress range at a variable amplitude fatigue limit.

The effective stress range (S_{re}) can be obtained from a spectrum analysis of strain gage data or a structural analysis of bridge structures with an applied live load given in terms of an equivalent fatigue truck. When the fatigue truck is used in the calculation, the effective stress range (S_{re}) can be determined from Eq. 4.5:

$$S_{re} = \frac{W \times (M_{IF}) \times GDF \times (1 + I) \times H}{S_x} \tag{4.5}$$

where W is a gross weight of the fatigue truck, M_{IF} is the moment range influence factor per unit weight of the fatigue truck, GDF is the girder distribution factor, I is the dynamic

load factor or impact factor, H is the headway factor, and S_x is the elastic section modulus of the flexural member.

4.3. Parameter Database

The statistical database of fatigue load and resistance parameters has been developed based on information obtained from an extensive literature review and the analysis results of the vehicle database. It should be noted that statistics of some parameters described herein were based on limited research; however, they were considered to be appropriate estimates and used in developing the AASHTO Fatigue Guide Specifications (1990). Therefore, unless updated statistics are found in the literature review, these values will also be utilized in the fatigue reliability model in this study. A statistical summary of the following parameters is presented:

- Uncertainty in Miner's Rule (Δ)
- Average daily truck traffic ($ADTT_{ave}$)
- An equivalent number of cycles per truck passage (NC)
- Fraction of truck traffic in a single lane (p)
- Intercept (b), slope constant (m), and fatigue limit of the S-N lines
- Effective stress range (S_{re})
- Gross weight of the fatigue truck (W)
- Moment range influence factor (M_{IF})
- Girder distribution factor (GDF)
- Dynamic load factor (I)
- Headway factor (H)
- Elastic section modulus (S_x)

Uncertainty in estimating the fatigue damage at failure predicted by Miner's rule is represented by a random variable Δ. The value of Δ depends on several factors, such as the definition of failure, type of specimen, mean stress, stress concentration, material,

temperature, and etc. (ASCE Committee on Fatigue and Fracture Reliability, 1982). It has been shown that Δ can be modeled as a lognormal distribution with a mean value equal to 1.0 and a coefficient of variation (C.O.V) equal to 15 percent (Nyman and Moses, 1985; Raju *et al*., 1990). Accordingly, 95 percent of the specimens tested under variable amplitude loadings are assumed to have a fatigue life within 70 to 130 percent of the life predicted by the Miner's rule.

$ADTT_{ave}$ is the average daily truck traffic for the time span over which the fatigue life is calculated. It is a function of the average daily traffic (ADT), percent truck in traffic, and traffic growth rate (r). Traffic volumes generally increase at an annual rate (r) of 3 to 5 percent until they reach a maximum physical traffic limit of roughly 20,000 vehicles per lane per day (AASHTO, 1998). By multiplying this limit with percent truck traffic, a maximum theoretical value of ADTT in a lane under consideration can be obtained. Generally, truck traffic should exclude panel, pickup, and other 2-axle trucks because these vehicles cause little fatigue damage. The same definition of truck traffic must be used when considering a gross weight distribution. The $ADTT_{ave}$ can be modeled as a lognormal distribution with a 10 percent coefficient of variation (Moses *et al.*, 1987).

An equivalent number of cycles per truck passage is represented by a random variable, NC, in the fatigue limit state function. The stress range associated with an equivalent number of cycles will cause the same amount of fatigue damage as that caused by a complex stress history. The equivalent number of cycles can be determined by decomposing a complex stress history into static and dynamic stress ranges and then employing the Miner's rule. Schilling (1984) refers to this effect as N_e . An equivalent number of cycles can be obtained by using either a simulation of the fatigue truck over analytical bridge models or the values specified in the AASHTO Specifications (1990). Because the statistical data for this parameter are limited and small variations are expected, Moses *et al.* (1987) suggested that the number of cycles per passage can be modeled as a lognormal distribution with a 5 percent coefficient of variation.

A fraction of truck traffic in a single lane (p) is an estimated percentile of truck passing the lane under consideration. The value provided in the AASHTO LRFD

Specifications (1998) is presented in Table 4.1. This parameter is assumed to be deterministic in the proposed fatigue reliability model.

Intercept (b), slope constant (m), and fatigue limit of the S-N lines are parameters representing the fatigue strength categories for various structural details. For bridge structures, Albrecht (1982) has found that the test data points have a lognormal distribution with approximately equal standard deviations for all ranges of fatigue life. This behavior was found to be true within all AASHTO categories of details. Moreover, the study performed by Keating and Fisher (1986) has shown that the slope (m) of the S-N lines for all AASHTO categories can be assumed to be 3.0 for simplicity. The mean values and coefficients of variation of stress ranges at 2 million cycles are provided in Table 4.2.

For practical-design purposes, the AASHTO Specifications selected S-N curves at two standard deviations below and parallel to the mean curves. These curves approximately encompass the lower 95 percent of the test data (Fisher, 1997). The nominal intercepts and constant amplitude fatigue limits (CAFL) shown in Table 4.2 are prescribed in the AASHTO Specifications (1998). However, instead of using two constant amplitude fatigue limits for category C fatigue details as previously performed in the old code provisions (AASHTO, 1992), the AASHTO LRFD Specifications (1998) classifies transverse stiffener-to-web and transverse stiffener-to-bottom flange fillet welds as category C′ details. The category C′ details have a nominal intercept of the S-N line similar to the category C details (Table 4.2), but the nominal constant amplitude fatigue limit for these details is suggested to be 12 ksi.

The study performed by Fisher *et al*. (1983) demonstrated that structures will have infinite fatigue life when the maximum and effective stress ranges are less than the constant amplitude fatigue limit. Therefore, a variable amplitude fatigue limit can be determined by multiplying the constant amplitude fatigue limit with a ratio of the effective stress range and the peak stress range, as shown in Eq. 4.6:

$$f_{VAFL} = \rho_e \times f_{FL} \tag{4.6}$$

where ρ_e is a ratio of the effective stress range to the peak stress range, and f_{FL} is a constant amplitude fatigue limit. It is assumed in the fatigue reliability model that ρ_e is deterministic; therefore, the variable amplitude fatigue limit (f_{VAFL}) in Eq. 4.6 has a distribution and a coefficient of variation similar to the constant amplitude fatigue limit (f_{FL}) (Table 4.2). In the AASHTO Specifications (1998), a nominal variable amplitude fatigue limit is defined as a stress range level at one-half of the nominal constant amplitude fatigue limit. This assumption has been observed to agree well with the WIM study performed by Albrecht and Wright (2000).

Uncertainty in estimating effective stress range is represented by S_{re}. Its mean is equal to the effective stress range or the root-mean-cube (RMC) of a stress range spectrum. The error associated with this parameter is in the order of 5 to 10 percent; however, a 9 percent coefficient of variation was suggested by Ang and Munse (1975) and Mohammadi *et al*. (1998). The AASHTO Specifications (1990) used a product of W, GDF, I, M_{IF}, and S_x to estimate the effective stress range for both the use of strain gage instrumentation and fatigue truck analysis. However, a coefficient of variation of the effective stress range computed from this product is not constant. It has a value approximately equal to 9 percent when the calculated stress ranges are in a range of 1 to 3 ksi, which are stress levels usually observed in most bridges (Moses *et al*., 1987). Therefore, a lognormal distribution with a 9 percent coefficient of variation will be used for a random variable S_{re} when strain gage instrumentation is utilized in the fatigue evaluation.

The gross vehicle weight of the fatigue truck is represented by the random variable W. The mean value of this parameter should be selected so that the fatigue truck will cause the same amount of fatigue damage as actual truck traffic for a given equivalent number of passages. In the AASHTO Specifications (1990), a 54-kip gross weight is suggested for the standard fatigue truck. However, when a gross weight distribution is known at an investigated site, the gross weight of the fatigue truck can be adjusted to be equal to the root-mean-cube value of the weight distribution.

In a fatigue evaluation, the gross weight distribution can be obtained from a few alternatives. However, the amount of uncertainty and bias corresponding to these

alternatives are not similar. The statistical parameters of the alternatives listed below, except Case 4 (traffic count data), were utilized in a code calibration of the AASHTO Specifications (1990) by Moses *et al*. (1987), and they will be employed in this study.

Case 1: Using the gross weight of the standard AASHTO fatigue truck – As mentioned earlier, the AASHTO Fatigue Guide Specifications (1990) stipulate a 54-kip gross weight for the fatigue truck. This gross weight was calculated based on the actual truck traffic spectra obtained from WIM studies that included 30 sites nationwide and over 27,000 observed trucks (Snyder *et al*., 1985). Therefore, this gross weight was assumed to be unbiased and had a lognormal distribution with a 10 percent coefficient of variation. Because no updated statistical values of this parameter have been found in the literature, this assumption will also be used in this study.

Case 2: Using static weigh station data – A biased value, corresponding to a ratio of the actual to estimated effective gross weights obtained based on weigh station data, is stipulated to be equal to 1.05. This ratio is defined to be slightly greater than 1.0 in order to account for a possibility that heavy trucks avoid weigh stations. W can be modeled as a lognormal distribution with a 3 percent coefficient of variation.

Case 3: Using WIM data - A biased value of the effective gross weight obtained from the WIM data is equal to 1.0. A random variable W can be modeled as a lognormal distribution with a 3 percent coefficient of variation. The coefficient of variation for this alternative is less than Case 1 (gross weight of the AASHTO fatigue truck) because actual gross weight distributions at investigated sites can be employed in the calculation.

Case 4: Using traffic count data – The analysis of truck traffic data collected from nine WIM sites in Indiana and the vehicle database available in the VTRIS software was conducted to investigate the amount of uncertainty inherently associated with use of traffic count data. It has been found that traffic count data can provide a relatively accurate estimate of the effective gross weight

when average gross weights at an investigated site or other sites with similar traffic characteristics are used in the calculation. The biased value and coefficient of variation of the gross weight obtained from this alternative procedure are equal to 1.10 and 5 percent, respectively. However, use of traffic count data provides a biased value of 1.21 and a 15 percent coefficient of variation, when a statewide average gross weight is used instead of site specific information (see Chapter 3). Similar to other parameters in the fatigue limit state function, the effective gross weight (W) obtained from traffic count data will be modeled as a lognormal distribution.

The moment range influence factor (M_{IF}) is the moment per unit weight obtained by dividing the maximum moment range by the gross vehicle weight of the fatigue truck. The magnitude of this parameter depends on bridge configuration, location of fatigue-prone details, and fatigue truck configuration. In a fatigue evaluation, the best estimate of the influence factor is assumed. A lognormal distribution with a 3 percent coefficient of variation will be used in the fatigue reliability model (Moses *et al*., 1987).

Girder distribution factor (GDF) is defined as a ratio of the load effect in a girder and the total moment or shear force. The girder distribution factor can be applied to one-dimensional-analysis moment to obtain the moment or shear value per girder. In the AASHTO Standard Specifications (1996), the girder distribution factor is defined as a function of girder spacing only. The formula is simple but provides conservative estimates for long spans and large girder spacings. However, it has been shown that the formulas provided in the AASHTO LRFD Specifications (1994, 1998), can provide a more accurate estimate and has a biased value close to 1.0 (Nowak and Szerszen, 1996). Therefore, the suggested use for this formula is to determine a mean value of the girder distribution factor. The study performed by Schilling (1982) has demonstrated that the girder distribution factor is generally in the range of 0.21 to 0.52 for steel bridge structures. Moses *et al*. (1987) suggested that the girder distribution factor had a lognormal distribution with a 13 percent coefficient of variation for the simplified

formula, and a 7 percent coefficient of variation for more rigorous methods, such as finite element methods.

Dynamic load factor or impact factor is defined as a random variable, I, in the fatigue limit state function. The magnitude of this parameter is a function of road surface roughness, bridge configuration, and dynamic characteristics of vehicle. In the study performed by Nowak and Zhou (1985), a dynamic load model was developed based on special simulation and test results of 22 bridges. The weights of test vehicles ranged from 54 kips to 130 kips. It was shown that the dynamic load factor in steel bridge structures could be modeled reasonably as a lognormal distribution with a mean value in a range of 0.08 to 0.20 with an average value of 0.14. A standard deviation was found to be in a range of 0.05 to 0.20 with an average value of 0.10. However, based on the simulations (Hwang and Nowak, 1991) and field measurements (Nassif and Nowak, 1995), a mean value of 15 percent and an 80 percent coefficient of variation were suggested for the dynamic load factor (Nowak and Szerszen, 1996). It should be noted that the AASHTO Specifications (1998) also use a 15 percent dynamic load factor for fatigue and fracture limit states.

The headway factor H is a random variable that reflects an increase in stress range due to the presence of multiple trucks on a bridge. The magnitude of this parameter is a function of traffic volume, a relative size of the population of cars and trucks, road grade, and traffic patterns or driving habits (Nyman and Moses, 1985; Raju *et al*., 1990). This parameter can be obtained from a simulation of WIM database. Generally, the headway factor increases as the traffic volume and bridge span increase. From simulation of several bridge spans and types, Nyman and Moses (1985) concluded that the headway factor has a mean value of 1.03 and a coefficient of variation of 0.6 percent.

The elastic section modulus is defined as a random variable (S_x) in the limit state function. It is assumed that S_x is obtained using the best estimate of the cross sectional properties; therefore, a biased value of this parameter is equal to 1.0. This parameter can be modeled reasonably as a lognormal distribution with a 10 percent coefficient of variation (Moses *et al*., 1987).

A statistical summary of the parameters in the limit state function is provided in Table 4.3. These values will be used in the proposed fatigue reliability model and in developing a safety factor for fatigue evaluation.

4.4. Sensitivity Study and Omission Factor

A sensitivity study can be used to reveal the relative importance of parameters in a limit state function. Correspondingly, the mean values and coefficients of variation of parameters in the fatigue reliability model were varied in the sensitivity study.

The original values used in the sensitivity study are summarized in Table 4.4. The ADTT shown in the table is average daily truck traffic at the first year of service. Based on the provided ADTT, traffic growth rate, and maximum highway capacity, the $ADTT_{ave}$ for a given fatigue life can be calculated.

In Case A, an effective stress range is assumed to be obtained from a spectrum analysis of strain gage data. Case A was used to study a variation influence of the following parameters: traffic growth rate (r), fraction of truck traffic in a single lane (p), percent truck traffic, a ratio of the variable to constant amplitude fatigue limits, Miner's rule uncertainty (Δ), fatigue category details, ADTT, and effective stress range (S_{re}).

In Case B, a fatigue truck analysis is assumed to be used in a fatigue evaluation. The parameters defined for this case were used to study a variation influence of the fatigue truck gross weight (W), girder distribution factor (GDF), dynamic load factor (I), and headway factor (H). The reliability indexes corresponding to the values provided in Table 4.4 and fatigue lives in a range of 15 to 75 years were determined, as each parameter was varied.

The variation results of deterministic parameters in the fatigue limit state function are graphically presented in Figure 4.1. Figures 4.2 and 4.3 illustrate an influence of the variation in means and coefficients of variation of the probabilistic parameters. These results were calculated by using the Rackwitz-Fiessler method. An extension of the S-N line was used to obtain most of the results. However, a variable amplitude fatigue limit concept was employed to study the sensitivity of the reliability index to a variation of the

variable amplitude fatigue limit. Based upon the sensitivity study, the following observations can be noted:

- It has been shown in Figure 4.1 that among deterministic parameters, variations in the fraction of truck traffic and percent truck traffic have a relatively small effect on the estimated fatigue life when compared with the variation effects of traffic growth rate and ratio of the variable amplitude fatigue limit to the constant amplitude fatigue limit.
- As a selected reliability index increases, the computed fatigue life tends to be less sensitive to a traffic growth rate and a ratio of the variable amplitude fatigue limit to the constant amplitude fatigue limit.
- A variable amplitude fatigue limit plays an important role in a fatigue evaluation when a large portion of the stress range distribution is below the constant amplitude fatigue limit. In the AASHTO Specifications (1998), the variable amplitude fatigue limit is assumed to be a stress range level at one-half of the constant amplitude fatigue limit. However, if an actual maximum stress range is selected, the ratio of the variable amplitude fatigue limit to the constant amplitude fatigue limit will generally be less than 0.5.

The Rayleigh distribution has been shown to be an appropriate representative of the stress range spectra caused by truck traffic loadings in many cases (Fisher *et al*., 1983 and 1993). For this one-parameter distribution, a cumulative probability between threshold and twice of the effective stress range is approximately equal to 99.2 percent. Therefore, a stress range level of the variable amplitude fatigue limit equal to half of the constant amplitude fatigue limit seems to be a reasonable value, if no further information is available.

In the fatigue reliability model, a finite fatigue life can be obtained even when an effective stress range is less than the variable amplitude fatigue limit. However, as the variable amplitude fatigue limit increases in comparison with the effective stress range, the estimated fatigue life tends to increase rapidly. This effect seems to be dramatic, especially when the reliability index decreases.

- As shown in Figure 4.2, variations of the mean values of the dynamic load factor and the headway factor have relatively small effects on the estimated fatigue life when compared with the other probabilistic parameters.
- As the selected reliability index decreases, the estimated fatigue life will be less sensitive to a variation in the mean value of ADTT at the first year of service. This is because for long fatigue life, the estimated truck traffic will reach the maximum highway capacity causing less difference in a total number of truck passages for each ADTT.
- As shown in Figure 4.3, the estimated fatigue life was not found to be sensitive to changes in the coefficient of variation of the fatigue truck gross weight and the girder distribution factor.
- The estimated fatigue life tends to be less sensitive to a variation in the coefficients of variation of the effective stress range and Miner's rule uncertainty (Δ), as the selected reliability index decreases.

Although, the sensitivity of the reliability index to coefficients of variation of ADTT, the number of cycles per passage (NC), and the headway factor (H) are not included in Figure 4.3, it will be shown later that the fatigue life is not particularly sensitive to uncertainties in these parameters.

The omission factor study can be used to identify the parameters that can be reasonably assumed as deterministic, while a specified level of accuracy still remains. An omission factor is defined as a ratio of the reliability index when the parameter being considered is replaced by a deterministic value, generally its median, and the reliability index when all parameters in the limit state function are modeled as probabilistic (Madsen, 1988). The original parameters provided in Table 4.4 were used in the omission factor study. The omission factors of selected parameters in the fatigue limit state function are summarized in Tables 4.5 and 4.6 for Cases A and B, respectively.

The results indicate that the omission factors of ADTT, number of cycles per truck (NC), and headway factor (H) are close to 1.0. Therefore, they can be reasonably modeled as deterministic parameters in the fatigue reliability model. However, the

probabilistic values of these parameters will be used in developing a safety factor for fatigue evaluation so that a more accurate result can be obtained.

4.5. Safety Factor for Fatigue Evaluation

A safety factor is generally used in design and evaluation codes to account for uncertainties inherent in load intensity, material strength, and assumptions used in the structural analysis. It can be employed in a fatigue evaluation to ensure that a certain level of safety is achieved without requiring a computational effort associated with the fatigue reliability concept. By utilizing a safety factor, the fatigue evaluation formulation can be expressed in terms of deterministic parameters. The safety factor for fatigue evaluation was developed based on the fatigue reliability model and parameter database presented in Sections 4.2 and 4.3.

A selected level of safety must be first defined. In the AASHTO Fatigue Guide Specifications (1990), two levels of safety were used to account for structural redundancy. The targeted probabilities that actual fatigue life exceeds the calculated fatigue life were selected to be 97.7 percent for redundant members and 99.9 percent for non-redundant members. These probabilities correspond to the reliability indexes equal to 2 and 3, respectively. A higher level of safety was applied to the non-redundant members because of the higher consequences of failure that were expected for these members. However, the structural redundancy concept has been excluded from the fatigue consideration in the AASHTO LRFD Specifications (1998). Only allowable stress ranges associated with the redundant members previously specified in the old design code provisions remain, and they are now to be used for both redundant and non-redundant members. This is because greater fracture toughness is specified for the non-redundant members. As a result, using both higher level of safety in the fatigue calculation and the greater fracture toughness could have constituted an unnecessary double penalty for the non-redundant members (Fisher *et al.*, 1998). To be consistent with the safety level used for a fatigue limit state in the AASHTO Specifications (1998), a level of safety corresponding to a reliability index equal to 2 was selected for this study.

Two methodologies regarding a fatigue limit consideration are generally used in a fatigue evaluation. An extension of S-N line approach is employed when a fatigue limit does not exist. For this methodology, all stress range levels in a variable amplitude spectrum contribute to the fatigue damage accumulation. As a result, this procedure always provides a finite fatigue life. However, as the fatigue limit is included in the fatigue calculation, structures are generally assumed to have an infinite fatigue life when all applied stress ranges are less than the constant amplitude fatigue limit.

The safety factor associated with both the extension of S-N line approach and the variable amplitude fatigue limit concept was investigated. The structural fatigue life is assumed to be infinite when the variable amplitude fatigue limit concept is used and an effective stress range (best estimate) is less than half of the nominal constant amplitude fatigue limit. This assumption is consistent with the AASHTO Specifications (1998). In addition to the fatigue limit consideration, several alternatives can be employed to estimate the effective stress range at the fatigue critical details. However, they are associated with different levels of uncertainty. Therefore, different safety factors must be assigned for these alternatives so that a uniform targeted level of safety can be obtained. In the study, the values of the safety factor were derived from a parametric study of the fatigue limit state function. The statistical values summarized in Tables 4.2 and 4.3 were utilized in the calculation. Each parameter in the limit state function was varied in a range of applications.

Strain gage instrumentation is one of the alternatives that can be utilized to estimate the effective stress range. The effective stress range obtained from this alternative is assumed to have a lognormal distribution with a 9 percent coefficient of variation in the fatigue reliability model (see Table 4.3). The parameter variations for this alternative are shown in Table 4.7. A total of 10 cases were examined. For each case, one of the parameters in the limit state function was varied from Case 1. The average daily truck traffic at the first year of service is represented by ADTT in the table. The stress ranges for each case were varied from 0.5 to 60 ksi with a 0.5-ksi increment; for an actual measurement the effective stress range would be inferred using strain data. Although high stress range levels are not expected to occur in typical steel bridge structures, they were,

however, included in the parametric study to reveal the required values of the safety factor over a range of stress ranges.

In addition, the effective stress range can be obtained from a product of the fatigue truck gross weight (W), moment range influence factor (M_{IF}), girder distribution factor (GDF), dynamic load factor (I), headway factor (H), and section modulus (S_x) when an analysis of the fatigue truck is used in the evaluation. The gross weight of the fatigue truck can be determined from the following alternatives: a 54-kip gross weight of the AASHTO fatigue truck, weigh station data, WIM measurements, and traffic count data. Table 4.8 shows the parameter variations for these alternatives. For each case number, the fatigue lives corresponding to each detail category and each coefficient of variation of the girder distribution factor (13 percent and 7 percent) were determined. The influence factors were varied from 2 to 40 kip-ft/kip with a 0.5-kip-ft/kip increment. These influence factors correspond to the moments caused by the AASHTO fatigue truck at the midspan of simple beam members with 20-ft to 190-ft span lengths. The maximum assumed girder distribution factor was equal to 0.5 in Case 14. This girder distribution factor is relatively close to the maximum value of 0.52 observed by Schilling (1982). A 15 percent dynamic load factor was used for all cases, which is equivalent to the value specified in the AASHTO LRFD Specifications (1998) for the fatigue limit state.

A computer program was developed in Microsoft Visual Basic software to calculate the total fatigue lives corresponding to the input parameters in Tables 4.7 and 4.8 and the target safety level of 97.7 percent. The statistical values provided in Tables 4.2 and 4.3 and the Rackwitz-Fiessler procedure was employed in the program. The required safety factors (R_s) were then calculated by using Eq. 4.7 for an extension of S-N line approach and Eq. 4.8 for the variable amplitude fatigue limit concept:

$$N = \frac{A}{(R_s S_{re})^3} \tag{4.7}$$

$$N = \frac{A}{(R_s S_{re})^3 - VAFL^3} \tag{4.8}$$

where N is the fatigue life (cycles) obtained from the fatigue reliability analysis, A is the constant for a given fatigue detail (Table 4.2), VAFL is the nominal variable amplitude fatigue limit (half of the nominal constant amplitude fatigue limit), and S_{re} is the estimated effective stress range provided by each alternative. Because a safety factor is utilized, all parameters in Eq. 4.7 and 4.8 are deterministic.

For the strain gage instrumentation approach, the estimated effective stress range (S_{re}) is unbiased and equal to the mean effective stress range provided in Table 4.7. However, for the other alternatives, S_{re} can be determined from Eq. 4.9, where M_{IF}, GDF, I, and S_x are equal to the mean values provided in Table 4.8. The gross weight of the fatigue truck (W) in Eq. 4.9 is an estimate obtained from one of the aforementioned alternatives and can be computed by dividing the actual effective gross weight in Table 4.8 by the biased value of each alternative in Table 4.3. Also, note that the headway factor (H) is not used in Eq. 4.9. This is because the headway factor is implicitly included in the safety factor used in the fatigue life calculation.

$$S_{re} = \frac{W \times (M_{IF}) \times GDF \times (1 + I)}{S_x} \tag{4.9}$$

Figure 4.4 graphically presents the safety factors required to achieve the target level of safety of 97.7 percent for stress range produced by use of strain gage instrumentation, AASHTO fatigue truck, or traffic count data when an extension of S-N line approach is used in the fatigue calculation. In this figure, a 13 percent coefficient of variation was assumed for the girder distribution factors. The results indicate that the safety factors are relatively constant over a wide envelope of stress ranges. The safety factors of categories A and E are slightly different from the safety factors of the other fatigue categories, mainly due to the difference in the coefficients of variation of each fatigue detail category.

The safety factors corresponding to a variable amplitude fatigue limit concept for the stress range by strain gage instrumentation, AASHTO fatigue truck, or traffic count data are presented in Figure 4.5. Again, a 13 percent coefficient of variation was used for

the girder distribution factors in this figure. As mentioned earlier, structures are assumed to have infinite fatigue life when the effective stress range (best estimate) is less than a variable amplitude fatigue limit; therefore, only effective stress ranges greater than or equal to half of the constant amplitude fatigue limit are presented in the figure. It has been found that as stress ranges increase, the safety factors of all categories tend to approach constant values, which are equal to the safety factors of an extension of the S-N line approach. However, the safety factors decrease as the effective stress ranges approach the variable amplitude fatigue limit.

An average safety factor for all fatigue detail categories was determined for each alternative. Figure 4.6 shows the average safety factor for a variable amplitude fatigue limit concept with a 13 percent coefficient of variation for the girder distribution factors. It has been found that a ratio of the safety factor for each alternative and the safety factor for the AASHTO fatigue truck case is relatively constant over a range of stress ranges for both the extension of the S-N line approach and the variable amplitude fatigue limit concept. Therefore, it is reasonable to develop a formula for the safety factor of the AASHTO fatigue truck case and apply additional factors to this safety factor for the other alternatives, as shown in Eq. 4.10:

$$R_s = R_{so} F_{s1} F_{s2} F_{s3} \tag{4.10}$$

where R_{so} is a basic safety factor for the AASHTO fatigue truck case, F_{s1} is a factor for strain gage instrumentation, F_{s2} is a factor accounting for the approach used to calculate the effective gross weight (WIM measurement, weigh station data, or traffic count data), and F_{s3} is a factor for the procedure used to determine the girder distribution factor. A formula similar to Eq. 4.10 is also used in the AASHTO Fatigue Guide Specifications (1990).

Based on the results obtained from the parametric study, R_{so} is equal to 1.29 when an extension of S-N line approach is used in the calculation. However, R_{so} is not constant for a wide distribution of stress ranges for the variable amplitude fatigue limit concept. Therefore, the best-fit curves of R_{so} provided by bilinear, polynomial, and exponential

functions were determined by utilizing the least-squares method. The R-squared value and maximum percent error of each function are presented in Table 4.9, and the various curves are shown in Figure 4.7. Although the exponential function provides the best fit of R_{so}, the R-squared values and maximum percent errors obtained from each function are relatively close. Therefore, the bilinear function is selected for simplification purposes.

To achieve a uniform targeted level of safety for all alternatives, the values of F_{s1}, F_{s2}, and F_{s3} must be determined. They can be obtained from a ratio of the safety factor required for the selected safety level of 97.7 percent of the considered alternative and the safety factor of the AASHTO fatigue truck (R_{so}). The values of these parameters are summarized in the following:

- F_{s1} = 0.83 when using strain gage instrumentation
- F_{s2} = 0.97 when using WIM measurement
  = 1.00 when using weigh station information
  = 1.07 when using traffic count data with average gross weights obtained from an investigated site or other similar highways
  = 1.28 when using traffic count data with statewide average gross weights
- F_{s3} = 0.96 when using rigorous method to determine a girder distribution factor

It should be noted that the actual value of F_{s2} for the weigh station case is equal to 1.01; however, the value equal to 1.00 was selected. In addition, unless addressed in the above cases, F_{s1}, F_{s2}, and F_{s3} are equal to 1.0.

4.6. Sample Calculation

An application of the developed safety factor is illustrated in the following two examples. It is assumed that effective stress ranges are obtained from strain gage

instrumentation in the first example and WIM measurements in the second example. The total fatigue lives were calculated by utilizing the developed safety factor and then compared with the estimates provided by the AASHTO Fatigue Guide Specifications (1990). The actual levels of safety corresponding to the computed fatigue lives are also presented.

4.6.1. Example 1

In this example, the fatigue strength of a stiffener-to-web connection in a steel plate girder bridge is evaluated. Strain gage instrumentation is used to examine the structural response of the bridge structure under routine truck traffic. Based upon the strain data collected near the stiffener detail, the nominal bending stresses at the end of the stiffener weld are inferred from linear-elastic response. After decomposing the recorded stress history with the rainflow counting method, the effective stress range at the transverse stiffener-to-flange fillet welds is found to be 7 ksi. This connection is classified as a category C′ detail per AASHTO (1998).

It is assumed that average daily truck traffic over the entire service life ($ADTT_{ave}$) is equal to 2500, and there is one traffic lane in each direction. The number of cycles per truck passage is equal to 1.0. Based on the provided information, total fatigue life corresponding to various fatigue limit concepts will be determined for the stiffener detail.

Because the effective stress range is obtained from strain gage instrumentation, the values of F_{s1}, F_{s2}, and F_{s3} are equal to 0.83, 1, and 1, respectively. For the C′ AASHTO fatigue category, the intercept of the nominal S-N line is $4.446(10)^9$ ksi^3, and the constant amplitude fatigue limit is 12 ksi (see Table 4.2). The fraction of the truck traffic in a single lane (p) is equal to 1 (see Table 4.1).

a) Extension of the S-N line

Based upon the variable discussed previously, the value of R_s can be computed as follows:

$R_{so} = 1.29$ and $R_s = R_{so}F_{s1}F_{s2}F_{s3} = 1.29 \times 0.83 \times 1 \times 1 = 1.07$

By using Eq. 4.7, $N = \frac{A}{(R_s S_{re})^3}$

$$N = \frac{4.446 \times 10^9}{(1.07 \times 7)^3} = 10.58 \times 10^6$$

Calculate the total fatigue life in years:

$$t = \frac{N}{ADTTave \times 365 \times p} = \frac{10.58 \times 10^6}{2500 \times 365 \times 1} = 11.6 \text{ years}$$

Based on the provided information and the statistical database in Section 4.3, the reliability index corresponding to the estimated fatigue life of 11.6 years is equal to 1.93. This reliability index provides a 97.3 percent confidence level that the actual fatigue life will exceed the calculated fatigue life.

b) Variable amplitude fatigue limit

Assuming that the bilinear curve for R_{so} is used, and since $\frac{S_{re}}{CAFL} = \frac{7}{12} = 0.583$ is greater than 0.50 but less than 1.22, then:

$$R_{so} = 0.05 \times \frac{S_{re}}{CAFL} + 1.229$$

$$R_{so} = 0.05 \times \frac{7}{12} + 1.229 = 1.258$$

Therefore, $R_s = R_{so}F_{s1}F_{s2}F_{s3} = 1.258 \times 0.83 \times 1 \times 1 = 1.044$

By using Eq. 4.8, $N = \frac{A}{(R_s S_{re})^3 - (VAFL)^3}$

$$N = \frac{4.446 \times 10^9}{(1.044 \times 7)^3 - (0.5 \times 12)^3} = 25.51 \times 10^6$$

Calculate the total fatigue life in years:

$$t = \frac{N}{ADTTave \times 365 \times p} = \frac{25.51 \times 10^6}{2500 \times 365 \times 1} = 28.0 \text{ years}$$

Based on the provided information and the statistical database in Section 4.3, the reliability index corresponding to the estimated fatigue life of 28.0 years is equal to 2.29. This reliability index provides a 98.9 percent confidence level that the actual fatigue life will exceed the calculated fatigue life.

c) AASHTO Fatigue Guide Specifications (1990)

The AASHTO Fatigue Guide Specifications (1990) use a similar formula as Eq. 4.10 to determine the safety factor. For strain gage instrumentation, R_{so} and F_{s1} are equal to 1.35 and 0.85, respectively. It should be noted that the AASHTO Specifications (1990) used an extension of S-N line approach in the code calibration.

Therefore, $R_s = R_{so}F_{s1}F_{s2}F_{s3} = 1.35\times0.85\times1\times1 = 1.148$

By using Eq. 4.7, $N = \dfrac{A}{(R_s S_{re})^3}$

$$N = \frac{4.446\times10^9}{(1.148\times7)^3} = 8.57\times10^6$$

Calculate the total fatigue life in years:

$$t = \frac{N}{ADTTave\times365\times p} = \frac{8.57\times10^6}{2500\times365\times1} = 9.4 \text{ years}$$

For the illustrated example, the AASHTO Specifications (1990) and the developed safety factor for an extension of the S-N line approach provide fairly similar estimates of the fatigue life. However, the variable amplitude fatigue concept predicts a fatigue life considerably longer - roughly three times longer - than the extension of S-N line approach.

4.6.2. Example 2

For the second example, assume that a 60-kip effective gross weight is estimated at the bridge structure based on WIM data collected near the bridge site. Moreover,

assume that the most critical fatigue detail in the structure is at the toe of the fillet weld at the end of a cover plate attached to the girder bottom flange, which can be classified as a category E detail per AASHTO (1998). It is assumed that average daily truck traffic over the entire service life ($ADTT_{ave}$) is equal to 2000, and the structure supports two traffic lanes in each direction. The number of cycles per truck passage is taken equal 1.0. A girder distribution factor of 0.30 is obtained from the formula specified in the AASHTO LRFD Specifications (1998). Based on a one-dimensional analytical model, it has been found that a moment range influence factor at the cover plate detail is 20 kip-ft/kip. Based on the cross sectional dimensions, the section modulus is equal to 1300 in^3. A 15 percent dynamic load factor is assumed at the investigated site.

In this example, F_{s1}, F_{s2}, and F_{s3} are equal to 1, 0.97, and 1, respectively because the effective gross weight is obtained from the WIM data and a simplified formula is used to determine the girder distribution factor. The intercept of the nominal S-N line is $1.072(10)^9$ ksi^3 for the E category fatigue detail, and the nominal constant amplitude fatigue limit is 4.5 ksi (see Table 4.2). The fraction of the truck traffic in a single lane (p) is equal to 0.85 for two-lane traffic (see Table 4.1).

a) Extension of the S-N line

$R_{so} = 1.29$ and $R_s = R_{so}F_{s1}F_{s2}F_{s3} = 1.29\times1\times0.97\times1 = 1.25$

Determine the effective stress range level at the category E fatigue detail:

$$S_{re} = \frac{W \times (M_{IF}) \times GDF \times (1+I)}{S_x}$$

$$S_{re} = \frac{60 \times (20\times12) \times 0.3 \times (1+0.15)}{1300} = 3.82 \text{ ksi}$$

By using Eq. 4.7, $N = \frac{A}{(R_s S_{re})^3}$

$$N = \frac{1.072\times10^9}{(1.25\times3.82)^3} = 9.85\times10^6$$

Calculate the total fatigue life in years:

$$t = \frac{N}{ADTT_{ave} \times 365 \times p} = \frac{9.85 \times 10^6}{2000 \times 365 \times 0.85} = 15.9 \text{ years}$$

The reliability index corresponding to the estimated fatigue life of 15.87 years is equal to 1.82, which provides a 96.6 percent confidence level that an actual fatigue life will exceed the calculated fatigue life.

b) Variable amplitude fatigue limit

$$R_{so} = 0.05 \times \frac{S_{re}}{CAFL} + 1.229$$

$$R_{so} = 0.05 \times \frac{3.82}{4.5} + 1.229 = 1.27$$

Therefore, $R_s = R_{so}F_{s1}F_{s2}F_{s3} = 1.27 \times 1 \times 0.97 \times 1 = 1.23$

By using Eq. 4.8, $$N = \frac{A}{(R_s S_{re})^3 - (VAFL)^3}$$

$$N = \frac{1.072 \times 10^9}{(1.23 \times 3.82)^3 - (0.5 \times 4.5)^3} = 11.61 \times 10^6$$

Calculate the total fatigue life in years:

$$t = \frac{N}{ADTTave \times 365 \times p} = \frac{11.61 \times 10^6}{2000 \times 365 \times 0.85} = 18.7 \text{ years}$$

The reliability index corresponding to the estimated fatigue life of 18.71 years is equal to 1.81, which provides a 96.5 percent confidence level that an actual fatigue life will exceed the calculated fatigue life.

c) AASHTO Fatigue Guide Specifications (1990)

For the WIM measurement, R_{so} and F_{s2} are equal to 1.35 and 0.95, respectively (AASHTO, 1990).

Therefore, $R_s = R_{so}F_{s1}F_{s2}F_{s3} = 1.35\times1\times0.95\times1 = 1.28$

By using Eq. 4.7, $$N = \frac{A}{(R_s S_{re})^3}$$

$$N = \frac{1.072\times10^9}{(1.28\times3.82)^3} = 9.17\times10^6$$

Calculate total fatigue life in years:

$$t = \frac{N}{ADTTave\times365\times p} = \frac{9.17\times10^6}{2000\times365\times0.85} = 14.8 \text{ years}$$

Similar to the previous example, the AASHTO Specifications (1990) provide a fatigue life relatively close to the developed safety factor for an extension of the S-N line approach. In addition, the calculated fatigue life increases when a variable amplitude fatigue limit is included in the calculation.

A Category E fatigue detail is assumed in this example to illustrate the minimum level of safety that can be obtained from the developed safety factor. As shown in Figures 4.4 and 4.5, actual safety factors required for category E are slightly higher than the other categories in most cases. Therefore, the developed safety factor, which is an average of the required safety factors of all categories, tends to provide the least conservative estimate of the fatigue life for fatigue category E. In this example, the probabilities of survival of 96.6 and 96.5 percent were obtained from the safety factors for an extension of the S-N line approach and the variable amplitude fatigue limit concept, respectively. These probabilities of survival are still relatively close to the target confidence level of 97.7 percent.

4.7. Summary

A fatigue reliability model has been developed based on a review of previous research studies on fatigue load and resistance parameters, as well as the analysis results of the vehicle database in Chapter 3. The proposed reliability model can incorporate

information obtained from an inspection at a specific site. An application of the fatigue reliability model and traffic count data in a fatigue evaluation will be illustrated in Chapter 5. In addition, the influences of various parameters in the fatigue limit state function were investigated using sensitivity and omission factor studies. The results indicate that the fatigue life is not sensitive to uncertainty inherent in the ADTT, the number of cycles per passage, and the headway factor. Also, it has been demonstrated that a variable amplitude fatigue limit concept can provide a considerably longer fatigue life than a simple extension of the S-N line. However, this effect is minimized as the selected level of safety and the effective stress range increase.

A safety factor for the fatigue evaluation of bridge details was developed based on the proposed fatigue reliability model. Its application has been demonstrated through two calculation examples. In addition to the procedure provided in the AASHTO Fatigue Guide Specifications (1990), the safety factors corresponding to a variable amplitude fatigue limit concept and the use of traffic count data are introduced.

Table 4.1 – Fraction of Truck Traffic in a Single Lane (p) (AASHTO, 1998)

Number of Lanes Available to Trucks	p
1	1.00
2	0.85
3 or more	0.80

Table 4.2 – Statistical Data for AASHTO S-N Curves (Moses *et a1*., 1987)

Detail Category	Stress Range at 2×10^6 Cycles		Intercept on The Nominal S-N Lines ($A = 10^b$)	C.O.V (%)	Fatigue Limit Stress Range	
	Mean (ksi)	Nominal (95%) (ksi)			Mean (ksi)	Nominal (95%) (ksi)
A	33.0	23.2	2.5×10^{10}	21.7	34.1	24.0
B	22.8	18.1	1.191×10^{10}	14.1	20.2	16.0
B'	18.0	14.5	6.109×10^{10}	13.2	14.9	12.0
C	16.7	13.0	4.446×10^{9}	15.3	12.8	10.0*
D	13.0	10.3	2.183×10^{9}	14.2	8.8	7.0
E	9.5	8.1	1.072×10^{9}	9.7	5.3	4.5
E'	7.2	5.8	3.908×10^{8}	13.2	3.2	2.6

* is equal to 12 ksi for transverse stiffener-to-flange and transverse stiffener-to-web fillet welds. These connections are classified as category C/ fatigue details per AASHTO (1998).

Table 4.3 – Summary of Parameters in Fatigue Reliability Model

Parameter	Description	Mean	C.O.V	Distribution
Δ	Uncertainty Miner's Rule	1	0.15	Lognormal
$ADTT_{ave}$	Average ADTT over Entire Fatigue Life	Varies	0.10	Lognormal
NC	Number of Cycles Per Truck	1-5	0.05	Lognormal
p	Fraction of Truck Traffic	0.8-1.0	-	Deterministic
t	Estimated Fatigue Life	-	-	Deterministic
b and VAFL	Fatigue Strength	Table 4.2	Table 4.2	Lognormal
S_{re}	Estimated Eff. Stress Range	Varies	0.09*	Lognormal
W	Estimated Eff. GVW	Biased Value		
	- Case 1: 54-kip AASHTO Fatigue Truck	1	0.10	Lognormal
	- Case2: Weigh Station Data	1.05	0.03	Lognormal
	- Case3: WIM Data	1	0.03	Lognormal
	-Case4: Traffic Count Data			
	with Average GVW of Investigated or Similar Sites	1.1	0.05	Lognormal
	with Statewide Average GVW	1.21	0.15	Lognormal
M_{IF}	Moment Range Influence Factor	Varies	0.03	Lognormal
GDF	Girder Distribution Factor	0.21-0.52	0.07 or 0.13	Lognormal
I	Dynamic Load Factor	0.15	0.80	Lognormal
H	Headway Factor	1.03	0.006	Lognormal
S_x	Section Modulus	Varies	0.10	Lognormal

* is used for the effective stress range computed from a spectrum analysis of strain gage data.

Table 4.4 – Original Parameters Used in Sensitivity Study

Parameter	Type	Mean	C.O.V	Value
Case A : Stress Range Information				
Uncertainty in Miner's Rule (Δ)	Lognormal	1	0.15	-
Effective Stress Range (S_{re}) (ksi)	Lognormal	2.5	0.09	-
Number of Cycles Per Truck (NC)	Lognormal	1	0.05	-
Traffic Growth Rate (r) (%)	Deterministic	-	-	3
ADTT	Lognormal	1000	0.10	-
Max Capacity (Vehicles/Day/Lane)	Deterministic	-	-	20000
Percent Truck (%)	Deterministic	-	-	20
Fatigue Category E	-	-	-	-
Case B : Fatigue Truck Information				
Uncertainty in Miner's Rule (Δ)	Lognormal	1	0.15	-
Influence Factor (M_{IF}) (kip-ft/kip)	Lognormal	4.13	0.03	
Gross Weight (W) (kips)	Lognormal	54	0.10	-
Dynamic Load Factor (I)	Lognormal	0.15	0.80	-
S_x (in^3)	Lognormal	440.43	0.10	-
Girder Distribution Factor (GDF)	Lognormal	0.348	0.13	-
Headway Factor (H)	Lognormal	1.03	0.006	-
Number of Cycles Per Truck (NC)	Lognormal	1	0.05	-
Traffic Growth Rate (r) (%)	Deterministic	-	-	3
ADTT	Lognormal	1000	0.10	-
Max Capacity (Vehicles/Day/Lane)	Deterministic	-	-	20000
Percent Truck (%)	Deterministic	-	-	20
Fatigue Category E	-	-	-	-

Table 4.5 – Omission Factors of Case A: Stress Range Information

Fatigue Life (years)	Reliability Index	Δ	ADTT	NC	b	S_{re}
15	7.37	1.06	1.03	1.00	1.20	1.33
30	5.02	1.06	1.02	1.00	1.21	1.35
45	3.35	1.06	1.02	1.01	1.21	1.37
60	2.02	1.08	1.02	1.01	1.22	1.38
75	1.11	1.08	1.01	1.01	1.24	1.44

Table 4.6 – Omission Factors of Case B: Fatigue Truck Information

Fatigue Life (years)	Reliability Index	Δ	ADTT	NC	b	W	GDF	H
15	3.71	1.01	1.01	1.00	1.02	1.03	1.03	1.00
30	2.89	1.01	1.01	1.00	1.03	1.05	1.05	1.00
45	2.12	1.02	1.01	1.00	1.05	1.08	1.08	1.00
60	1.37	1.02	1.01	1.00	1.06	1.11	1.11	1.00
75	0.82	1.03	1.00	1.00	1.07	1.12	1.12	1.00

Table 4.7 – Parameter Variations for Strain Gage Instrumentation

Case	r	ADTT	p	NC	Percent Truck	Fatigue Details	S_{re} (ksi)	VAFL
1	0.03	1000	0.85	1	0.2	A - E'	0.5-60	0, 0.5CAFL
2	0.01	1000	0.85	1	0.2	A - E'	0.5-60	0, 0.5CAFL
3	0.05	1000	0.85	1	0.2	A - E'	0.5-60	0, 0.5CAFL
4	0.03	100	0.85	1	0.2	A - E'	0.5-60	0, 0.5CAFL
5	0.03	2500	0.85	1	0.2	A - E'	0.5-60	0, 0.5CAFL
6	0.03	1000	0.8	1	0.2	A - E'	0.5-60	0, 0.5CAFL
7	0.03	1000	1	1	0.2	A - E'	0.5-60	0, 0.5CAFL
8	0.03	1000	0.85	2	0.2	A - E'	0.5-60	0, 0.5CAFL
9	0.03	1000	0.85	5	0.2	A - E'	0.5-60	0, 0.5CAFL
10	0.03	1000	0.85	1	0.1	A - E'	0.5-60	0, 0.5CAFL

Table 4.8 – Parameter Variations for AASHTO Fatigue Truck, Weigh Station Information, WIM Measurement, and Traffic Count Data

Case	r	ADTT	p	NC	Percent Truck	Fatigue Details	Influence Factor (kip-ft/kip)	Actual Eff. Gross Wt. (kips)	GDF	I	H	S_x (in^3)	VAFL
1	0.03	1000	0.85	1	0.2	A - E'	2-40	54	0.3	0.15	1.03	400	0, 0.5CAFL
2	0.01	1000	0.85	1	0.2	A - E'	2-40	54	0.3	0.15	1.03	400	0, 0.5CAFL
3	0.05	1000	0.85	1	0.2	A - E'	2-40	54	0.3	0.15	1.03	400	0, 0.5CAFL
4	0.03	100	0.85	1	0.2	A - E'	2-40	54	0.3	0.15	1.03	400	0, 0.5CAFL
5	0.03	2500	0.85	1	0.2	A - E'	2-40	54	0.3	0.15	1.03	400	0, 0.5CAFL
6	0.03	1000	0.8	1	0.2	A - E'	2-40	54	0.3	0.15	1.03	400	0, 0.5CAFL
7	0.03	1000	1	1	0.2	A - E'	2-40	54	0.3	0.15	1.03	400	0, 0.5CAFL
8	0.03	1000	0.85	2	0.2	A - E'	2-40	54	0.3	0.15	1.03	400	0, 0.5CAFL
9	0.03	1000	0.85	5	0.2	A - E'	2-40	54	0.3	0.15	1.03	400	0, 0.5CAFL
10	0.03	1000	0.85	1	0.1	A - E'	2-40	54	0.3	0.15	1.03	400	0, 0.5CAFL
11	0.03	1000	0.85	1	0.2	A - E'	2-40	40	0.3	0.15	1.03	400	0, 0.5CAFL
12	0.03	1000	0.85	1	0.2	A - E'	2-40	80	0.3	0.15	1.03	400	0, 0.5CAFL
13	0.03	1000	0.85	1	0.2	A - E'	2-40	54	0.2	0.15	1.03	400	0, 0.5CAFL
14	0.03	1000	0.85	1	0.2	A - E'	2-40	54	0.5	0.15	1.03	400	0, 0.5CAFL
15	0.03	1000	0.85	1	0.2	A - E'	2-40	54	0.3	0.15	1.03	850	0, 0.5CAFL
16	0.03	1000	0.85	1	0.2	A - E'	2-40	54	0.3	0.15	1.03	1300	0, 0.5CAFL
17	0.03	100	0.85	1	0.2	A - E'	2-40	80	0.5	0.15	1.03	200	0, 0.5CAFL

Table 4.9 – Fitted Curves of R_{so}

Curve #	Equation	Function	R-squared Value	Maximum Error (%)
1	$0.5<=S_{re}/CAFL<=1.22$, $y = ax+b$ $S_{re}/CAFL>1.22$, $y = 1.29$ Where $x = S_{re}/CAFL$ a = 0.050 b = 1.229	Bilinear	0.96	0.36
2	$0.5<=S_{re}/CAFL<=1.5$, $y = ax^2+bx+c$ $S_{re}/CAFL>1.5$, $y = 1.29$ Where $x = S_{re}/CAFL$ a = -0.0325 b = 0.107 c = 1.209	Polynomial	0.98	0.20
3	$0.5<=S_{re}/CAFL<=2$, $y = a-b*\exp(-cx)$ $S_{re}/CAFL>2$, $y = 1.29$ Where $x = S_{re}/CAFL$ a = 1.291 b = 0.142 c = 2.510	Exponential	0.99	0.24

Note: R_{so} is equal to the value y in the table above.

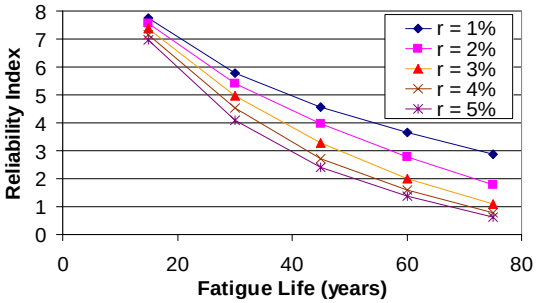

a) Traffic Growth Rate (r)

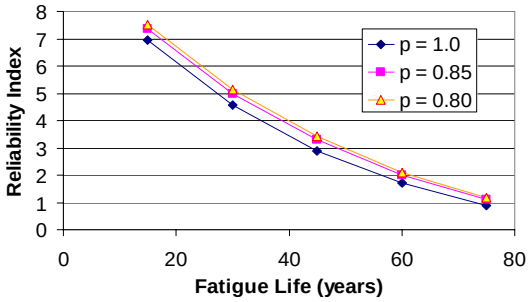

b) Fraction of Truck Traffic (p)

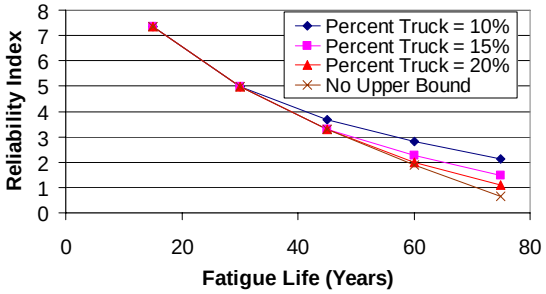

c) Percent Truck Traffic

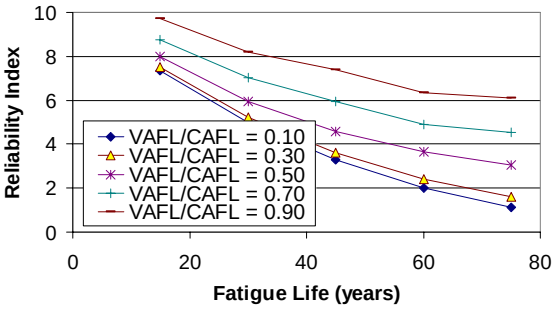

d) Ratio of VAFL and CAFL

Figure 4.1 – Effect of Variation of Deterministic Parameters

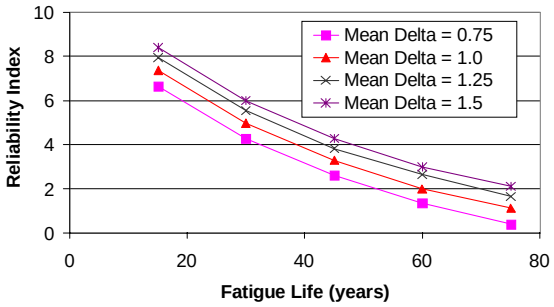

a) Uncertainty in Miner's Rule (Δ)

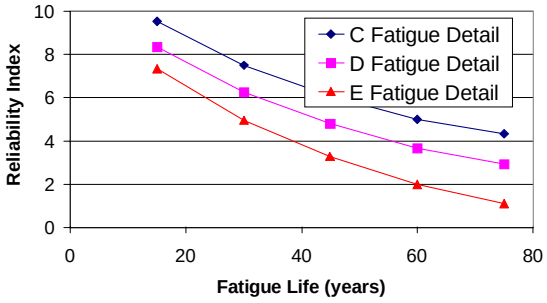

b) Fatigue Category Details

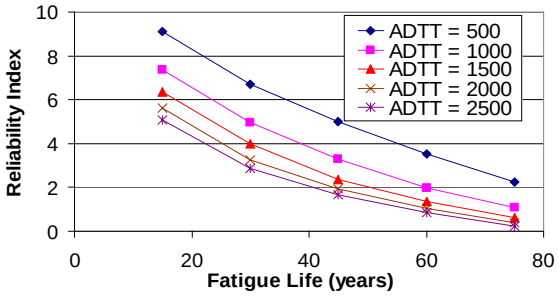

c) ADTT

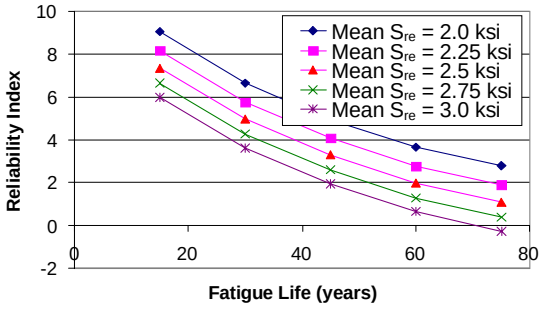

d) Effective Stress Range (S_{re})

Figure 4.2 – Effect of Variation of Mean Value of Probabilistic Parameters

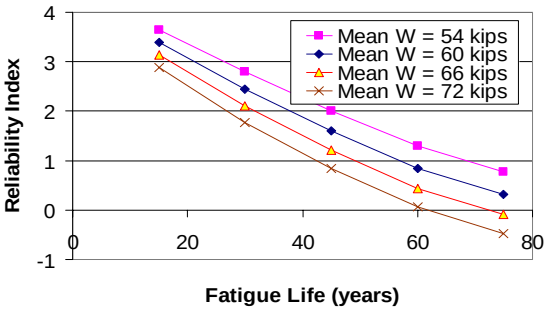

e) Fatigue Truck Gross Weight (W)

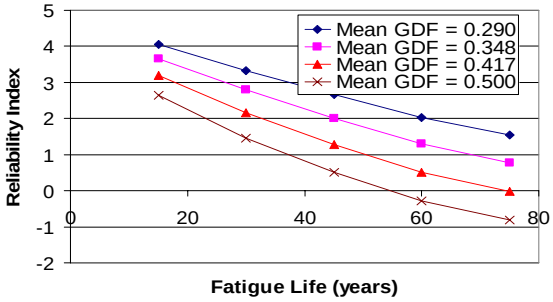

f) Girder Distribution Factor (GDF)

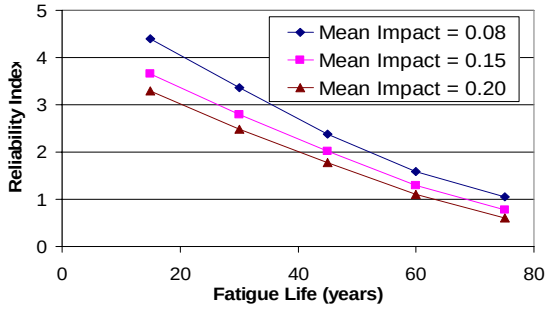

g) Dynamic Load Factor (I)

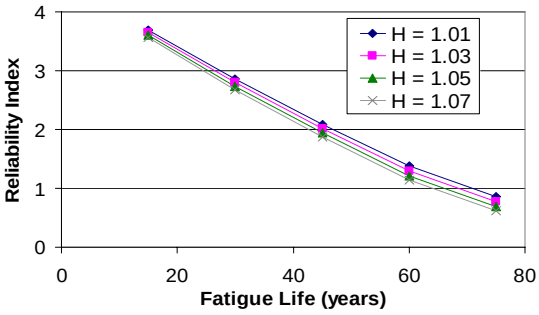

h) Headway Factor (H)

Figure 4.2 (Cont.) – Effect of Variation of Mean Value of Probabilistic Parameters

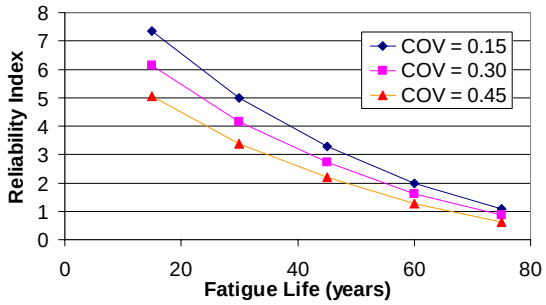

a) Uncertainty in Miner's Rule (Δ)

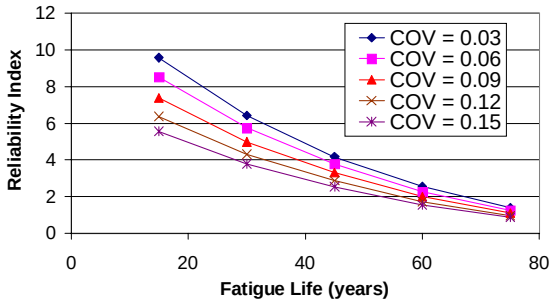

b) Effective Stress Range (S_{re})

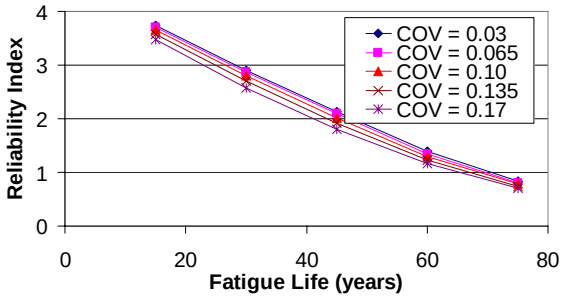

c) Fatigue Truck Gross Weight (W)

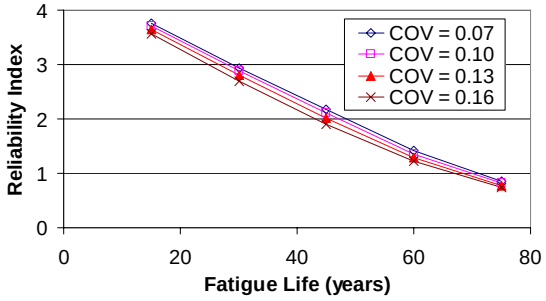

d) Girder Distribution Factor (GDF)

Figure 4.3 – Effect of Variation of C.O.V of Probabilistic Parameters

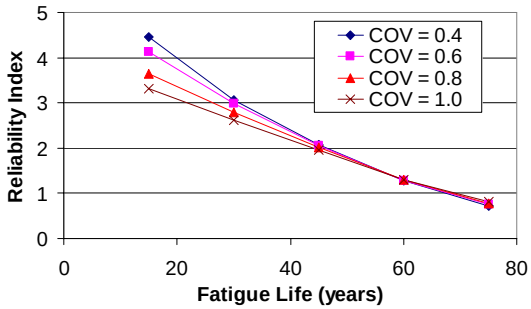

e) Dynamic Load Factor

Figure 4.3 (Cont.) – Effect of Variation of C.O.V of Probabilistic Parameters

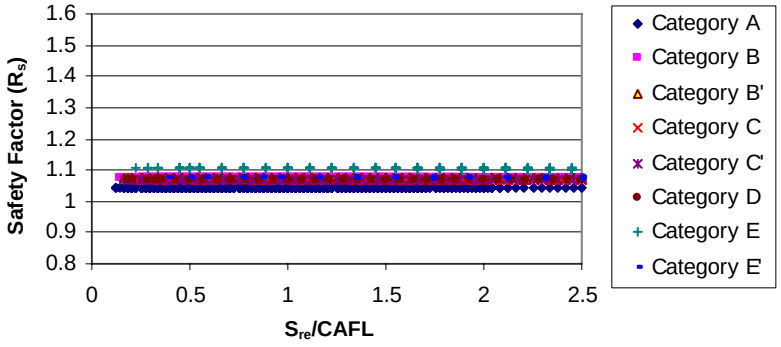

a) Strain Gage Instrumentation

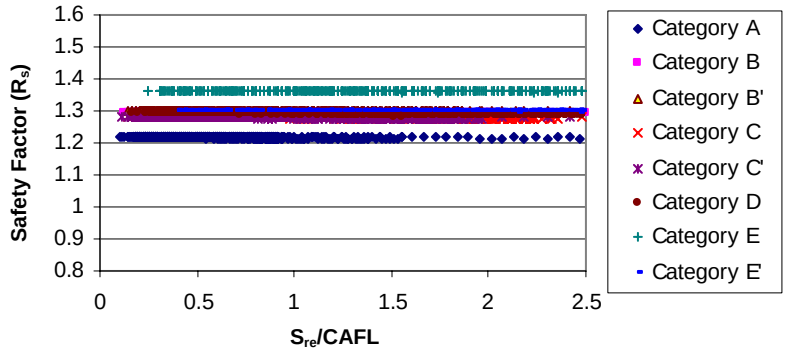

b) AASHTO Fatigue Truck

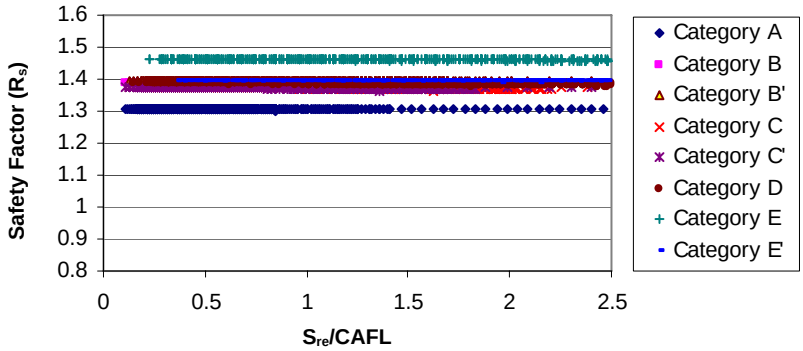

c) Traffic Count Data with Average Gross Weights of Investigated Site

Figure 4.4 – Example of Safety Factors for Extension of S-N Line Approach

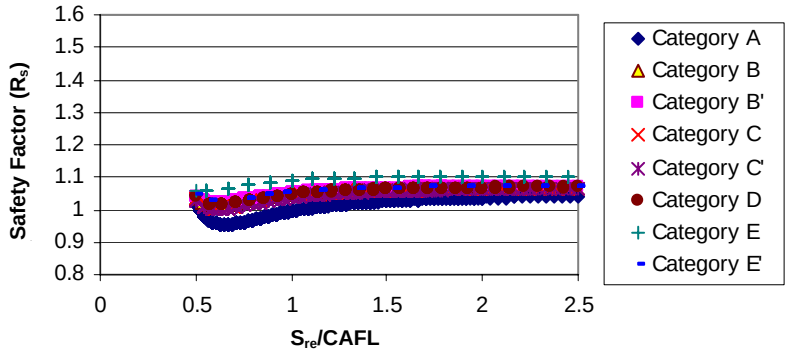

a) Strain Gage Instrumentation

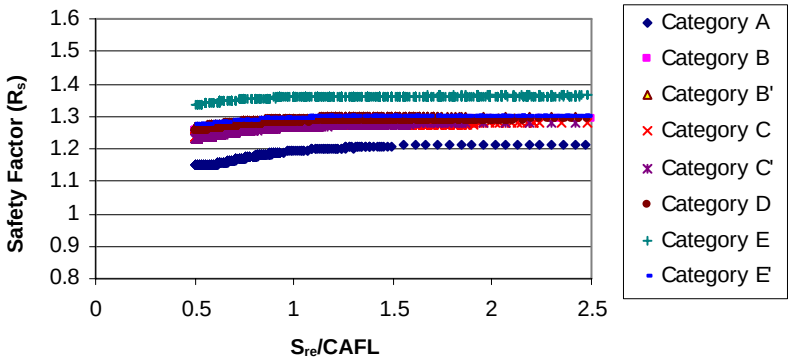

b) AASHTO Fatigue Truck

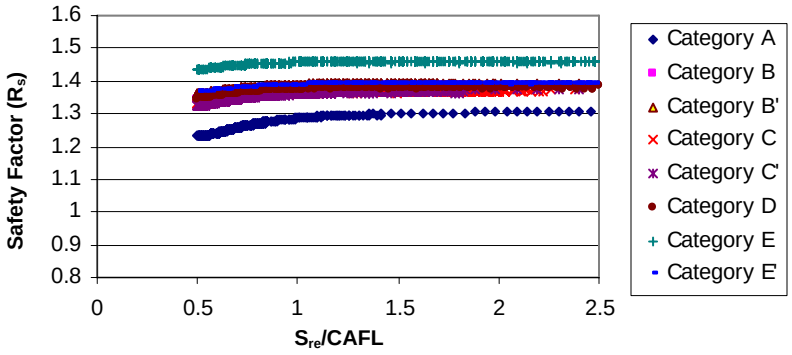

c) Traffic Count Data with Average Gross Weights of Investigated Site

Figure 4.5 – Example of Safety Factors for Variable Amplitude Fatigue Limit Concept

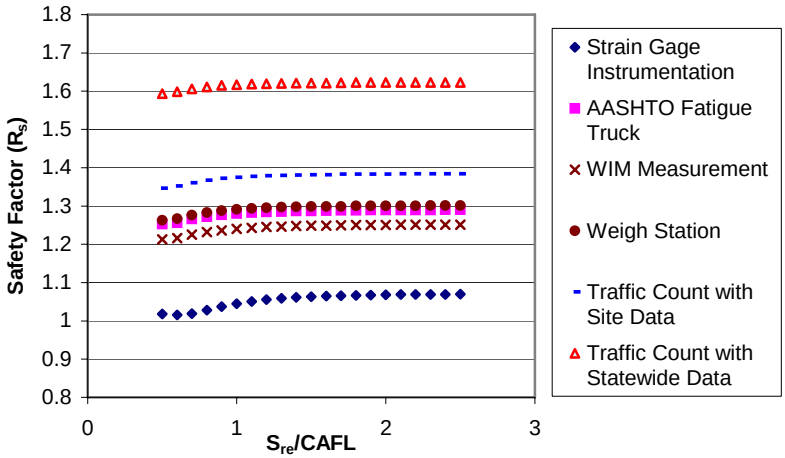

Figure 4.6 – Safety Factor for Variable Amplitude Fatigue Limit Concept

(Use 13 Percent Coefficient of Variation for GDF)

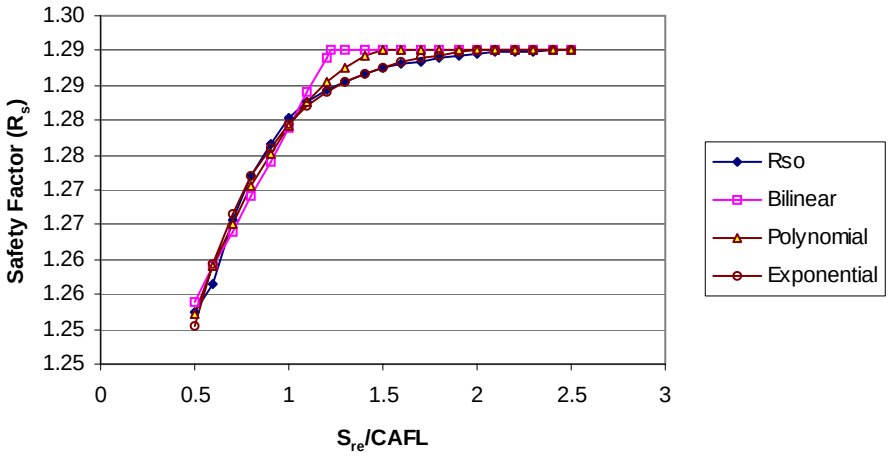

Figure 4.7 – Fitted Curves of R_{so} for Variable Amplitude Fatigue Limit Concept

CHAPTER 5. EXPERIMENTAL PROGRAM AND APPLICATION OF PROPOSED FATIGUE RELIABILITY MODEL

5.1. Introduction

An experimental program was conducted to evaluate the fatigue strength of two steel bridge structures. The first structure is located on U.S. 20 along the extra heavy duty corridor near Michigan City in northwest Indiana. This corridor provides an important route for steel and other manufacturers to transport cargos between northwest Indiana and the state of Michigan. Multi-trailer, multi-axle trucks - generally referred to as "Michigan Trains" - are a typical truck type traveling along this route. Gross weights of the "Michigan Train" trucks can be considerably heavier than trucks typically found on state and interstate highways. The second structure was located on I-65 over the Kankakee River in northwest Indiana. The structure has experienced distortion-induced fatigue cracking in the girder web at several of the diaphragm-to-stiffener terminal welds. A retrofit detail was installed in 1992 to minimize web gap distortion and arrest the cracking that had occurred.

Strain gage instrumentation was used for both structures to monitor stress range levels at the sections of fatigue critical details and to evaluate the overall structural response under routine truck traffic. In addition, a WIM system was installed at the first bridge structure to collect truck traffic data.

Two different cycle counting procedures were utilized to decompose the recorded strain data. The rainflow counting method was employed in the first procedure, while the racetrack method was used in conjunction with rainflow counting in the second procedure. By comparing the cycle counting results obtained from these two procedures, a potential benefit of using the racetrack method to facilitate the cycle counting procedure was examined.

Based upon effective stress ranges obtained from the collected strain gage data, WIM measurement, and traffic count data with the statewide average gross weights provided in Chapter 3, the fatigue lives of the structures were evaluated. The fatigue reliability model described in Chapter 4 and the procedure provided in the AASHTO Fatigue Guide Specifications (1990) were utilized to perform the fatigue life calculation. A comparison of the fatigue lives predicted by these alternative procedures is presented herein.

Additionally, a basic procedure which can be used to perform a fatigue evaluation is discussed. This method, along with the fatigue reliability model, was utilized to evaluate the remaining fatigue lives of an additional twelve steel bridge structures located along various segments of the extra heavy duty corridor. Because strain gage data were not available at these bridge structures, one-dimensional analytical models along with the AASHTO girder distribution factor (AASHTO, 1998) were employed in the fatigue calculation.

5.2. Fatigue Evaluation of U.S.-20 Bridge near Michigan City

The structure was selected among several bridges located along segments of the extra heavy duty corridor. The structure provided good accessibility for installation of strain gages on the members and near the fatigue critical details. The bridge and the instrumentation details are described in much greater detail in Volume 1 of this report. For convenience, the salient features of the bridge field measurements and results are also provided herein.

5.2.1. Structural Description

The bridge structure is located at milepost 37.37 on U.S. 20 over Railroad/Chandler Avenue and an Amtrak rail line in the Town of Pines, IN, near Michigan City, IN. The structure is a ten-continuous-span non-composite steel beam bridge supporting four lanes, two each in eastbound and westbound directions. The bridge has two separate structures, one for each traffic direction. Each structure is

composed of six continuous steel beams with a 9.75-inch concrete deck. A view of the framing plan for the eastbound structure is shown in Figure 5.1. The structure has a total length of 410 ft and a beam spacing of 6.67 ft.

Four different rolled beam sections (WF27x84, WF27x94, WF27x102, and WF27x114) were used as longitudinal members. These sections are connected at each support by bolted splice plates as shown in Figure 5.2. The diaphragms (Type 16B26) are connected perpendicular to the longitudinal members at the middle of each span and at each support to provide lateral stiffness. The diaphragms are attached to the beam web by one of two connection types: either attached directly to the beam web with an intermittent fillet weld (Figure 5.3), or attached with a shear plate that is bolted to the diaphragm and welded to the beam web (Figure 5.4).

In addition to the bolted splice plate and diaphragm connections, the other fatigue critical detail is at an improperly located attachment plate (Figure 5.5). The plate was intended to be used as a shear plate for the diaphragm connection; however, it was installed at a wrong location. Therefore, it was not used and, instead, was simply left intact. The plate is located in the outmost span of beam line 9 at 20.13 ft from the east support.

5.2.2. Instrumentation

Strain gage instrumentation was used to monitor the strain history of the structure under normal truck traffic. In addition, a WIM system was used to collect truck traffic data, including axle weights, axle spacings, gross weights, and truck classifications. The truck traffic data provided crucial information in estimating ADTT and an effective gross weight of the truck distribution, as well as developing the fatigue load model for the investigated structure. From a combination of information obtained from these two systems, a complete scenario of both fatigue loading and bridge response can be obtained.

The strain gage locations were selected in such a way that an overall response of the structure and strain levels at the sections of fatigue critical details could be obtained. Based on previous traffic data, the greatest number of heavy trucks were expected to be

in the eastbound direction. In addition, due to optimum accessibility, the two outmost spans of the eastbound structure were chosen for instrumentation. Forty strain gages were installed at nine sections in both interior and exterior spans of beam lines 8 and 10 and in the exterior span of beam line 9 (see Reisert, 2003). The location and assigned number of each monitored section are shown in Figure 5.6.

The strain gages were installed at the expected maximum moment and diaphragm sections in the interior and exterior spans of beam lines 8 and 10. The location monitored on beam line 9 was at the improperly located attachment plate. The gage locations and numbering scheme are provided in Table 5.1. At each maximum moment section, four strain gages were installed, one located on the bottom of the top flange, two gages located on the web, and one on top of the bottom flange, as shown in Figure 5.7. Six strain gages were installed at each diaphragm section, two gages located on the bottom of the top flange, two gages located slightly under the diaphragms, and two gages located on top of the bottom flange, as shown in Figure 5.8.

Based on a preliminary analysis of the bridge structure, it has been found that a natural frequency of the structure is approximately 5.7 Hz (Reisert, 2003). Therefore, a selected 100-Hz scan rate would be able to capture all peaks and valleys in a strain history. In each span, a trigger channel was set on the bottom flange gage of the maximum moment section. Once the strain level on the trigger channel equaled or exceeded 30 microstrain, the strain data in both maximum moment and diaphragm sections in the corresponding span and beam line were recorded for five seconds, 2.5 seconds before and after reaching the trigger level.

A Campbell Scientific data acquisition system (Model CR 5000) was used in the study to collect the strain results. The system was selected because it provided a remote connection capability and allowed the strain data to be downloaded through a telephone line. The system also provided a sufficient scan rate capability.

The piezoelectric WIM sensors provided by International Road Dynamics (IRD) were installed at a location one-mile west of the bridge structure. (This WIM site is referred in Chapter 3 as Station 001.) The recorded gross weights of trucks traveling across the bridge were found to be as high as 236 kips. The effective gross weight, based

on one-year of truck data, was found to be 75.3 kips. Approximately 16 percent of the truck traffic in the eastbound direction was composed of Class-13 trucks, which are 7-or-more axle multi-trailer trucks. Additional information of the truck traffic characteristics at this site is provided in Chapter 3.

5.2.3. Cycle Counting Results

The strain gage data were collected from December 2001 to May 2002, six months in total. All strain data were decomposed by using two different cycle counting procedures. The rainflow counting method was employed in the first procedure. For the second procedure, the racetrack method with a 20-microstrain track width was used first to condense the recorded strain history. Then, the rainflow counting method was utilized to decompose the remaining strain history.

Stress range levels at all monitored sections were determined based on the cycle counting results and the assumption of a linear stress-strain relationship. Table 5.2 shows the maximum strain ranges observed at the bottom flange gages of the maximum moment sections. The maximum strain range was found to be 255 microstrain at Section # 8. This strain range is well below the yield strain of 1240 microstrain for ASTM A36 steel. Therefore, assuming a reasonably small strain value for dead load, the assumption of a linear stress-strain relationship is valid.

The cycle counting results of strain data recorded over a six-month period at the bottom flange gages on the south side of the diaphragm sections are graphically presented in Figure 5.9. The results revealed that most of the stress range values were less than 3 ksi. Best fit curves of the stress range histograms in Figure 5.9 were determined by utilizing the statistical software SAS. The lognormal, exponential, Rayleigh, and Weibull distributions were used to fit the histograms. Tables 5.3 and 5.4 summarize the mean value, standard deviation, and effective stress range provided by each distribution. The results indicated that the Weibull distribution provided the best fit of stress range histograms and the closest estimates of the effective stress range at all diaphragm sections.

Average stress range and the number of cycles per truck passage at the bottom flange gages of diaphragm sections obtained from the two counting procedures are summarized in Tables 5.5 and 5.6. The one-week cycle counting results of the first two weeks in March and April and the six-month counting results are summarized in the tables. The results indicate that effective stress ranges for each week of data were not significantly different. Among monitored diaphragm sections, the diaphragm located in the exterior span of beam line 10 (Section # 4) had the highest effective stress range. The number of cycles per passage obtained from the rainflow counting method (Procedure # 1) was in the range of 1.24 to 1.85. However, when the racetrack method was used first before performing the cycle count (Procedure # 2), a number of cycles per passage was in a range of 1.15 to 1.53. Although the numbers of cycles per passage provided by the two procedures were different, the effective stress ranges were relatively close. The difference between the effective stress ranges provided by the two counting procedures was found to be less than 7 percent.

5.2.4. Dynamic Load Factor

The dynamic load factor, or impact factor, is an important parameter in a fatigue evaluation. It is used to represent the dynamic response inherent in a strain history. Many definitions have been provided by various researchers to determine the dynamic load factor (McLean and Marsh, 1998). However, in this study, the dynamic load factor was determined from the ratio of the maximum instantaneous dynamic response and maximum static response.

Nassif and Nowak (1995) demonstrated that the dynamic response and an equivalent static response can be obtained from a recorded strain history by employing a signal analysis procedure. The complex strain history, which displays in a time domain, must first be transformed into a frequency domain by using the fast fourier transform (FFT) technique. The strain history can then be represented by using the power spectral density to describe how the power of strain responses is distributed with frequency (Grover and Deller, 1999). An example of the power spectral density of the strain data collected at Section # 4 is presented in Figure 5.10. A cutoff frequency is determined to

define a static frequency response. After eliminating all frequencies above the cutoff level, the equivalent static response present in a time domain can be obtained by employing the invert FFT. By applying this procedure to all recorded events, the distribution of the dynamic load factors can be determined. This procedure can be used to estimate a dynamic response when the strain data from a calibration truck are not available. Therefore, the procedure was used in the present study.

The dynamic load factors calculated from a one-week period of strain data collected from the bottom flange gages on the south side of Sections # 3 and # 4 are shown in Figures 5.11 and 5.12. The cutoff frequency used in the figures was selected based on an estimated period that trucks used to cross over the monitored span. The results indicate that the dynamic load factor decreases as the magnitude of the static strain increases. The explanation is that the rate of increase in static response is higher than the rate of increase in dynamic response as the static response increases.

Statistics of the dynamic load factor at four different diaphragm sections are summarized in Table 5.7. Mean values of the dynamic load factor in the interior and exterior spans of beam line 10 were found to be 8 percent and 12 percent, respectively. (The 15-percent dynamic load factor required in the AASHTO Specifications (1998) is slightly higher.) In addition, the coefficient of variation of the dynamic load factor at the diaphragm sections was in the range of 44 percent to 63 percent. This coefficient of variation is less than an 80 percent coefficient of variation used in the proposed fatigue reliability fatigue model.

5.2.5. Analytical Model

The effective stress ranges at the monitored and fatigue-prone detail sections were estimated by two types of analytical models: one-dimensional and three-dimensional models. These stress ranges were used to identify the most critical diaphragm section in the monitored structure. Although the structure was originally built as a non-composite structure, a partially composite-section behavior was observed by reviewing the strain gage data (Reisert, 2003). Therefore, the structural responses corresponding to both non-composite and fully composite-section behaviors were determined in the analytical

models. The AASHTO fatigue truck and the 4-axle fatigue truck developed in Chapter 3 were used as applied loads in the models. An effective gross weight estimated from the collected WIM data was used to estimate the gross weight of the fatigue trucks.

5.2.5.1. One-Dimensional Analytical Model

Two one-dimensional beam-line type analytical models were developed by using the SAP 2000 structural analysis software. Frame elements were used to model the beams for a non-composite section and both bridge deck and beams for a composite section. The influence lines were obtained in each model by applying a unit load on the finite element models at 1-foot increments along the beam line. Then, a computer program was developed to calculate stress range envelopes of the moving loads. The AASHTO fatigue truck and the proposed 4-axle fatigue trucks were used as applied loads. An effective weight of 75.3 kips calculated from the one-year WIM data was used as a gross vehicle weight of the fatigue trucks. The AASHTO girder distribution factor and dynamic load factor (AASHTO, 1998) were utilized in the calculation.

Stress range envelopes caused by each fatigue truck in both non-composite and composite models are shown in Figure 5.13. The composite model loaded with the 4-axle fatigue truck provided the lowest estimated effective stress ranges at all locations. The results obtained from both the AASHTO fatigue truck and the 4-axle fatigue truck suggested that a diaphragm section located in the first span had an effective stress range slightly greater than the one in the last span (Section # 4) and was the most critical diaphragm section. In addition, the maximum stress range over the interior supports was found to be at pier 10 supporting the outmost span.

5.2.5.2. Three-Dimensional Analytical Model

Two three-dimensional finite element models were developed using the SAP 2000 analysis program. Shell elements were employed to model the bridge deck, and frame elements were used to model the beams. Two different constraints were utilized to represent non-composite and composite sections, as shown in Figure 5.14. For a non-

composite section, vertical displacements of nodes located at centroid of the beams and middle depth of the concrete deck were constrained. However, for a composite section, rigid elements were connected between the beams and bridge deck. Diaphragms were not included in the models. Figure 5.15 shows an isometric view of the three-dimensional finite element model for a composite section.

Similar to the one-dimensional models, the AASHTO and 4-axle fatigue trucks with a 75.3-kip gross weight were used as applied loads. Maximum estimated stress ranges at diaphragm sections in the two monitored spans of beam 10 and at the bolted splice plate over pier 10 were obtained by placing the fatigue trucks at different locations in the models. The dynamic load factor provided in the AASHTO Specifications (1998) was used to account for the increase in stress range magnitude due to dynamic response.

5.2.6. Analysis Comparison

A comparison of the effective stress ranges obtained from the strain gage data and the analytical models is summarized in Table 5.8. The stress ranges shown in the table are located at the top of the bottom flange of the diaphragm section in the first span, Section # 4, and Section # 9, and at the outmost fibers of the top and bottom splice plates for the bolted splice plate over pier 10. The stress ranges for the bolted splice plate detail were determined from non-composite-section models. For the strain gage case, the effective stress ranges at the diaphragm section in the first span and the bolted splice plate were obtained based on the stress range envelope of the three-dimensional finite element model with a non-composite section. Strain at the section of interest was computed by multiplying the measured strain by the ratio of the stress range at the section of interest to the stress range at the section with the strain gages.

The results indicated that, regardless of the fatigue truck type, the one-dimensional models provided estimates of the effective stress ranges higher than the three-dimensional models. Additionally, the effective stress ranges computed from the three-dimensional models with the 4-axle fatigue truck were relatively close to the values obtained from the strain gage data. Based on the collected strain data, the effective stress range at the top of the bottom flange at Section # 4 was found to be 2.45 ksi, while the

non-composite and composite three-dimensional models with the 4-axle fatigue truck provided the estimated effective stress ranges of 3.13 ksi and 2.95 ksi, respectively, at the corresponding location.

In addition, the traffic count data with statewide average gross weights was used to estimate a gross weight of the fatigue truck. An effective gross weight was found to be 54.2 kips, which is considerably less than the actual effective gross weight of 75.3 kips. The effective stress ranges provided by the one-dimensional models with the 4-axle fatigue truck having a 54.2-kip gross weight are shown in Table 5.8.

A comparison of the neutral axis locations in both interior and exterior spans of beam line 10 (Sections # 3 and # 4) provided by the strain gage data and the analytical model with the 4-axle fatigue truck is graphically presented in Figure 5.16. The lines shown in the figure are obtained by connecting the estimated effective stress range in Table 5.8 and the estimated neutral axis locations. For the strain gage case, the neutral axis locations were determined from roughly 6-7 arbitrarily selected strain data recorded at the cross sections of interest. These neutral axes were found to be between the locations estimated by the non-composite and composite models.

The results indicated that a certain amount of composite action existed at the monitored sections. Additionally, both one-dimensional and three-dimensional analytical models provided relatively close estimated locations of the neutral axis when a similar section behavior was assumed in the models. It also should be noted that although the effective stress ranges at the bottom flange of three-dimensional models with 4-axle fatigue truck are relatively close to the values obtained from the strain gage data, the estimated stress ranges at fatigue critical details can be different due to an error in estimating the neutral axis location.

5.2.7. Fatigue Life Estimation

The fatigue life was evaluated based on the proposed fatigue reliability model from Chapter 4 and the AASHTO Fatigue Guide Specifications (1990). The estimated effective stress ranges obtained from the strain gage data and analytical models at an

intermittent weld detail of the diaphragm section, an improperly located attachment plate, and a bolted splice plate detail were used in the calculation.

A study on diaphragm details that are directly welded to the beam web was performed by Barth and Bowman (2002). They suggested that the intermittent weld diaphragm detail has a fatigue resistance somewhere between AASHTO Categories C and D. The fillet weld detail at the improperly located attachment plate is classified as a Category C detail, while the bolted splice plate detail is a Category B detail per AASHTO (1998). Two different traffic growth rates were assumed. The input parameters used in the fatigue evaluation are summarized in Table 5.9. The ADTT was estimated based on one-year record of WIM data collected at the investigated structure.

An extension of the S-N line approach was used. For this approach, a fatigue limit is not included in the calculation. As a result, all stress range levels are assumed to cause fatigue damage at a fatigue detail. The estimated total fatigue lives of the bridge structure corresponding to effective stress ranges provided by the strain gage data at the diaphragm section, improperly located attachment plate, and bolted splice plate detail are summarized in Table 5.10. Computed lives in excess of 150 years are shown in the table as >=150 years. The total fatigue life was found to exceed 150 years at all three of the details. Since the bridge is approximately 35 years old, a remaining fatigue life in excess of 100 years still remains.

In addition, the fatigue lives were computed based on effective stress ranges provided by the one-dimensional and three-dimensional models with gross weights obtained from the WIM data and traffic count data with statewide average gross weights. The number of trucks for each FHWA truck classification was obtained based on the collected WIM data. By using traffic count data and the statewide average gross weights provided in Chapter 3, the effective gross weight was found to be 54.2 kips. The biased values and coefficients of variation of the parameter database in Chapter 4 were employed in the calculation. The fatigue lives at the diaphragm sections were computed from the effective stress ranges obtained from both non-composite and composite models. These fatigue lives are compared with the lives estimated based on the strain gage data in Figures 5.17 and 5.18 for 2-percent and 4-percent traffic growth rates. Upper

and lower bounds of the fatigue lives for each case in these two figures correspond to the AASHTO category C and category D, respectively. For a 4-percent traffic growth rate and the AASHTO category D, the fatigue lives at the diaphragm sections predicted by the one-dimensional model with the 4-axle fatigue truck, the measured strain data, and the use of traffic count data are equal to 70.6, 225.5, and 75.8 years, respectively.

Figure 5.19 shows a comparison of the fatigue lives at a bolted splice plate detail. In this figure, the upper and lower bounds correspond to 2-percent and 4-percent traffic growth rates, respectively. The results indicate that the one-dimensional analytical model provided the most conservative fatigue life, followed by the three-dimensional analytical model, and then the use of strain gage data. The three-dimensional analytical models with the 4-axle fatigue truck provided the closest estimate of the fatigue life to the strain gage data. Moreover, it was found that the fatigue lives predicted by the one-dimensional model with effective gross weights estimated from WIM information was vary similar to that predicted by using traffic count data.

In addition, the fatigue life corresponding to the measured stress ranges was also computed by using the AASHTO Fatigue Guide Specifications (1990), along with an extension of the S-N line approach. The AASHTO Specifications (1990) provide a reliability factor or a safety index for the fatigue evaluation. By using this reliability factor, a fatigue limit state function can be expressed in terms of deterministic parameters. Mean values of the parameters listed in Table 5.9 with a 4-percent traffic growth rate and the maximum estimated effective stress ranges of 1.96 ksi at an intermittent welded diaphragm and 3.08 ksi at a bolted splice plate detail were used in the calculation. These stress ranges were estimated from the strain gage data. The total fatigue lives were found to be more than 150 years at both the welded diaphragm and bolted splice plate details. Therefore, the remaining fatigue life of the structure is still greater than 100 years.

5.3. Fatigue Evaluation of I-65 Bridge over the Kankakee River

A field investigation was performed to study the structural response and fatigue strength of a bridge structure on I-65. Strain gage instrumentation was used to monitor

the strains developed in critical girders under routine truck traffic. The strain data collected were decomposed by using two different cycle counting procedures. The cycle counting results were then compared with the estimated effective stress ranges calculated from finite element models developed in the present study. By combining results obtained from the field testing and the analytical study, the effective stress ranges at the fatigue critical details were determined and used as crucial information in a fatigue evaluation.

5.3.1. Structure Description

The structures that were evaluated are located on I-65 over the Kankakee River at the border of Lake and Newton Counties in northwest Indiana. The structures are each a three-span continuous steel plate girder bridge supporting two traffic lanes. One bridge carries northbound traffic, the other southbound traffic. Each structure is composed of seven continuous girders with an 8-inch concrete deck. The overall length of each structure is 310-feet, with span lengths of 86'-6", 137'-0", and 86'-6". A typical girder profile is illustrated in Figure 5.20. The depth of girder web varies from 3 ft in the end spans region to 7 ft over the interior piers.

The bridges were built and opened to traffic in 1967. After a few years, it was observed that the bridge structures had experienced distortion-induced fatigue cracking at a number of the transverse stiffener details located at the diaphragm sections. The cracking occurred in the girder web and propagated around the ends of the stiffener weld at the bottom cope.

A repair was performed to minimize the out-of-plane displacement at the transverse stiffener connections and deter further crack growth. (The repair was performed in conjunction with a project to widen the bridges and add additional girder lines.) Angles were used as a rigid attachment to stiffen the connections. The angles were welded to the transverse stiffeners and bolted to the bottom flange of the plate girder. In addition, holes were drilled through the web at the crack tips to minimize (or arrest) further fatigue crack extension in the girder web. A typical retrofit angle detail is shown

in Figure 5.21. This figure also shows that multiple holes were used to arrest crack growth before the retrofit angles were installed.

5.3.2. Instrumentation

Strain gage instrumentation was used to investigate the response of the southbound bridge structure under routine truck traffic. Four different strain gage locations were selected to obtain an understanding of the overall structural response. The following criteria were used to consider the strain gage locations.

1) Ideally, at least eight strain gages should be attached at each monitored section so that the actual structural behavior (composite/ non-composite action) can be assessed.
2) The most critical fatigue life locations should be monitored. These locations are subjected to the greatest loading from truck traffic.
3) The strain range levels in both interior and exterior spans should be monitored.

Based on the criteria listed above, thirty strain gages were attached at four different locations on girder lines 10 and 11 of the southbound structure, as shown in Figure 5.22 and Table 5.11. These two girder lines were selected because they were expected to carry a substantial amount of traffic and experience the greatest stress ranges. Also, most of the cracking was limited to diaphragms along these two girder lines.

Strain gages on Sections # 1, # 2, and # 3 were located 18 inches south of the diaphragm sections, while Section # 4 was located 4 inches south of Diaphragm # 12 (38.53 ft from the north support). Figures 5.23 to 5.25 illustrate the strain gage locations at each monitored section. Strain gages were not installed on the top flange of Section # 2 because it was not accessible with the reach-all equipment utilized during strain gage installation.

Based on a preliminary analysis of the structure, it was found that the bridge natural frequency is approximately 4.2 Hz. Therefore, a 50-Hz scan rate was selected in

the study to capture all peaks and valleys of the strain response. The strains at all monitored sections were triggered separately by using a strain gage located on the bottom flange on the west side of the girder as the trigger channel. The strain data at each section were recorded only when a 30-microstrain level was achieved or exceeded at the trigger channel.

A Campbell Scientific (Model CR5000) data acquisition system was used to collect the strain data. This data acquisition system provided triggering capabilities and a suitable scan rate. Moreover, it was able to be operated by using a simple 12-volt car battery for the power source. The test setup is shown in Figure 5.26.

5.3.3. Cycle Counting Results

Strain gage data were collected continuously from August 29, 2003 to September 22, 2003, a total of 24 days. Point-to-point recorded strain data are generally erratic with a number of small reversals intermixed within a large reversal. Therefore, a cycle-counting procedure is required to decompose the strain history for each loading event. In this study, two different cycle-counting procedures were performed. A rainflow cycle counting method was used in the first procedure. In the second procedure, a racetrack method was first used to eliminate small strain ranges from the strain history, followed by a rainflow counting method to decompose the remaining strain history. In this study, a 20-microstrain boundary size was used as a track width in the racetrack method.

After a complex strain histogram is decomposed, stress ranges can be determined based on an assumption that a structure is still in the elastic region. Table 5.12 summarizes the maximum strain ranges observed at the bottom flange gages on the west side of the girders 10 and 11. The results indicate that an assumption of a linear relationship between stress and strain is valid since all of the measured strain values are well below the yield strain of 1240 microstrain for an ASTM A36 steel.

Cycle counting results of the 24-day strain data collected from the bottom flange gages located on the girder west side were converted to stress units and are graphically presented in Figure 5.27. The histograms show that most of the stress ranges are below 2.3 ksi. Best fit curves for the stress range histograms in these figures were determined by

using the SAS software - a statistical computer program available at Purdue University. The stress range histograms were fitted with lognormal, exponential, Weibull, and Rayleigh distributions. Tables 5.13 and 5.14 summarize the estimated effective stress ranges provided by each distribution and the actual effective stress ranges of the histograms in Figure 5.27. It was found that the Weibull distribution provides the best fit and closest estimates of the effective stress ranges at all monitored sections.

Average effective stress ranges at the top of the bottom flange obtained from the two different cycle counting procedures are summarized in Tables 5.15 and 5.16. From the results in the tables, it can be observed that the effective stress ranges between each week of data are relatively close. It can also be observed that the effective stress range values determined by the two different cycle-counting procedures are very similar at all four sections. The differences between the effective stress ranges provided by the two counting procedures are found to be less than 7 percent. The number of cycles per truck ranges from 1.02 to 1.24 when the racetrack method is applied first before performing the rainflow counting method (Procedure # 2). Meanwhile, the number of cycles per truck obtained from the rainflow counting method (Procedure # 1) ranges from 1.15 to 1.33. The cycle counting results also indicate that Section # 1 (exterior span) is subjected to higher stress range values than Section # 2 (middle span). These cycle counting results will be compared with the estimates obtained from analytical models in the following section.

5.3.4. Dynamic Load Factor

Similar to the field investigation of the bridge structure located on the extra heavy duty corridor (Section 5.2), a signal analysis procedure used by Nassif and Nowak (1995) in the study of the dynamic load spectra of bridge girders was utilized.

The dynamic load factors at Sections # 1 and # 2 are shown in Figures 5.28 and 5.29, respectively, for all recorded events. Only data from the bottom flange gages located on west side of Girder # 11 are included in these figures. The results are consistent with observations obtained from the other field investigation in that the dynamic load factor increases as the magnitude of static response decreases.

Statistical parameters of the dynamic load factors at all monitored sections are listed in Table 5.17. It has been found that the dynamic load factors in exterior and interior spans are approximately 11 percent and 7 percent, respectively. Therefore, the 15-percent dynamic load factor required in the AASHTO Specifications (1998) provides a conservative estimate and is relatively close to a mean dynamic load factor observed in an exterior span of the monitored structure. The coefficient of variation of the dynamic load factor ranged from 33 percent to 40 percent, which is less than the 80 percent coefficient of variation used in the proposed fatigue reliability model.

5.3.5. Analytical Model

Two analytical models were developed to estimate the structural response of the monitored structure. The analytical results are compared with the recorded strain history and used to estimate effective stress ranges at the diaphragm sections. The results obtained from the analytical models are summarized in the following.

5.3.5.1. One-Dimensional Analytical Model

A one-dimensional beam-line type analytical model was developed using the SAP 2000 structural analysis software. Frame elements were used to model the bridge deck and plate girders. Influence lines were developed by applying a unit load on the finite element model at 1-foot increments along the length. Then, the corresponding frame element forces were determined. Once the influence lines were obtained, a computer program was developed to calculate the stress range envelopes of the moving loads. In the calculation, the girder distribution factor and dynamic load factor specified in the AASHTO Specifications (1998) were used.

The stress range envelopes of the AASHTO fatigue truck, AASHTO HL-93 design truck (no lane load), and various superload vehicles are presented in Figures 5.30 and 5.31. The configurations of superload vehicles are shown in Appendix B. From both figures, it is evident that the largest stress range at the diaphragm sections occurs in the exterior span.

5.3.5.2. Three-Dimensional Analytical Model

The SAP 2000 analysis program was also utilized to develop a three-dimensional finite element model. Shell elements were selected to represent the bridge deck and girder webs. Frame elements were used to model the girder flanges. Rigid elements were connected between the slab and the top girder flange to represent composite-section behavior, as shown in Figure 5.32. Diaphragms were not included in the model. An isometric view of the three-dimensional finite element model is shown in Figure 5.33.

The AASHTO fatigue truck with a 54-kip gross vehicle weight was used in the model. The wheel load locations were applied to cause maximum stress ranges at the critical diaphragm sections in the exterior and interior spans (Diaphragms # 2, # 7, and # 12, if counting left-to-right for diaphragm locations noted in Figure 5.31), as well as at the monitored locations. The 15-percent dynamic load factor specified in the AASHTO Specifications (1998) was used to amplify the estimated stress ranges in order to account for dynamic response. Analytical results of the three-dimensional model will be summarized and compared with the estimates obtained from both the one-dimensional model and the strain gage instrumentation.

To examine the stress range levels at the transverse stiffener details under distortion-induced fatigue loading, a modified cross section of the three-dimensional finite element model was employed. Truss elements were added to the previous three-dimensional model to represent the X-type cross-frame diaphragms. These elements were connected directly to the girder web, as shown in Figure 5.34. The truss elements were selected to simulate the behavior of the cross-frame diaphragms, which were anticipated to develop little moment magnitudes and rotate under traffic loadings. The AASHTO fatigue truck with a 54-kip gross weight was applied along a centerline of the outside lane. Then, the relative rotations of the diaphragm members and girder web at the critical diaphragm sections (Diaphragms # 2 and # 7) were monitored. The maximum rotations at Diaphragms # 2 and # 7 of girder line 11 were found to be $1.225*10^{-4}$ and $1.813*10^{-4}$ radians, respectively. Based on these rotations, the distortion-induced stresses can be estimated by utilizing Eq. 5.1 (Jajich and Schultz, 2003):

$$\sigma_{wg} = \left(\frac{2 \times E \times t_w \times \theta}{g} \right) \tag{5.1}$$

where σ_{wg} is the web gap stress range, E is the young's modulus of elasticity, t_w is the web thickness, θ is the diaphragm rotation, and g is the web gap. This equation was developed based on the assumption that a web gap stress is dominated by a rotation of the transverse stiffener rather than an out-of-plane translation of the web gap. In the study performed by Jajich and Schultz (2003), a web gap stress calculated from Eq. 5.1 was compared with finite element results and strain gage data and found to provide a reasonable estimate.

By using Eq. 5.1, the diaphragm rotations obtained from the three-dimensional model, and a configuration of the bridge being studied (t_w = 0.375", g = 0.5"), the distortion-induced stresses at Diaphragms # 2 and # 7 of girder line 11 were found to be 5.33 ksi and 7.89 ksi, respectively. The results indicate that under a distortion-induced fatigue loading, Diaphragm # 7 is more critical than Diaphragm # 2. To further explain the fatigue problem experienced in this bridge before a retrofit was performed, the fatigue lives corresponding to the estimated distortion-induced stresses will be evaluated in the following section.

5.3.6. Analysis Comparison

A summary and comparison of the girder stress-range results obtained from the one-dimensional model, the three-dimensional finite element model, and the strain gage data are presented in Table 5.18. The stresses were computed at the following locations: vertical diaphragm connection plate at 0.5-inch above top of the bottom flange, transverse intermediate stiffener at top of bottom flange, and the web-flange fillet weld detail at the top of the bottom flange. For the strain gage case, the effective stress ranges at the critical diaphragm sections (Diaphragms # 2, # 7, and # 12) were estimated based on the stress range envelope of the three-dimensional finite element model. Strain at the section of

interest was computed by multiplying the measured strain by the ratio of the stress range at the section of interest to the stress range at the section with the strain gages.

The results indicate that the three-dimensional model provides closer estimates of the strain-gage based effective stress ranges at Sections # 1 and # 2 than the one-dimensional model. Therefore, the actual bridge response can be assessed more accurately by utilizing the three-dimensional model.

In addition to stress range values, the neutral axis locations estimated by the one-dimensional and the three- dimensional models are compared with the structural behavior obtained from strain gage instrumentation. The stress distributions of Sections # 1 and # 2 are shown in Figure 5.35. The neutral axis locations of the strain gage case in the figure are estimated from roughly 6-7 arbitrarily selected strain data values recorded at each cross section. The line shown in the figure is obtained by connecting the neutral axis position and the bottom flange effective stress range value obtained from rainflow cycle counting for all strain gage measurements. The strain data neutral axis position confirms that a significant percentage of composite action exists at the monitored cross sections. The results also indicate that the neutral axis locations predicted by one-dimensional and three-dimensional models are relatively close to the actual structural response.

5.3.7. Fatigue Life Estimation

The fatigue life corresponding to the estimated stress ranges at the fatigue-prone details were evaluated based on the proposed fatigue reliability model and the AASHTO Fatigue Guide Specifications (1990). The estimated stress ranges at the lower portion of the transverse stiffener detail and at the web-to-flange fillet weld were used in the calculation. The retrofit bolted angle detail shown in Figure 5.21 is similar to a detail that was classified as a category B fatigue detail according to Keating (1994). The longitudinal web-to-flange fillet weld is also a category B detail per AASHTO (1998). However, the fillet welds of transverse stiffeners to the web and to the bottom flange are classified as category C$'$ details (AASHTO, 1998). Three different traffic growth rates were assumed for the fatigue life calculation. The input parameters used in the fatigue evaluation are summarized in Table 5.19. An extension of the S-N line is used in the

cyclic damage calculation. This method assumes that a fatigue limit does not exist in the fatigue resistance curves (S-N lines), meaning that all stress range levels will cause fatigue damage at the structural detail.

The fatigue behavior of the bridge prior to the installation of any retrofit details was examined to see if the observed cracking was consistent with the out-of-plane distortion-induced fatigue model discussed earlier. The estimated distortion-induced fatigue stresses obtained from the three-dimensional finite model were used to evaluate the structural fatigue life. The input parameters listed in Table 5.19 with a 4-percent traffic growth rate and a fatigue strength corresponding to category C′ were used in the calculation. The fatigue lives corresponding to the estimated stress levels at Diaphragms # 2 and # 7, which are equal to 5.33 and 7.89 ksi, were found to be 32.9 and 15.2 years, respectively. These fatigue lives are fairly consistent with cracking observed on the I-65 bridges. This calculation demonstrates that distortion-induced stress can cause a serious fatigue problem and significantly reduce the fatigue life of a structure, unless addressed by a retrofit that minimizes the out-of-plane distortion.

Based on the measured strain gage data, the estimated fatigue lives of the southbound structure corresponding to the maximum effective stress ranges in the girder at the diaphragm sections in the exterior and interior spans, the transverse intermediate stiffener detail with the largest stress range, and the web-flange fillet weld with the greatest stress range were determined, as presented in Table 5.20. For a computed life in excess of 150 years, the value shown is >= 150 years.

A couple of significant observations can be drawn from the results in Table 5.20. First, and foremost, the fatigue life was found to exceed 150 years for all of the details examined based upon the stress ranges being experienced. Secondly, the retrofit detail was assumed to exhibit category B behavior based upon information from Keating (1994). The only way to truly know the fatigue strength of the bolted retrofit detail is to conduct a number of experimental fatigue tests to accurately classify the fatigue behavior. However, in this case, if an even lower strength corresponding to category C′ was more representative of the true fatigue behavior, the detail was still found to exhibit a satisfactory fatigue life due to the low stress ranges.

In addition, weigh-in-motion data were collected on I-65 at milepost 218.4 from July, 2002 to December, 2002. These data indicate that the effective gross vehicle weights of truck traffic in the southbound and northbound directions are 45.0 and 51.1 kips, respectively. Consequently, these data suggest that the loads in the northbound direction are heavier and maybe more critical. Therefore, the ratio of these two effective gross vehicle weights was used to estimate effective stress ranges in the northbound structure. The estimated total fatigue lives of the northbound structure corresponding to stress ranges at the aforementioned sections as noted in Table 5.20 are summarized in Table 5.21. The increased gross vehicle weight in the northbound direction, as expected, resulted in shorter fatigue lives in the northbound structure than in the southbound structure. The predicted fatigue strength at the transverse intermediate stiffener detail is still 111 years. Since the bridge is approximately 37 years old, this means that the remaining fatigue life is 74 years. Note, however, that even this remaining life could be extended if the critical transverse intermediate stiffeners were retrofitted after fatigue cracking occurred. Lastly, it should be pointed out that the critical diaphragm detail had a remaining predicted fatigue life of 138 years at the time retrofit was initiated. Consequently, since the retrofit was installed about 12 years ago, a considerable fatigue life (in excess of 100 years) still remains.

The fatigue lives were also calculated based on the effective stress ranges obtained from the analytical bridge models using a 54-kip gross weight for the AASHTO fatigue truck and an effective gross weight estimated from traffic count data together with the statewide average gross weights provided in Chapter 3. The traffic count data collected from the WIM site located on I-65 at milepost 218.4 was used in the calculation. This WIM site is located approximately 16-miles south of the bridge structure and labeled in Chapter 3 as Station 410. For comparison purposes, the estimated effective gross weight computed from the traffic count data together with the statewide average gross weight values for various truck classes was found to be 48.7 kips in the northbound direction. The biased values and coefficients of variation provided in Chapter 4 were employed in the fatigue life calculation.

Figures 5.36 and 5.37 show the fatigue lives of the northbound structure estimated based on the strain gage data, the 54-kip AASHTO fatigue truck, and the traffic count data at the transverse intermediate stiffener and web-to-flange fillet weld details. A range in fatigue lives is shown based upon 0 percent and 4 percent growth rates in traffic. The one-dimensional model provides the most conservative estimate of the fatigue life, followed by the three-dimensional model and the strain gage data, respectively. In addition, the fatigue lives estimated from the 54-kip AASHTO fatigue truck and traffic count data are not significantly different. For a 4-percent traffic growth rate, the fatigue lives provided by strain gage data, a one-dimensional model with the 54-kip AASHTO fatigue truck, and use of traffic count data are equal to 111.3, 30.0, and 23.8 years, respectively.

It should be noted that for a short fatigue life, a 4-percent traffic growth rate provides a fatigue life in years greater than a 0-percent traffic growth rate. This is because the same ADTT at the 35^{th} year of service were assumed for both growth rates. The estimated ADTT at the first year of service for a 4-percent growth rate is therefore less than a 0-percent growth rate. As a result, for a short fatigue life, a 4-percent traffic growth rate provides a total number of cycles less than a 0-percent growth rate; however, this effect reverses for long fatigue lives.

In addition, the fatigue life corresponding to the measured stress ranges was also evaluated by using the AASHTO Fatigue Guide Specifications (1990). An extension of the S-N line was utilized in the calculation. By using a reliability factor provided in the Specifications (1990), the fatigue life can be computed from deterministic values of the load and resistance parameters. Therefore, the mean values of the input parameters listed in Table 5.19 with a 4-percent traffic growth rate and the maximum estimated effective stress ranges of 2.51 ksi at the transverse stiffener detail and 2.58 ksi at the web-to-flange fillet weld (Table 5.21) were used in the calculation. These stress range values were obtained by using measured strain values in the southbound structure, and were then adjusted for the northbound direction using WIM data. It should be mentioned that a transverse stiffener detail is classified as a category C fatigue detail in the Specifications (1990). The total fatigue lives corresponding to the stress ranges at the transverse

stiffener detail and the web-to-flange fillet weld detail were found to be 98.5 years and greater than 150 years, respectively. These results indicate that the structure still has a remaining fatigue life of 61 years.

5.4. Fatigue Evaluation Procedure

The fatigue life estimated for a selected level of safety can vary due to uncertainties inherent in alternative procedures used in a fatigue evaluation. It has been illustrated in the experimental program conducted in this study that strain gage instrumentation is likely to provide an estimate of the effective stress range that is less than that predicted using an analytical bridge model. Additionally, a rigorous analysis method, such as a three-dimensional finite element model can provide a better prediction of the stress range level in a bridge structure than a one-dimensional model. Although the aforementioned alternative procedures can be utilized, a simplified evaluation procedure for the fatigue reliability-based analysis of a bridge structure is still desirable to facilitate rapid implementation and evaluation of bridge structures. The evaluation procedure used herein is described as follows:

1. Identify the fatigue critical details used in a given bridge structure.
2. Based on detail geometry, the fatigue strength corresponding to a given fatigue detail can be determined from the parameter database provided in Chapter 4. Fatigue strength data on a similar detail can also be used, if such data are available.
3. Evaluate the effective stress range at the detail by using information obtained from strain gage instrumentation or a fatigue truck analysis.
4. If a one-dimensional analytical model is utilized in the fatigue evaluation, an effective stress range at a fatigue detail can be estimated by using the proposed fatigue truck model with the girder distribution factor and dynamic load factor in the AASHTO Specifications (1998).

5. Estimate the number of trucks traveling across a structure in the past, present, and future. The estimated value can be presented in terms of ADTT and traffic growth rate.
6. Select a level of safety, or a confidence level, for the fatigue analysis. This corresponds to the statistical confidence that the actual fatigue life is greater than a given computed fatigue life.
7. A fatigue life can be determined by using either a safety factor or a structural reliability analysis with the fatigue limit state function. When a safety factor is utilized, the fatigue life can be computed from nominal or deterministic values of fatigue load and resistance parameters. The safety factor developed in Chapter 4 can be used when a 97.7-percent probability of survival (or a reliability index equal to 2) is selected. However, if the reliability analysis is employed, the amount of uncertainty and the probability distribution functions of the fatigue load and resistance parameters must be first determined. Alternatively, the statistics of the parameter database provided in Chapter 4 can be used in the calculation. By employing a numerical procedure or a simulation technique, the fatigue life corresponding to a selected level of safety can then be determined.
8. If the computed fatigue life does not satisfy the service life requirements, a field investigation or a rigorous analysis method can be used to provide a better prediction of the fatigue life.
9. Based on the computed fatigue life, a recommendation can be formulated and required follow-up procedures can be established. The follow-up procedure can be one or more of the following:
    a) Inspect the structure more frequently.
    b) Restrict the number of trucks or the maximum gross weight of trucks traveling across a structure.
    c) Modify an existing fatigue detail so that a lower stress level or a higher fatigue resistance can be obtained.

d) Use a mechanical method to produce a compressive residual stress at a fatigue critical detail.

e) Schedule the structure for replacement.

The procedure described above is also illustrated in Figure 5.38. The flowchart indicates that the loading information can be obtained in multiple ways, including the use of strain data, WIM information, traffic count information, or use of standard fatigue trucks. For the procedure utilized herein, the fatigue analysis can be conducted in a deterministic manner with a prescribed safety factor or by use of fatigue reliability. If a fatigue reliability method is used, then the uncertainty levels in the load and the resistance of the detail must also be provided. The total fatigue life is then computed. As indicated in Figure 5.38, the remaining fatigue life is then determined by considering the information on-hand for the previous load history.

5.5. Evaluation of Steel Bridges along Extra Heavy Duty Corridor

The remaining fatigue lives of the steel bridge structures located along segments of the extra heavy duty corridor in northwest Indiana were evaluated by using the fatigue evaluation procedure discussed in the previous section (Section 5.4) and the fatigue reliability model described in Chapter 4. The effective stress range at a given fatigue critical detail can be obtained from a couple of alternatives. The results obtained from the experimental program conducted on two significantly different steel bridge structures have shown that use of a one-dimensional analytical model along with the AASHTO girder distribution factor (AASHTO, 1998) provides a conservative estimate of the fatigue life. Additionally, it can be conveniently used in the fatigue calculation. Therefore, this approach was selected to determine the fatigue lives of the structures on the extra heavy duty corridor.

The bridge numbering, location, and year built are provided in Table 5.22 for bridges along the extra heavy duty corridor. Figure 5.39 shows an overview of the extra heavy duty corridor in 2002 and the location of the bridge structures along the corridor. For each structure, only the last four numbers of the nomenclature provided in Table 5.22

are shown in the figure. It should be mentioned that Structure # 20-64-2458A is the steel bridge on U.S. 20 near Michigan City as noted in the experimental program (Section 5.2).

A bridge inspection was performed to identify fatigue critical details used in each structure. Appendix C contains photographs of the fatigue critical details and an overview of the structures. The dimension of longitudinal members, deck thickness, and location of the fatigue critical details were determined from the bridge plans. A summary of the structural configurations is presented in Table 5.23. This information was obtained from the 1999-2000 Inventory of Bridges - State Highway System of Indiana. Structures # 31-71-5805A, # 31-71-5807A, and # 149-64-4467B are composite continuous plate girder bridges, while the other structures use rolled sections for the longitudinal members.

Diaphragms are attached to the longitudinal members by one of the following four connection types: 1) intermittent fillet weld diaphragm connection, 2) bolted diaphragm connection, 3) riveted diaphragm connection, and 4) continuous fillet weld connection at diaphragm-transverse stiffeners (see Figure 5.40). Figure 5.40d also shows that the transverse stiffeners at the cross-frame diaphragm sections are stiffened by a base plate that is welded to the stiffener and bolted to the bottom flange plate. The base plates are welded to the transverse stiffeners and bolted to the girder bottom flange. This connection type is used in Structures # 31-71-5805A and # 31-71-5807A. A summary of the fatigue critical details and diaphragm connection types used in each structure is presented in Table 5.24. A bolted splice plate connection is used in most of the structures, except Structure # 21-4 which uses a riveted connection, to provide continuity of the longitudinal members.

One-dimensional beam-line type analytical models were developed using the SAP 2000 structural analysis software. Frame elements were used to represent the bridge deck and girders. The bending moment influence lines were generated by applying a unit load along the length of the model. A computer program was then developed to compute the stress range responses at the fatigue critical details. The proposed 4-axle fatigue truck with a 75.3-kip effective gross weight was used as the applied live load. This effective gross weight was obtained from the one-year database of truck traffic data collected at the WIM site (Station 001) located at approximately one-mile west of Structure # 20-64-

2458A. It should be noted that this effective gross weight tends to provide a conservative estimate of the actual traffic load spectrum for the structures located on U.S. 31, S.R. 149, and S.R. 249 considering that heavy trucks are allowed to travel along S.R. 39 to enter the state of Michigan (Figure 5.38). Thus, these structures may be subjected to truck traffic with a lower value of the effective gross weight. Clearly, a more accurate estimate of the effective gross weight would result in a better fatigue life prediction.

The remaining fatigue lives corresponding to a reliability index equal to 2 were calculated by using the proposed fatigue reliability model. A mean ADTT equal to 776 trucks in 2002 and 20-percent truck traffic were assumed at all structures. This ADTT was estimated based on the one-year WIM data collected at Station 001. In addition, the number of cycles per passage corresponding to the proposed 4-axle fatigue truck was used in the calculation.

Table 5.24 provides the remaining fatigue lives computed based on the estimated effective stress ranges at fatigue critical details and traffic growth rates of 2 and 4 percent. For a computed life in excess of 150 years, the value shown is >= 150 years. An extension of S-N lines was utilized in the calculation. The results indicated that among all of the structures, Structure # 31-71-5805A has the shortest remaining fatigue life of 29.2 and 25.0 years for the traffic growth rates of 2 and 4 percent, respectively. As mentioned earlier, a conservative estimate of the effective gross weight was used in the fatigue calculation of this structure. Moreover, it is also known that the use of the one-dimensional analysis will provide higher effective stresses. Therefore, an actual remaining fatigue life of greater than 25 years undoubtedly still remains for the structure.

In addition, distortion-induced stresses at web gaps of the diaphragm-transverse stiffeners were determined for Structures # 31-71-5805A and # 31-71-5807A by using the formula (Eq. 5.1) proposed by Jajich and Schultz (2003). The key parameter required in computing web gap stresses is the diaphragm rotation. For negative-moment regions, the diaphragm rotation is approximately equal to a ratio of the differential deflection between adjacent girders and girder spacing. It should be noted that the critical web gap stresses in the structures are at the diaphragm sections in negative moment regions because an out-

of-plane displacement in the positive moment regions is minimized with the bolted base plate connection at the transverse stiffeners (Figure 5.40d).

The differential deflections were determined from the one-dimensional and three-dimensional analytical models developed in the present study. For the one-dimensional model, the deflection at the critical diaphragm section in the beam line of interest was computed by using the proposed 4-axle fatigue truck with a 75.3-kip gross weight as an applied live load and the AASHTO girder distribution factor (AASHTO, 1998). The diaphragm rotation was then calculated with the assumption that the other girders in the structure did not deflect. It has been found that the one-dimensional analytical model with the AASHTO girder distribution factor (AASHTO, 1998) considerably overestimates the differential deflections and provides unreasonably high web gap stress ranges in the investigated structures.

Three-dimensional analytical models were developed for Structures # 31-71-5805A and # 31-71-5807A. Shell elements were selected to represent the bridge deck and girder webs. Frame elements were used to model the girder flanges. Rigid elements were connected between the slab and the top girder flanges to represent a composite-section behavior. The proposed 4-axle fatigue truck with a 75.3-kip gross weight was used as an applied live load in the bridge models. Based on the differential deflections obtained from the three-dimensional models and section geometries, the distortion-induced stresses at the critical diaphragm section of Structures # 31-71-5805A and # 31-71-5807A were found to be 4.99 ksi and 5.35 ksi, respectively. The remaining fatigue lives corresponding to the estimated stress levels, the AASHTO category C' fatigue strength, and a 4-percent traffic growth rate were equal to 31.6 years for Structure # 31-71-5805A and 27.1 years for Structure # 31-71-5807A. It has been found that among the fatigue critical details used in Structure # 31-71-5807A, the web gap stress provides the shortest fatigue life. The most critical detail in Structure # 31-71-5805A, however, is at the fillet weld of a longitudinal attachment plate.

5.6. Conclusions

A fatigue evaluation was performed on fourteen steel bridge structures by utilizing the proposed fatigue reliability model. Among these structures, the fatigue lives of two bridges were determined based on the results obtained from strain gage instrumentation and various analytical bridge models. For the other structures, the fatigue lives were evaluated by utilizing a one-dimensional analytical model together with the AASHTO girder distribution factor (AASHTO, 1998).

The cycle counting results obtained from two steel bridges with different structural configurations and traffic characteristics have shown that the effective stress ranges provided by the two cycle counting procedures, one with and one without the racetrack method, are not significantly different. This observation indicates that the racetrack method might be a useful tool in the cycle counting procedure. Therefore, the computational time required to identify all ranges in the recorded strain history can be significantly reduced.

Additionally, by comparing the structural responses determined from the measured strain data and that from analytical bridge models, it has been shown that a three-dimensional model provides a more accurate estimate of the effective stress range than a one-dimensional model. Meanwhile, strain gage instrumentation can provide a realistic estimate of the structural response and tends to predict a longer fatigue life than a structural analysis of bridge models. An application of traffic count data in a fatigue evaluation was also demonstrated in the study. By comparing the fatigue lives predicted by using traffic count data along with statewide average gross weights, WIM data, and a 54-kip gross weight of the AASHTO fatigue truck, it has been demonstrated that use of traffic count data can provide a reasonable, albeit conservative, estimate of the fatigue life.

In addition, an evaluation procedure for the fatigue reliability-based analysis is provided in the chapter. The procedure can be utilized by practical engineers to determine the remaining fatigue life of steel bridge structures.

Table 5.1 – Summary of Gage Locations for the U.S.-20 Bridge

Member/Gage Location	Gage #	Location
Beam #8/Diaphragm-Interior Span (Section #1)	1-8-D-N-1	Bottom of Top Flange
	1-8-D-N-2	Beam Web at Bottom of Diaphragm
	1-8-D-N-3	Top of Bottom Flange
	1-8-D-S-1	Bottom of Top Flange
	1-8-D-S-2	Beam Web at Bottom of Diaphragm
	1-8-D-S-3	Top of Bottom Flange
Beam #8/Diaphragm-End Span (Section #2)	2-8-D-N-1	Bottom of Top Flange
	2-8-D-N-2	Beam Web at Bottom of Diaphragm
	2-8-D-N-3	Top of Bottom Flange
	2-8-D-S-1	Bottom of Top Flange
	2-8-D-S-2	Beam Web at Bottom of Diaphragm
	2-8-D-S-3	Top of Bottom Flange
Beam #10/Diaphragm-Interior Span (Section #3)	3-10-D-N-1	Bottom of Top Flange
	3-10-D-N-2	Beam Web at Bottom of Diaphragm
	3-10-D-N-3	Top of Bottom Flange
	3-10-D-S-1	Bottom of Top Flange
	3-10-D-S-2	Beam Web at Bottom of Diaphragm
	3-10-D-S-3	Top of Bottom Flange
Beam #10/Diaphragm-End Span (Section #4)	4-10-D-N-1	Bottom of Top Flange
	4-10-D-N-2	Beam Web at Bottom of Diaphragm
	4-10-D-N-3	Top of Bottom Flange
	4-10-D-S-1	Bottom of Top Flange
	4-10-D-S-2	Beam Web at Bottom of Diaphragm
	4-10-D-S-3	Top of Bottom Flange
Beam #8/Moment-Interior Span (Section #5)	1-8-M-N-1	Bottom of Top Flange
	1-8-M-N-2	Beam Web In-Line w/ Top of Diaphragm
	1-8-M-N-3	Beam Web In-Line w/Bottom of Diaphragm
	1-8-M-N-4	Top of Bottom Flange
Beam #8/Moment-End Span (Section #6)	2-8-M-N-1	Bottom of Top Flange
	2-8-M-N-2	Beam Web In-Line w/ Top of Diaphragm
	2-8-M-N-3	Beam Web In-Line w/Bottom of Diaphragm
	2-8-M-N-4	Top of Bottom Flange
Beam #10/Moment-Interior Span (Section #7)	3-10-M-N-1	Bottom of Top Flange
	3-10-M-N-2	Beam Web In-Line w/ Top of Diaphragm
	3-10-M-N-3	Beam Web In-Line w/Bottom of Diaphragm
	3-10-M-N-4	Top of Bottom Flange
Beam #10/Moment-End Span (Section #8)	4-10-M-N-1	Bottom of Top Flange
	4-10-M-N-2	Beam Web In-Line w/ Top of Diaphragm
	4-10-M-N-3	Beam Web In-Line w/Bottom of Diaphragm
	4-10-M-N-4	Top of Bottom Flange
Beam #9/Attachment Plate-End Span (Section #9)	5-9-S-S-1	Bottom of Top Flange
	5-9-S-S-2	Beam Web In-Line w/Bottom of Diaphragm
	5-9-S-S-3	Top of Bottom Flange

Table 5.2 – Maximum Strain Range at Maximum Moment Section for U.S.-20 Bridge

Section #	Maximum Strain Range (microstrain)
5	175
6	235
7	185
8	255

Table 5.3 – Statistical Parameters Obtained from Fitting Distribution of Rainflow Counting Results (Procedure #1) for U.S.-20 Bridge

Distribution	Parameter	Section 1 1-8-D-S-3	Section 2 2-8-D-S-3	Section 3 3-10-D-S-3	Section 4 4-10-D-S-3
Lognormal	Mean	1.60	1.63	1.72	2.00
	Std.	0.57	0.80	0.83	1.12
	Kolmogorov-Smirnov	0.18	0.13	0.12	0.10
	Est. Eff. Stress (ksi)	1.80	2.02	2.12	2.62
Exponential	Mean	1.60	1.63	1.72	1.99
	Std.	1.60	1.63	1.72	1.99
	Kolmogorov-Smirnov	0.40	0.36	0.34	0.31
	Est. Eff. Stress (ksi)	2.90	2.96	3.12	3.61
Weibull	Mean	1.59	1.63	1.72	2.00
	Std.	0.56	0.76	0.77	1.00
	Kolmogorov-Smirnov	0.16	0.12	0.11	0.12
	Est. Eff. Stress (ksi)	1.77	1.95	2.03	2.44
Rayleigh	Mean	1.49	1.59	1.67	1.98
	Std.	0.78	0.83	0.87	1.03
	Kolmogorov-Smirnov	0.29	0.15	0.14	0.10
	Est. Eff Stress (ksi)	1.85	1.97	2.07	2.45
Actual Effective Stress (ksi)		1.77	1.97	2.03	2.45

Table 5.4 – Statistical Parameters Obtained from Fitting Distribution of Racetrack and Rainflow Counting Results (Procedure #2) for U.S.-20 Bridge

Distribution	Parameter	Section 1 1-8-D-S-3	Section 2 2-8-D-S-3	Section 3 3-10-D-S-3	Section 4 4-10-D-S-3
Lognormal	Mean	1.57	1.67	1.68	2.05
	Std.	0.50	0.70	0.75	1.03
	Kolmogorov-Smirnov	0.19	0.15	0.11	0.10
	Est. Eff. Stress (ksi)	1.73	1.96	2.01	2.57
Exponential	Mean	1.56	1.66	1.67	2.05
	Std.	1.56	1.66	1.67	2.05
	Kolmogorov-Smirnov	0.43	0.37	0.35	0.32
	Est. Eff. Stress (ksi)	2.82	2.99	3.01	3.64
Weibull	Mean	1.55	1.66	1.67	2.05
	Std.	0.53	0.72	0.74	0.95
	Kolmogorov-Smirnov	0.18	0.11	0.16	0.09
	Est. Eff. Stress (ksi)	1.72	1.94	1.97	2.44
Rayleigh	Mean	1.45	1.59	1.61	2.00
	Std.	0.76	0.83	0.84	1.05
	Kolmogorov-Smirnov	0.32	0.19	0.15	0.12
	Est. Eff. Stress (ksi)	1.80	1.98	2.00	2.48
Actual Effective Stress (ksi)		1.70	1.95	1.98	2.46

Table 5.5 – Rainflow Counting Results (Procedure #1) of Bottom Flange Gages at Diaphragm Sections (U.S.-20 Bridge)

Parameters	Period	Section 1	Section 2	Section 3	Section 4
Effective Stress Range (ksi)	1st Week of March	1.78	2.02	2.01	2.42
	2nd Week of March	1.78	2.02	2.02	2.41
	1st Week of April	1.76	1.94	2.05	2.47
	2nd Week of April	1.78	1.95	2.02	2.48
	Total (Dec-May)	1.77	1.96	2.02	2.45
Number of Cycles Per Truck	1st Week of March	1.26	1.54	1.55	1.76
	2nd Week of March	1.24	1.53	1.58	1.78
	1st Week of April	1.27	1.56	1.67	1.85
	2nd Week of April	1.28	1.52	1.65	1.81
	Total (Dec-May)	1.26	1.54	1.56	1.79

Table 5.6 – Racetrack and Rainflow Counting Results (Procedure #2) of Bottom Flange Gages at Diaphragm Sections (U.S.-20 Bridge)

Parameters	Period	Section 1	Section 2	Section 3	Section 4
Effective Stress Range (ksi)	1st Week of March	1.72	1.97	1.95	2.46
	2nd Week of March	1.71	1.97	1.98	2.45
	1st Week of April	1.65	1.89	1.98	2.49
	2nd Week of April	1.67	1.91	1.96	2.50
	Total (Dec-May)	1.69	1.94	1.99	2.46
Number of Cycles Per Truck	1st Week of March	1.17	1.27	1.31	1.53
	2nd Week of March	1.15	1.24	1.26	1.47
	1st Week of April	1.18	1.28	1.32	1.50
	2nd Week of April	1.20	1.24	1.34	1.53
	Total (Dec-May)	1.17	1.25	1.32	1.52

Table 5.7 – Dynamic Load Factors of South-Side Bottom-Flange Gages at Diaphragm Sections (U.S.-20 Bridge)

Section	Gage #	Dynamic Load Factor				Number of Trucks
		Average	Std. Dev.	C.O.V.	Maximum	
1	1-8-D-S-3	0.06	0.03	0.50	0.36	4113
2	2-8-D-S-3	0.09	0.04	0.44	0.59	4116
3	3-10-D-S-3	0.08	0.05	0.63	0.34	5511
4	4-10-D-S-3	0.12	0.07	0.58	0.52	4828

Table 5.8 – Comparison of Effective Stress Ranges Computed Using Strain Gage Data and Analytical Models (U.S.-20 Bridge)

Model	Diaphragm in Span 1	Section 4	Section 9	Bolted Splice Plate over Pier 10
1-D AASHTO Non-Composite	6.35	6.02	6.11	6.16
1-D AASHTO Truck Composite	4.39	4.17	4.23	-
1-D 4-Axle Truck Non-Composite	5.36	5.06	5.28	5.47
1-D 4-Axle Truck Composite	3.68	3.52	3.66	-
3-D AASHTO Non-Composite	3.84	3.71	3.91	4.65
3-D AASHTO Truck Composite	3.57	3.39	3.63	-
3-D 4-Axle Truck Non-Composite	3.21	3.13	3.17	3.93
3-D 4-Axle Truck Composite	3.02	2.95	3.02	-
Strain Gage Data (Dec-May)	2.51*	2.45	2.43	3.08*
Traffic Count with 1-D 4-Axle Non-Composite	3.86	3.64	3.80	3.94
Traffic Count with 1-D 4-Axle Composite	2.65	2.53	2.63	-

***** Estimated from stress range envelope of three-dimensional finite model with 4-axle fatigue truck

Table 5.9 – Input Parameters Used in Fatigue Life Estimation for U.S.-20 Bridge

Parameters	Mean	C.O.V	Distribution
Uncertainty in Miner's Rule	1	0.15	Lognormal
Effective Stress Range (ksi)	Varies	0.09	Lognormal
Number of Cycles Per Passage	1	0.05	Lognormal
ADTT at 33th year of service	776	0.1	Lognormal
Traffic Growth Rate (%)	2, 4	-	Deterministic
Fraction of Truck Traffic in a Single Lane	0.85	-	Deterministic
Maximum Highway Capacity (Vehicles/Day/Lane)	20000	-	Deterministic
Percent Truck Traffic (%)	18	-	Deterministic
Categories C and D for Diaphragm-to-Web Weld, Category C for Improperly Located Attachment Plate, and B for Bolted Splice Plate Detail			
Probability of Survival = 0.9775 (Reliability Index =2)			

Table 5.10 – Estimated Total Fatigue Life (in Years) for U.S.-20 Bridge Based upon Strain Data

Location	S_{re} (ksi)	Traffic Growth Rate (%)	Category		
			B	C	D
Diaphragm Section	1.96	2	-	>=150	>=150
		4	-	>=150	>=150
Improperly Located Attachment Plate	1.53	2	-	>=150	-
		4	-	>=150	-
Bolted Splice Plate Detail	3.08	2	>=150	-	-
		4	>=150	-	-

Table 5.11 – Summary of Strain Gage Locations for the I-65 SBL Bridge

Section #	Gage #	Location
Section #1 Located At 18" South of the Diaphragm # 12 - Girder Line 11	1	Top Flange - East Side
	2	Top Flange - West Side
	3	Girder Web - 1' from the Top Flange - East Side
	4	Girder Web - 1' from the Top Flange - West Side
	5	Girder Web - 2' from the Top Flange - East Side
	6	Girder Web - 2' from the Top Flange - West Side
	7	Bottom Flange - East Side
	8	Bottom Flange - West Side
Section #2 Located At 18" South of the Diaphragm # 7 - Girder Line 11	9	Girder Web - 1'-8" from the Top Flange - East Side
	10	Girder Web - 1'-8" ft from the Top Flange - West Side
	11	Girder Web - 3'-4" ft from the Top Flange - East Side
	12	Girder Web - 3'-4" ft from the Top Flange - West Side
	13	Bottom Flange - East Side
	14	Bottom Flange - West Side
Section #3 Located At 18" South of the Diaphragm # 12 – Girder Line 10	15	Top Flange - East Side
	16	Top Flange - West Side
	17	Girder Web - 1 ft from the Top Flange – East Side
	18	Girder Web - 1 ft from the Top Flange – West Side
	19	Girder Web - 2 ft from the Top Flange – East Side
	20	Girder Web - 2 ft from the Top Flange – West Side
	21	Bottom Flange - East Side
	22	Bottom Flange - West Side
Section #4 Located At 4” South of the Diaphragm # 12 - Girder Line 11	23	Top Flange - East Side
	24	Top Flange - West Side
	25	Girder Web - 1 ft from the Top Flange – East Side
	26	Girder Web - 1 ft from the Top Flange – West Side
	27	Girder Web - 2 ft from the Top Flange – East Side
	28	Girder Web - 2 ft from the Top Flange – West Side
	29	Bottom Flange - East Side
	30	Bottom Flange - West Side

Table 5.12 – Maximum Strain Range of West Side Gages for the I-65 SBL Bridge

Section #	Maximum Strain Range (microstrain)
1	210
2	170
3	190
4	200

Table 5.13 – Statistical Parameters Obtained from Fitting Distribution of Rainflow Counting Results (Procedure #1) for the I-65 SBL Bridge

Distribution	Parameter	Section1 Strain #8	Section2 Strain #14	Section3 Strain #22	Section4 Strain #30
Lognormal	Mean (ksi)	1.71	1.59	1.50	1.65
	Std.	0.82	0.58	0.60	0.77
	Kolmogorov-Smirnov	0.23	0.22	0.23	0.24
	Est. Eff. Stress (ksi)	2.10	1.81	1.74	2.01
Exponential	Mean (ksi)	1.70	1.59	1.50	1.65
	Std.	1.70	1.59	1.50	1.65
	Kolmogorov-Smirnov	0.40	0.42	0.44	0.41
	Est. Eff. Stress (ksi)	3.07	2.87	2.72	2.98
Weibull	Mean (ksi)	1.71	1.59	1.50	1.66
	Std.	0.73	0.53	0.60	0.69
	Kolmogorov-Smirnov	0.21	0.21	0.18	0.21
	Est. Eff. Stress (ksi)	1.99	1.75	1.72	1.92
Rayleigh	Mean (ksi)	1.64	1.48	1.43	1.59
	Std.	0.86	0.77	0.75	0.83
	Kolmogorov-Smirnov	0.20	0.28	0.25	0.21
	Est. Eff. Stress (ksi)	2.04	1.84	1.77	1.97
Actual Effective Stress (ksi)		1.97	1.74	1.70	1.90

Table 5.14 – Statistical Parameters Obtained from Fitting Distribution of Racetrack and Rainflow Counting Results (Procedure #2) for the I-65 SBL Bridge

Distribution	Parameter	Section1 Strain #8	Section2 Strain #14	Section3 Strain #22	Section4 Strain #30
Lognormal	Mean	1.68	1.63	1.47	1.60
	Std.	0.78	0.55	0.58	0.70
	Kolmogorov-Smirnov	0.14	0.18	0.13	0.13
	Est. Eff. Stress (ksi)	2.04	1.82	1.70	1.91
Exponential	Mean	1.67	1.63	1.47	1.60
	Std.	1.67	1.63	1.47	1.60
	Kolmogorov-Smirnov	0.35	0.39	0.39	0.37
	Est. Eff. Stress (ksi)	3.01	2.94	2.67	2.89
Weibull	Mean	1.68	1.62	1.47	1.60
	Std.	0.67	0.51	0.59	0.64
	Kolmogorov-Smirnov	0.09	0.13	0.13	0.11
	Est. Eff. Stress (ksi)	1.92	1.77	1.69	1.83
Rayleigh	Mean	1.60	1.51	1.40	1.52
	Std.	0.84	0.79	0.73	0.80
	Kolmogorov-Smirnov	0.15	0.28	0.20	0.16
	Est. Eff. Stress (ksi)	1.98	1.87	1.74	1.89
Actual Effective Stress (ksi)		1.92	1.77	1.69	1.83

Table 5.15 – Rainflow Counting Results (Procedure #1) of Bottom Flange Gages (I-65 SBL Bridge)

Parameters	Period	Section 1	Section 2	Section 3	Section 4
Effective Stress Range (ksi)	Week1	1.88	1.68	1.70	1.82
	Week2	1.88	1.69	1.66	1.81
	Week3	1.88	1.67	1.69	1.82
	Week4 (3 Days)	1.87	1.66	1.65	1.82
	Total (24 Days)	1.88	1.68	1.68	1.82
Number of Cycles Per Truck	Week1	1.28	1.15	1.21	1.31
	Week2	1.28	1.18	1.22	1.30
	Week3	1.33	1.21	1.22	1.31
	Week4 (3 Days)	1.31	1.16	1.20	1.31
	Total (24 Days)	1.32	1.18	1.21	1.30

Table 5.16 – Racetrack and Rainflow Counting Results (Procedure #2) of Bottom Flange Gages (I-65 SBL Bridge)

Parameters	Period	Section 1	Section 2	Section 3	Section 4
Effective Stress Range (ksi)	Week1	1.78	1.70	1.67	1.76
	Week2	1.84	1.75	1.64	1.79
	Week3	1.80	1.76	1.67	1.75
	Week4 (3 Days)	1.75	1.69	1.63	1.77
	Total (24 Days)	1.83	1.72	1.66	1.77
Number of Cycles Per Truck	Week1	1.20	1.02	1.08	1.22
	Week2	1.22	1.02	1.08	1.24
	Week3	1.24	1.07	1.04	1.24
	Week4 (3 Days)	1.20	1.02	1.06	1.22
	Total (24 Days)	1.24	1.02	1.07	1.23

Table 5.17 – Dynamic Load Factors of Bottom Flange Gages (I-65 SBL Bridge)

Section #	Gage #	Dynamic Load Factor				Number of Trucks
		Average	Std. Dev.	C.O.V.	Maximum	
1	Gage #7	0.13	0.05	0.38	0.53	12444
	Gage #8	0.11	0.04	0.36	0.53	14248
2	Gage #13	0.08	0.03	0.38	0.66	10178
	Gage #14	0.06	0.02	0.33	0.34	11816
3	Gage #21	0.10	0.04	0.40	0.44	9543
	Gage #22	0.10	0.04	0.40	0.66	10995
4	Gage #29	0.13	0.05	0.38	0.51	13018
	Gage #30	0.11	0.04	0.36	0.48	13845

Table 5.18 – Comparison of Effective Stress Range Computed Using Strain Gage Data and Analytical Results (I-65 SBL Bridge)

Location	Effective Stress Range (ksi)		
	1-D Model	3-D Model	Strain Gage Data
Diaphragm #12 - Toe of Transverse Stiffener Weld to Girder Web	3.63	2.54	1.80*
Section #1 – Top of Bottom Flange	3.73	2.64	1.88
Diaphragm #7-Toe of Transverse Stiffener Weld to Girder Web	2.97	2.22	1.65*
Section #2 – Top of Bottom Flange	3.02	2.26	1.68
Diaphragm #2 - Toe of Transverse Stiffener Weld to Girder Web	3.79	2.68	2.00*
Fillet Weld of Transverse Stiffener to Bottom flange (Max)	4.73	3.09	2.20*
Web-to-Flange Fillet Weld (Max)	4.80	3.18	2.26*

* Estimated from stress range envelope of three-dimensional finite element model

Table 5.19 – Input Parameters Used in Fatigue Life Estimation for the I-65 SBL Bridge

Parameters	Mean	COV	Distribution
Uncertainty in Miner's Rule	1	0.15	Lognormal
Effective Stress Range (ksi)	Varies	0.09	Lognormal
Number of Cycles Per Passage	1	0.05	Lognormal
ADTT at 35th year of service	4392	0.1	Lognormal
Traffic Growth Rate (%)	0, 2, 4	-	Deterministic
Fraction of Truck Traffic in a Single Lane	0.85	-	Deterministic
Maximum Highway Capacity (Vehicles/Day/Lane)	20000	-	Deterministic
Percent Truck Traffic (%)	37	-	Deterministic
Category C′ (Transverse Stiffener Details) and Category B (Retrofit Bolted Connection and Web-to-Flange Fillet Weld)			
Probability of Survival = 0.9775 (Reliability Index =2)			

Table 5.20 – Estimated Total Fatigue Life Based on Measured Strains for the Southbound I-65 Structure (in Years)

Location	Traffic Growth Rate (%)	Category C′ Transverse Stiffener	Category B Bolt Connection and Builtup Members
Diaphragm Section in Exterior Span (Effective Stress Range = 2.0 ksi)	0	>=150	>=150
	2	>=150	>=150
	4	>=150	>=150
Diaphragm Section in Interior Span (Effective Stress Range = 1.65 ksi)	0	>=150	>=150
	2	>=150	>=150
	4	>=150	>=150
Transverse Intermediate Stiffener (Effective Stress Range = 2.20 ksi)	0	>=150	-
	2	>=150	-
	4	>=150	-
Web-to-Flange Fillet Weld (Effective Stress Range = 2.26 ksi)	0	-	>=150
	2	-	>=150
	4	-	>=150

Table 5.21 – Estimated Total Fatigue Life Based on Measured Strains for the Northbound I-65 Structure (in Years)

Location	Traffic Growth Rate (%)	Category C′ Transverse Stiffener	Category B Bolt Connection and Buitup Members
Diaphragm Section in Exterior Span (Effective Stress Range = 2.28 ksi)	0	>=150	>=150
	2	139.7	>=150
	4	138.2	>=150
Diaphragm Section in Interior Span (Effective Stress Range = 1.88 ksi)	0	>=150	>=150
	2	>=150	>=150
	4	>=150	>=150
Transverse Intermediate Stiffener (Effective Stress Range = 2.51 ksi)	0	>=150	-
	2	112.8	-
	4	111.3	-
Web-to-Flange Fillet Weld (Effective Stress Range = 2.58 ksi)	0	-	>=150
	2	-	>=150
	4	-	>=150

Table 5.22 – Locations of Steel Bridges Examined on Extra Heavy Duty Corridor

Structure No.	Highway	County	Log Mile	Feature Crossed	Year Built
20-64-1010A	U.S. 20	Porter	1.4	CSX Transportation	1931
20-64-2458A	U.S. 20	Porter	16.44	Amtrak & Chandler Road	1969
21-4	U.S. 20	La Porte	14.36	Toll Road Interstate 80-90	1956
20-71-2205B	U.S. 20	St. Joseph	11.25	Ardmore Trail & 2 Railroads	1958
20-71-4045B	U.S. 20	St. Joseph	12.33	State Route 2	1958
20-71-4047B	U.S. 20	St. Joseph	14.01	Mayflower Road	1961
20-71-2206B	U.S. 20	St. Joseph	14.13	G.T.W. RR & Private Farm Road	1961
20-71-2207C	U.S. 20	St. Joseph	14.43	Abandoned RR & Private Farm Road	1964
31-71-5805A	U.S. 31	St. Joseph	19.04	U.S. Route 20 & U.S.20X	1975
31-71-5807A	U.S. 31	St. Joseph	20.73	Toll Road Interstate 80-90	1975
249-64-4238B	U.S. 249	Porter	0.24	Interstate 94	1967
249-64-5414C	U.S. 249	Porter	0.95	Little Calumet River	1972
149-64-4467B	U.S. 249	Porter	7.91	Interstate 94	1969

Table 5.23 – Geometrical Details of Steel Bridges on the Extra Heavy Duty Corridor (1999-2000 Inventory of Bridges – State Highway System of Indiana)

Structure No.	Skew Angle	Type	Span Length	Roadway Width
20-64-1010A	45°	Continuous Steel Beam	44'-8",45'-8",66',45'-8",44'-8"	54'-00"
20-64-2458A	45°	Continuous Steel Beam	42'-3",43'-0",23'-5",2@44'-3",50'-11",44'-3",23'-5",43'-0"	-
21-4	19°	Continuous Steel Beam	32',45',32',45',32'	85'-04"
20-71-2205A	10°	Continuous Steel Beam	37'-2",50',60',72',60',37'-2"	2@32'-11"
20-71-4045A	-	Continuous Steel Beam	38'-1",2@55'-3",38'-1"	2@46'-05"
20-71-4047A	35°	Continuous Steel Beam	40'-6",58'-0",47'-6",51'-0"	32'-11",44'-11"
20-71-2206A	31°	Continuous Steel Beam	60',72',60'	2@32'-11"
20-71-2207B	13°	Continuous Steel Beam	30',50',60',50',40'	2@32'-11"
31-71-5805A	26°	Steel Beam, Composite Continuous Steel Girder, Steel Beam	39',144'-6",39'	52'-07"
31-71-5807A	-	Composite Continuous Steel Girder	2@115'	52'-08"
249-64-4238B	-	Composite Continuous Steel Beam	38'-7",2@82',38'-7"	51'-08"
249-64-5414B	30°	Composite Continuous Steel Beam	62',88',62'	39'-06"
149-64-4467A	-	Composite Continuous Steel Girder	2@105'	2@47'-10"

Table 5.24 – Estimated Remaining Fatigue Life of Bridges on Extra Heavy Duty Corridor

Structure #	Fatigue Detail (AASHTO Category - Description)	Stress Range (ksi)	Remaining Fatigue Life (Years) with Traffic Growth Rate	
			2%	4%
20-64-1010A	1. D - Welded Diaphragm Connection	2.64	84.2	61.0
	2. B - Bolted Splice Plate	4.88	77.2	55.1
20-64-2458A	1. D - Welded Diaphragm Connection	3.54	45.6	35.6
	2. B - Bolted Splice Plate	5.47	61.4	44.8
21-4	1. D - Riveted Diaphragm Connection	3.12	59.6	44.3
	2. D - Riveted Splice Plate	3.96	29.4	26.7
20-71-2205B	1. B - Bolted Diaphragm Connection	1.14	>=150	>=150
	2. D - Riveted Diaphragm Connection	2.87	71.1	51.3
	3. B - Bolted Splice Plate	4.36	91.1	68.4
20-71-4045B	1. D - Longitudinal Weld at Diaphragm	3.58	42.1	34.2
	2. D - Riveted Diaphragm Connection	2.89	70.2	50.7
	3. B - Bolted Diaphragm Connection	0.77	>=150	>=150
	4. B - Bolted Splice Plate	5.77	52.9	40.4
20-71-4047B	1. D - Riveted Diaphragm Connection	3.17	58.2	43.2
	2. B - Bolted Diaphragm Connection	0.94	>=150	>=150
	3. B - Bolted Splice Plate	4.89	75.4	54.3
20-71-2206B	1. D - Riveted Diaphragm Connection	3.28	53.7	40.7
	2. B - Bolted Diaphragm Connection	0.55	>=150	>=150
	3. B - Bolted Spliced Plate	4.00	105.7	82.8
20-71-2207C	1. D - Welded Diaphragm Connection	3.08	62.3	45.5
	2. B - Bolted Diaphragm Connection	1.37	>=150	>=150
	3. B - Bolted Splice Plate	4.89	75.7	54.4

Table 5.24 (Cont.) – Estimated Remaining Fatigue Life of Bridges on Extra Heavy Duty Corridor

Structure #	Fatigue Detail (AASHTO Category - Description)	Stress Range (ksi)	Remaining Fatigue Life (Years) with Traffic Growth Rate	
			2%	4%
31-71-5805A	1. B - Web-to-Flange Fillet Weld	3.27	>=150	135.8
	2. B - Bolted Splice Plate	2.68	>=150	>=150
	3. B - Bolted Diaphragm Connection	1.77	>=150	>=150
	4. C′ - Transverse Intermediate Stiffener	3.14	93.4	69.9
	5. C′ - Transverse Stiffener at Diaphragm	3.15	92.9	69.4
	6. B - Bolted Transverse Stiffener to Bottom Flange	3.36	>=150	126.7
	7. E – Fillet Weld at Longitudinal Attachment Plate	3.12	29.2	25.0
	8. B - Bottom Flange Butt Weld	3.25	161.3	137.9
	9. C′ - Web Gap at Cross-Frame Diaphragm	4.99	40.1	31.6
31-71-5807A	1. C′ - Transverse Intermediate Stiffener	4.67	42.5	33.3
	2. C′ - Transverse Stiffener at Diaphragm	3.68	71.8	51.1
	3. B - Bolted Transverse Stiffener to Bottom Flange	3.94	111.7	87.7
	4. B - Bolted Splice Plate	4.56	86.3	62.9
	5. B – Web-to-Flange Fillet Weld	4.83	78.6	56.2
	6. B - Bottom Flange Butt Weld	4.97	74.8	53.3
	7. C′ - Web Gap at Cross-Frame Diaphragm	5.35	32.5	27.1
249-64-4238B	1. B - Bolted Diaphragm Connection	4.33	95.8	71.6
	2. B - Bolted Splice Plate	5.19	72.3	50.8
249-64-5414C	1. D - Welded Diaphragm Connection	3.85	36.5	29.8
	2. B - Bolted Diaphragm Connection	3.12	>=150	>=150
	3. B - Bolted Splice Plate	5.70	56.6	41.9
149-64-4467B	1. D - Welded Diaphragm Connection	3.95	32.8	27.8
	2. C′ - Transverse Stiffener at Middle Support	3.09	95.9	72.3
	3. B - Bolted Splice Plate	6.79	35.1	29.2
	4. B – Web-to-Flange Fillet Weld	5.54	59.8	43.8

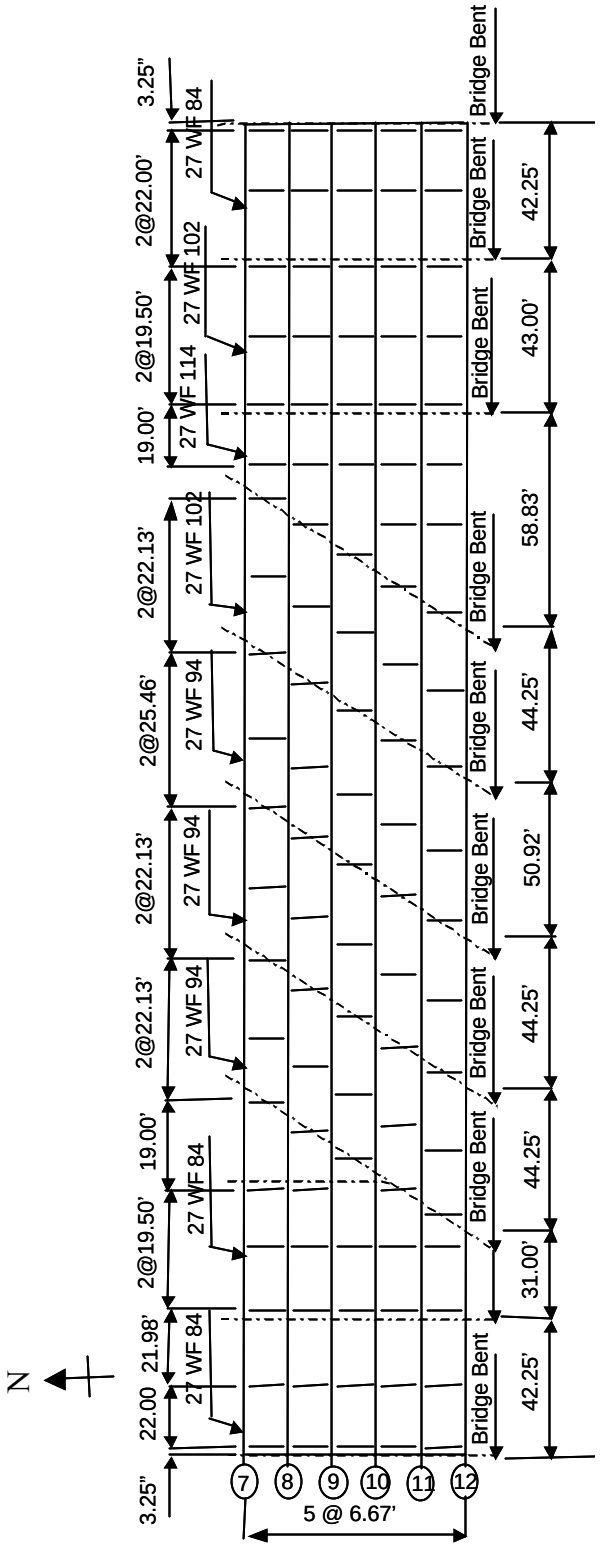

Figure 5.1 – Framing Plan of U.S.-20 Bridge near Michigan City

Figure 5.2 – Typical Bolted Splice Plate at Support

Figure 5.3 – Intermittent-Welded Diaphragm

Figure 5.4 – Shear-Plate Connection at Diaphragm Section

Figure 5.5 – Improperly Located Shear Plate

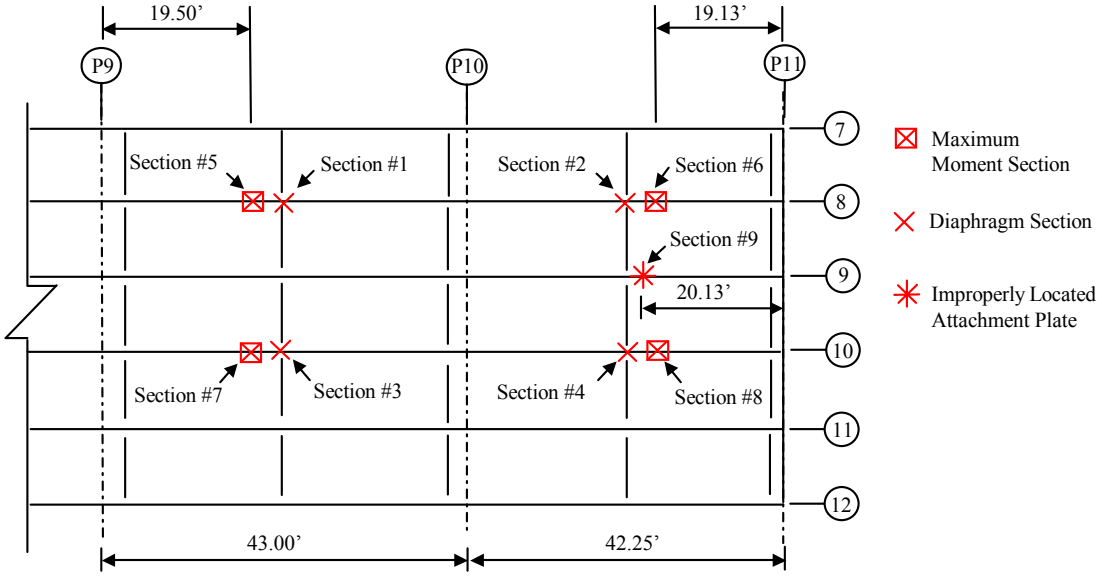

Figure 5.6 – Sections Monitored for U.S.-20 Bridge

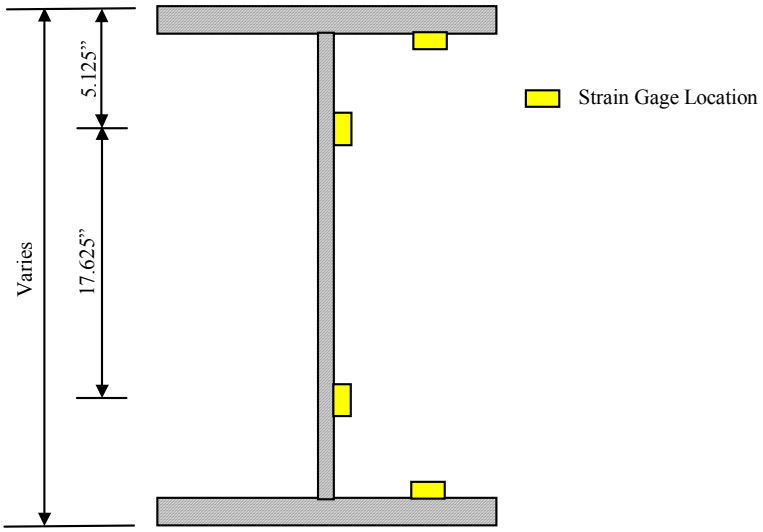

Figure 5.7 – Strain Gage Locations at the Maximum Moment Section

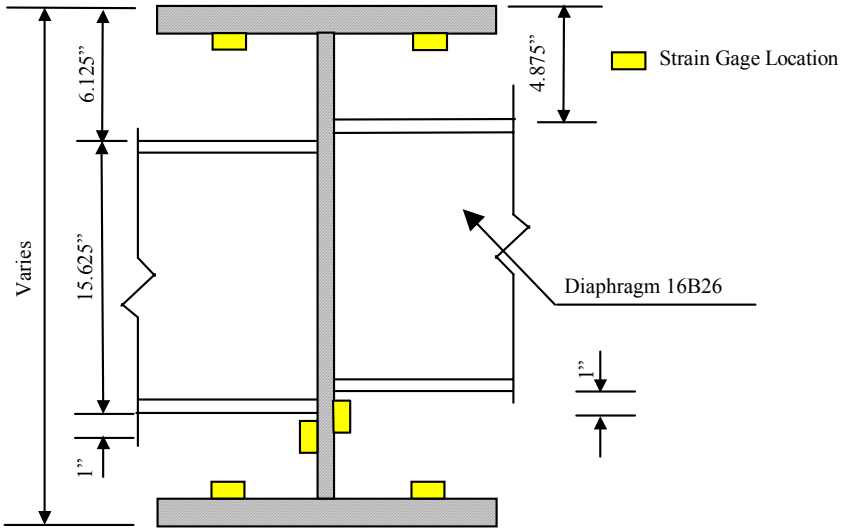

Figure 5.8 – Strain Gage Locations at the Diaphragm Section

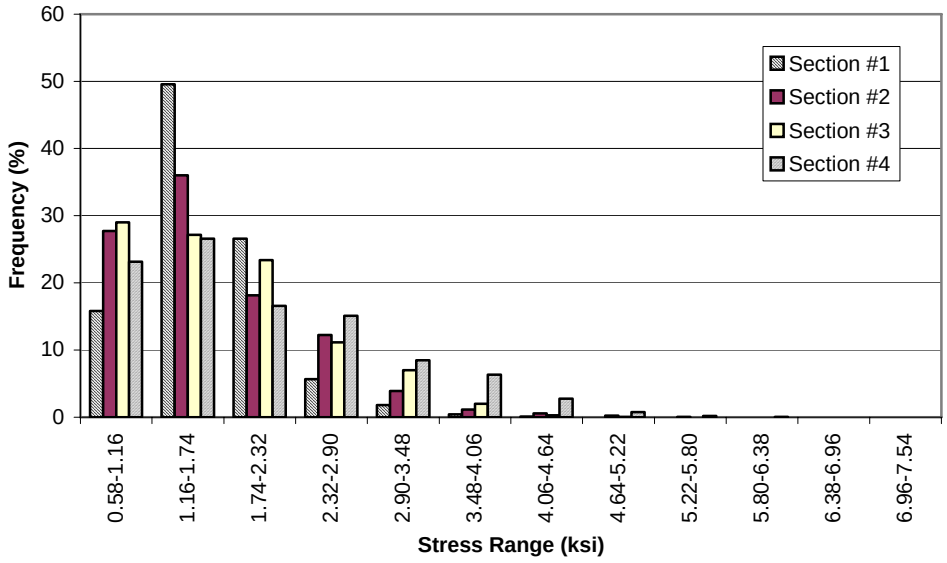

a) Rainflow Counting Method (Procedure #1)

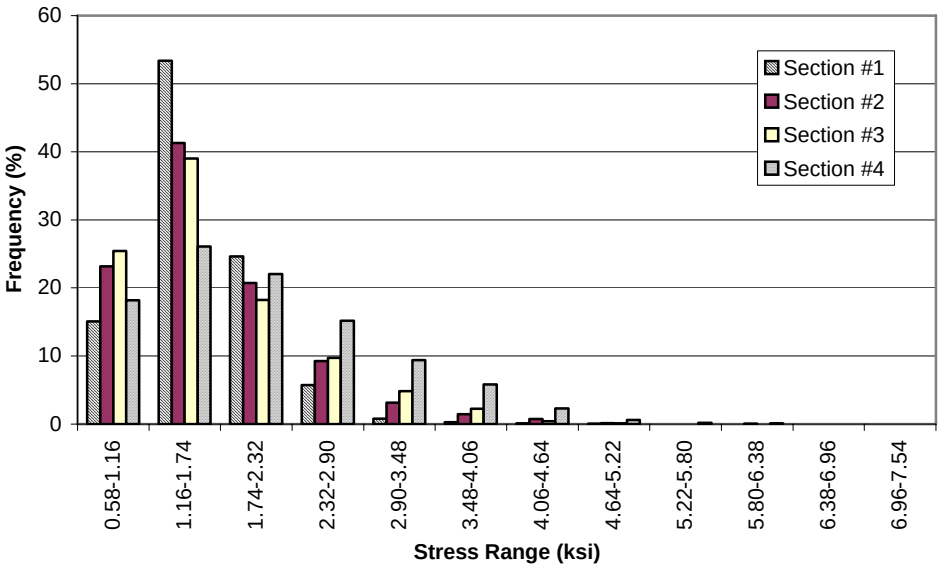

b) Racetrack and Rainflow Counting Methods (Procedure #2)

Figure 5.9 – Cycle Counting Results of South-Side Bottom-Flange Gages (U.S.-20 Bridge)

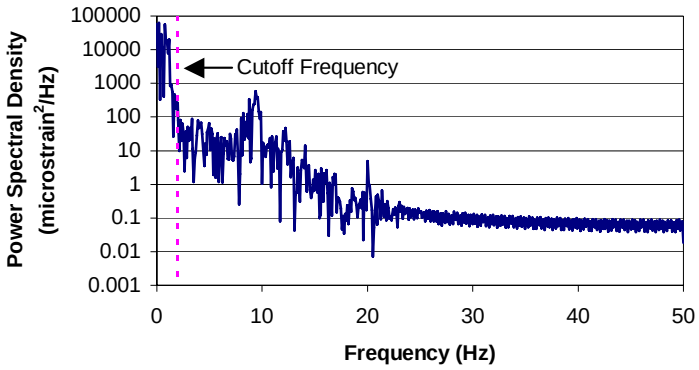

Figure 5.10 – Power Spectral Density of Sampled Strain Data at South-Side Bottom-Flange Gage of Section # 4 (U.S.-20 Bridge)

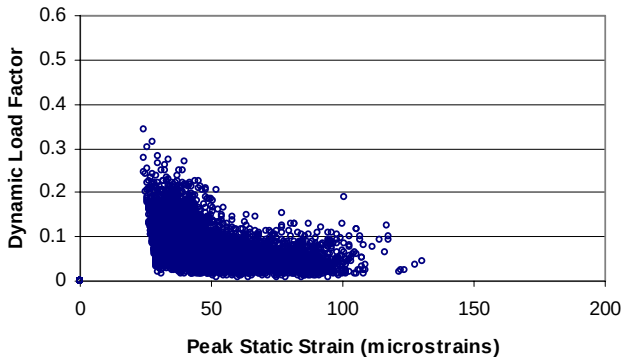

Figure 5.11 – Dynamic Load Factors at South-Side Bottom-Flange Gage of Section # 3 (U.S.-20 Bridge)

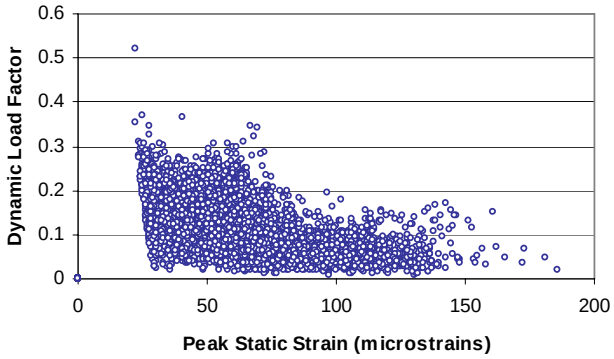

Figure 5.12 – Dynamic Load Factors at South-Side Bottom-Flange Gage of Section # 4 (U.S.-20 Bridge)

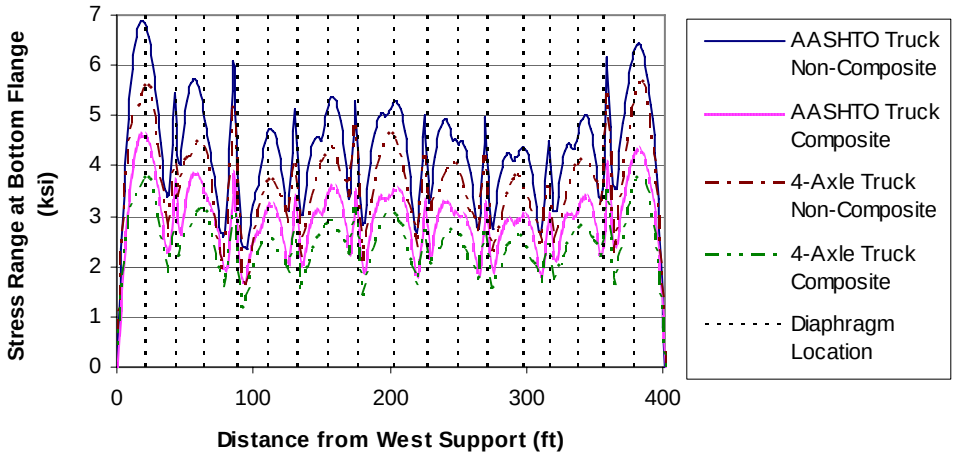

a) All Spans

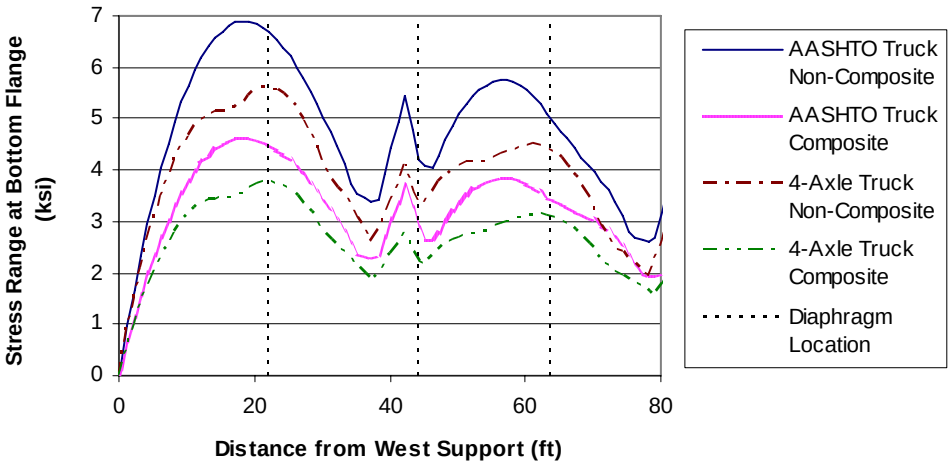

b) First Two Spans

Figure 5.13 – Stress Range Envelope Curves of One-Dimensional Model for U.S.-20 Bridge

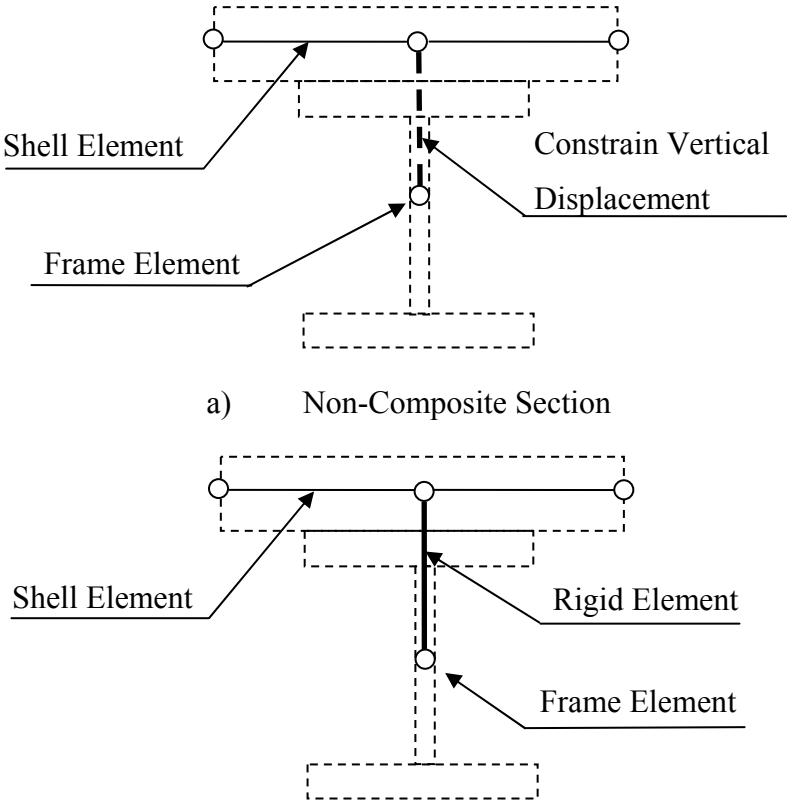

Figure 5.14 – Cross Section of Three-Dimensional Finite Element Model for U.S.-20 Bridge

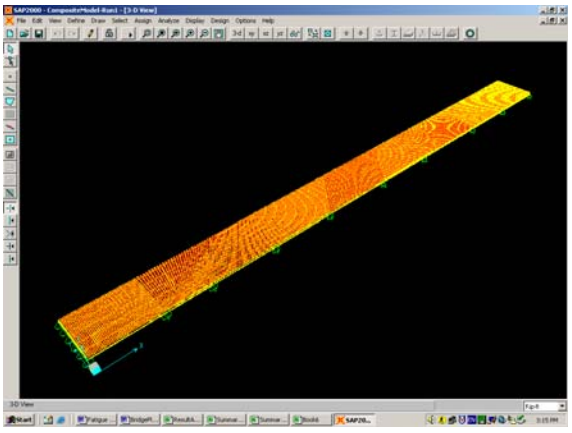

Figure 5.15 – Isometric View of Three-Dimensional Finite Element Model for Composite Section (U.S.-20 Bridge)

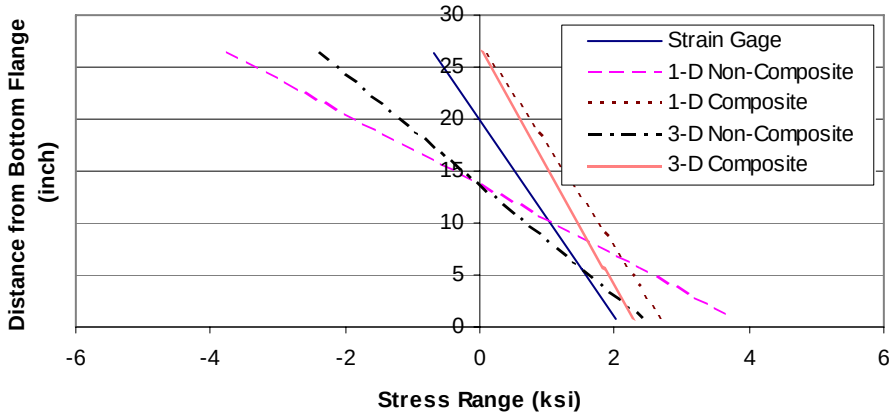

a) Interior Span (Section #3)

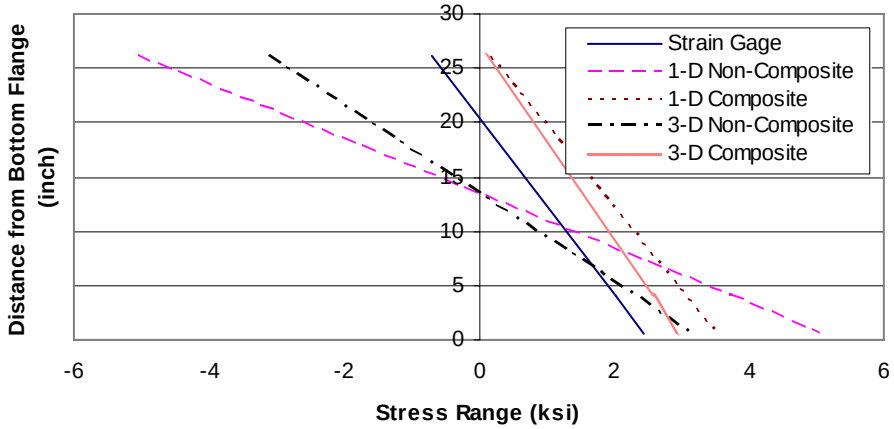

b) Exterior Span (Section #4)

Figure 5.16 – Comparison of Neutral Axis Locations of Strain Gage Data and Analytical Models with 4-Axle Fatigue Truck (U.S.-20 Bridge)

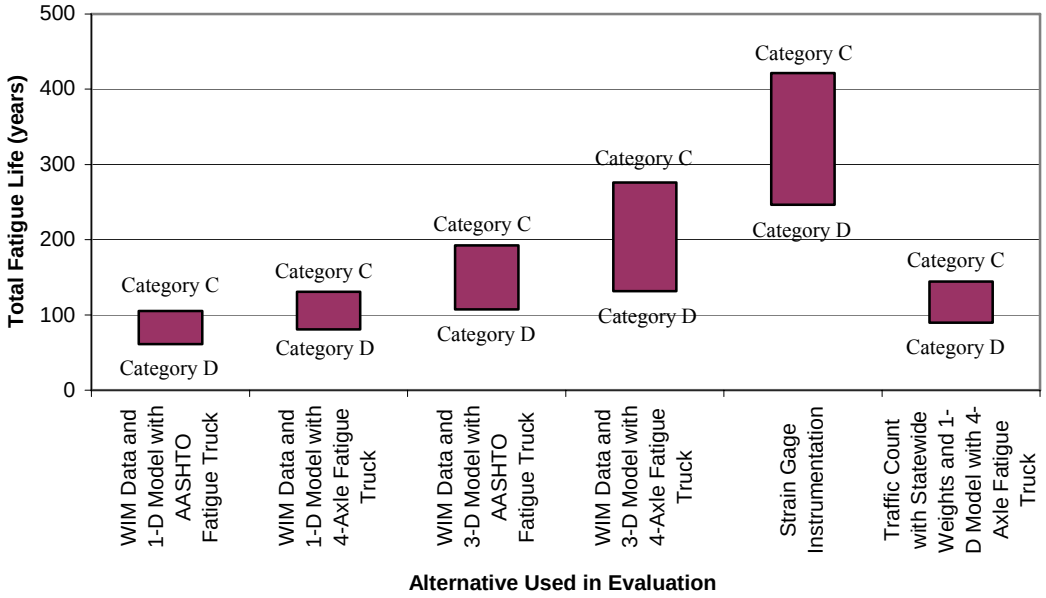

Figure 5.17 – Fatigue Life at Diaphragm Section with
A 2-Percent Traffic Growth Rate (U.S.-20 Bridge)

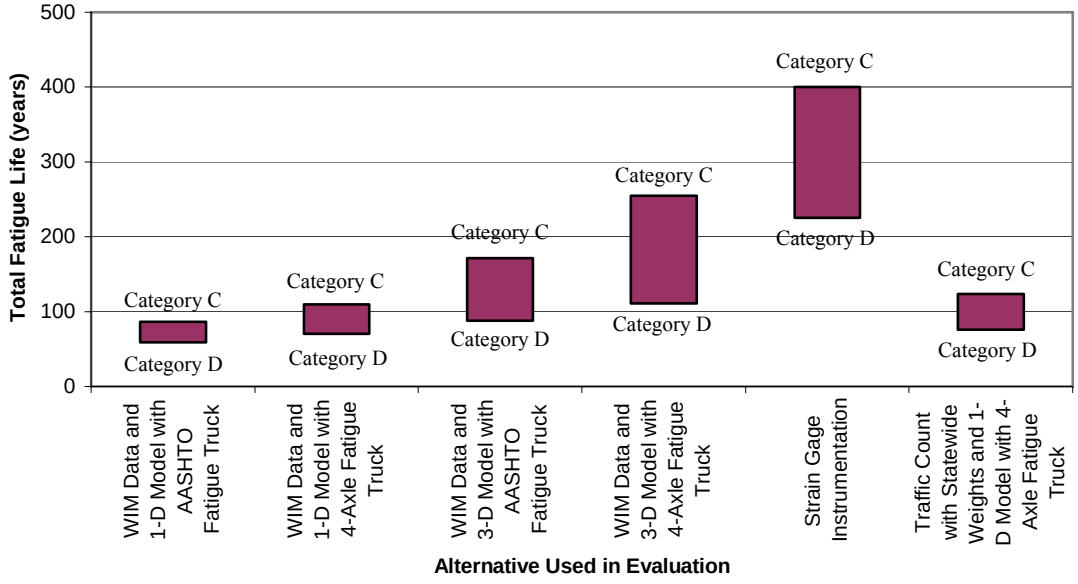

Figure 5.18 – Fatigue Life at Diaphragm Section with
A 4-Percent Traffic Growth Rate (U.S.-20 Bridge)

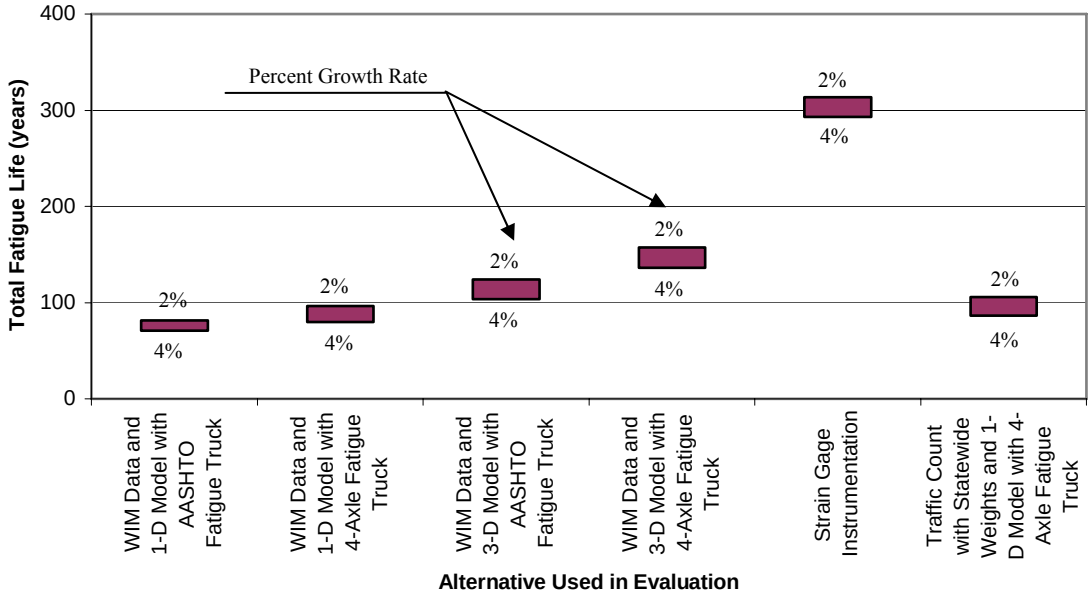

Figure 5.19 – Fatigue Life at Bolted Splice Plate Detail (U.S.-20 Bridge)

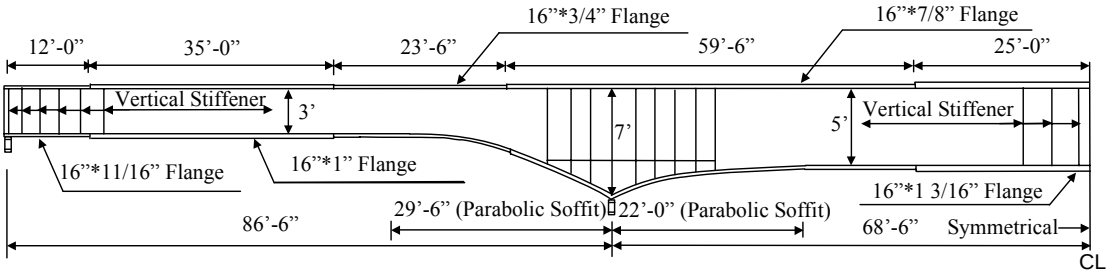

Figure 5.20 – Typical Profile of Longitudinal Plate Girder

Figure 5.21 – Retrofit Angle Detail at Diaphragm Section

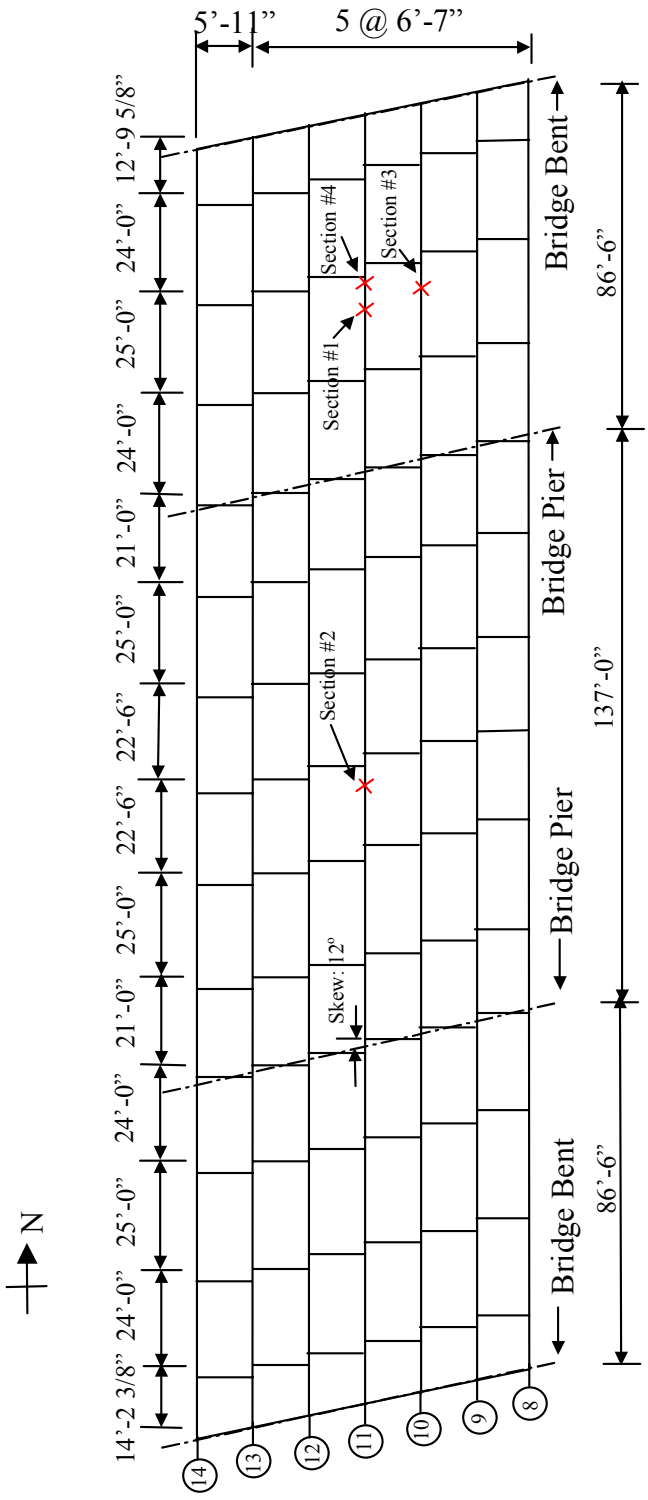

Figure 5.22 – Framing Plan and Monitored Locations for the I-65 SBL Bridge

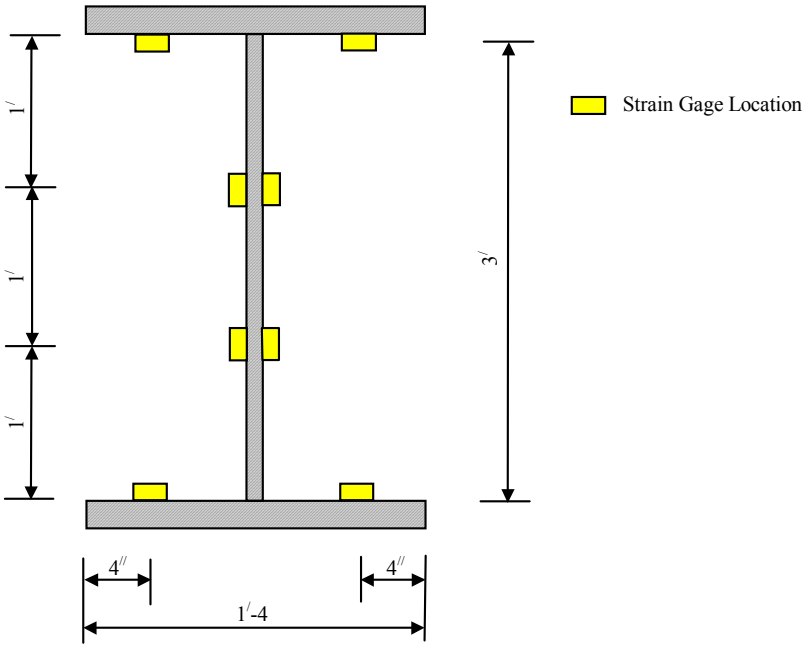

Figure 5.23 – Strain Gage Locations at Sections # 1 and # 3

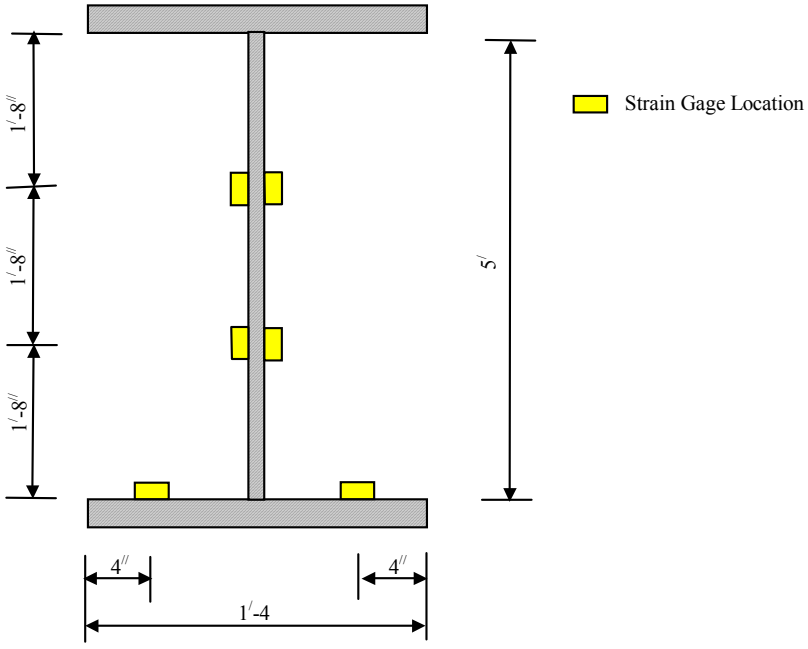

Figure 5.24 – Strain Gage Locations at Section # 2

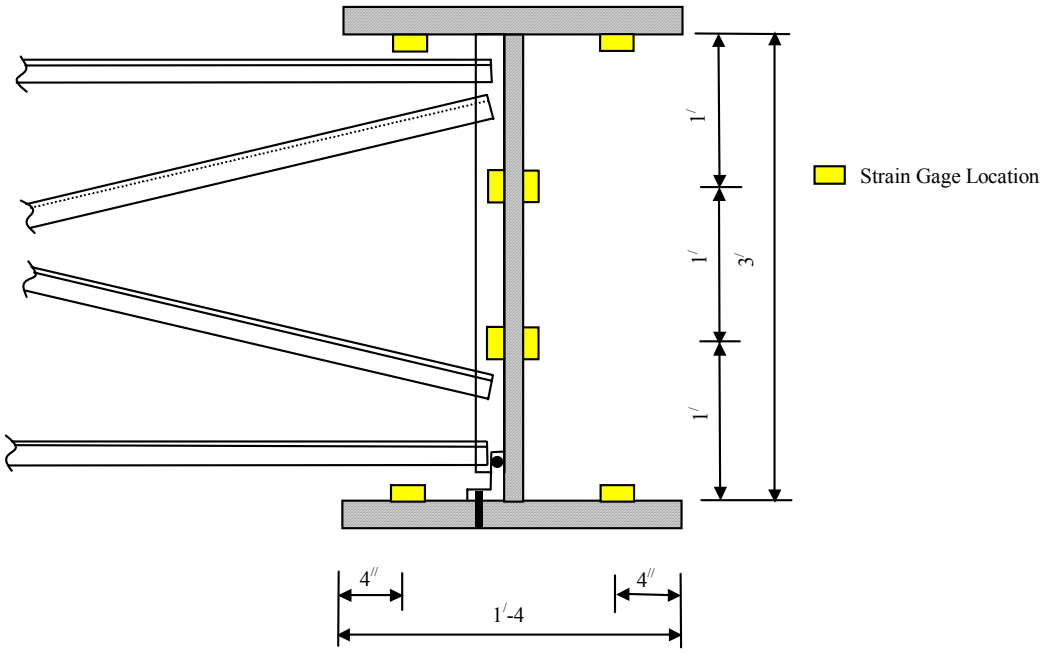

Figure 5.25 – Strain Gage Locations at Section # 4

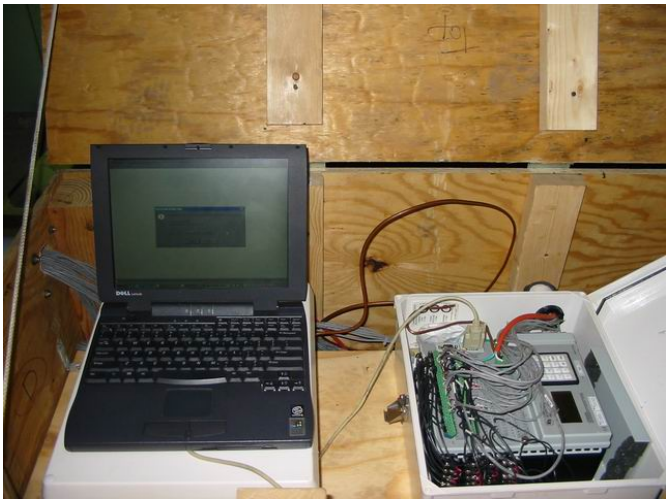

a) CR 5000 Data Acquisition System and Cable Wiring

b) Strain Gage Instrumentation at Section #2

Figure 5.26 – Test Setup for I-65 Bridge

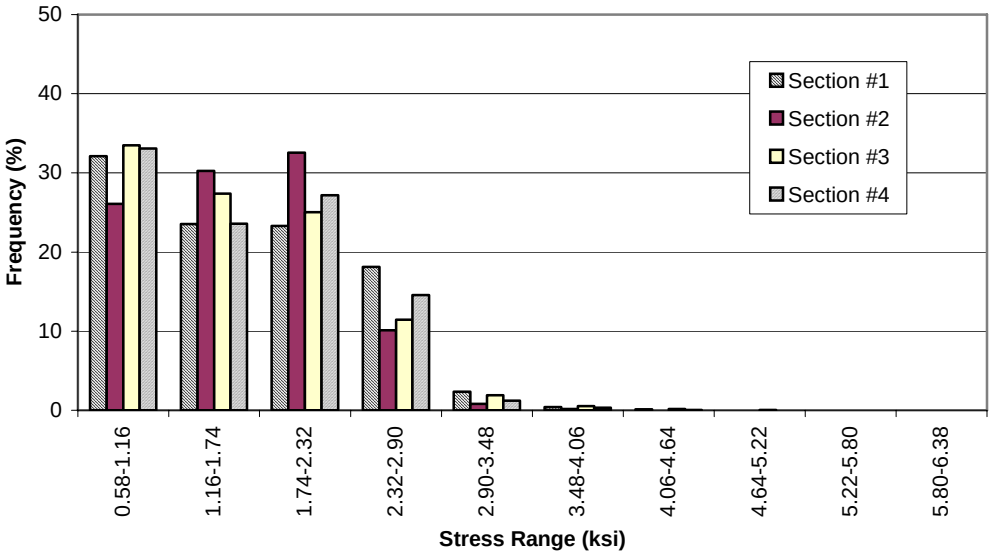

a) Rainflow Counting Method (Procedure #1)

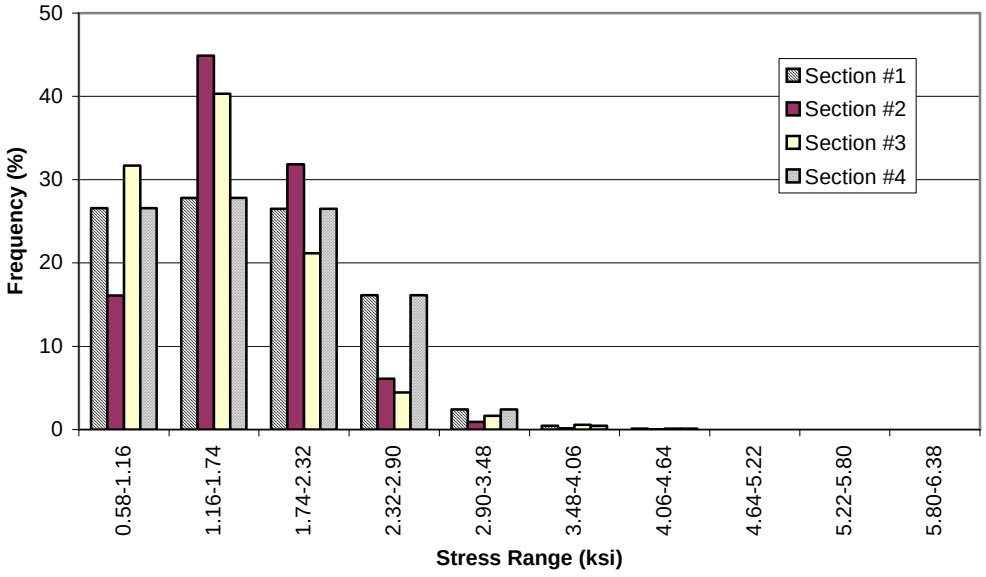

b) Racetrack and Rainflow Counting Methods (Procedure #2)

Figure 5.27 – Cycle Counting Results of West-Side Bottom-Flange Gages (I-65 Bridge)

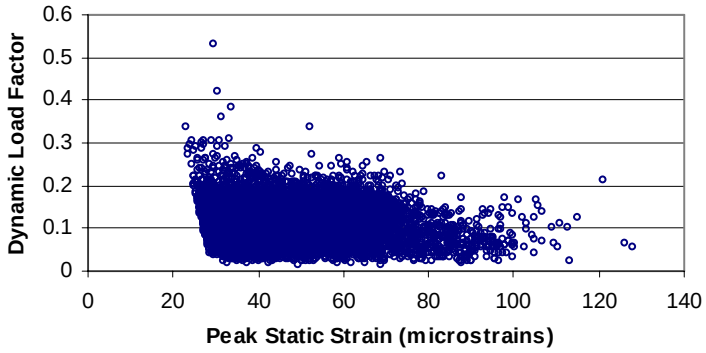

Figure 5.28 – Dynamic Load Factors of Events Recorded from Gage # 8 at Section #1 (I-65 Bridge)

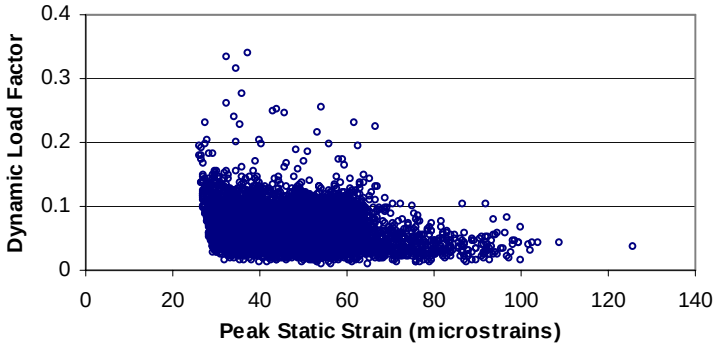

Figure 5.29 – Dynamic Load Factors of Events Recorded from Gage #14 at Section #2 (I-65 Bridge)

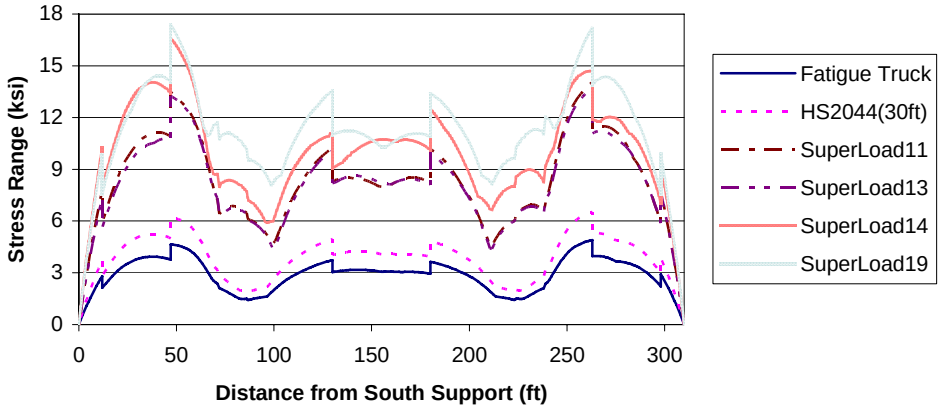

Figure 5.30 – Stress Range Envelopes of One-Dimensional Model for I-65 Bridge

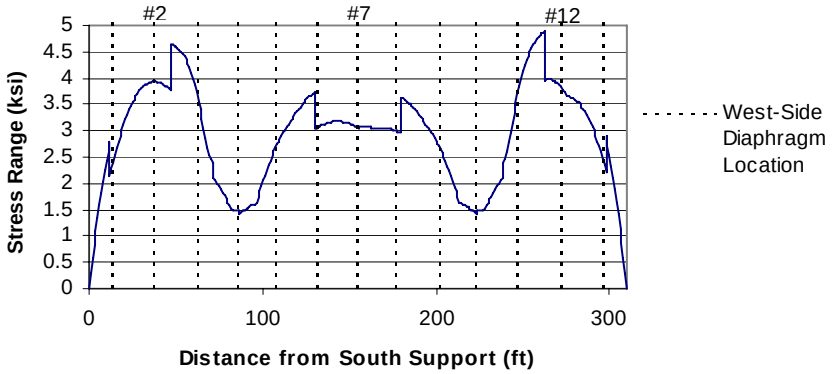

Figure 5.31 – Stress Range Envelope of AASHTO Fatigue Truck for I-65 Bridge

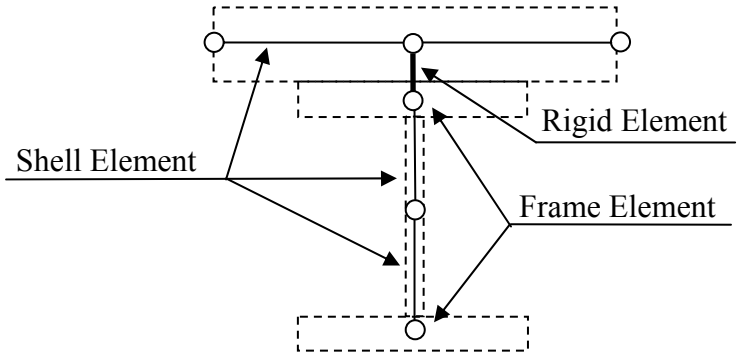

Figure 5.32 – Cross Section of Finite Element Model for I-65 Bridge

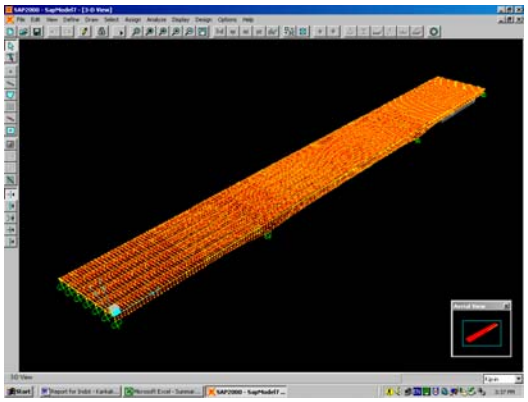

Figure 5.33 – Isometric View of Three-Dimensional Finite Element Model for I-65 Bridge

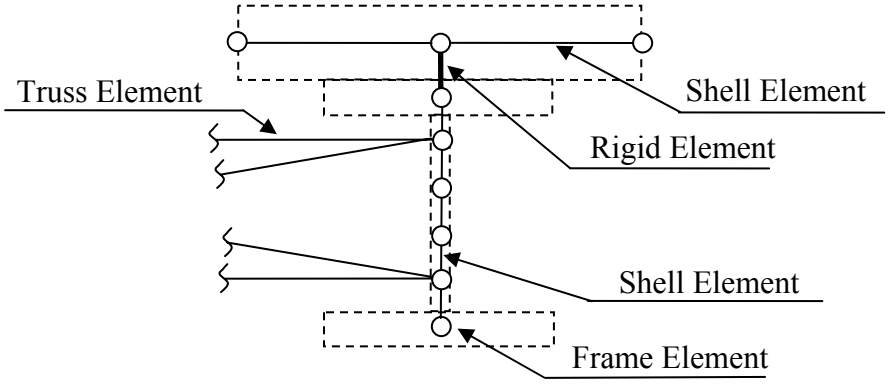

Figure 5.34 – Modified Cross Section of Finite Element Model for I-65 Bridge

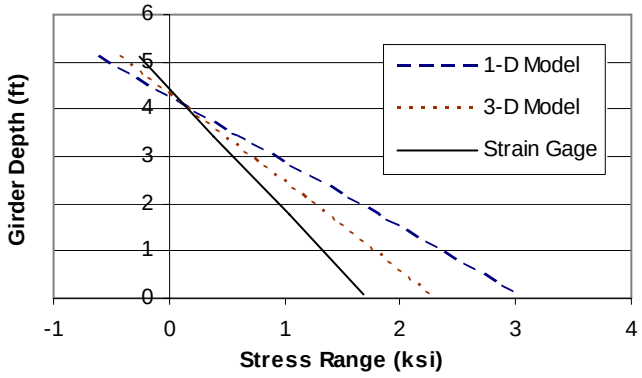

a) Interior Span (Section #2)

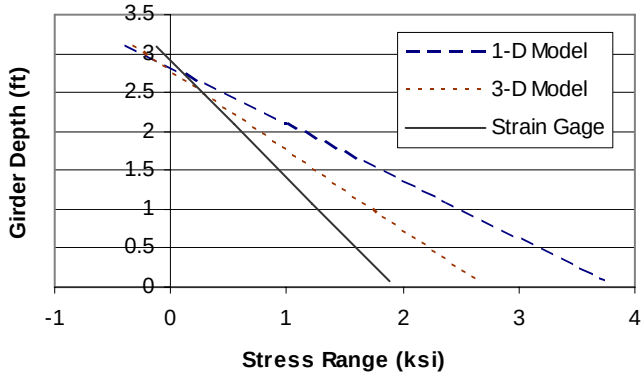

b) Exterior Span (Section #1)

Figure 5.35 – Comparison of Neutral Axis Locations of Strain Gage Data and Analytical Models (I-65 Bridge)

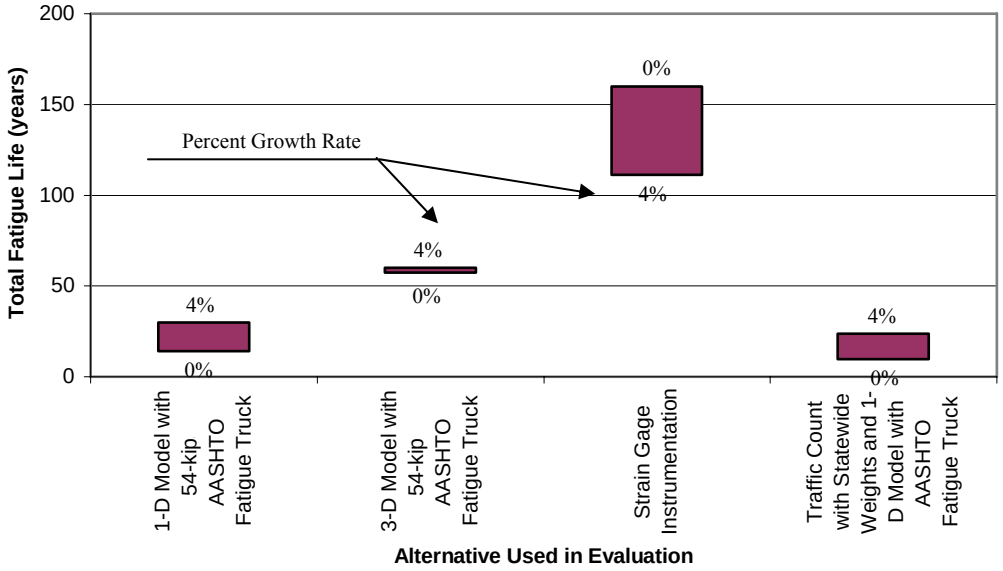

Figure 5.36 – Fatigue Life at Transverse Intermediate Stiffener (I-65 Bridge)

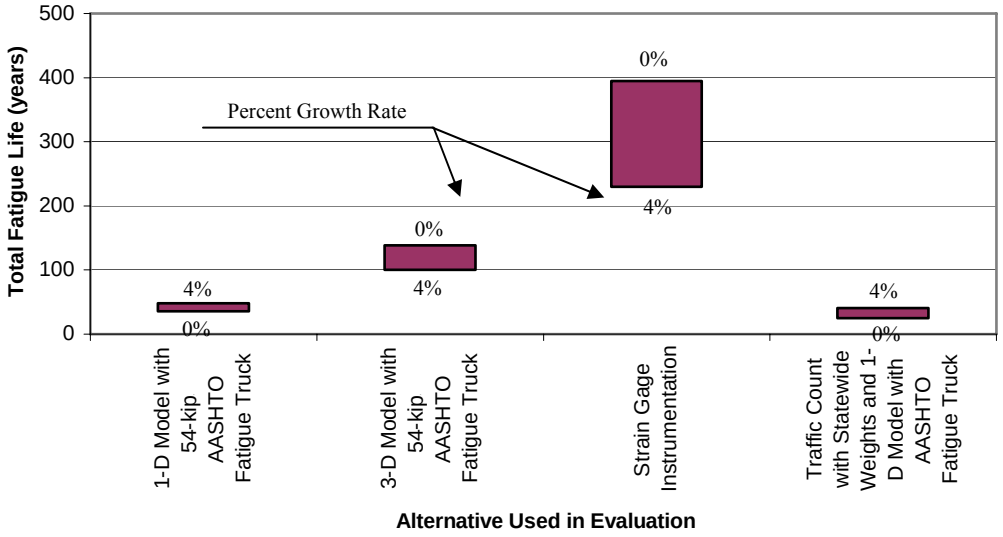

Figure 5.37 – Fatigue Life at Web-to-Flange Fillet Weld (I-65 Bridge)

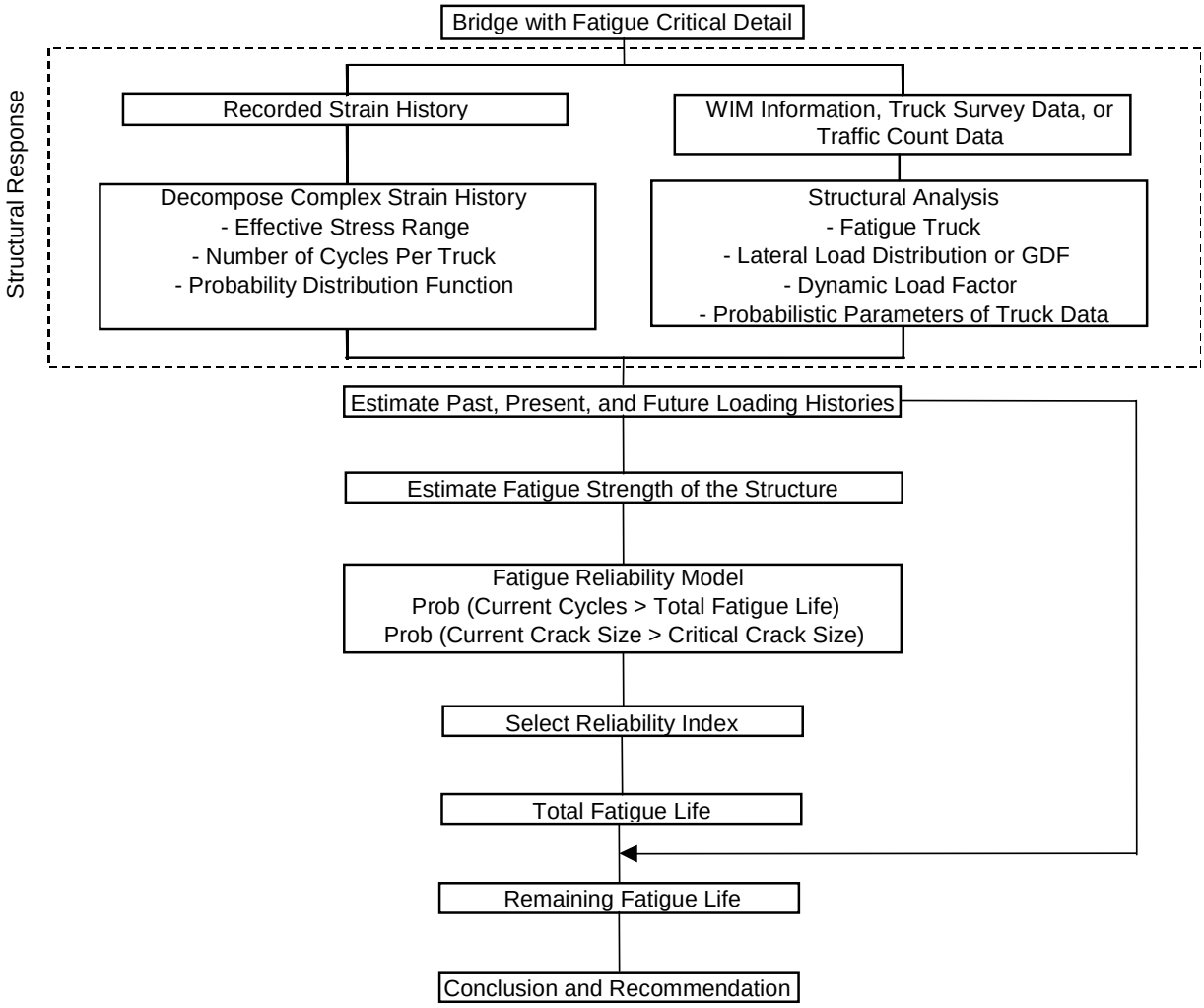

Figure 5.38 – Procedure Used to Determine Remaining Fatigue Life

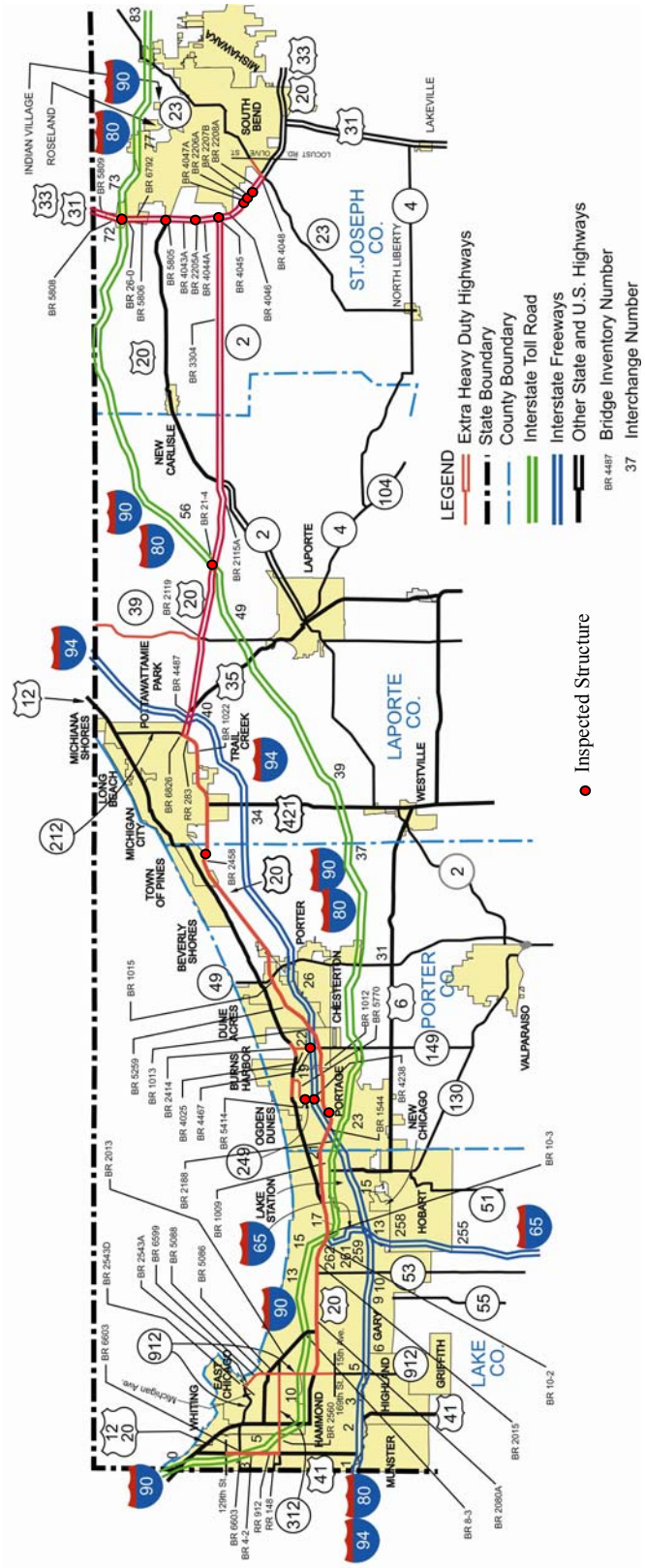

Figure 5.39 – Locations of Inspected Structures on Extra Heavy Duty Corridor

a) Intermittent Fillet Weld Diaphragm Connection

b) Bolted Diaphragm Connection

Figure 5.40 – Diaphragm Connection Types Used in Steel Bridges on Extra Heavy Duty Corridor

c) Riveted Diaphragm Connection

d) Continuous Fillet Weld Connection at Diaphragm-Transverse Stiffeners

Figure 5.40 (Cont.) – Diaphragm Connection Types Used in Steel Bridges on Extra Heavy Duty Corridor

CHAPTER 6. SUMMARY AND CONCLUSIONS

6.1. Summary

The variability of current available fatigue load models in estimating the fatigue damage accumulation of steel bridge structures was evaluated. Truck traffic data collected from three different WIM sites, including more than 60,000 trucks, were simulated by using various distribution functions. The simulated load history was then applied to simple and two-span continuous bridge models to investigate moment range responses of bridge structures under truck traffic loadings. The simulation results indicate that the fatigue truck models given by AASHTO (1990) and Laman and Nowak (1996) do not provide an accurate estimate of the fatigue damage for a wide range of span lengths when compared with the damage predicted using the WIM database. The fatigue damage predicted by these fatigue truck models could be significantly overestimated especially in short span girders. Accordingly, new 3-axle and 4-axle fatigue trucks were developed in the present study. These two new fatigue trucks have been shown to more accurately estimate the fatigue damage accumulation for the full range of span lengths investigated.

Uncertainties associated with using traffic count data to estimate the effective gross weight of a given truck weight distribution were evaluated based on the analysis results of truck traffic data collected at nine WIM sites in Indiana and the vehicle database available in the VTRIS software. Use of traffic count data can provide a relatively accurate estimate of the effective gross weight when the frequency of occurrence and average gross weight of each truck type at an investigated site or other similar highways are utilized in the calculation. However, statewide average gross weights can be employed when gross weight information is not available at a given site.

For this later case, the use of traffic count data tends to underestimate the actual effective gross weights of the truck traffic data investigated.

A review of previous research studies on fatigue load and resistance parameters was conducted to develop a statistical database necessary for a fatigue reliability calculation. Based upon the parameter database and the analysis results of the vehicle database, a fatigue reliability model was developed. The fatigue reliability model can incorporate information obtained from an inspection at a particular site into the fatigue life calculation. The model can be used to provide an estimate of the fatigue life for a level of safety selected by the user. In addition, the safety factor for fatigue evaluation was calibrated based on the parametric study of the proposed fatigue reliability model. The safety factor was developed for both the extension of the S-N line approach and the variable amplitude fatigue limit concept.

An application of the proposed fatigue load model was demonstrated through a field investigation of two steel bridge structures and a fatigue evaluation of twelve steel bridge structures located along segments of the extra heavy duty corridor in northwestern Indiana. Strain gage instrumentation was utilized at the two bridge structures to investigate actual bridge responses under routine truck traffic.

The collected strain data were decomposed by using two different cycle counting procedures, one with and one without the racetrack method. By comparing the cycle counting results obtained from the two procedures, an application of the racetrack method as a pre-filtering process in the counting procedure was examined. The results reveal that the effective stress ranges computed from the two procedures are relatively close. Additionally, more than half of the computational time required in the analysis of strain gage data can be reduced when the racetrack method is utilized in the counting procedure. This indicates that the racetrack method may be a useful tool to facilitate the cycle counting procedure and significantly reduce the computational time required to predict the fatigue life.

Statistics developed for use of traffic count data were compiled into the fatigue reliability model to predict the expected fatigue life of the two bridge structures. The results indicate that use of traffic count data can provide a reasonable estimate of the

fatigue life. This approach shows promise in using information commonly recorded at a site, such as traffic count data, in a fatigue evaluation.

Additionally, a simplified evaluation procedure for a structural reliability-based analysis was discussed. The procedure can be used to provide an estimate of the remaining fatigue life of steel bridge structures so that an operating procedure and a maintenance plan can be properly performed.

6.2. Conclusions and Recommendations

The following are the major conclusions and recommendations that result from this study:

1. The fatigue reliability model and the described fatigue evaluation procedure can be used to determine the remaining fatigue life of in-service steel bridge structures. It is anticipated that the fatigue reliability model can provide a more accurate estimate of the fatigue life than the AASHTO Fatigue Guide Specifications (1990).
2. The variable amplitude fatigue limit concept can provide a considerably longer fatigue life than that predicted by an extension of the S-N line approach. This effect is minimized, however, as the effective stress range is higher in comparison with the variable amplitude fatigue limit.
3. Strain ranges for each week of data do not significantly differ. Therefore, one-week strain data can provide a reasonable estimate of the actual strain range level in bridge structures.
4. The racetrack method can be used as a pre-filtering process in a cycle counting procedure so that the computational time required to identify all ranges in a complex reversal history can be significantly reduced.
5. The effective gross weight of trucks used for a fatigue evaluation is site-specific and can be dramatically different from the 54-kip gross weight of the AASHTO fatigue truck.

6. The current AASHTO fatigue truck can notably overestimate the fatigue damage accumulation, especially in short span girders.
7. The accuracy in estimating the fatigue damage accumulation can be dramatically improved by using the actual truck traffic information at an investigated site in a fatigue calculation, instead of the 54-kip gross weight of the standard AASHTO fatigue truck.
8. A one-dimensional analytical model with the girder distribution factor and dynamic load factor available in the AASHTO LRFD Specifications (1998) provides a conservative estimate of the fatigue life. However, the accuracy in a fatigue life prediction of bridge structures can be improved by using either a more rigorous analysis method or field-measured data.
9. Traffic count data can be used as another alternative procedure in a fatigue evaluation. By compiling the developed statistics for use of traffic count data in estimating an effective gross weight into the fatigue reliability model, a fatigue life can be reasonably estimated and is not significantly different from the fatigue life determined based on the WIM data.
10. The proposed 3-axle and 4-axle fatigue trucks can be used to represent the actual truck traffic with a variety of gross vehicle weights and axle configurations. It is recommended to use the new 3-axle fatigue truck for typical highways with a majority of the fatigue damage dominated by 2- to 5-axle trucks and the 4-axle fatigue trucks for heavy duty highways with more than 10 percent of the truck traffic dominated by 8- to 11-axle trucks.
11. The fatigue behavior of thirteen steel bridge structures along the extra heavy-duty corridor was evaluated using the fatigue reliability model in conjunction with predicted strains from a one-dimensional, beam-line analysis for the fatigue truck loading. It was found that a remaining fatigue life in excess of 25 years was predicted for all bridges along the corridor, and most bridge details were predicted to have fatigue lives well in excess of fifty years. Moreover, it is believed that a life well in excess of 25 years

still remains for the two bridges that had the shortest remaining lives since the one-dimensional beam analysis is known to provide conservative fatigue life estimates.

6.3. Implementation Recommendations

A reliability-based analytical model was developed to predict the fatigue life of steel bridge structures. Based upon truck gross vehicle weights measured using a weigh-in-motion sensor installed on the extra heavy-weight corridor, the effective gross weight of a four-axle fatigue truck was determined. By using stresses predicted for the fatigue truck loading along with the reliability-based model, the fatigue strength for thirteen bridge structures on the extra heavy-weight corridor was evaluated. Based upon this information, the following implementation recommendations are provided. First, the fatigue critical details for the steel bridges along the extra heavy-duty corridor should continue to be monitored through the routine biennial (two-year) inspection monitoring program. Second, if any cracking or unusual rusting is detected during the routine biennial inspection, then it may be desirable to conduct a closer, arms-length inspection of the fatigue critical details, especially for the bridges which have the shortest predicted remaining fatigue lives. Third, the characterization of the loading on the extra heavy-weight corridor should be periodically monitored to see if the trends in truck weights change significantly. Lastly, the analytical model developed in this study can be used to evaluate steel bridge structures at locations other than the extra heavy duty corridor. To perform such an evaluation, the user would need to define the stress at the fatigue detail using either structural analysis along with the appropriate fatigue truck or strain data to infer the stress level.

LIST OF REFERENCES

LIST OF REFERENCES

Albrecht, P. (1982). "Fatigue Reliability Analysis of Highway Bridges." *Transportation Research Record*, Issue 871, Washington, D.C.

Albrecht, P. and Wright, W.J. (2000). "Near-Threshold Fatigue Strength of a Welded Steel Bridge Detail." *Fatigue Crack Growth Thresholds, Endurance Limits, and Design: STP 1372*, pp. 374-399.

American Association of State Highway and Transportation Officials (AASHTO). (1984). *Standard Specifications for Highway Bridges*, 13th Edition, Washington, D.C.

American Association of State Highway and Transportation Officials (AASHTO). (1990). *Guide Specifications for Fatigue Evaluation of Existing Steel Bridges*, Washington, D.C.

American Association of State Highway and Transportation Officials (AASHTO). (1992). *Standard Specifications for Highway Bridges*, 15th Edition, Washington D.C.

American Association of State Highway and Transportation Officials (AASHTO). (1998). *LRFD Bridge Design Specifications*, Second Edition, Washington D.C.

ASTM Standard E1049-85 (1997). *Standard Practices for Cycle Counting in Fatigue Analysis*, American Society for Testing and Materials.

Aziz, T.S. and Alizadeh, A. (1976). "Transverse Distribution of Vehicle Loads on Highway Bridges." Acres Consulting Services Limited, Toronto, Canada.

Ang, A. H-S. and Munse, W.H. (1975). "Practical Reliability Basis for Structural Fatigue." *ASCE National Structural Engineering Convention*, Preprint No. 2494.

Bannantine, J.A., Comer, J.J., and Handrock, J.L. (1990). *Fundamentals of Metal Fatigue Analysis*, Prentice Hall, Englewood Cliffs, NJ.

Barth, A.S. and Bowman, M.D. (2002). "Fatigue Behavior of Beam Diaphragm Connections with Intermittent Fillet Welds: Part I, Volume 2, Laboratory Fatigue Evaluation." *Final Report FHWA/IN/JTRP-2001/10-I-2*, Indiana Department of Transportation.

Clarke, S.N., Deatherage, J.H., Goodpasture, D.W., and Burdette, E.G. (1998). "Influence of Bridge Approach, Surface Condition, and Velocity on Impact Factors for Fatigue-Prone Details." *Transportation Research Record 1624*, pp. 166-179.

Committee on Fatigue and Fracture Reliability of the Committee on Structural Safety and Reliability of the Structural Division. (1982). "Fatigue Reliability: Variable Amplitude Loading." *Journal of Structural Division*, Vol. 108, No.1, pp.47-69.

Dowling, N.E. (1972). "Fatigue Failure Predictions for Complicated Stress-Strain Histories." *Journal of Materials*, Vol. 7, No. 1, pp. 71-87.

Fisher, J.W. (1997). "Evolution of Fatigue-Resistant Steel Bridges." *Transportation Research Record*, No. 1594, pp. 5-17.

Fisher, J.W., Albrecht, P.A., Yen, B.T., Klingerman, D.J., and McNamee, B.M. (1974). "Fatigue Strength of Steel Beams with Welded Stiffeners and Attachments." *NCHRP Report 147*, Transportation Research Board, Washington, D.C.

Fisher, J.W., Frank, K.H., Hirt, M.A., and McNamee, B.M. (1970). "Effect of Weldments on the Fatigue Strength of Steel Beams." *NCHRP Report 102*, Transportation Research Board, Washington, D.C.

Fisher, J.W., Hausammann, H., Sullivan, M.D., and Pense, A.W. (1979). "Detection and Repair of Fatigue Damage in Welded Highway Bridges." *NCHRP 206*, Transportation Research Board, Washington, D.C.

Fisher, J.W., Kulak, G.L., and Smith, I.F.C. (1998). *A Fatigue Primer for Structural Engineers*, National Steel Bridge Alliance.

Fisher, J.W., Mertz, D.R., and Zhong, A. (1983). "Steel Bridge Members Under Variable Amplitude Long Life Fatigue Loading." *NCHRP 267*, Transportation Research Board, Washington, D.C.

Fisher, J.W., Nussbaumer, A., and Keating, P.B. (1993). "Resistance of Welded Details Under Variable Amplitude Long-Life Fatigue Loading." *NCHRP 354*, Transportation Research Board, Washington, D.C.

Fuchs, H.O., Nelson, D.V., Burke, M.A., and Toomay, T.L. (1973). "Shortcuts in Cumulative Damage Analysis." *SAE Automobile Engineering Meeting*, Paper 730565.

Grover, D. and Deller, J.R. (1999). *Digital Signal Processing and the Microcontroller*, Prentice Hall, NJ.

Hasofer, A.M. and Lind, N.C. (1974). "Exact and Invariant Second Moment Code Format." *Journal of Engineering Mechanics*, Vol. 100, No. EM1, February, pp. 111-121.

Hwang, E-S. and Nowak, A.S. (1991). "Simulation of Dynamic Load for Bridges." *ASCE Journal of Structural Engineering*, Vol. 117, No.5, pp.1413-1434.

Indiana Design Manual (1994). Part-V Road Design, Volume I.

Jajich, D. and Schultz, A.E. (2003). "Measurement and Analysis of Distortion-Induced Fatigue in Multigirder Steel Bridges." *Journal of Bridge Engineering*, Vol. 8, No. 2, pp. 84-91.

Keating, P.B. (1994). "Focusing on Fatigue." *Civil Engineering*, ASCE, November, pp. 54-57.

Keating, P.B. and Fisher J.W. (1986). "Evaluation of Fatigue Tests and Design Criteria on Welded Details." *NCHRP Report 286*, Transportation Research Board, Washington, D.C.

Laman, J.A. (1996). "Probabilistic Fatigue Models for Bridge Evaluation." *Probabilistic Mechanics & Structural Reliability, Proceedings of the Seventh Specialty Conference*, August.

Laman, J.A. and Nowak, A.S. (1996). "Fatigue-Load Models for Girder Bridges." *Journal of Structural Engineering*, Vol. 122, July, pp.726-33.

Mabsout, M, Tarhini, K.M., Frederick, G.R., and Kesserwan, A. (1998). "Effect of Continuity on Wheel Load Distribution in Steel Girder Bridges." *Journal of Bridge Engineering*, Vol. 3, No. 3, August, pp. 103-110.

Madsen, H.O. (1988). "Omission Sensitivity Factors." *Structural Safety*, Vol. 5, pp. 35-45.

Madsen, H.O., Krenk, S., and Lind, N.C. (1986). *Methods of Structural Safety*, Prentice Hall, Englewood Cliffs, NJ.

Matsuishi, M. and Endo, T. (1968). "Fatigue of Metals Subjected to Varying Stress - Fatigue Lives under Random Loading." *Preliminary Proceedings of the Kyushu District Meeting*, The Japan Society of Mechanical Engineers, March, pp. 37-40.

Mauser, J. (2001). *Bridge Load Rating and Fatigue Life Report I65 over the Kankakee River Lake County*, Indiana, Janssen & Spaans Engineering (JSE).

McLean, D. I. and Marsh, M. L. (1998). "Dynamic Impact Factors for Bridges." *Synthesis of Highway Practice 266*.

Melchers, R.E. (1987). *Structural Reliability Analysis and Prediction*, John Wiley & Sons, New York.

Miner, M. A. (1945). "Cumulative Damage in Fatigue." *Transactions of the American Society of Mechanical Engineers*, Vol. 67.

Mohammadi, J., Guralnick, S.A., and Polepeddi, R. (1998). "Bridge Fatigue Life Estimation from Field Data." *Practice Periodic on Structural Design and Construction*, Vol. 3, No. 3, August, pp. 128-133.

Moses, F., Schilling, C.G., and Raju, K.S. (1987). "Fatigue Evaluation Procedures for Steel Bridge." *NCHRP Report 299*, Transportation Research Board, Washington, D.C.

Najafi, F. T. and Blackadar, B. (1998). "Analysis of Weigh-In-Motion Truck Traffic Data." *Proceedings of the Annual Meeting of the Transportation Research Forum 40th*, Vol. 1, pp. 139-162.

Nassif, H.H. and Nowak, A.S. (1995). "Dynamic Load Spectra for Girder Bridges." *Transportation Research Record 1476*, pp.69-83.

Nowak, A.S., Hong, Y., and Hwang, E. (1991). "Modeling Live Load and Dynamic Load for Bridges." *Transportation Research Record*, Issue 1290, pp. 110-118.

Nowak, A.S. and Szerszen, M.M. (1996). "Bridge Load and Resistance Models." *Proceedings of the Workshop on Structural Reliability in Bridge Engineering*, October, pp. 30-41.

Nowak, A.S. and Zhou, J. (1985). "Reliability Models for Bridge Analysis." *Report No. UMCE 85-3*, March.

Nyman, W.E. and Moses, F. (1985). "Calibration of Bridge Fatigue Design Model." *Journal of Structural Engineering*, ASCE, Vol. 11, June, pp. 1251-66.

Palmgren, A. (1924). "Die Lebensdauer von Kugellagern," ZDVDI, Vol. 68, No.14, p339 (In German).

Paris, P. and Erdogan, F. (1963). "A Critical Analysis of Crack Propagation Laws." *Journal of Basic Engineering*, Transactions of the American Society of Mechanical Engineers, December, Vol. 85, No. 4, pp.528-534.

Rackwitz, R. and Fiessler, B. (1978). "Structural Reliability Under Combined Random Load Sequences." *Computers and Structures*, Vol. 9., No. 5, pp. 484-494.

Raju, S.K., Moses, F., and Schilling, C. G. (1990). "Reliability Calibration of Fatigue Evaluation and Design Procedures." *Journal of Structural Engineering*, Vol. 116, May, pp.1356-69.

Reisert, J.A. (2003). "Bridge and Weigh-In-Motion Measurements on the Northern Indiana Extra Heavy Duty Truck Corridor." Master Thesis Presented to Purdue University.

Schilling, C.G. (1982). "Lateral-Distribution Factors for Fatigue Design." *Journal of the Structural Division*, ASCE, Vol. 108, No. ST9, September.

Schilling, C.G. (1984). "Stress Cycles for Fatigue Design of Steel Bridges." *Journal of Structural Engineering*, ASCE, Vol.110, No.6, June.

Schilling, C.G. and Klippstein, K.H. (1978). "New Method for Fatigue Design of Bridges." *Journal of Structural Division*, Vol. 104.

Sih, G.C. (1973). *Handbook of Stress-Intensity Factors for Researchers and Engineers*, Institute of Fracture and Solid Mechanics, Lehigh University, Bethlehem, PA.

Stephens, R.I., Fatemi, A., Stephens, R.R., and Fuchs, H.O. (2001). *Metal Fatigue in Engineering*, John Wiley & Sons, Second Edition.

Synder, R.E., Likins, G.E., and Moses, F. (1985). "Loading Spectrum Experienced by Bridge Structures in the United States." *Report FHWA/RD-85/012*, Bridge Weighing Systems Inc., Warrensville, Ohio.

Tada, H., Paris, P.C., and Irwin, G.R., Eds. (1985). *Stress Analysis of Cracks Handbook*, Del Research Corporation, St. Louis, MO.

Traffic Monitoring Guide. August 2003. FHWA Office of Highway Policy Information. 22 March. 2004 <http://www.fhwa.dot.gov/ohim/tmguide>.

Vehicle Travel Information System (VTRIS). April 2003. FHWA Office of Highway Policy Information. 25 August. 2003 <http://apps.fhwa.dot.gov/vtris>.

Zokaie, T. (1992). “Distribution of Wheel Loads on Highway Bridges.” *Research Results Digest*, Number 187.

APPENDICES

APPENDIX A. FHWA VEHICLE CLASSIFICATION

In the mid-1980's, the FHWA developed the 13-category scheme used for most federal vehicle classification count reporting. The classification scheme is separated into categories depending on whether the vehicle carries passengers or commodities. Non-passenger vehicles are further subdivided by number of axles and number of units, including both power and trailer units. Note that the addition of a light trailer to a vehicle does not change the classification of the vehicle. The definitions of FHWA vehicle classifications are provided in the followings (http://www.fhwa.dot.gov/ohim/tmguide/):

Class 1 - Motorcycles: All two- or three-wheeled motorized vehicles. Typical vehicles in this category have saddle type seats and are steered by handle bars rather than wheels. This category includes motorcycles, motor scooters, mopeds, motor-powered bicycles, and three-wheeled motorcycles. This vehicle may be reported at the option of the State.

Class 2 - Passenger Cars: All sedans, coupes, and station wagons manufactured primarily for the purpose of carrying passengers and including those passenger cars pulling recreational or other light trailers.

Class 3 - Other Two-Axle, Four-Tire, Single Unit Vehicles: All two-axle, four-tire, vehicles other than passenger cars. Included in this classification are pickups, panels, vans, and other vehicles such as campers, motor homes, ambulances, hearses, carryalls, and minibuses. Other two-axle, four-tire single unit vehicles pulling recreational or other light trailers are included in this classification.

Class 4 - Buses: All vehicles manufactured as traditional passenger-carrying buses with two axles and six tires or three or more axles. This category includes

only traditional buses (including school buses) functioning as passenger-carrying vehicles. Modified buses should be considered to be trucks and be appropriately classified.

Note: In reporting information on trucks the following criteria should be used:

a. Truck tractor units traveling without a trailer will be considered single unit trucks.

b. A truck tractor unit pulling other such units in a “saddle mount” configuration will be considered as one single unit truck and will be defined only by axles on the pulling unit.

c. Vehicles shall be defined by the number of axles in contact with the roadway. Therefore, “floating” axles are counted only when in the down position.

d. The term “trailer” includes both semi- and full trailers.

Class 5 - Two-Axle, Six-Tire, Single Unit Trucks: All vehicles on a single frame including trucks, camping and recreational vehicles, motor homes, etc., having two axles and dual rear wheels.

Class 6 - Three-axle Single unit Trucks: All vehicles on a single frame including trucks, camping and recreational vehicles, motor homes, etc., having three axles.

Class 7 - Four or More Axle Single Unit Trucks: All trucks on a single frame with four or more axles.

Class 8 - Four or Less Axle Single Trailer Trucks: All vehicles with four or less axles consisting of two units, one of which is a tractor or straight truck power unit.

Class 9 - Five-Axle Single Trailer Trucks: All five-axle vehicles consisting of two units, one of which is a tractor or straight truck power unit.

Class 10 - Six or More Axle Single Trailer Trucks: All vehicles with six or more axles consisting of two units, one of which is a tractor or straight truck power unit.

Class 11 - Five or Less Axle Multi-Trailer Trucks: All vehicles with five or less axles consisting of three or more units, one of which is a tractor or straight truck power unit.

Class 12 - Six-Axle Multi-Trailer Trucks: All six-axle vehicles consisting of three or more units, one of which is a tractor or straight truck power unit.

Class 13 - Seven or More Axle Multi-Trailer Trucks: All vehicles with seven or more axles consisting of three or more units, one of which is a tractor or straight truck power unit.

APPENDIX B. SUPERLOAD VEHICLES

This section provides a configuration of superload vehicles provided by INDOT for load rating of the I-65 bridges over the Kankakee River.

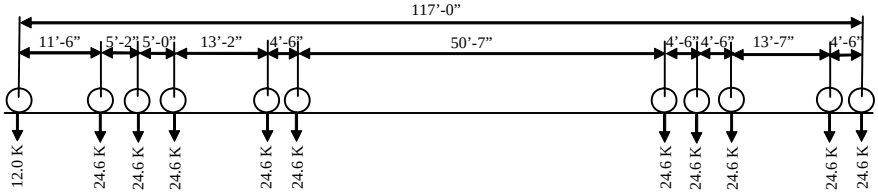

a) Superload 11-Axle Vehicle (Total Gross Weight = 258 kips)

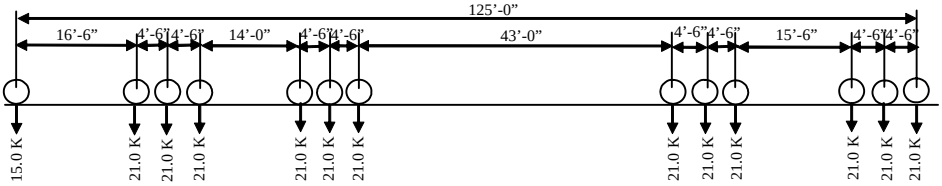

b) Superload 13-Axle Vehicle (Total Gross Weight = 267 kips)

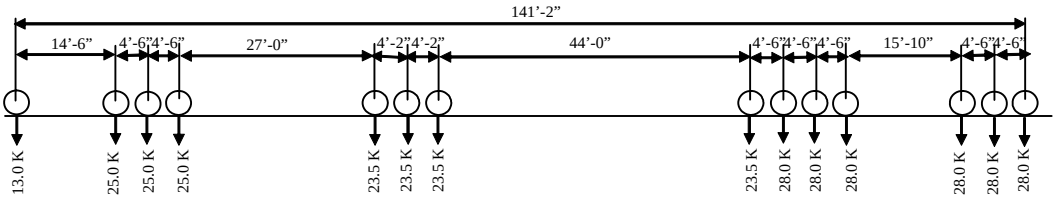

c) Superload 14-Axle Vehicle (Total Gross Weight = 350 kips)

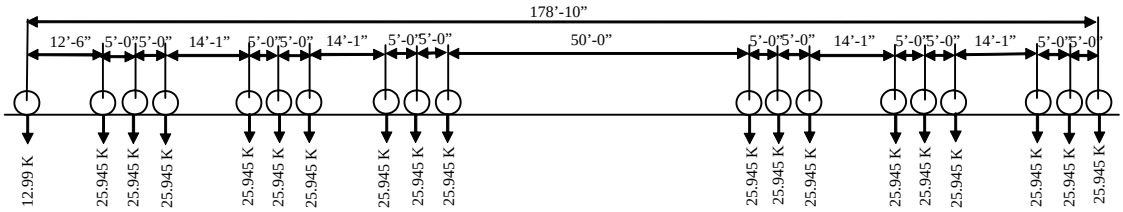

d) Superload 19-Axle Vehicle (Total Gross Weight = 480 kips)

Figure B1 – Superload Vehicles (Mauser, 2001)

APPENDIX C. INSPECTION OF BRIDGES ON EXTRA HEAVY DUTY HIGHWAY

This section contains photographs taken during an inspection of the bridge structures located along various segments of the extra heavy duty corridor. Included are pictures of an overview and fatigue details used in each structure.

a) Overview

b) Intermittent Weld Diaphragm Connection

Figure C.1 – Overview and Fatigue Details of Structure No. 20-64-1010A

c) Bolted Splice Plate Connection

Figure C.1 (Cont.) – Overview and Fatigue Details of Structure No. 20-64-1010A

a) Overview

b) Structural Framing

Figure C.2 – Overview and Fatigue Details of Structure No. 21-4

c) Riveted Diaphragm Connection

d) Riveted Splice Plate Connection

Figure C.2 (Cont.) – Overview and Fatigue Details of Structure No. 21-4

a) Overview

b) Bolted Diaphragm Connection

c) Riveted Diaphragm Connection

Figure C.3 – Overview and Fatigue Details of Structure No. 20-71-2205B

d) Bolted Splice Plate Connection

Figure C.3 (Cont.) – Overview and Fatigue Details of Structure No. 20-71-2205B

a) Overview

b) Riveted Diaphragm Connection

Figure C.4 – Overview and Fatigue Details of Structure No. 20-71-4045B

c) Bolted Diaphragm Connection

d) Bolted Splice Plate Connection

Figure C.4 (Cont.) – Overview and Fatigue Details of Structure No. 20-71-4045B

a) Overview

b) Bolted Diaphragm Connection

c) Riveted Diaphragm Connection

Figure C.5 – Overview and Fatigue Details of Structure No. 20-71-4047B

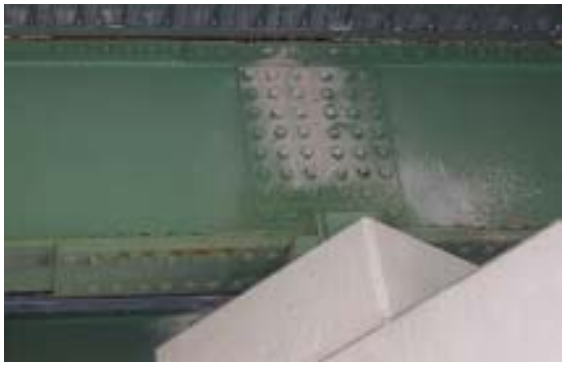

d) Bolted Splice Plate Connection

Figure C.5 (Cont.) – Overview and Fatigue Details of Structure No. 20-71-4047B

a) Overview

b) Bolted Diaphragm Connection

Figure C.6 – Overview and Fatigue Details of Structure No. 20-71-2206B

c) Riveted Diaphragm Connection

d) Bolted Splice Plate Connection

Figure C.6 (Cont.) – Overview and Fatigue Details of Structure No.20-71-2206B

a) Overview

b) Bolted Diaphragm Connection

c) Intermitted Weld Diaphragm Connection

Figure C.7 – Overview and Fatigue Details of Structure No. 20-71-2207C

d) Bolted Splice Plate Connection

Figure C.7 (Cont.) – Overview and Fatigue Details of Structure No. 20-71-2207C

a) Overview

b) Structural Framing

c) Jacking Frame at Middle Support

Figure C.8 – Overview and Fatigue Details of Structure No. 31-71-5805A

d) Bolted Diaphragm Connection

e) Longitudinal Attachment Plate

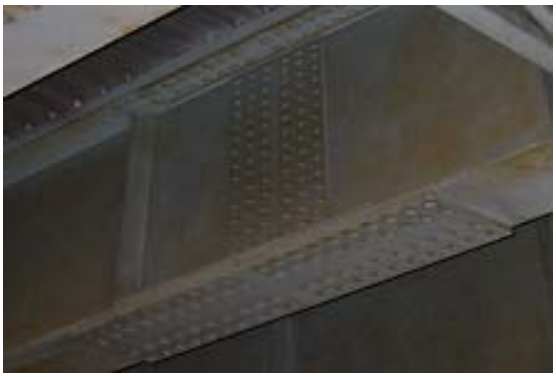

f) Bolted Splice Plate Connection

Figure C.8 (Cont.) – Overview and Fatigue Details of Structure No. 31-71-5805A

a) Overview

b) Diaphragm Framing

c) Cross-Frame Diaphragm

Figure C.9 – Overview and Fatigue Details of Structure No. 31-71-5807A

d) Bolted Splice Plate Connection

Figure C.9 (Cont.) – Overview and Fatigue Details of Structure No. 31-71-5807A

a) Overview

b) Structural Framing

Figure C.10 – Overview and Fatigue Details of Structure No. 249-64-4238B

c) Bolted Diaphragm Connection

d) Bolted Splice Plate Connection

Figure C.10 (Cont.) – Overview and Fatigue Details of Structure No. 249-64-4238B

a) Overview

b) Structural Framing

c) Bolted Diaphragm Connection

Figure C.11 – Overview and Fatigue Details of Structure No. 249-64-5414C

d) Intermittent Weld Diaphragm Connection

e) Bolted Splice Plate Connection

Figure C.11 (Cont.) – Overview and Fatigue Details of Structure No. 249-64-5414C

a) Overview

b) Structural Framing

c) Intermittent Weld Diaphragm Connection

Figure C.12 – Overview and Fatigue Details of Structure No. 149-64-4467B

d) Jacking-Frame and Cross-Frame Diaphragms at Middle Support

e) Bolted Splice Plate Connection

Figure C.12 (Cont.) – Overview and Fatigue Details of Structure No. 149-64-4467B